FY24 NRL DOD HPCMP ANNUAL REPORTS

U.S. NAVAL RESEARCH LABORATORY

FY24 NRL DoD
High Performance Computing Modernization Program Annual Reports

Edited by
Dr. Yu Yu Khine
Dr. Robert Rosenberg
Benjamin Bateman

Prepared by
Beth A. Howell

Center for Computational Science
Information Technology Division

August xx, 2025

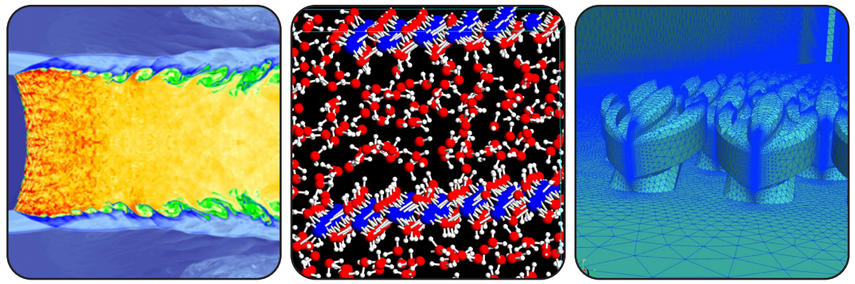

REVIEWED AND APPROVED
NRL/5590/PU--2025/1
IR-5594-25-2-U
August 2025

Center for Computational Science
Information Technology Division

Introduction

This book is a compilation of reports on all the work accomplished by NRL scientists and engineers and their collaborators using the DoD High Performance Computing Modernization Program's (HPCMP) resources for fiscal year 2024. The reports encompass work performed by researchers at all three NRL sites: Washington, D.C., Stennis Space Center, Mississippi, and Monterey, California.

These reports are categorized according to the primary Computational Technology Areas (CTAs) as specified by the HPCMP and include resources at the DOD Supercomputing Resource Centers (DSRC) as well as the Affiliated Resource Centers (ARC). This volume includes three indices for ease of reference: an author index, a site index, and an NRL hierarchical index of reports from the branches and divisions in the Laboratory.

THIS PAGE INTENTIONALLY LEFT BLANK

Table of Contents

Computational Structural Mechanics (CSM)

Geometric, Constitutive and Loading Complexities in Structural Materials 2
S.A. Wimmer,[1] N. Wade,[2] and A. Arcari[1]
[1]U.S. Naval Research Laboratory, Washington, DC
[2]American Society for Engineering Education Postdoctoral Fellow at the U.S. Naval Research Laboratory, Washington, DC

Stochastic Methods for Uncertainty Quantification in Computational Mechanics.....4
K. Teferra,[1] N. Wade,[2] and A. Chadwick[1]
[1]U.S. Naval Research Laboratory, Washington, DC
[2]American Society for Engineering Education Postdoctoral Fellow at the U.S. Naval Research Laboratory, Washington, DC

Atomistic Simulations of Structural Materials 6
E. Antillon
U.S. Naval Research Laboratory, Washington, DC

Computational Analysis of Warfighter Brain Injury and Protective Equipment.....8
X.G. Tan and A.E. Moser
U.S. Naval Research Laboratory, Washington, DC

Computational Fluid Dynamics (CFD)

Airbreathing Combustion for Hypersonics 12
G.B. Goodwin[1] and R. DeBoskey[2]
[1]U.S. Naval Research Laboratory, Washington, DC
[2]Commonwealth Technology Innovation LLC, Alexandria, VA

Predicting Fluid-Structure Interaction for Military Applications.....14
Y. Khine and D.R. Mott
U.S. Naval Research Laboratory, Washington, DC

Numerical Investigation of Advanced Military Aircraft Noise Reduction Concepts.....16
J. Liu
U.S. Naval Research Laboratory, Washington, DC

High-fidelity Modeling of Gaseous Detonations.....18
V.N. Gamezo[1] and A.Y. Poludnenko[2]
[1]U.S. Naval Research Laboratory, Washington, DC
[2]University of Connecticut, Storrs, CT

Numerical Simulations of Noise Generated by Non-Circular Advanced Military Aircraft Nozzles.....20
K. Viswanath
U.S. Naval Research Laboratory, Washington, DC

High-Fidelity CFD Simulations of High-Speed Flows in Realistic Atmospheric Conditions.....22
D. Kessler, T.K. Patel, R.F. Johnson, A. Hess, and B. Bojko
U.S. Naval Research Laboratory, Washington, DC

Applications of FEFLO Incompressible Flow Solver.....24
R. Ramamurti
U.S. Naval Research Laboratory, Washington, DC

Direct Numerical Simulation of Fluid-Sediment Wave Bottom Boundary Layer.....26
J. Simeonov, I. Adams, A. Penko, S. Schoenauer, S. Bateman, K. Edwards, R. Phillip, and J. Veeramony
U.S. Naval Research Laboratory, Stennis Space Center, MS

Detonations with Multi-Phase Flows for Propulsion.....28
D.A. Schwer
U.S. Naval Research Laboratory, Washington, DC

Multidimensional Chemically Reacting Fluid Dynamics with Application to Flameless Combustors.....30
R.F. Johnson
U.S. Naval Research Laboratory, Washington, DC

Computational Biology, Chemistry, and Materials Science (CCM)

Calculation of Materials Properties via Density Functional Theory and Its Extensions.....34
J.L. Lyons
U.S. Naval Research Laboratory, Washington, DC

Point Defects and Interfaces in Two-Dimensional Materials.....36
D. Wickramaratne
U.S. Naval Research Laboratory, Washington, DC

Materials for Energy Storage and Generation.....38
M. Johannes
U.S. Naval Research Laboratory, Washington, DC

Computational Materials Design for Targeted Applications.....40
S. Mukhopadhyay
U.S. Naval Research Laboratory, Washington, DC

Numerical Studies of Semiconductor Nanostructures.....42
T.L. Reinecke[1] and I. Welland[2]
[1]U.S. Naval Research Laboratory, Washington, DC
[2]National Research Council Research Associate at the U.S. Naval Research Laboratory, Washington, DC

Machine Learning Interatomic Potentials for Materials Science.....44
M.W. Swift
U.S. Naval Research Laboratory, Washington, DC

Materials Properties of Surfaces and Two-dimensional Systems.....46
M. Phillips
U.S. Naval Research Laboratory, Washington, DC

Multiple Length and Time Scale Simulations of Material Properties 48
N. Bernstein
U.S. Naval Research Laboratory, Washington, DC

Optimization Algorithms for Quantum Computers.....50
C.S. Hellberg
U.S. Naval Research Laboratory, Washington, DC

Evaluating the Active Site of Metal-Zeolite Combinations for Selective Catalytic Reactions.....52
C.F. Holder,[1] A.R. Shabaev,[1] and J.R. Morse[2]
[1]U.S. Naval Research Laboratory, Washington, DC
[2]Applied Research Laboratory at Penn State University, State College, PA

Target Material Detection by Comparison of Measured DFT-calculated Absorbance Spectra 54
A.R. Shabaev, C.F Holder, and S. Lambrakos
U.S. Naval Research Laboratory, Washington, DC

Surfaces and Interfaces in Oxides and Semiconductors 56
C.S. Hellberg
U.S. Naval Research Laboratory, Washington, DC

First-principles Simulations of Condensed-phase Decomposition of Energetic Materials.....58
I.V. Schweigert
U.S. Naval Research Laboratory, Washington, DC

Marine Biofilm Metaproteomics 60
W.J. Hervey, M.R. Kardish, and G.J. Vora
U.S. Naval Research Laboratory, Washington, DC

Synthetic Biology for Military Environments **62**
W.J. Hervey and G.J. Vora
U.S. Naval Research Laboratory, Washington, DC

Atomistic Simulations of Navy-relevant Materials **64**
D. Fragiadakis
U.S. Naval Research Laboratory, Washington, DC

Computational Electromagnetics and Acoustics (CEA)

Low Grazing Angle Radar Backscatter **68**
J.V. Toporkov, M.A. Sletten, and J.D. Ouellette
U.S. Naval Research Laboratory, Washington, DC

Acoustic Parameter Variability over an Ocean Reanalysis (AVORA) **70**
B.A. Melzer
U.S. Naval Research Laboratory, Stennis Space Center, MS

Computer-Aided Design of Vacuum Electronic Devices **72**
G. Stantchev,[1] S. Cooke,[1] J. Petillo,[2] A. Jensen,[2] and S. Ovtchinnikov[2]
[1]*U.S. Naval Research Laboratory, Washington, DC*
[2]*Leidos, Tewksbury, MA*

Particle-In-Cell Simulations of Two Cylindrical Reflex Triodes in Parallel **74**
I.M. Rittersdorf, B.V. Weber, S.B. Swanekamp, and D.D. Hinshelwood
U.S. Naval Research Laboratory, Washington, DC

Three-Dimensional Empire Particle-in-cell Simulations of a Magnetically-insulated Transmission Line Terminated by a Large-area Diode **76**
S.B. Swanekamp,[1] J.C. Zier,[1] N.D. Isner,[1] I.M. Rittersdorf,[1] A.R. Vazsonyi,[1] and M.D. Johnston[2]
[1]*U.S. Naval Research Laboratory, Washington, DC*
[2]*Sandia National Laboratories, Albuquerque, NM*

Infrared Scattering by Micro-particles **78**
R. Furstenberg and A.R. Shabaev
U.S. Naval Research Laboratory, Washington, DC

Three-Dimensional Acousto-Elastic Modeling **80**
S. Dey
U.S. Naval Research Laboratory, Washington, DC

Underwater Electrical Impedance Tomography **82**
G.R. Gatling and E.M. Tejero
U.S. Naval Research Laboratory, Washington, DC

Climate Weather Ocean Modeling (CWO)

COAMPS-TC® Tropical Cyclone Rapid Intensification Prediction 86
J.D. Doyle
U.S. Naval Research Laboratory, Monterey, CA

Improved Mixed Layer Depth and Upper Ocean Structures via Turbulent Mixing Advancements 88
Y. Fan
U.S. Naval Research Laboratory, Stennis Space Center, MS

Dynamics of Coupled Models 90
I. Shulman, S. Cayula, E. Jarosz, and E.J. Metzger
U.S. Naval Research Laboratory, Stennis Space Center, MS

Coastal Mesoscale Modeling 92
P.M. Finocchio
U.S. Naval Research Laboratory, Washington, DC

Eddy-Resolving Global/Basin-Scale Ocean Modeling – Winter Convection and Water Mass Formation in the Northern Arabian Sea 94
P.G. Thoppil
U.S. Naval Research Laboratory, Stennis Space Center, MS

Eddy-Resolving Global/Basin-Scale Ocean Modeling 96
E.J. Metzger
U.S. Naval Research Laboratory, Stennis Space Center, MS

Eddy-Resolving Global/Basin-Scale Ocean Modeling – Phase-accurate Internal Tides in a Global Ocean Forecast Model: Potential Applications for Nadir and Wide-swath Altimetry 98
J.F. Shriver and E.J. Metzger
U.S. Naval Research Laboratory, Stennis Space Center, MS

Eddy-Resolving Global/Basin-Scale Ocean Modeling – Optimization of Ice Rheology for Advancing Sea Ice Forecast 100
G. Panteleev, D. Hebert, M. Yaremchuk, and R. Allard
U.S. Naval Research Laboratory, Stennis Space Center, MS

Eddy-Resolving Global/Basin-Scale Ocean Modeling – Ocean Forecast Compression for Resource-limited Environments 102
C.B. Trott
U.S. Naval Research Laboratory, Stennis Space Center, MS

Eddy-Resolving Global/Basin-Scale Ocean Modeling – Dynamical Controls of the East China Sea/Yellow Sea 104
J.F. Shriver and L.T. Gulliver
U.S. Naval Research Laboratory, Stennis Space Center, MS

Eddy-Resolving Global/Basin-Scale Ocean Modeling – Accelerating Ocean Forecasts Through Mixed Precision Data Representation 106
C. Rowley
U.S. Naval Research Laboratory, Stennis Space Center, MS

Eddy-Resolving Global/Basin-Scale Ocean Modeling – Ocean Submesoscale Eddy Evolution.....108
J. May, T. Smith, J.M. D'Addezio, D. Hebert, and B. Krause
U.S. Naval Research Laboratory, Stennis Space Center, MS

Eddy-Resolving Global/Basin-Scale Ocean Modeling – Resolving Northern High Latitude Water-mass Formation Mechanisms.....110
S.R. Smith,[1] R.W. Helber,[1] and H. Kaur[2]
[1]U.S. Naval Research Laboratory, Stennis Space Center, MS
[2]University of Southern Mississippi, Hattiesburg, MS

Data Assimilation Studies Project 112
J. Tsu and W.F. Campbell
U.S. Naval Research Laboratory, Monterey, CA

Performance Study and Potential Optimization Exploration of an Ocean Modeling Code 114
Y. Khine
U.S. Naval Research Laboratory, Washington, DC

Ocean Data Assimilation – Multiscale, Multiphysics Ocean Data Assimilation.....116
J.M. D'Addezio,[1] A.J. Iversen,[2] G. Jacobs,[1] S.R. Smith[1]
[1]Naval Research Laboratory, Stennis Space Center, MS
[2]Peraton, Stennis Space Center, MS

Velocity Data Assimilation 118
S.R. Smith, R.W. Helber, and G. Jacobs
U.S. Naval Research Laboratory, Stennis Space Center, MS

Impact of SWOT Observations on the Ocean Subsurface.....120
B. Rester[1] and M.J. Carrier[2]
[1]American Society for Engineering Education Postdoctoral Fellow at the U.S. Naval Research Laboratory, Stennis Space Center, MS
[2]U.S. Naval Research Laboratory, Stennis Space Center, MS

Ocean Modeling for Acoustic Impacts.....122
J.J. Osborne,[1] C.M. Amos,[2,3] G.A. Jacobs,[1] J.W. Book,[1] C.N. Barron,[1] and A. Lawrence[4]
[1]U.S. Naval Research Laboratory, Stennis Space Center, MS
[2]American Society for Engineering Education Postdoctoral Fellow at the U.S. Naval Research Laboratory, Stennis Space Center, MS
[3]Applied Physics Laboratory, Johns Hopkins University
[4]Peraton, Inc., Stennis Space Center, MS

Atmospheric Process Studies 124
J.A. Ridout, T.R. Whitcomb, M.A. Janiga, and J.M. McLay
U.S. Naval Research Laboratory, Monterey, CA

Coupled Ocean-Wave-Air-Ice Prediction System.....126
R. Allard,[1] T. Campbell,[1] E. Douglass,[1] D. Hebert,[1] T. Jensen,[1] G. Panteleev,[1]
M. Phelps,[2] and T. Smith[1]
[1]Naval Research Laboratory, Washington, DC
[2]Peraton, Inc., Stennis Space Center, MS

Multiscale Characterization and Prediction of the Global Atmosphere from Ground to the Edge of Space using Next-Generation Navy Modeling Systems 128
C.A. Barton, S.D. Eckermann, J.F. Kelly, M.A. Herrera, K.W. Hoppel, D.D. Kuhl,
D.R. Allen, J. Ma, and T. Rhodes
U.S. Naval Research Laboratory, Washington, DC

Electronics, Networking, and Systems/C4I (ENS)

Simulations of Passively Mode-locked and Frequency Modulated Interband Cascade Laser Frequency Combs 132
M. Povolotskyi,[1] I. Vurgaftman,[2] and J.R. Meyer[2]
[1]Jacobs, Hanover MD
[2]U.S. Naval Research Laboratory, Washington, DC

Signal Image Processing (SIP)

Retrieving Surface Soil Moisture from CyGNSS Reflectivity Measurements.....136
J.D. Ouellette, E.M. Twarog, L. Li, and S.M. Grossman
U.S. Naval Research Laboratory, Washington, DC

Application of Physics-based Machine Learning to Navy Problems 138
L.N. Smith
U.S. Naval Research Laboratory, Washington, DC

Task Force Lima 140
L.N. Smith
U.S. Naval Research Laboratory, Washington, DC

Space and Astrophysical Science (SAS)

Searches for Millisecond Pulsars and Pulsar Emission Modeling.....144
P.S. Ray[1] and J. Deneva[2]
[1]U.S. Naval Research Laboratory, Washington, DC
[2]George Mason University, Fairfax, VA, resident at U.S. Naval Research Laboratory, Washington, DC

Modeling Propagation of Ionospheric Disturbances Initiated by Magnetospheric Substorms 146
J. Haiducek and J. Helmboldt
U.S. Naval Research Laboratory, Washington, DC

Particle-in-Cell Simulations of Plasma Waves and Turbulence.....148
A.R. Soto-Chavez and J.D. Huba
U.S. Naval Research Laboratory, Washington, DC

Thermosphere & Ionosphere Numerical Models and Ensemble Methods.....150
D.P. Drob, M. Jones, and J. Emmert
U.S. Naval Research Laboratory, Washington, DC

Navy Ionosphere Model for Operations 152
M.R. Burleigh,[1] S.E. McDonald,[1] J.L. Tate,[2] E. Morgan,[1] C.A. Metzler,[1] D. Hodyss,[1] R. Schaefer,[3] G. Romeo[3]
[1]U.S. Naval Research Laboratory, Washington, DC
[2]Computational Physics, Inc., Springfield, VA
[3]Johns Hopkins University Applied Physics Laboratory, Laurel, MD

Environmental Quality Modeling and Simulation (EQM)

Data-Driven Prediction of Global Seabed Environmental Properties.....156
B.J. Phrampus and T.R. Lee
U.S. Naval Research Laboratory, Stennis Space Center, MS

Data and Decision Analytics (DDA)

The Impact of Foam and Aerosol Dynamics on Fire, Explosion Safety, and Suppression (Mechanisms of Water Mist Suppression of a Burning Solid Surface) 160
J.A. Cramer and R. Ananth
U.S. Naval Research Laboratory, Washington, DC

Other (OTH)

Modeling Low-Temperature Plasmas for Atomic Precision Processing 164
M. Meyer[1] and S.G. Walton[2]
[1]National Research Council Postdoctoral Research Associate at the U.S. Naval Research Laboratory, Washington, DC
[2]U.S. Naval Research Laboratory, Washington, DC

Simulation of High Energy-Radiation Environments 166
J. Finke and W. Duvall
U.S. Naval Research Laboratory, Washington, DC

Author Index 169

Division Index.....172

Site Index 175

THIS PAGE INTENTIONALLY LEFT BLANK

CSM

Computational Structural Mechanics

CSM covers the high-resolution multidimensional modeling of materials and structures subjected to a broad range of loading conditions including quasistatic, dynamic, electromagnetic, shock, penetration, and blast. It also includes the highly interdisciplinary research area of materials design, where multiscale modeling from atomistic scale to macroscale is essential. CSM encompasses a wide range of engineering problems in solid mechanics, such as material or structural response to time- and history-dependent loading, large deformations, fracture propagation, shock wave propagation, isotropic and anisotropic plasticity, frequency response, and nonlinear and heterogeneous material behaviors. High-performance computing for CSM addresses the accurate numerical solution of conservation equations, equations of motion, equations of state, and constitutive relationships to model simple or complex geometries and material properties, subject to external boundary conditions and loads. CSM is used for basic studies in continuum mechanics, stress analysis for engineering design studies, predicting structural and material response to impulsive loads, and modeling response of heterogeneous embedded sensors/devices. DoD application areas include conventional underwater explosion and ship response, structural acoustics, coupled field problems, space debris, propulsion systems, structural analysis, total weapon simulation, weapon systems' lethality and survivability (e.g., aircraft, ships, submarines, and tanks), theater missile defense lethality analyses, optimization techniques, and real-time, large-scale soldier- and hardware-in-the-loop ground vehicle dynamic simulation.

Title: Geometric, Constitutive and Loading Complexities in Structural Materials
Author(s): S.A. Wimmer,[1] N. Wade,[2] and A. Arcari[1]
Affiliation(s): [1]U.S. Naval Research Laboratory, Washington, DC; [2]American Society for Engineering Education Postdoctoral Fellow at the U.S. Naval Research Laboratory, Washington, DC
CTA: CSM

Computer Resources: HPE SGI 8600, HPE Cray EX [NAVY, MS]

Research Objectives: The research strives to develop rational bases and mathematical descriptions of complex material responses for structural and novel evolving materials. Structural integrity and life cycle evaluations require an understanding of material responses. Analytical models and techniques cannot describe complex materials and often do not account for interactions, complex geometries, or multiphysics loading. Finite element methods are used to develop models involving multifunctional materials, novel evolving materials, and multiphysics. In order to accurately model the nonlinear response of conventional structural materials, rate dependence, large deformation, and damage accumulation mechanisms must be understood and accurately represented. The performance of the overall structure or system is also examined via parameters such as kinematics, geometric complexities, loading path dependencies, and interaction between loading types.

Methodology: The project uses finite-element methods extensively. Nonlinear material constitutive response features are highlighted in much of the work. Implicit and explicit solution methods are used as appropriate. The primary finite element codes used are MOOSE and ABAQUS. Coupled material responses, such as electric-thermal or electrical-mechanical-thermal, are exercised for evaluation of these effects. Model development is done with CUBIT, ABAQUS/CAE, or in-house software. Large run times and large model sizes are often required for the multistep nonlinear finite element analysis jobs. We also have expanded into alternative methods for solving these problems to include neural network development using TENSORFLOW.

Results: This project involves work in several topics. Illustrative results for physics-informed neural networks (PINNs) for stochastic applications are shown. One significant finding is that because PINNs traditionally are designed for deterministic problems, they struggle to capture the entire range of a stochastic solution field. This limitation arises from the network's tendency to overfit regions of the domain that are more common or similar. The main challenge in solving stochastic problems is accurately capturing the outliers within the solution field. To overcome this, a weighted residual-based training approach was used that reduced test data errors from 10%–15% to 2%–3% (see Fig. 1). This improvement makes PINN training more generalizable, allowing the network to learn the underlying physics governing the problem, rather than merely mapping deterministic solution fields. Figure 2 illustrates these results, showing a variety of inputs from a highly variable stochastic field and their corresponding PINN network outputs.

DoD Impact/Significance: This project provides several key benefits to the DoD. First, PINNs offer a powerful tool for addressing advanced numerical problems, with the potential to reduce the computational cost of their evaluation significantly. Second, the expertise gained in training these machine learning models can be applied across a range of artificial intelligence/machine learning (AI/ML) applications, bolstering the DoD’s capacity to develop, train, and leverage similar models in the future. Additionally, this work enhances our understanding of the relationships between AI/ML approaches and classical methods like finite element analysis, contributing to more informed decision-making in computational problem-solving strategies.

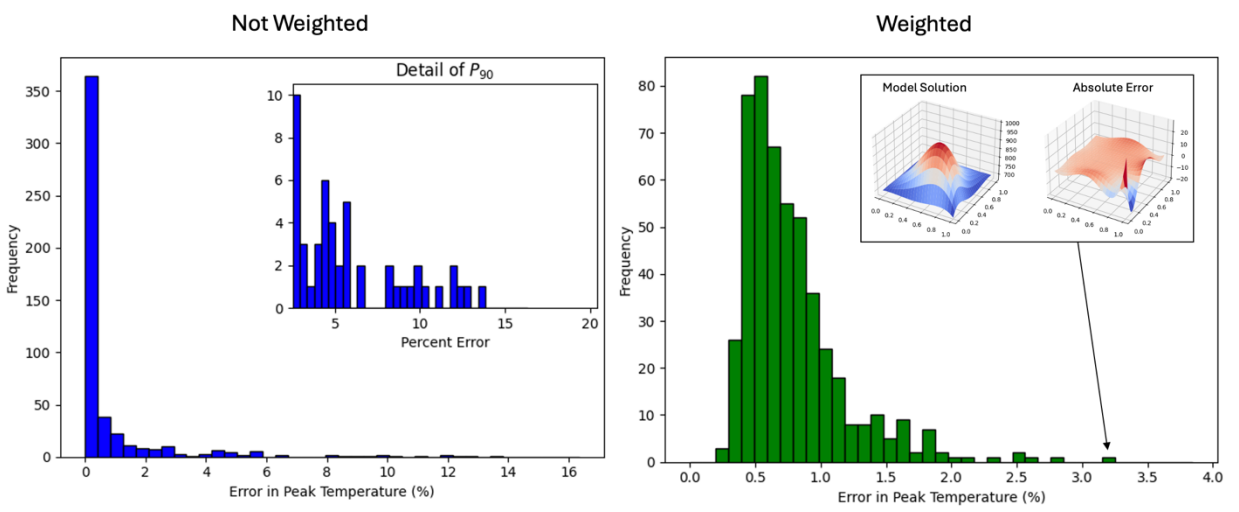

Figure 1. Histograms of the error between the finite-element solution and PINN network output with and without weighted training. The weighted training had a greatly reduced mean (0.98%) and maximum (3.2%) error.

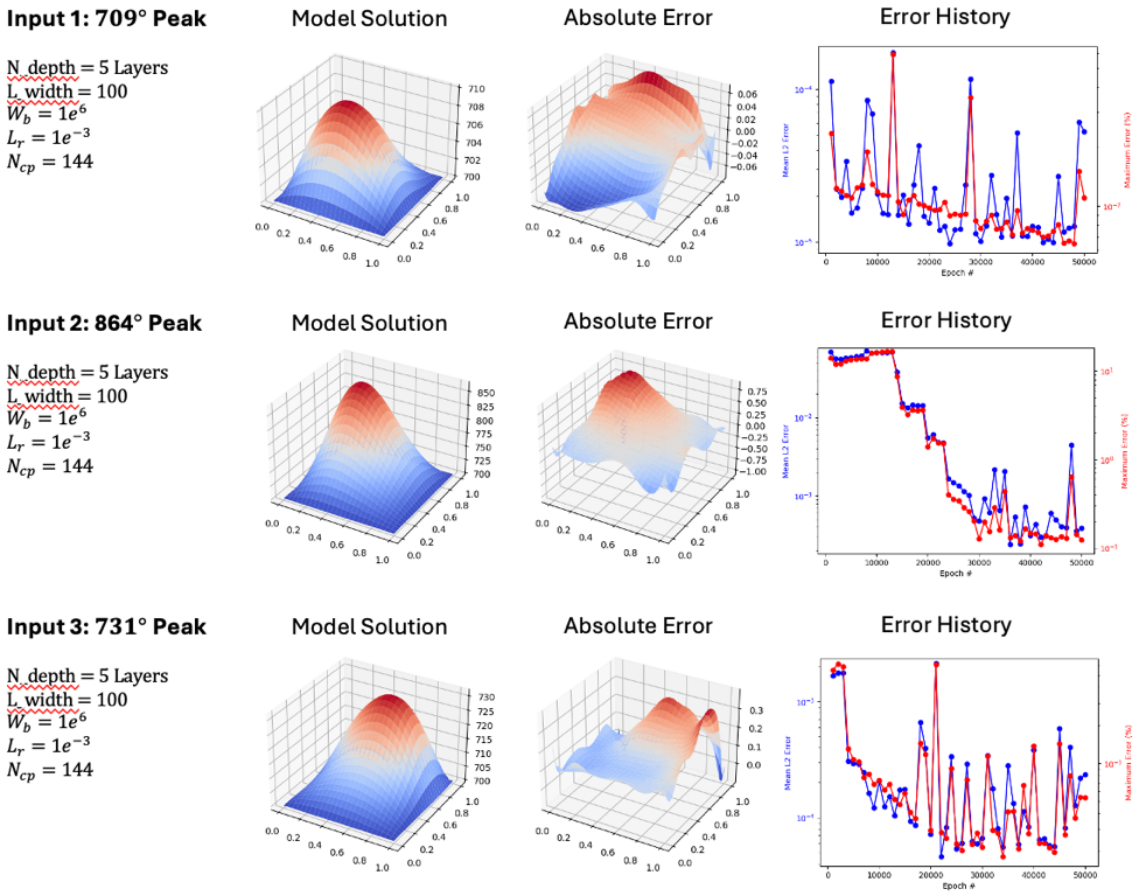

Figure 2. Solution fields and error histories for various inputs trained using the PINN network. The diversity in peak temperatures and their locations demonstrates the network's ability to capture a range of stochastic solution fields beyond a single deterministic outcome. In all cases, the absolute error remains less than 1°C, well within the acceptable tolerance, highlighting the model's accuracy and robustness.

Title: Stochastic Methods for Uncertainty Quantification in Computational Mechanics
Author(s): K. Teferra,[1] N. Wade,[2] and A. Chadwick[1]
Affiliation(s): [1]U.S. Naval Research Laboratory, Washington, DC; [2]American Society for Engineering Education Postdoctoral Fellow at the U.S. Naval Research Laboratory, Washington, DC
CTA: CSM

Computer Resources: HPE SGI 8600 [AFRL, OH], [NAVY, MS]; HPE Cray EX 4000 [ERDC, MS], HPE Cray EX [NAVY, MS]

Research Objectives: The research objective for the work in FY24 that is highlighted in this report is effort to establish reduced order and surrogate models of crystal plasticity finite element simulations of residual stress in additively manufactured (AM) metals. These modeling techniques serve the purpose of increasing the affordability of constructing a database of material mechanical information from which fast-running, data-driven models can be developed. The intent is to establish a database of processing conditions, microstructural features, and material properties for a range of scenarios. Thus, the challenges are, firstly, to be able to develop this database efficiently over high-dimensional input data, and secondly, to develop surrogate models that establish mappings between input and output spaces. If successful, this surrogate model is capable of providing high-throughput prediction of process-structure-property relationships for a large range of parameter values that otherwise would be too costly to interrogate.

Methodology: The aim of this project is to develop methodologies within the hyperreduced order modeling (HROM) concept and with the physics-informed neural network surrogate modeling concept. The HROM algorithm is "numerically intrusive," meaning that it is coupled with a numerical-solution methodology for solving partial differential equations in a way that it cannot be treated as a wrapper around existing code. Thus, a crystal plasticity finite element model must be developed in order to have complete access to the code. The HROM will identify a low-dimensional basis representing the solution field as a function of input parameter, allowing for Monte Carlo-type simulation to be conducted through interpolation of base functions over the parameter space. Further, techniques for efficiently optimizing neural networks to reconstruct solution fields computed from HROMs are being researched and implemented.

Results: During FY24 a crystal plasticity finite-element model has been hand-coded in order to have access to all aspects of the numerical solution routines. This code has been implemented on DoD HPC machines, using the PETSc library for parallel solution methodologies for nonlinear equations, and has been benchmarked against existing crystal plasticity finite element models in built-in Multiphysics Object Oriented Simulation Environment (MOOSE) code. Additionally, the HROM algorithm and the Energy Conserving Sampling and Weighting algorithm have been implemented and benchmarked on nonlinear Euler-Bernoulli beams. The figures illustrate the results of this effort.

DoD Impact/Significance: The enhanced structural material performance in terms of durability, strength-to-weight ratio, and manufacturability are essential ingredients toward transforming fleet capabilities. Understanding the nuances of processing parameters is increasingly more important as additive manufacturing becomes a more commonplace manufacturing technique not only for military applications, but also for civilian applications. Understanding the influence of additive manufacturing processing parameters on resulting parts is integral to providing guidance to material designers to achieve manufacturing of materials with not only desired properties, but also maximally optimized properties. The development of high-throughput modeling techniques lowers the cost of exploring the materials design space.

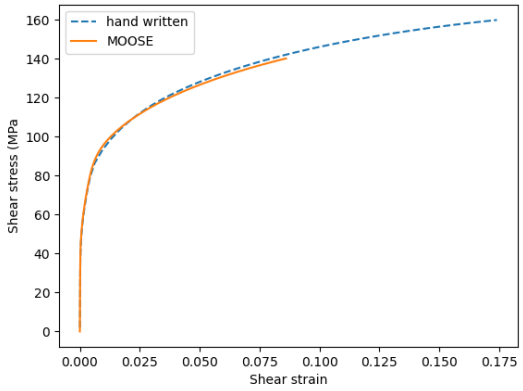

Figure 1. Stress-strain curves for a single-element patch test comparing the handwritten crystal plasticity finite-element model with that in the MOOSE software. The good match provides verification of the handwritten code, as MOOSE is heavily benchmarked software.

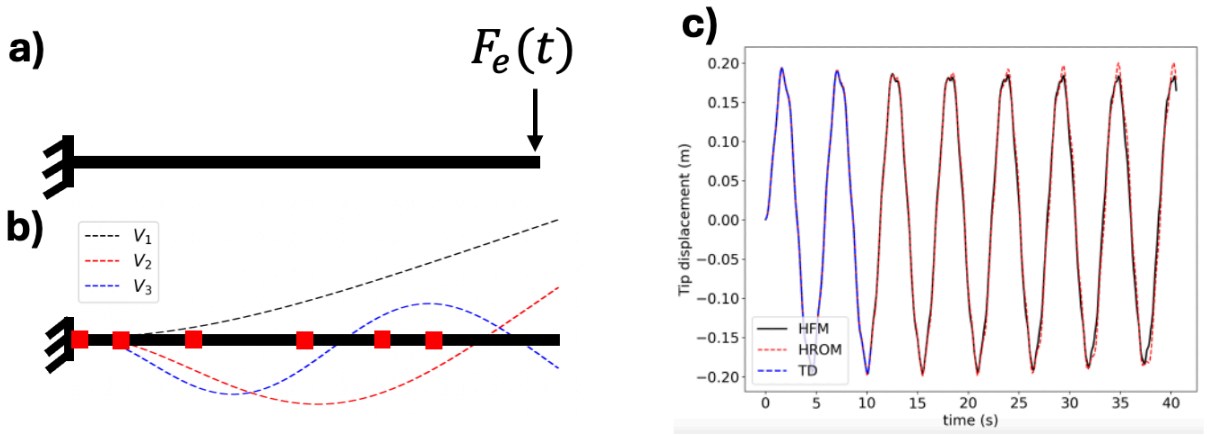

Figure 2. Benchmarking of the HROM algorithm: a) an Euler-Bernoulli beam with a nonlinear material constitutive law is loaded at the end with an impact force, b) the three retained mode shapes (dashed lines), and the six retained interpolation points for internal force vector reconstruction (red dots), c) the tip displacement history showing the full order model and the HROM. The blue section of the time history is the only part of the history that the HROM is trained on. The red part of the time history curve shows the HROM solution for time duration beyond that for which it was trained. Although the HROM is a low-order representation of the solution field, it retains extrapolation capability because it still solves the governing equations, in contrast to neural network surrogates.

Title: Atomistic Simulations of Structural Materials
Author(s): E. Antillon
Affiliation(s): U.S. Naval Research Laboratory, Washington, DC
CTA: CSM

Computer Resources: HPE SGI 8600, Penguin Open Compute Platform (OCP) [AFRL, OH]; Cray XC40/50 [ERDC, MS]

Research Objectives: The objective is to understand atomistic processes that are responsible for mechanical strength and phase stability in structural materials, specifically steel alloys.

Methodology: We utilize atomistic simulations, combining first-principles calculations and classical interatomic potentials, to evaluate material properties of a promising manganese-rich austenitic steel. The remarkable strengthening behavior is thought to result from the interaction between nanoprecipitates and dislocation movement within the lattice. In this study, we compute dislocation-precipitate interactions using an effective interatomic potential developed by Farkas et al. [1] via molecular dynamics, focusing on the influence of precipitate size on material strength. The stability energetics of various coherent precipitate structures are calculated, minimizing strain energy through density functional theory (DFT). This data then is integrated into discrete dislocation dynamics (DDD) simulations and, together with microstructural information from atom-probe tomography (APT), is used to predict theoretical yield strength across different stages of precipitation, varying with precipitate composition and volume fraction.

Results: We study how thermal aging plays a role in the various contributions affecting dislocation mobility. As the steel is exposed to prolonged annealing, it develops a distribution of nanoscale precipitates that provide an additional resistance to dislocation motion and lead to impressive strengthening surpassing ferritic naval steels. Initially, hardness measurements of the solution-treated material are compared with yield-strength predictions from an analytical model by Varvenne et al. [2], which uses inputs from atomic misfit volumes to predict lattice friction within the matrix. As precipitation progresses, we analyze the impact of precipitate strengthening through analytical models that describe the mechanisms of either shearing the precipitate or overcoming the precipitate via a dislocation-bowing mechanism. Figure 1(a) illustrates a crossover point for a precipitate radius of approximately 2.5 nm, though this value is highly dependent on the anti-phase boundary (APB) energy, i.e., the energy required to shear the precipitate by one Burgers vector. Figure 1(b) presents predicted yield stresses from a multiscale model incorporating coarse-grained discrete dislocation dynamics across various APB energy values in comparison to experimental microhardness measurements. The findings reveal that during early aging, the precipitates transition from coherent, lower-APB energy structures to more stable, incoherent precipitates with higher APB energy, indicating significant changes in precipitate characteristics between the 3-hour and 10-hour aged samples.

DoD Impact/Significance: Understanding the impact of processing conditions on local microstructure and how the microstructure, in turn, influences material properties is essential for designing advanced alloys tailored to withstand extreme conditions. Ordering or phase segregation at the atomic level can introduce substantial variations in material strength and stability. Therefore, it is important to assess how current strengthening predictive models can deviate under such circumstances in order to improve material performance.

References

[1] Farkas, D., and Caro, A., (2020), "Model interatomic potentials for Fe–Ni–Cr–Co–Al high-entropy alloys," *Journal of Materials Research*, **35**, 3031-3040. DOI: 10.1557/jmr.2020.294
[2] Varvenne, C., Luque, A., and Curtin, W. A., Theory of strengthening in fcc high entropy alloys, Acta Materialia, Volume 118, 2016, Pages 164-176, ISSN 1359-6454, https://doi.org/10.1016/j.actamat.2016.07.040

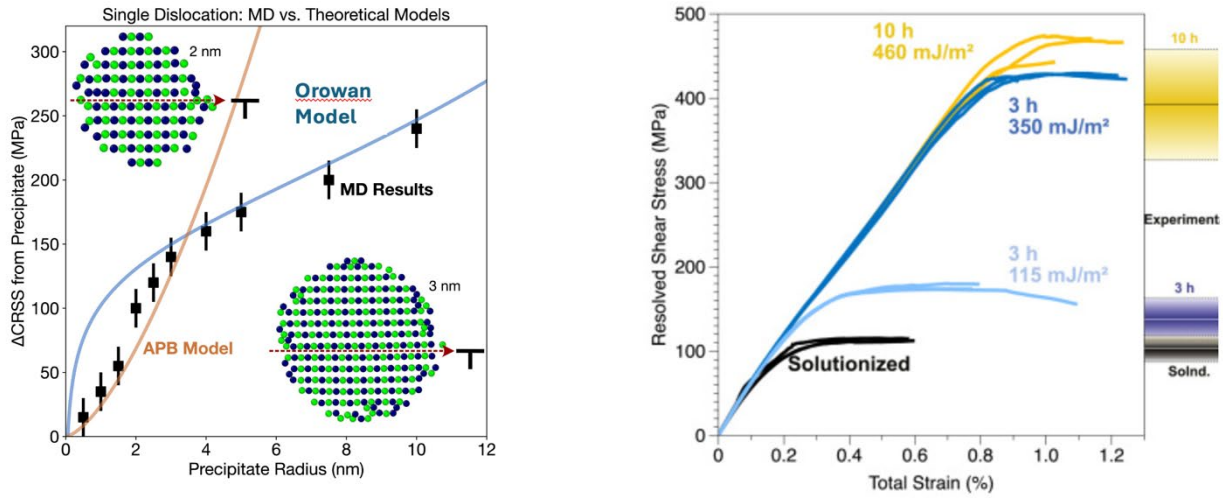

(a) (b)

Figure 1. (a) MD results (symbols) as a function of precipitate size and corresponding predictions (lines) using Orowan-type mechanism and APB shearing. (b) Multiscale prediction vs. strain for various APB energies (lines) compared to measured prediction from mechanical hardness (bands).

Title: Computational Analysis of Warfighter Brain Injury and Protective Equipment
Author(s): X.G. Tan and A.E. Moser
Affiliation(s): U.S. Naval Research Laboratory, Washington, DC
CTA: CSM

Computer Resources: HPE SGI 8600 [AFRL, OH], [NAVY, MS]; HPE Cray EX [NAVY, MS]

Research Objectives: The research objective of this project is the development of methods to prevent and mitigate injury to warfighters. This involves computational analysis of ballistic/blunt impacts on personal protective equipment (PPE) and blast-induced traumatic brain injury (TBI). Computational methods, such as finite-element analysis, are used to conduct the simulation analysis. The use of HPC resources is vitally important to this project due to the high fidelity of the models of interest. A typical model to analyze traumatic brain injury requires approximately 24 hours on 128 CPUs. One of the primary outcomes of this research will be the accumulation of a significant number of simulations that will be used to construct the correspondence relationship between humans and animals and to optimize the design of protective equipment.

Methodology: The project uses finite-element methods extensively, but the work is not restricted to finite-element methodologies. Nonlinear material mechanical constitutive response features are highlighted in much of the work performed. Implicit and explicit solution methods are used as appropriate. The primary finite-element codes used are Abaqus, CoBi, and CTH. User subroutines are used for specialized material constitutive response when applicable. Multiphysics analysis is used to capture the fluid/acoustic-structure interaction and electromagnetically (EM) induced thermomechanical effects. Typically, Abaqus/Viewer, ParaView, VisIt, IDL, and Matlab are used for visualization of results in formats such as VTU and HDF5, including animation. For model development, the project typically uses CUBIT, ABAQUS/CAE, Simpleware, IDL, and in-house code. Large run times and large model sizes are often required for the multiphysics/multistep nonlinear finite-element/volume analysis jobs.

Results: This project involves work in several topical areas. Work has been performed in the numerical investigation of sound-dampening structure using commercially available materials to attenuate the bone-conducted impulse noise to the inner ears. The high-fidelity modeling approach was used to analyze biomechanical effects of impulse noise from the firing of weapons and explosion incidents. Simulation results highlight differences in sound transmission between bone-conduction and air-conduction pathways. Results show significant sound-pressure transmission through the bone-conduction pathway. The comparative analysis indicates that the protection of temporal bone can be effective in reducing the pressure in the inner ear due to bone-conducted impulse noise. Based on the parametric simulation results, the multilayer sound-absorbing pad structure covering the temporal bone, as shown in Fig. 1, was found to be effective and to provide a practical solution for attenuating impulse noise to the inner ears. This work supports the development of improved hearing protection devices (HPDs) and predicts auditory injury risk in military high-risk environments, specifically including firing ranges and airfields.

DoD Impact/Significance: Insights gained from this project are necessary for the advancement from concept to application. Expected outcomes include a deeper understanding of the mechanisms underlying traumatic brain injury and impulse noise-induced hearing loss relevant to Navy and DoD operations. New insights will be gained through quantifying the effects of anatomical and material property differences on the mechanical response of variables associated with traumatic brain injuries and hearing loss. These findings will protect warfighters' health by contributing to the development of improved protective gear and advancing the understanding of the correlation between mechanical response thresholds and traumatic brain injuries. The development of techniques to model population-wide anatomical variability will provide insight into the importance of the fit of protective gear.

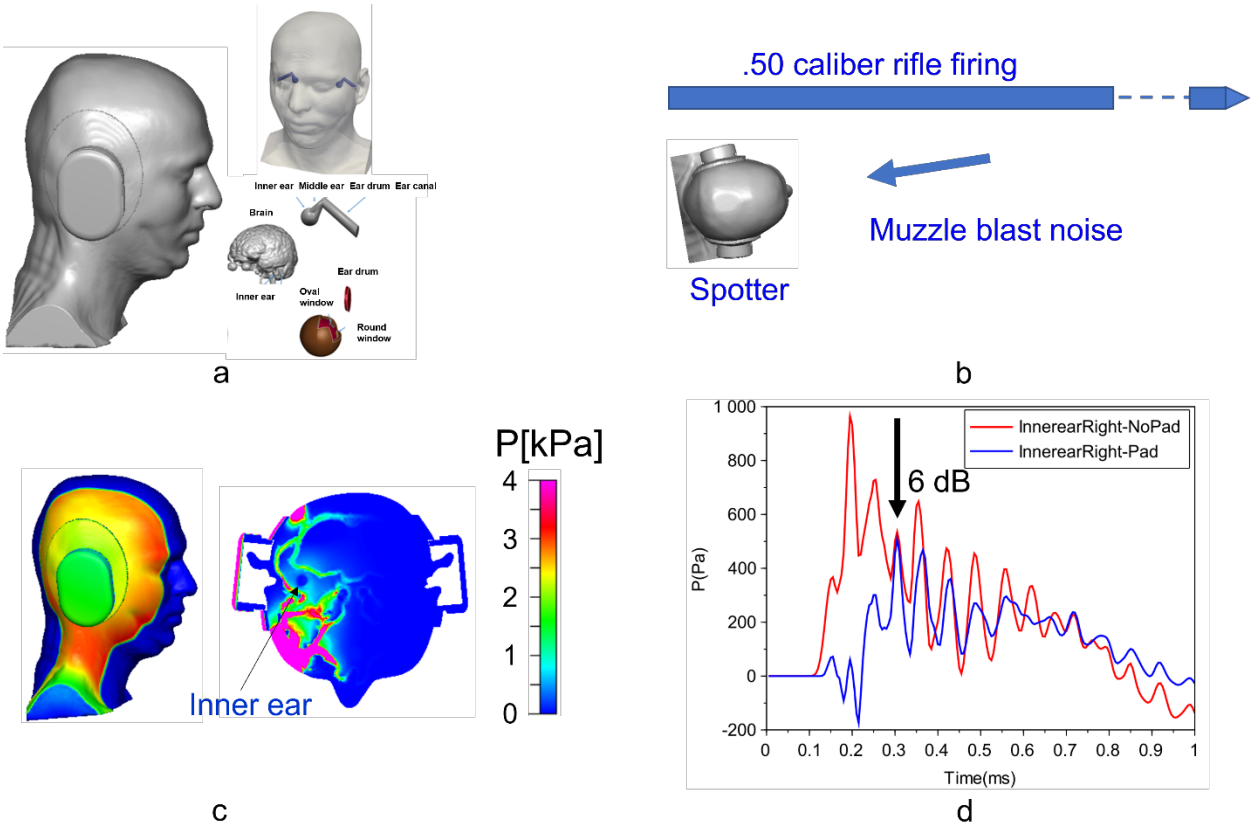

Figure 1. Simulation of impulse noise reduction: a) finite-element (FE) model of head and ear with both earmuff and temporal pad protection, b) loading condition of muzzle blast noise from a .50-caliber rifle firing near the spotter's head, c) snapshot of pressures on the head surface and on the transverse plane for blast noise from the right side, d) peak pressure inside the right inner ear reduced by 6 dB for the head with both earmuff and temporal pad protection, compared to earmuff-only protection.

THIS PAGE INTENTIONALLY LEFT BLANK

CFD

Computational Fluid Dynamics

CFD covers high-performance computations whose goal is the accurate numerical solution of the equations describing fluid motion and the related use of digital computers in fluid dynamics research. CFD is used for basic studies of fluid dynamics for engineering design of complex flow configurations and for predicting the interactions of chemistry with fluid flow for combustion and propulsion. It is also used to interpret and analyze experimental data and to extrapolate into regimes that are inaccessible or too costly to study. Work in the CFD CTA encompasses all Reynolds number flow regimes and scales of interest to the DoD. Incompressible flows are generally slow (e.g., governing the dynamics of submarines, slow airplanes, pipe flows, and air circulation) while compressible flows are important at higher speeds (e.g., controlling the behavior of transonic and supersonic planes, missiles, and projectiles). Fluid dynamics itself involves some very complex physics, such as boundary layer flows, transition to turbulence, and turbulence dynamics, that require continued scientific research. CFD also must incorporate complex additional physics to deal with many real-world problems. These effects include additional force fields, coupling to surface atomic physics and microphysics, changes of phase, changes of chemical composition, and interactions among multiple phases in heterogeneous flows. Examples of these physical complexities include direct simulation Monte Carlo and plasma simulation for atmospheric reentry, microelectromechanical systems (MEMS), materials processing, and magnetohydrodynamics (MHD) for advanced power systems and weapons effects. CFD has no restrictions on the geometry and includes motion and deformation of solid boundaries defining the flow.

Title: Airbreathing Combustion for Hypersonics
Author(s): G.B. Goodwin[1] and R. DeBoskey[2]
Affiliation(s): [1]U.S. Naval Research Laboratory, Washington, DC; [2]Commonwealth Technology Innovation LLC, Alexandria, VA
CTA: CFD

Computer Resources: HPE Cray EX [NAVY, MS]

Research Objectives: The objective of this research is to build a reduced-order solid-fuel ramjet (SFRJ) modeling capability and to evaluate its accuracy and utility as compared to the results obtained with higher-fidelity methods.

Methodology: Solid-fuel ramjets are a promising technology for enabling air-breathing supersonic flight with reduced cost and complexity as compared to liquid-fueled systems. The methodology for this research is to use reduced-order computational fluid dynamics (CFD) to simulate the high-speed reactive flow in the combustor of an SFRJ. The purpose is to gauge the ability of the reduced-order methods to reproduce the temperature field, the fuel regression rate, the flame structure, and other important data as compared to that obtained with higher-fidelity methods. Simulation of combustion in an SFRJ of realistic scale can take weeks for a single flow residence time using higher-fidelity methods, such as large-eddy simulation (LES), warranting investigation of the utility of the reduced-order methods in reproducing the physics of interest. In this study, combustion in a bench-test SFRJ combustor was simulated using Reynolds averaged Navier-Stokes (RANS) and LES, representing reduced and high-fidelity modeling methodologies, respectively. Pyrolysis at the fuel grain surface was modeled using a mass inflow boundary condition, in which the rate of gaseous fuel flow into the domain was a function of boundary heat flux, fuel density, and enthalpy of gasification. Gas-phase combustion was modeled using global and skeletal ethylene-air combustion mechanisms.

Results: Figure 1 shows a snapshot of the cavity-stabilized flame using the RANS and LES models with several different combustion mechanisms. All simulations resulted in a cavity-stabilized flame. The RANS simulation using the three-step mechanism showed temperature elevated higher than that observed in the LES case, with a sharper reaction front and flame attachment directly to the cavity leading edge. The RANS case with a six-step mechanism agreed better with the LES results, with lower temperature throughout and a more diffuse reaction front and recirculation zone. Using the skeletal mechanism, the RANS model was able to capture the flame attachment region accurately as compared to the LES case, but again overpredicted the maximum temperature. Further study is required, but these results indicate that RANS can be useful as a first-order approximation tool in SFRJ simulation, but experimental or higher-fidelity CFD data is required for anchoring the RANS model assumptions to ensure satisfactory agreement.

DoD Impact/Significance: The impact of this research is an improved understanding of the ability of RANS simulations to reproduce the results of higher-fidelity LES in simulating combustion in an SFRJ engine. The simulations are run in tandem with accompanying experiments for validation and comparison.

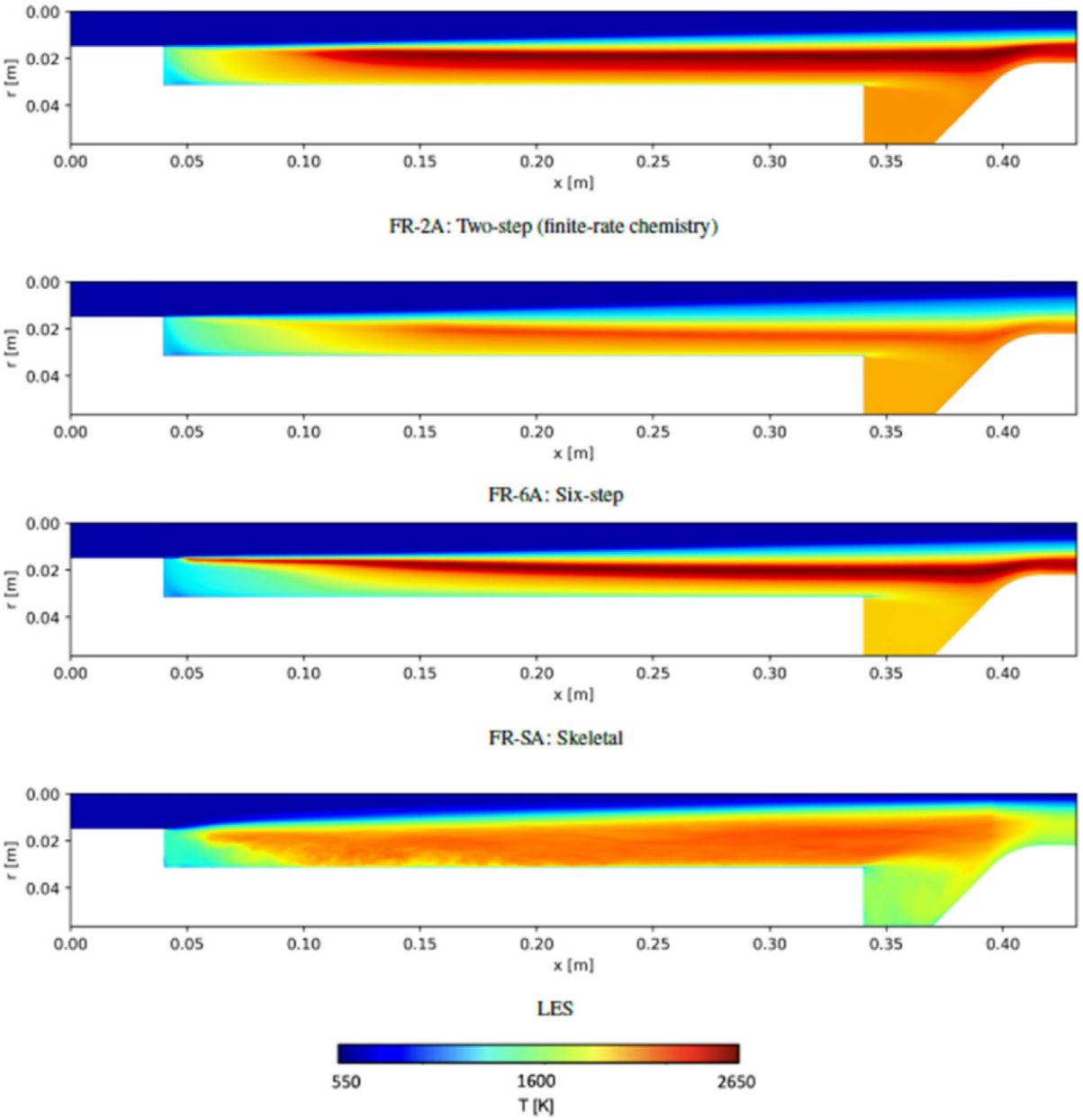

Figure 1. Steady-state temperature field in RANS simulations using two- and six-step global and skeletal ethylene-air combustion mechanisms and an LES using the same skeletal mechanism.

Title: Predicting Fluid-Structure Interaction for Military Applications
Author(s): Y. Khine and D.R. Mott
Affiliation(s): U.S. Naval Research Laboratory, Washington, DC
CTA: CFD

Computer Resources: HPE Cray EX [NAVY, MS]

Research Objectives: Create the computational capability to predict the interaction of fluids with complex structures and apply these capabilities to solve emerging problems critical to DON and the broader defense community. In the current context, simulations were used to assess various design criteria for helmets including blunt, ballistic, and blast performance, as well as thermal performance (highlighted below), and new methodologies for combining these performance parameters into a unified design approach were developed and explored.

Methodology: In FY22, transport phenomena around a warfighter in different ambient wind conditions was studied in order to assess the impact of helmet configuration on passive cooling potential through perspiration and to inform the unified design approach cited above. In FY24, additional simulations were performed to study the effects of various wind directions on the warfighter wearing two different helmet configurations. Baseline simulations without a helmet are performed to compare with those with five-pad and seven-pad helmets. CFD++ Software by Metacomp Technologies, Inc. that is available on DoD HPC resources is used to simulate various scenarios of interest. Transport of the saturated air away from the head surface through forced convection enabled the prediction of a maximum cooling effect through evaporation.

Results: Figure 1 shows the temperature distribution of baseline (bare head/no helmet) studies with various wind angles of attack. In Fig. 1(a), the warfighter is exposed to a frontal wind (0 degree) and the temperature variation around the head is more or less in symmetry. In Fig. 1(b), the wind is blown at a 45-degree angle toward the warfighter from the right front corner, and the temperature variation is seen at the left back of the head. In Fig. 1(c), the wind is exposed from the right (90 degree), and the air on the left of the head is affected by the wind. In Fig. 1(d), the wind is blown from the back (180 degree) and the front part of the face is cooled by the wind. Figure 2 displays the temperature distribution at the head and the helmet for five-pad and seven-pad helmet configurations. In Fig. 2(a), with five-pad configuration, there is a larger gap area between the head and the helmet, and this helps the evaporation process compared to the seven-pad configuration in Fig. 2(b).

Table 1 displays the detail thermal loading response for baseline (bare head/no helmet), five-pad, and seven-pad helmet configurations in various wind directions exposed to the warfighter. From Table 1, the thermal loading score, $S_{thermal}$, that is based on the evaporative cooling of a scenario is the best for the frontal wind (0 degree) for both five-pad and seven-pad helmet configurations. Of the two helmet configurations considered here, the five-pad configuration performs better than the seven-pad configuration.

DoD Impact/Significance: Thermal loading in the field not only undermines concentration and performance of cognitive tasks, it also can result in heat-related injury. A design approach that accurately emphasizes the relative importance of a variety of design factors and threats, and that can be weighted differently for different scenarios, can produce optimal configuration options for targeted theaters and operations.

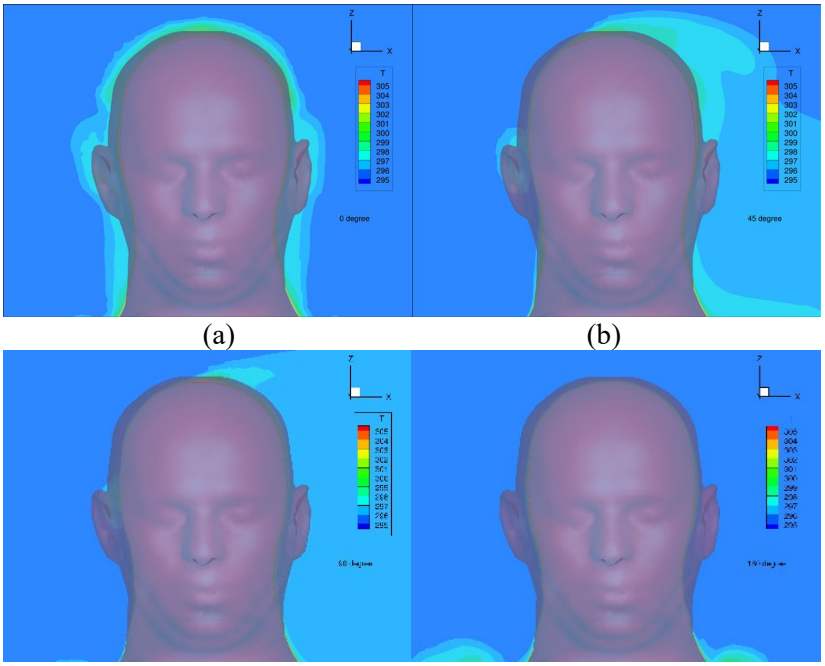

Figure 1. Temperature distribution for baseline (bare head/no helmet). (a) frontal wind (0 degree), (b) wind from right front corner (45 degree), (c) side wind from right (90 degree), and (d) wind from back (180 degree).

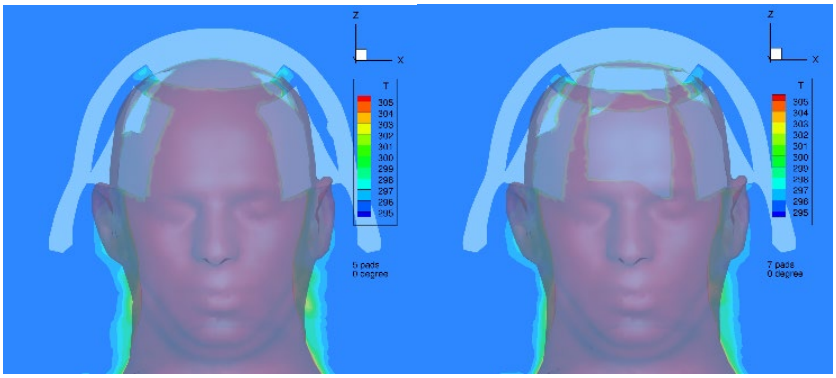

Figure 2. Temperature distribution at midplane of head for five-pad and seven-pad configurations with frontal wind (0 degree).

	Baseline (no helmet)	Five pads		Seven pads	
Air flow direction (deg)	Heat dissipation rate, q (W)	Heat dissipation rate, q (W)	Thermal loading score, $S_{thermal}$ (%)	Heat dissipation rate, q (W)	Thermal loading score, $S_{thermal}$ (%)
0	51.70	51.45	99.50	46.84	90.60
45	55.66	53.48	96.09	48.64	87.39
90	53.24	45.74	85.91	42.83	80.45
135	56.87	44.53	78.30	42.83	75.32
180	57.74	47.53	82.15	44.98	77.91

Table 1. Helmet system thermal loading response

Title: Numerical Investigation of Advanced Military Aircraft Noise Reduction Concepts
Author(s): J. Liu
Affiliation(s): U.S. Naval Research Laboratory, Washington, DC
CTA: CFD

Computer Resources: HPE Cray EX [NAVY, MS]; HPE Cray EX 4000, Cray XC40/50, [ERDC, MS]; Penguin Open Compute Platform (OCP), HPE Cray EX [AFRL, OH]

Research Objectives: Use HPC computational resources to predict details of turbulent flow structures and noise generation in supersonic exhaust jets from representative military aircraft jet engine nozzles and use this information to investigate and assess promising jet noise reduction concepts in support of the ongoing jet noise reduction programs.

Methodology: The flow solver is an extended development version of the JENRE® multiphysics framework. The JENRE® multiphysics framework can take structured meshes and unstructured meshes with arbitrary cell types and has multiple levels of parallelism: multicore CPUs or multicore GPUs, and MPI for interprocessor communication. The JENRE® multiphysics framework has achieved exceptional computational performance and scalability. Because using large-eddy simulations (LES) to fully resolve wall-bounded flows at high Reynolds numbers is computationally prohibitive due to the limitations of the available numerical methods and computational resources, the wall-model method is implemented in this extended version to simulate the boundary-layer effect of the wall-bounded flows. The far-field noise prediction is based on the Ffowcs Williams-Hawkings (FW-H) surface integral method. To simulate the high-temperature effect observed in realistic jet engine exhausts, a temperature-dependent specific heat ratio is used.

Results: LES has become an important tool in developing and optimizing the jet noise-reduction technologies. The noise-reduction methods of using lower jet Mach numbers and inverted velocity profiles have been assessed numerically in the mode-scale supersonic jet exhaust nozzles last year. This year, we have conducted the assessment in full-scale supersonic jet engine nozzles. Both LES assessments show that using a jet Mach number barely above 1 can reduce the shock-associated noise up to 5 dB to 6 dB and can reduce the mixing noise about 1.5 dB. Using an inverted velocity profile can reduce the mixing noise further by 2 dB. Furthermore, if a lower jet velocity can be used, for example, a velocity decrease by 9% to 10%, an additional noise reduction of 2.5 dB to 3.0 dB can be obtained. LES predictions show that the combination of the three noise-reduction methods, a lower jet Mach number, an inverted velocity profile, and a lower jet velocity, can achieve a noise reduction up to 6 dB in both upstream and downstream directions. Figure 1 shows the instantaneous pressure distribution in the jet plume and the near field without the noise-reduction treatment. Figure 2 shows the instantaneous pressure distribution with the noise reduction treatment. The acoustic pressure waves are clearly weaker in Fig. 2 than those in Fig. 1. This work involves many large-eddy simulations of supersonic jets at multiple jet operating conditions. Each test often involves several iterations to match the required thrust and mass flow. The author is thankful for the HPCMP resources because they are critical to the success of these jet noise reduction assessments.

DoD Impact/Significance: There is a growing need to reduce the noise generated by high-performance, supersonic military aircraft significantly. The noise generated during takeoffs and landings on aircraft carriers has direct impact on shipboard health and safety issues. It is estimated that the U.S. Veterans Administration pays $5.0 billion or more for hearing-disability claims each year. The results of our work will provide better understanding of the noise production for both industrial and military aircraft and will aid the current effort of noise reduction, especially for supersonic aircraft.

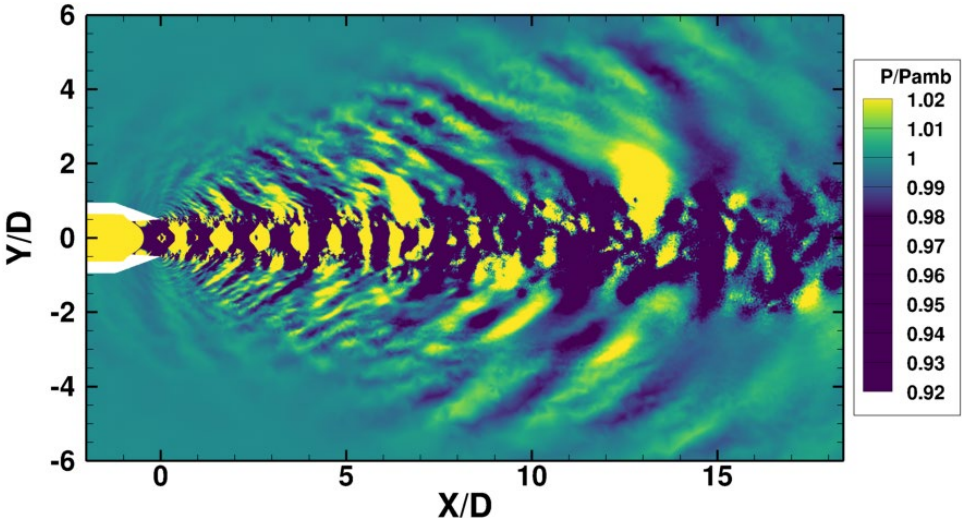

Figure 1. Instantaneous pressure distribution near the nozzle without the jet noise reduction treatment. "D" is a scaling length. P stands for pressure and Pamb stands for ambient pressure.

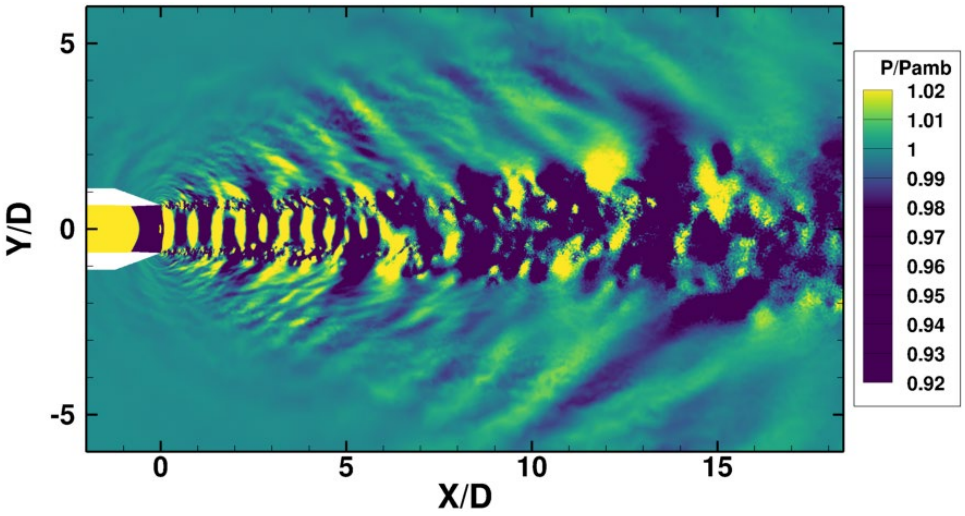

Figure 2. Instantaneous pressure distribution near the nozzle with the jet noise reduction treatment. "D" is a scaling length. P stands for the pressure and Pamb stands for ambient pressure.

Title: High-fidelity Modeling of Gaseous Detonations
Author(s): V.N. Gamezo[1] and A.Y. Poludnenko[2]
Affiliation(s): [1]U.S. Naval Research Laboratory, Washington, DC; [2]University of Connecticut, Storrs, CT
CTA: CFD

Computer Resources: HPE Cray EX 4000, Cray XC40/50 [ERDC, MS]; HPE Cray EX, Penguin TrueHPC [NAVY, MS]; HPE Cray EX, Penguin Open Compute Platform (OCP) [AFRL, OH]

Research Objectives: High-fidelity numerical modeling of detonations in gaseous mixtures and liquid fuel sprays is central for the understanding of these complex reacting flow phenomena and for the design of advanced energy conversion and propulsion systems of direct DoD and Navy relevance. These include novel detonation-based systems, as well as safe storage and handling of fuels both on board and on shore. The focus of this effort is on the development of a systematic and first-principles understanding of detonations to enable robust predictive capability of modern numerical simulations of detonations. Prior studies by the authors showed that modern state-of-the-art thermochemical models are not able to predict the detonation structure in hydrogen/air mixtures at any practically relevant conditions, with errors in the characteristic detonation cell sizes exceeding an order of magnitude for some mixtures. This, in turn, does not allow modern numerical simulations to predict with any degree of accuracy key dynamical characteristics, e.g., the minimum channel size and detonability limits, which are crucial for the design of practical systems. The goal of this work is to perform the first comprehensive suite of high-fidelity detonation simulations for a wide range of fuels, including hydrogen, methane, acetylene, ethylene, and Navy-relevant fuels, such as JP10. Furthermore, in an effort to explore alternative novel detonation engine concepts, we have performed detailed preliminary analysis of the jet-stabilized detonation wave concept in the two-dimensional (2D) geometry using simplified single-step chemical kinetics.

Methodology: In FY24, we performed a large suite of 2D and three-dimensional (3D) high-fidelity numerical simulations of freely propagating detonations in rectangular channels. The focus has been on the five primary fuels: H_2, C_2H_2, C_2H_4, CH_4, and JP10, for a wide range of equivalence ratios, diluent mass fractions, and initial mixture pressures and temperatures, for which experimental data exists that would enable direct comparison with the simulation results. Chosen fuels span virtually the entire thermochemical parameter space of reacting mixtures relevant to the DoD. All simulations were performed using the code Athena-RFX++, a massively parallel, higher-order, structured grid code with the adaptive mesh refinement capability. The physical model was based on the state-of-the-art FFCM1 and HyChem families of reduced chemical kinetics mechanisms developed at Stanford University. Finally, a wide range of additional factors has been explored, including the effect of wall losses and the sensitivity to resolution, the chemical mechanism, steam addition, etc.

Results: The suite of numerical simulations performed represents the largest survey to date of the detonation properties with the state-of-the-art numerical code and physicochemical model. These simulations have demonstrated that modern numerical simulations generally are not able to reproduce detonation structure and dynamics, with the exception of low-pressure or preheated conditions, as well as mixtures with monoatomic diluents (Fig. 1). These results highlight the deficiencies of the existing models, and they form the foundation for the development of the next generation of chemical kinetics mechanism, the work on which is underway in FY25. Finally, we also performed the first systematic exploration of the jet-stabilized detonation waves (JSDW, Fig. 2) and developed a detailed theoretical framework for predicting the range of flow conditions required to achieve stable detonative burning. The work on JSDW is complimentary to the ongoing experimental effort at NRL led by Dr. Christopher Reuter.

DoD Impact/Significance: Numerical models of gaseous detonations obtained in this work represent the state of the art in the field. They constitute a key step toward the development of accurate and predictive physicochemical models for supersonic combustion. Such models will provide critical modeling capability for the development of advanced propulsion systems by the U.S. Navy. Work carried out in this project is tightly connected with the ongoing efforts at the U.S. Naval Research Laboratory under the 6.1 Base Program, and more broadly at the Office of Naval Research under the MURI program and at other DoD agencies, such as AFOSR, aimed at studying detonations.

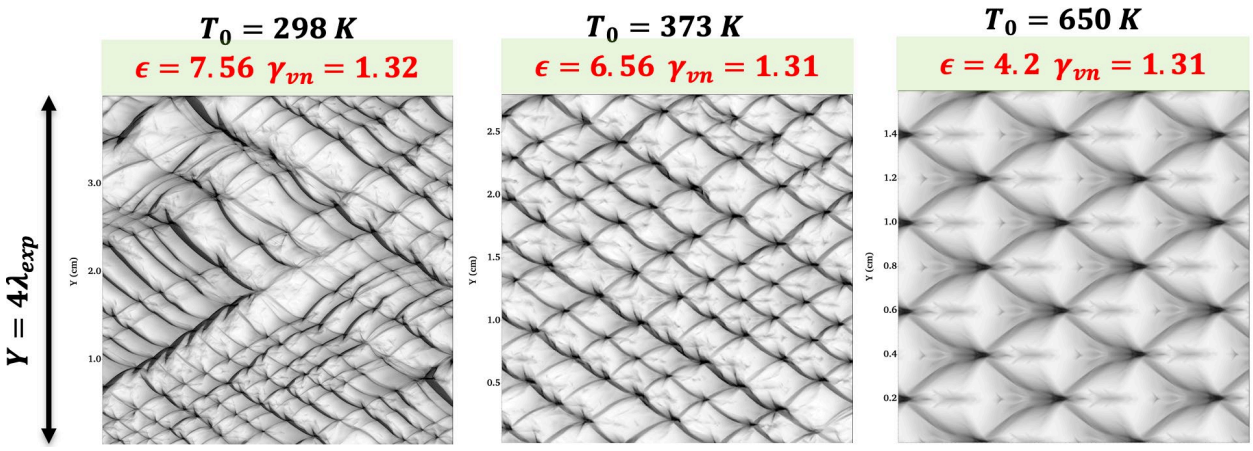

Figure 1. Synthetic soot foils showing cellular structure of a detonation in a stoichiometric H_2/air mixture at 1 atm pressure for a range of temperatures. Detonation propagates from right to left and the channel height is equal to 4 times the experimental cell size. Simulations are performed in a 2D geometry with the code Athena-RFX++ using FFCM1 chemical kinetics mechanism for the H_2 oxidation. Ratio of specific heats (γ_{VN}) and the logarithmic temperature sensitivity (ϵ) of the mixture in the postshock state are given above each panel. These calculations are a sample from a large, comprehensive survey of detonation properties for a wide range of fuels and flow conditions. Note that out of these three cases, only the case with the preheated upstream mixture (T = 650 K) is in agreement with the experiments, while at lower temperatures, existing thermochemical models significantly underpredict the detonation cell size.

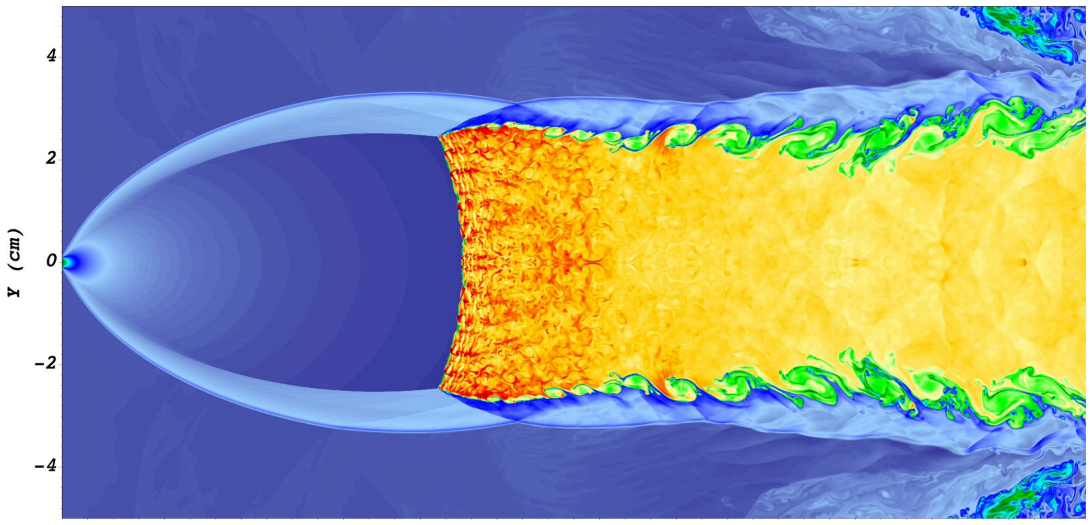

Figure 2. Structure of a jet-stabilized detonation wave (JSDW) in a 2D underexpanded reacting jet. Shown is the distribution of temperature in a high-fidelity simulation performed with the code Athena-RFX++ using simplified single-step Arrhenius reaction kinetics.

Title: Numerical Simulations of Noise Generated by Non-Circular Advanced Military Aircraft Nozzles
Author(s): K. Viswanath
Affiliation(s): U.S. Naval Research Laboratory, Washington, DC
CTA: CFD

Computer Resources: HPE Cray EX [NAVY, MS]; Cray XC40/50 [ERDC, MS]

Research Objectives: Use HPC computational resources to predict details of turbulent flow structures and noise generation in supersonic noncircular asymmetric exhaust jets from representative military aircraft jet engine nozzles. This information will be used to investigate and assess promising jet noise reduction concepts in support of the ongoing testing program.

Methodology: Simulations are performed using the JENRE® multiphysics framework, developed by the U.S. Naval Research Laboratory (NRL) with collaborating institutions. This U.S. Government-owned code provides unsteady compressible flow-solver capabilities that support various numerics, as well as cell-centered finite-volume or nodal finite-element methods, while delivering high throughput on calculations. It was developed with an emphasis on raw performance and the ability to exploit emerging massively parallel, high-performance computing (HPC) architectures. It supports different HPC parallel-programming paradigms for message passing such as MPI, OpenMP, CUDA, HIP, and hybrid models, depending on the HPC cluster architecture. A key bottleneck of HPC throughput is data input-output (IO). The code supports parallel IO via MPI/IO to complement the multiple levels of parallelism further. Taylor-Galerkin finite-element method with second-order spatial accuracy for tetrahedral cells is used with the finite-element flux-corrected transport (FEM-FCT) method. The multidimensional FCT flux limiter provides an implicit subgrid stress model, which ensures monotonicity at shocks and sharp gradients with minimal artificial dissipation. We use an extended version of the code that features a wall model that supports high-speed flows and surface-roughness effects while significantly reducing grid resolution requirements.

Results: Simulations of a supersonic twin jet at overexpanded operating condition and canted inward at 4 degrees was investigated to understand the twin jet interaction and their spectral POD (SPOD) fluid dynamic modes, along with far-field noise behavior, and to compare with experimental results collected at Monash University, Australia. Figure 1 shows the inward-canted twin jet nozzle, each of aspect ratio 2, with separation distance of 2.25D (equivalent diameter D = 0.0076 m). Experimental results had both thin- and thick-lipped nozzles, while the simulations were done with an in-between lip thickness. To accurately calculate the SPOD modes, more than 10,000 snapshots were required for each plane, making this a resource-intensive calculation in processors utilized, output data storage, and throughput. Results are shown for the nozzle pressure ratio of 3.0 and the temperature ratio of 1.0. Figure 2 shows the comparison of mean fields of u and v velocities between LES and PIV thin-lipped case. Shock cell strength and locations, potential core, and center line mixing match very well. However, the LES results are closer to the thick-lipped nozzle PIV results when comparing mean fields. Figure 3 shows the SPOD spectra results comparing LES with schlieren from both thin- and thick-lipped nozzles. LES captures the major mode and its exact frequency and again, the results are closer to the thick-lipped case. For the strongest screech frequencies, experiments had two alternating modes, and the same is seen in our data.

DoD Impact/Significance: The results of our work will provide better understanding of the noise production for both industrial and military aircraft and will aid the current effort of noise reduction, especially for supersonic aircraft, to reduce the impact of the jet noise on shipboard health and safety issues.

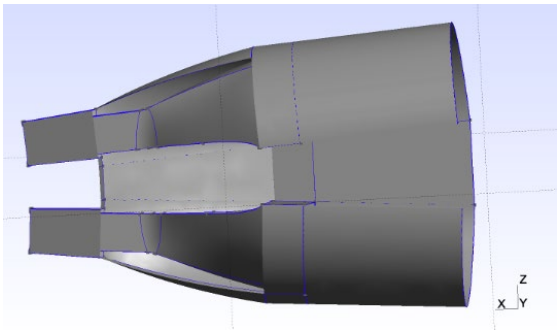

Figure 1. Twin-jet nozzle geometry, aspect ratio 2 nozzles with inward cant angle of 4 degrees and separation distance of 2.25D.

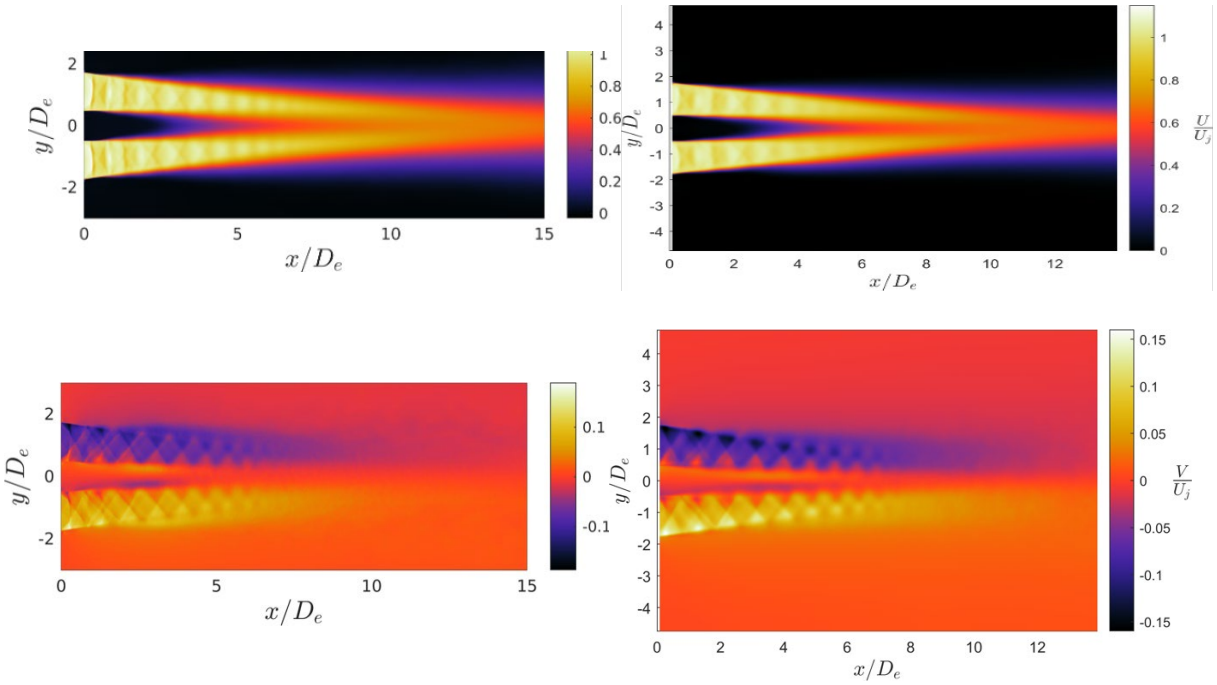

Figure 2. Comparison of mean fields of u and v velocities between LES (left) and PIV (right) thin-lipped case. General agreement is good, with the LES results closer to the thick-lipped nozzle PIV results.

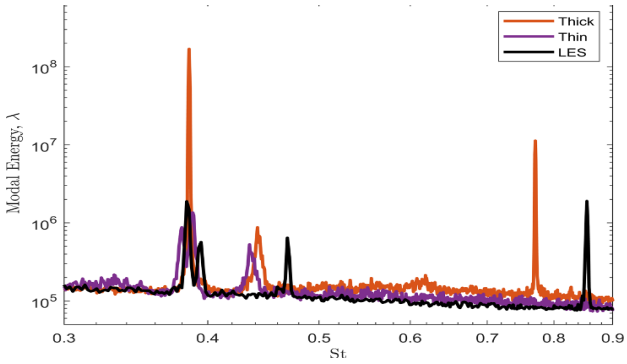

Figure 1. Twin-jet interaction SPOD spectra results comparing LES with schlieren from both thin- and thick-lipped nozzles. LES captures the major mode and harmonics similar to the thick-lip case.

Title: High-Fidelity CFD Simulations of High-Speed Flows in Realistic Atmospheric Conditions
Author(s): D. Kessler, T.K. Patel, R.F. Johnson, A. Hess, and B. Bojko
Affiliation(s): U.S. Naval Research Laboratory, Washington, DC
CTA: CFD

Computer Resources: HPE Cray EX [AFRL, OH], [NAVY, MS]; Penguin TrueHPC [NAVY, MS]

Research Objectives: Determine the impact of chemical kinetics and multidimensional flow effects on the local and average regression rates of solid fuel strands measured in commonly used experimental material characterization facilities.

Methodology: We are using the JENRE® multiphysics framework to perform high-fidelity and high-resolution simulations of the chemically reacting flows associated with high-Mach-number supersonic and hypersonic flight.

Results: The solid-fuel ramjet (SFRJ) is a type of air-breathing propulsion system that could be used to power high-supersonic-flight vehicles and weapon systems that travel at speeds in excess of Mach 3. These systems promise a host of benefits over similar liquid-fueled systems, including high specific impulse and, consequently, increased range. Achieving this goal requires the development of high-performance solid fuels, the combustion of which need to be characterized thoroughly in order to generate a robust engine design. One specific characterization method measures the rate of regression of the solid fuel surface caused by an attached flame in an opposed flow burner. In this configuration, air is accelerated through a nozzle perpendicular to the fuel surface. Upon ignition, a flame spreads across the surface of the pellet, following the air flow as it wraps around the burner. Classical one-dimensional theory suggests a uniform, constant burning rate across the surface. Experimental measurements show a significant deviation from these predictions.

During FY24, our team has performed a series of high-resolution large-eddy simulations (LES) with the goal of accurately describing the multiphase combustion process in the solid-fuel opposed flow burner (OFB). The general configuration is shown in Fig. 1a, in which a subsonic air jet issues from the nozzle and flows from top to bottom, where it impinges on the solid fuel pellet. Validation of the simulated results with experimental shadowgraph, flame thickness, and regression rate indicate that axisymmetric LESs are a suitable tool for exploring the combustion physics in the OFB geometry. Figures 1b–1e display the instantaneous temperature, the azimuthal vorticity, the mass fraction of carbon monoxide, and the mass fraction of carbon dioxide, respectively. The instantaneous flame markers elucidate the unsteady nature of the OFB combustion dynamics in which azimuthal vorticity contours display regular vortex shedding from the nozzle lip, advected downstream toward the fuel grain lip. The temperature and mass fraction contours capture flame roll-up and wrinkling as a consequence of the interactions with the vorticity. Most of the larger flame roll-up occurs downstream of the fuel grain, resulting in smaller perturbations to the flame thickness above the fuel grain surface. This suggests that the main driver of the unsteady combustion and regression dynamics is the vortex shedding from the nozzle lip. Figure 1f shows a comparison between the regression rate prediction of the high-resolution simulations described above and the classical quasi-one-dimensional model compared to experimental measurements. Here, we find a significant improvement in regression prediction using the multidimensional model.

DoD Impact/Significance: Achieving a long-range strike capability and countermeasures for similar technologies under development by our adversaries are critical for protecting our fleet and maintaining naval superiority. This work will provide a better understanding of how solid fuels can be used in high-speed weapon systems to provide a significant increase in range.

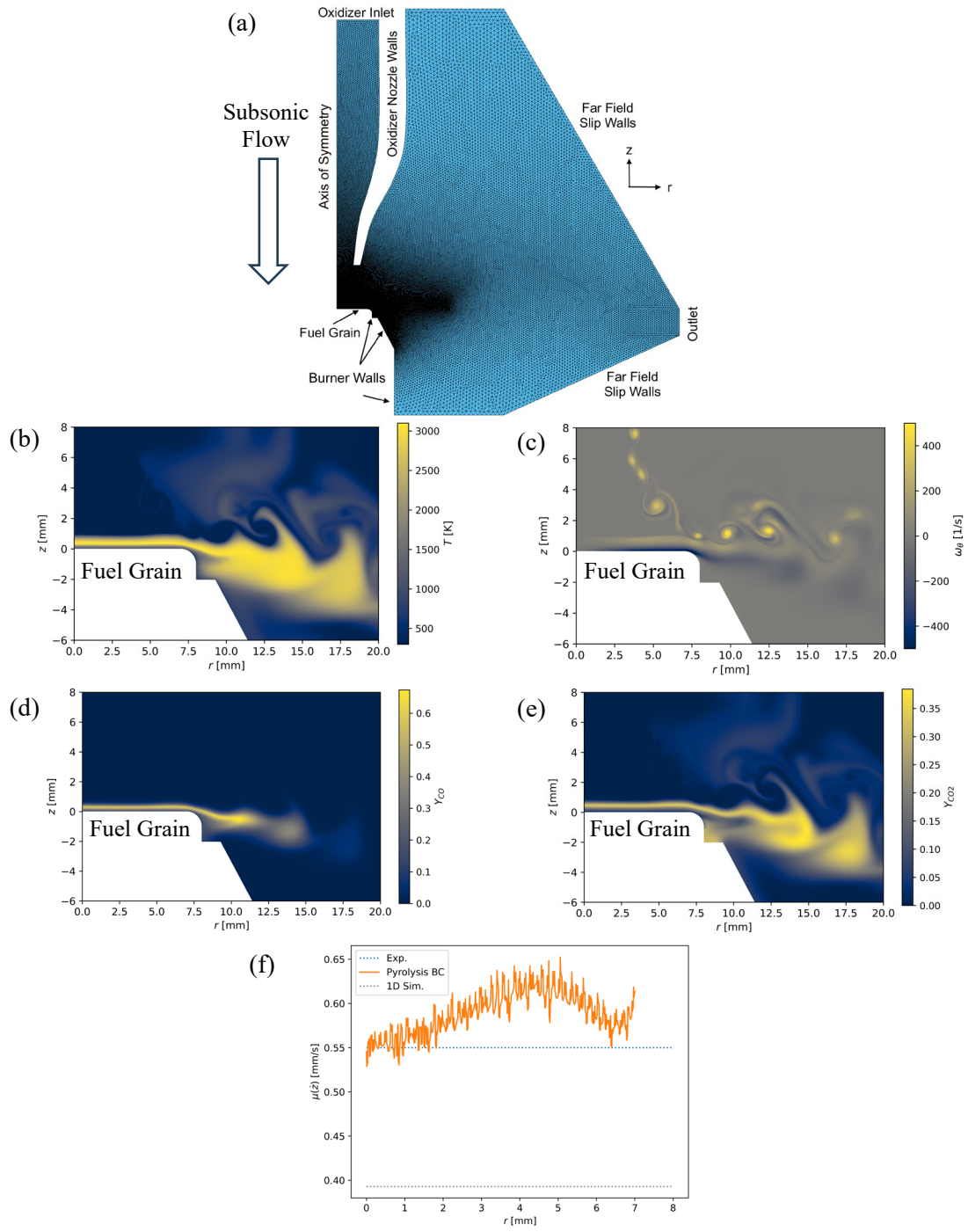

Figure 1. (a) Illustration of OFB geometry and computation mesh. Instantaneous contours of (b) temperature, (c) vorticity, (d) carbon monoxide mass fraction, and (e) carbon dioxide mass extracted from a representative reacting flow calculation. (f) Comparison of fuel regression rates predicted by the simulation (orange line) compared to that predicted by the quasi-1D model and that measured in experiments.

Title: Applications of FEFLO Incompressible Flow Solver
Author(s): R. Ramamurti
Affiliation(s): U.S. Naval Research Laboratory, Washington, DC
CTA: CFD

Computer Resources: HPE Cray EX [AFRL, OH]; Cray XC40/50 [ERDC, MS]; Liqid [ARL, MD]

Research Objectives: Perform three-dimensional (3D) numerical simulations of flow past complex configurations. The proposed studies will investigate the use of bioinspired skins for drag reduction for unmanned underwater vehicles and unsteady flow past acoustic sensor enclosures.

Methodology: A finite-element solver, called FEFLO, for 3D incompressible flows based on unstructured grids is used. The flow solver is combined with adaptive remeshing techniques for transient problems with moving grids and also is integrated with the rigid body motion in a self-consistent manner that allows the simulation of fully coupled fluid-rigid body interaction problems of arbitrary geometric complexity in three dimensions. NRL has developed a coupled fluid-structure interaction solver for simulating flapping-fin propulsion for operations. In addition to baseline simulations past a flat plate with denticles, simulations are performed over an Eppler airfoil placed at various angles of attack in the hydroacoustic flow channel facility.

Results: The baseline configuration used for simulations is a flat plate with denticles in both aligned and staggered configurations. The configuration consists of a flat plate for one half of the span and the plate with denticles for the other half of the span. The inflow velocity is set to 1 m/s. The unsteady velocity and pressure distribution are monitored at several locations downstream of the plate and are provided to the NRL Acoustics Division for further postprocessing. Simulations were performed over this baseline configuration with a 9 in-long plate and the results are shown in Fig. 1. The unsteady surface pressure data and the pressure and velocity at several station points in the wake of the denticles will be postprocessed to measure the acoustic noise that is propagated into the housing. In addition to the baseline simulation, the flow over the Eppler airfoil at 5° and 10° angles of attack were performed to study the self-aligning property of the airfoil. The potential for noise reduction using proper foil shape then can be explored.

DoD Impact/Significance: Simulations have enabled characterization of the unsteady flow behind a circular cylinder and an airfoil. This will provide the next steps toward development of a low-noise acoustic sensor enclosures in complex environments.

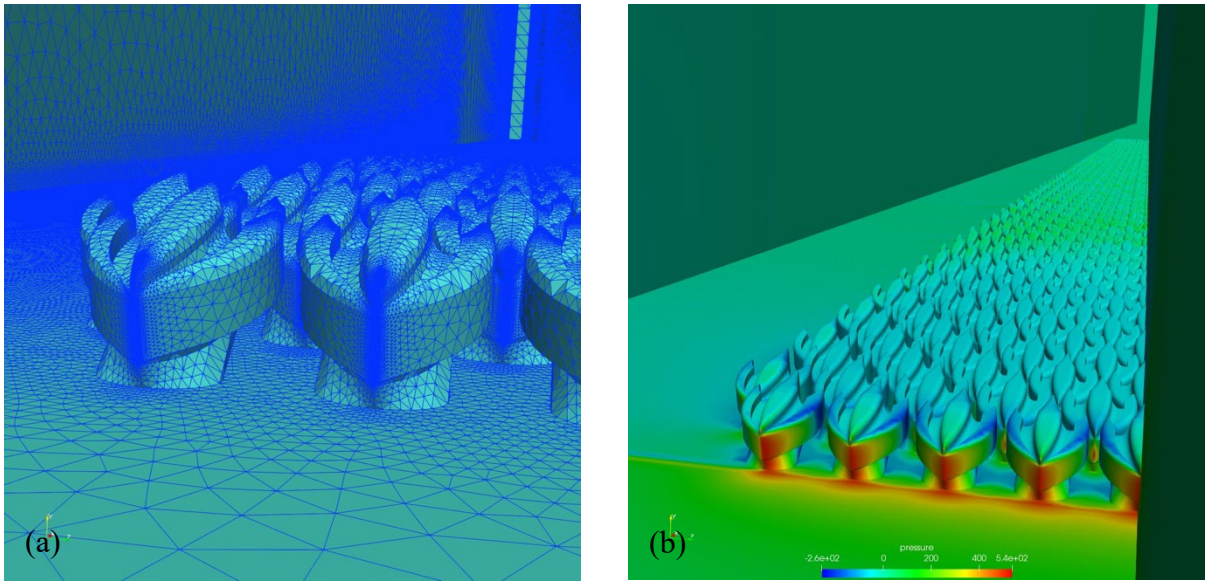

Figure 1. (a) Surface triangulation and (b) pressure distribution for the baseline flat plate with denticles.

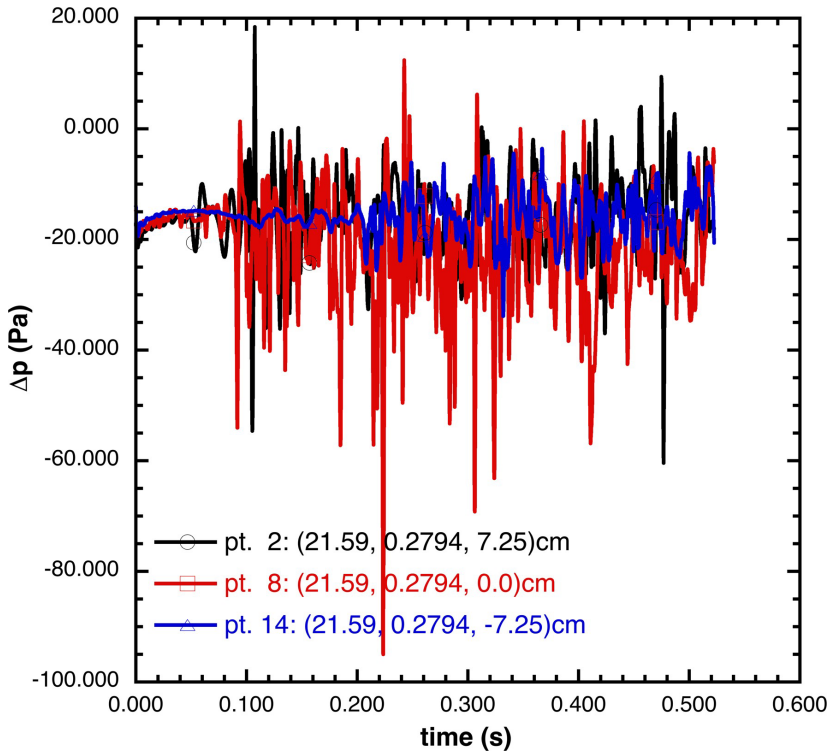

Figure 2. Time history of pressure at selected points downstream of the denticles.

Title: Direct Numerical Simulation of Fluid-Sediment Wave Bottom Boundary Layer
Author(s): J. Simeonov, I. Adams, A. Penko, S. Schoenauer, S. Bateman, K. Edwards, R. Phillip, and J. Veeramony
Affiliation(s): U.S. Naval Research Laboratory, Stennis Space Center, MS
CTA: CFD

Computer Resources: HPE SGI 8600, HPE Cray EX [NAVY, MS]

Research Objectives: Predictive models for nearshore bathymetry and beach topography evolution require a complete understanding of the physics of fluid-sediment interactions in the wave bottom boundary layer (WBBL) and the atmospheric boundary layer. Since such variable three-dimensional (3D) processes are difficult to quantify in situ, we performed coupled fluid-sediment numerical simulations to increase our understanding of the sediment and hydrodynamics in the boundary layer. Fundamental concepts used in describing the phenomena of sediment transport such as particle size and shape, turbulent bottom stress, mixture viscosity and diffusivity, hindered settling, bed failure criterion, and bedforms and their effect of the bottom stress variability are addressed with our models. The models produce high-resolution results necessary to gain insight into the small-scale boundary-layer processes and clarify new directions for measurement techniques needed to improve predictive capabilities.

Methodology: Utilization and development of a suite of discrete and continuum WBBL multiphase models for simulating sediment transport in the nearshore environment from the microscale (cm–m) to the mesoscale (km) is ongoing with HPC resources. At the mesoscale, we use Reynolds-averaged Navier-Stokes simulations (RANS) to predict wave- or current-induced bottom stress and the resulting sediment fluxes (e.g., using Delft3D model). At this scale, the sediment bed is usually modeled as continuum and its kinematics and morphology are determined by simple mass conservation. At the microscale (<10 cm), the 3D sediment phase is simulated with a discrete-element method (DEM) that allows individual grains and their interactions to be specified uniquely, and the fluid model varies in its complexity. In the eddy viscosity DEM approach, the fluid flow is resolved only at scales larger than individual particles, and as a result, the fluid forces (e.g., drag) induced by the flow are parameterized using drag and lift coefficients. Below, we discuss new parameterizations of the fluid forces acting on spherical triangle shapes considered as a model for seashell fragments.

Results: To estimate the hydrodynamic forces acting on the shell fragments, we performed RANS CFD simulations on special meshes (e.g., Fig. 1) with O(y+ = 1) grid size near boundaries, which allows the explicit resolution of the viscous boundary layer and is needed to produce accurate estimates of drag and lift forces. The RANS simulations for particle Reynolds number of 34,000 were carried out with OpenFoam using the Shear Stress Transport k-omega model to simulate turbulence. We considered nine different fragments with base width of 2 cm, length/width aspect ratios varying from 0.2 to 1, and flatness varying from 0.02 to 0.2, and having 64 different orientations with respect to the mean flow. The simulations demonstrated that the fluid forces in the fragment frame of reference can be modeled as a linear combination of the velocity components in the same frame of reference (Fig. 2).

DoD Impact/Significance: All process-based models for nearshore bathymetric evolution are limited by shortcomings in fundamental knowledge of the boundary-layer physics. The microscale simulations provide an unprecedented level of detail for the study of fluid-sediment interactions that is impossible to obtain with available measuring technologies in the field or the laboratory. These results are utilized to improve parameterizations of small-scale processes in larger-scale models. At the mesoscale, our models are well suited for coupling to regional operational hydrodynamic models. The computational resources consumed were in direct support of NRL base programs “Observations and modeling of biological cohesion on seafloor evolution time scales,” “Modeling sediment sorting in sand-shell environments,” and “Predicting wind driven topographic change in sandy, coastal battlespace environments.”

Figure 1. The cross-sectional area of the meshed domain around a rotated shell fragment shape with an aspect ratio of 1 and a flatness parameter of 0.2. The fragment is centered within the hydrodynamic boundary at a distance 15 cm away from the inlet and 6 cm from the bottom surface. Refinement zones in the wake and bottom wall surfaces increase the resolution to 0.7 mm and 0.3 mm, respectively. The resolution of the wall boundary layers at the shell fragment surface is 0.059 mm, corresponding to $y+$ of order 1, fully resolving the viscous sublayer. Resolving the wall boundary layer allows us to forgo the use of wall functions, resulting in a more accurate measure of the surface forces experienced by the shell fragment.

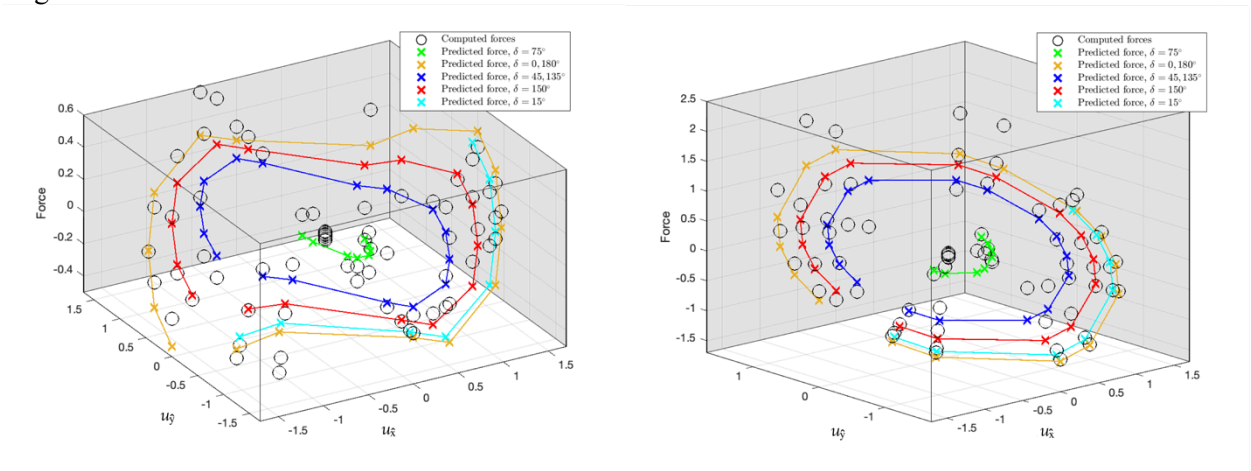

Figure 2. Colored lines (with crosses) show predicted longitudinal (left) and normal (right) force using linear combinations of the longitudinal and normal velocity components in the object frame of reference. The predictions are in good agreement with the forces calculated in the CFD OpenFOAM simulations for 64 unique orientations (black circles).

Title: Detonations with Multi-Phase Flows for Propulsion
Author(s): D.A. Schwer
Affiliation(s): U.S. Naval Research Laboratory, Washington, DC
CTA: CFD

Computer Resources: HPE Cray EX [NAVY, MS]

Research Objectives: The main research goal of the present HPC project is to study high- and low-speed multiphase reacting flows for further understanding advanced engine concepts, with the specific application for detonation engines.

Methodology: We have used two modeling codes for our research into blast and detonation engine simulations. Simulations are done primarily using the JENRE® multiphysics framework. Due to our extensive experience with using the DET3D codes for detonation propulsion, we continue to use them as a benchmark for comparison with the JENRE® framework. The framework utilizes unstructured meshes and both continuous- and discontinuous-Galerkin-FEM techniques to solve a wide variety of complex fluid dynamical phenomena. It has been built from the ground up to make efficient use of CUDA, HIP, Thread-Building-Blocks, OpenMP, and MPI through the use of template libraries. By utilizing unstructured meshes, the solver easily can handle complex flowpaths from rig assemblies and engine concepts while remaining relatively efficient. Extensive work has gone into improving the JENRE® framework for both reacting and multiphase flows during the past several years.

Results: Simulations were conducted investigating an augmentor concept proposed at the Naval Postgraduate School. This concept proposes separating the core mixture from a fairly standard rotation detonation combustor (RDC) using the inner wall of the RDC. Pilot holes then are cut into the inner wall connecting the RDC to the interior core flow. Penetration of gases through these channels into the core serves as a pilot for the core reactant mixture. Fully coupled simulations initially were run, and then a one-way coupling procedure was developed to enable parametric studies to be accomplished efficiently. The one-way coupling simulations explored the amount of penetration of hot, detonated gases through these channels into the core gas, given two different RDC geometries and core conditions, as well as the location of channels. RDC channel flow rates varied between 0.66 kg/s up to 1.16 kg/s, and the core flow was set at 2 kg/s. Results show good penetration for both a high-pressure RDC channel and a low-pressure RDC channel, with hot gas penetration into the core consistently between 30 and 41 mm for the examined cases, without the benefit of core reactions. Further parametric studies were conducted to investigate the benefit of more complex pilot hole arrangements, including multiple pilot holes at azimuthal locations. Results from these simulations showed that substantially improved penetration could be generated through interactions between the holes in the multihole setup beyond just the additional area provided by the second hole.

DoD Impact/Significance: The physics involved in RDCs and other detonation engines is substantially different than for gas-turbine engines. Simulations of RDC systems from basic concepts all the way to full propulsion devices are necessary to understand these devices as well as to contribute to the design process. The work accomplished this year approaches understanding RDC-piloted augmenters from both ends. More detailed simulations are conducted to investigate the underlying physics, while approximations are made to enable parametric studies of a wide range of conditions and geometries.

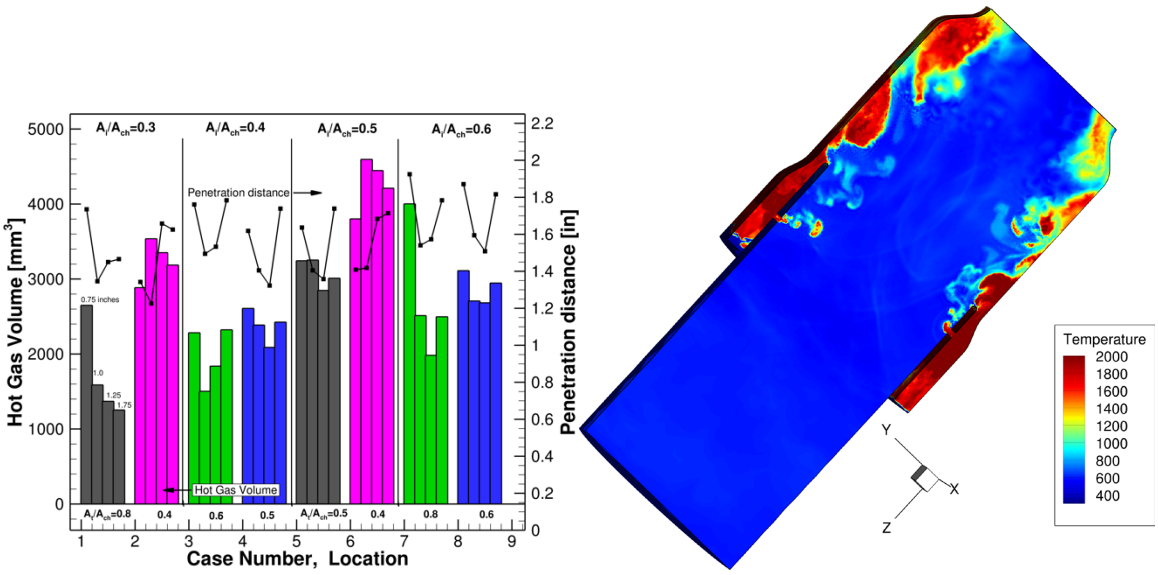

Figure 1. One-way coupling results (left) of a parametric study showing hot gas volume and penetration distance from RDC channel into core, (right) validation simulation of one-way coupling procedure with a coupled core/RDC simulation showing temperature.

Title: Multidimensional Chemically Reacting Fluid Dynamics with Application to Flameless Combustors
Author(s): R.F. Johnson
Affiliation(s): U.S. Naval Research Laboratory, Washington, DC
CTA: CFD

Computer Resources: HPE SGI 8600 [AFRL, OH]; HPE Cray EX [NAVY, MS]

Research Objectives: Conduct computationally intensive simulations of chemically reacting fluid dynamics in diverse multidimensional configurations using HPC resources. The primary aim is to improve our understanding of complex, multiscale combustion phenomena.

Methodology: The Laboratories for Computational Physics and Fluid Dynamics employ high-fidelity simulation codes to predict precise flow fields across various configurations. These codes leverage high-order numerical methods, which are particularly effective for simulating unsteady flows with strong shocks, chemical reactions, and intricate multiscale interactions. This work focuses on developing advanced methodologies for simulating chemically reacting flows at high and low speeds using state-of-the-art numerical techniques. This year, we made significant strides in demonstrating the robustness of our approach in modeling chemically reacting flows.

Results: In this work, we utilized the discontinuous Galerkin (DG) method. One of the DG method's strengths lies in its ability to resolve flow structures with high-order accuracy without requiring additional mesh refinement. While challenges in shock capturing persist — necessitating stabilization near discontinuities — we refined our entropy-preserving limiters to prevent oscillations at high orders. This year, we successfully generated three-dimensional simulations of chemically reacting hydrogen jets in supersonic cross flow for a variety of chemical mechanisms. These simulations leveraged HPCMP resources and an extension of the high-order DG solver in the JENRE® multiphysics framework.

Although these investigations are preliminary, evaluating the impact of different chemistry models reveals a sensitivity in flow structures to the choice of kinetics model. Figure 1 demonstrates the effect of various chemistry models on predicting the behavior of a hydrogen jet in a supersonic cross flow. These results showcase the capability of our methodologies to simulate multidimensional chemically reacting flow phenomena, accurately capturing the complex physics of jet mixing in supersonic air. Simultaneously, they enable us to assess the influence of the underlying chemical kinetic models.

DoD Impact/Significance: Advancing numerical techniques for simulating propulsion devices contributes to improved understanding and prediction of Navy/DoD aircraft performance. This year in particular saw impressive capabilities demonstrated for simulating multicomponent chemically reacting flows on fully unstructured grids, further solidifying our methodologies' role in cutting-edge propulsion research.

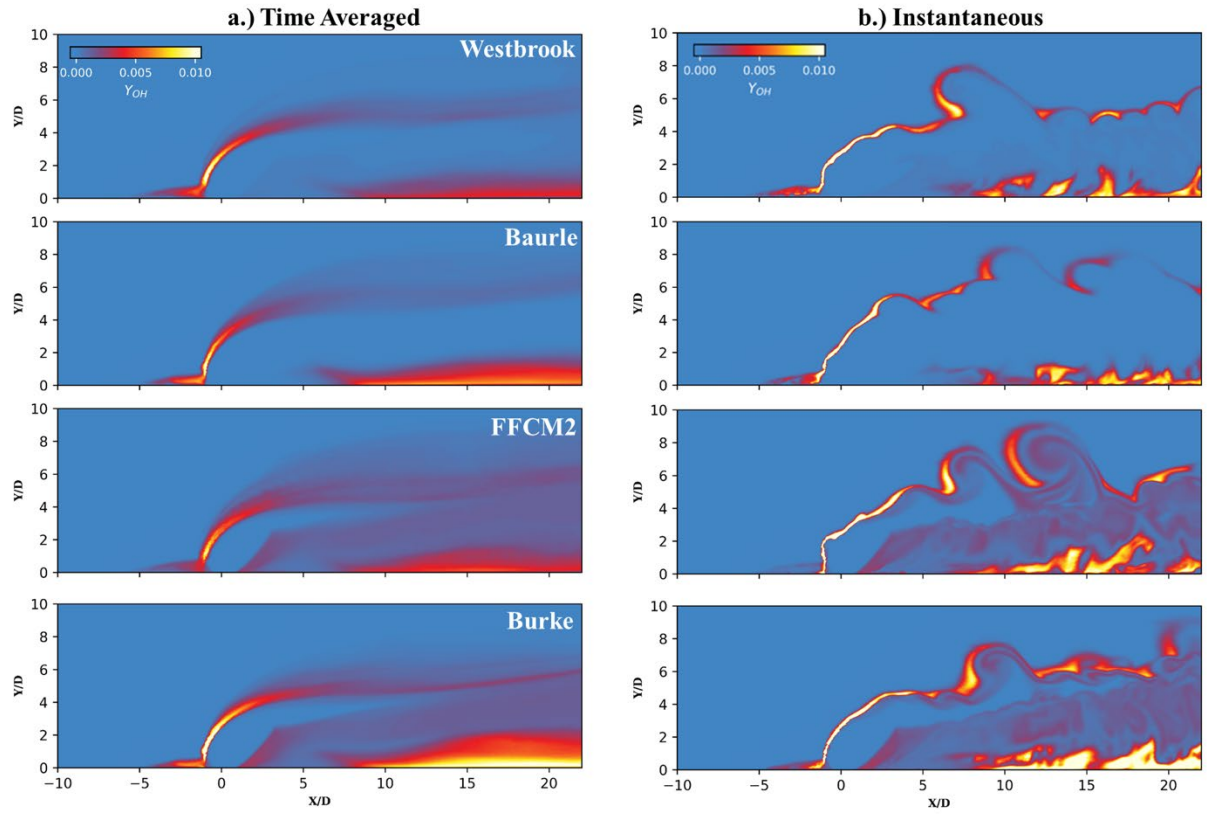

Figure 1. Time average and instantaneous OH profiles for a hydrogen jet in supersonic cross flow. The chemistry models used, Westbrook, Baurle, FFCM2, and Burke, are all various available hydrogen models. The Burke and FFCM2 models are more recent chemistry models.

THIS PAGE INTENTIONALLY LEFT BLANK

CCM

Computational Biology, Chemistry, and Materials Science

CCM covers computational tools used to predict basic properties of chemicals and materials, including nano- and biomaterials. Properties such as molecular geometries and energies, spectroscopic parameters, intermolecular forces, reaction potential energy surfaces, and mechanical properties are being addressed. Within the DoD, quantum chemistry, molecular dynamics, statistical mechanics, and multiscale methods are used to design new chemical, polymer, nanomolecular, and biomolecular systems for fuel, lubrication, laser protection, explosives, rocket propulsion, catalysis, structural applications, fuel cells, and chemical defense. Solid-state modeling techniques are employed in the development of new high-performance materials for electronics, optical computing, advanced sensors, aircraft engines and structures, semiconductor lasers, advanced rocket engine components, and biomedical applications. Of recent emerging interest in the Computational Biology, Chemistry, and Materials Science (CCM) CTA are methodologies that cover bioinformatics tools, computational biology, and related areas, such as cellular modeling.

Title: Calculation of Materials Properties Via Density Functional Theory and Its Extensions
Author(s): J.L. Lyons
Affiliation(s): U.S. Naval Research Laboratory, Washington, DC
CTA: CCM

Computer Resources: HPE SGI 8600, Penguin Open Compute Platform (OCP) [AFRL, OH]; Cray XC40/50 [ERDC, MS]

Research Objectives: To determine the electronic structure, as well as the role of defects and dopants, for ultrawide-bandgap semiconductors (UWBGSs) such as gallium oxide (Ga_2O_3) and lithium gallate ($LiGa_5O_8$), and novel materials such as cesium lead bromide ($CsPbBr_3$), using hybrid density functional theory (DFT).

Methodology: DFT has long been the workhorse for determining semiconductor electronic structure. Although in principle, DFT requires no experimental input, when applied to UWBGS, the so-called "bandgap problem" makes quantitative prediction of defect properties difficult. To overcome this issue, we employ hybrid DFT, which mixes in a fraction of screened Hartree-Fock exchange into the exchange-correlation functional. This approach provides accurate, quantitative prediction of bandgaps and defect transition levels, even for UWBGS. Using hybrid DFT, defect-related charge-state transition levels, formation energies, and optical transitions are calculated. For the lead halide perovskites (e.g., $CsPbBr_3$), spin-orbit coupling is also required due to the heavy lead atom.

Results: In FY24, we studied the role of deep nitrogen acceptors in beta (monoclinic) Ga_2O_3 by calculating the formation energies and configuration-coordinate diagrams of these dopants. In conjunction with deep-level optical spectroscopy measurements, we demonstrated the nitrogen acceptor as a nearly ideal defect for establishing the Fermi level in the midgap region for achieving semi-insulating material.

Using hybrid functional calculations, we also examined the role of self-trapped holes (STHs) in limiting *p*-type conductivity in UWBGSs. We found that STHs were highly stable in a recently discovered UWBGS, $LiGa_5O_8$ (see Fig. 1). This strongly limits the prospects of p-type (hole) conductivity in $LiGa_5O_8$ because holes then also bind strongly to acceptor dopants such as Mg.

We also explored rutile UWBG oxides such as germanium oxide (r-GeO_2), which recently has been touted as one of the few UWBG oxides that can exhibit hole conductivity. Motivated by those results, we also examined rutile silicon dioxide (r-SiO_2, a metastable polymorph). We find that STHs are not stable in this compound due to its very small Si−O bond lengths. Concurrently, acceptor ionization energies from group 3 elements such as Al or Ga are small (less than 200 MeV; see Fig.1), indicating that *p*-type conductivity should be possible in this UWBGS.

Finally, we examined the optimal heterostructures for β-Ga_2O_3 using DFT modeling of oxide alloys containing In_2O_3 and Al_2O_3. We find that an alloy of $(In_{0.25}Al_{0.75})_2O_3$, in the monoclinic structure, will be particularly interesting because it closely matches the lattice constants of Ga_2O_3. At the same time, this alloy provides a large bandgap (5.70 eV) and a substantial conduction-band offset (1 eV), meaning it should be an effective carrier-blocking barrier layer.

DoD Impact/Significance: Along with GaN, UWBGS such as Ga_2O_3 can be deployed in power electronics that provide a crucial role in many Navy-relevant applications and afford significant SWaP-C when outperforming components based on traditional semiconductor materials. Newer materials such as the halide perovskites are attractive as potentially low-cost, highly efficient energy materials. Controlling electrical conductivity via impurity doping, understanding contaminant species, and characterizing unintentional native defects is crucial for improving such materials and optimizing device designs.

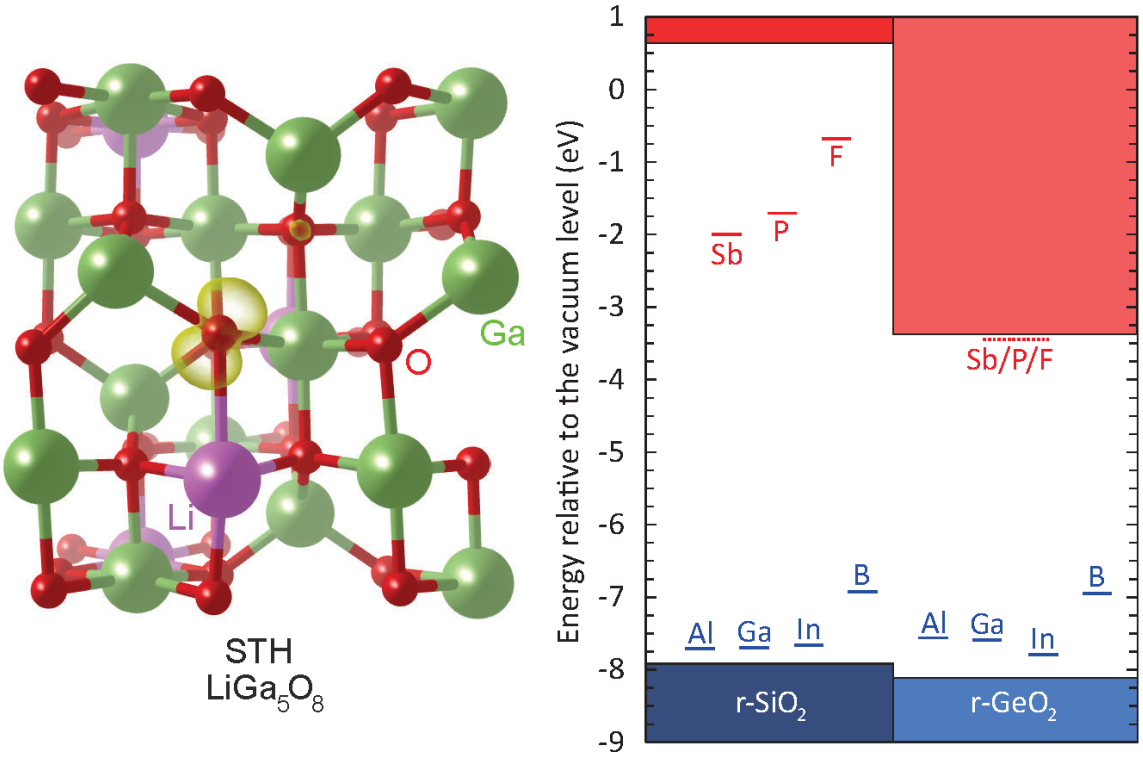

Figure 1. Hybrid DFT calculations indicated that self-trapped holes (STHs) were stable in $LiGa_5O_8$, limiting *p*-type conductivity (left). However, in r-SiO_2, which has very small Si-O bond lengths, STH are not stable, and acceptor ionization energies are small (right).

Title: Point Defects and Interfaces in Two-Dimensional Materials
Author(s): D. Wickramaratne
Affiliation(s): U.S. Naval Research Laboratory, Washington, DC
CTA: CCM

Computer Resources: HPE SGI 8600 [AFRL, OH]; Cray XC40/50 [ERDC, MS]

Research Objectives: To understand and predict the electronic, structural and optical properties of point defects, dopants, and interfaces in bulk and low-dimensional semiconductors.

Methodology: We use density functional theory (DFT) and the projector augmented-wave (PAW) method as implemented in the Vienna Ab Initio Simulation (VASP) code for our calculations. To describe the bandgap of semiconductors accurately, we use screened hybrid functional calculations. Accurate forces and total energy calculations are required to identify the most stable configurations of point defects in their various charge states. We use this information to determine the formation energies, charge-state transition levels, and optical transitions of various defects.

Results: We performed first-principles calculations of carbon in aluminum nitride (AlN) to determine the optical and hyperfine properties of this impurity. We compared our results against photo-EPR measurements of the hyperfine parameters and optical cross sections to photoionize and quench the EPR spectra. Our calculations provide clear evidence that carbon substitutes on the nitrogen site in AlN lead to an optical absorption band at ~4.7 eV that can hamper the operation of AlN ultraviolet optoelectronic devices, and we revise the interpretation of hyperfine spectra that was presented in previous studies of defects in AlN by showing that it is due to substitutional carbon on the nitrogen site.

DoD Impact/Significance: Aluminum nitride (AlN) is a candidate ultrawide-bandgap semiconductor for ultraviolet optoelectronics and power electronics with multiple application areas that are relevant to the DoD. While carbon is known to incorporate unintentionally in AlN, its configuration within the AlN lattice has been debated widely despite several decades of defect spectroscopy investigations. Our work highlights the importance of controlling the incorporation of carbon because it leads to optical absorption that would hinder the operation of any ultraviolet AlN optoelectronic device.

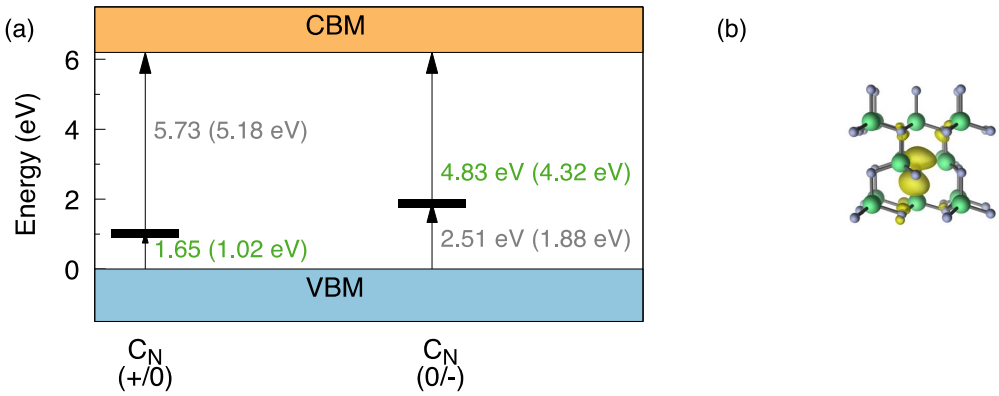

Figure 1. (a) The peak absorption energy and zero-phonon line (in parentheses) for the C_N (+/0) and (0/−) levels is listed alongside each arrow denoting possible optical absorption processes. Processes that lead to an EPR active state are denoted in green font. (b) Configuration-coordinate diagram illustrating photoionization of electrons from the VBM to the C_N (0/−) level converting the EPR active charge state to an EPR silent state. The inset in (b) illustrates the spin density of the hole introduced by the EPR active neutral charge state of C_N.

Title: Materials for Energy Storage and Generation
Author(s): M. Johannes
Affiliation(s): U.S. Naval Research Laboratory, Washington, DC
CTA: CCM

Computer Resources: HPE SGI 8600 [AFRL, OH]

Research Objectives: The objectives of this program are to calculate the materials properties with relevance to functionality in materials relevant to energy storage and generation using density functional theory (DFT) and its extensions including molecular dynamics. Materials of particular interest include battery cathode, anode, and electrolyte materials, electrolytes for solid acid fuel cells (SAFC), and magnetic and superconducting materials. Substantial concentration is on the mechanisms and phase diagram of hydration/dehydration as a function of temperature.

Methodology: Our primary methodology is molecular dynamics based on ab initio calculation of forces and energies using first-principles projector-augmented plane-wave (PAW) methods as implemented in Vienna Ab Initio Software Program (VASP). Incorporation of the chemical potential water was accomplished by consulting the JANAF Tables and extrapolating the measured entropy to temperatures and relative humidities of interest.

Results: In FY24, the project's focus on SAFC electrolytes shifted to include calculation of the tendency of this family of materials either to dehydrate or to overhydrate and subsequently hydrolyze. Our calculations successfully reproduced the dehydration sequence of well-known electrolyte materials CsH_2PO_4 and analogue RbH_2PO_4, lending confidence to our prediction that the reverse process occurs in the borophosphate materials developed at NRL. Specifically, we showed that Cs-based borophosphate was susceptible to uptake of water molecules, even at fairly low relative humidity, and that once absorbed, these molecules were very mobile within the framework structure and exhibited proton exchange with nearby PO_4 units. This indicates that in addition to the intrinsic p^+ conduction previously observed and calculated, some of the conductivity may stem from proton exchange under the influence of a voltage.

We also carried out extensive calculations of Ni dopants in Ceria. We found that without oxygen vacancies, Ni always adopts the Ni^{3+} valency, but that if oxygen vacancies are present, 2+ valency is also possible. Importantly, our calculations show that with or without vacancies present, the substitutional Ni (for Ce) does not remain on the Ce site, but shifts to a more energetically favorable square planar interstitial environment.

DoD Impact/Significance: Energy materials are an obvious naval need and our investigation of the SAFC electrolyte not only has revealed how its record-setting conductivity takes place, but also maps out the temperature dependence of dehydration/hydration that can aid in conduction within certain bounds. Proper control of this water interaction will be crucial to enable all-solid-state fuel cells without the necessity for large overpotentials or dangerously high temperatures.

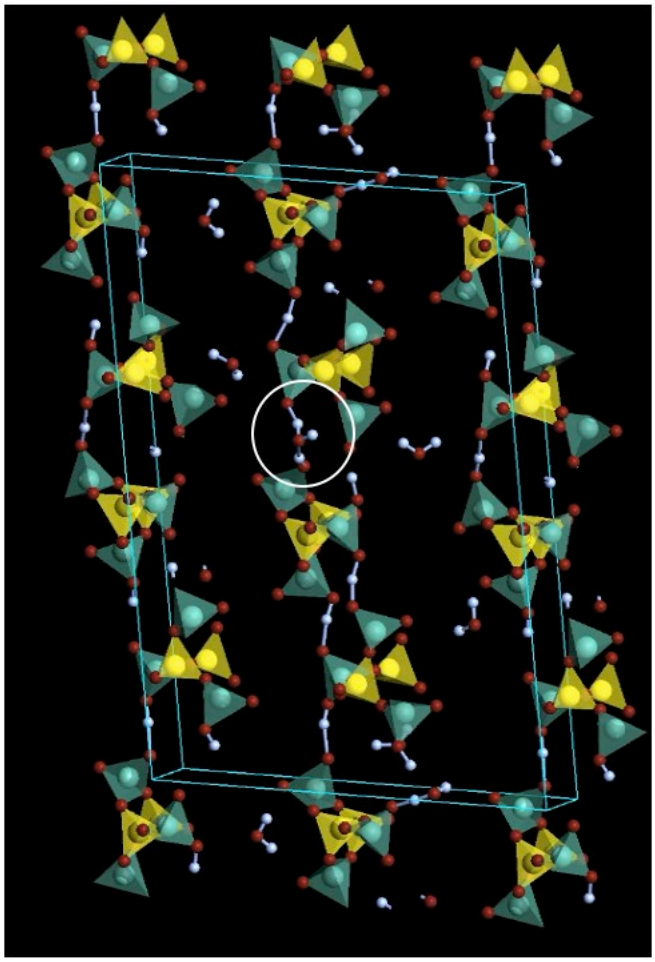

Figure 1. Cs-borophosphate with water molecules intercalated. White circle highlights a molecule mid-protonic exchange with an intrinsic p^+ located at its typical PO_4 site.

Title: Computational Materials Design for Targeted Applications
Author(s): S. Mukhopadhyay
Affiliation(s): U.S. Naval Research Laboratory, Washington, DC
CTA: CCM

Computer Resources: HPE SGI 8600, Penguin Open Compute Platform (OCP) [AFRL, OH]; HPE Cray EX 4000 [ERDC, MS]; HPE Cray EX, Penguin TrueHPC [NAVY, MS]

Research Objectives: (i) In order to minimize the heat generated in the device, it is important to reduce the thermal boundary resistance so that the generated heat could be dissipated promptly. Our objective in this research was to find ways to minimize the thermal boundary resistance in GaN/diamond interfaces. (ii) Materials with high permittivity play a critical role to improve device performance by reducing the leakage current. In this study, we aim at obtaining the maximum dielectric permittivity in Sc-doped AlN.

Methodologies: (i) Ab initio density functional methods using Quantum ATK was used to simulate the GaN/diamond interfaces and for optimizing the interfaces prior to calculating the transport properties. Subsequently, the thermal boundary resistance was calculated using RNEMD (reverse nonequilibrium molecular dynamics) and NEGF (nonequilibrium Green function)-based methods as implemented in Quantum ATK. (ii) The randomly substituted Sc-doped AlN was simulated using MedeA, and then structural, vibrational, and dielectric properties were calculated using density functional theory as implemented in VASP.

Results: (i) We calculated the interfacial thermal conductivity of GaAs/diamond interface using RNEMD and NEGF-based methods. The thermal conductance from the NEGF method was found to be 42.3 MW/Km^2 as compared to 51.8 MW/Km^2 from the RNEMD method. Subsequently, we explored several interlayer materials to reduce the interfacial thermal conductivity. The calculated thermal boundary conductance of the GaAs/AlN/diamond trilayer interface is 61.86 MW/m^2K. Although AlN was found to stabilize the interface better than just the GaAs/diamond interface, the TBR was not reduced significantly in contrast to the case with the GaN/AlN/diamond interface. Nevertheless, having the interlayer system was found to be beneficial, and therefore, it motivates exploring various interlayer materials such as TiN, TaN and NbN to boost thermal boundary conductivity. (ii) We calculated dielectric properties of randomly generated Sc-doped AlN structures. The calculated results were able to explain the previously measured data and predicted the optimum Sc-doping for achieving the highest permittivity in the ScAlN system. The calculation predicted a discrete jump around 40% doping (optimum doping for highest permittivity. This was confirmed by the NRL experiment.)

DoD Impact/Significance: (i) The theoretical framework developed here to calculate the thermal boundary resistance for interfaces will help identify a suitable interlayer system to reduce heat generated that negatively impacts the device performance. Size-, weight-, and power (SWaP)-constrained platforms that simply do not have the luxury of extensive secondary support systems, such as active liquid cooling for microelectronics, would benefit highly from these innovations in heat extraction and reduction in heat generation. (ii) The scheme to obtain the maximum dielectric constant in ScAlN would help reduce the leakage current in the electronic devices that would enhance their performance.

Graphics:

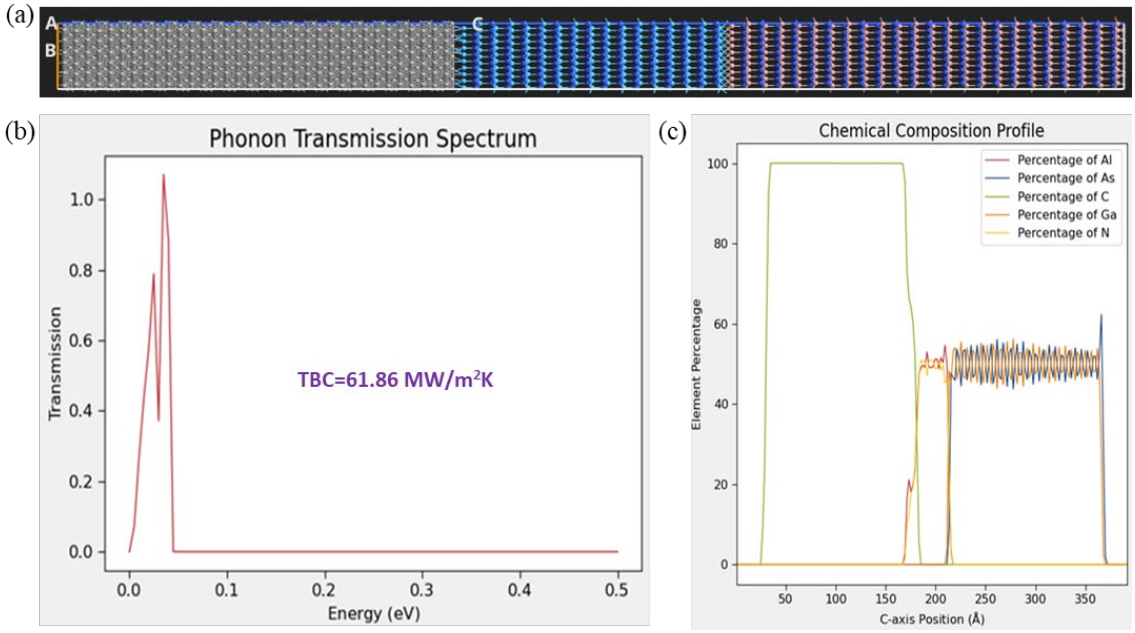

Figure 1. (a) Schematic of the diamond/GaAs interface with an AlN interlayer in the middle. (b) Effective phonon transmission through the trilayer (diamond/AlN/GaAs) interface that leads to an equivalent thermal boundary conductivity (TBC) of 62 MW/m^{2}K. (c) Chemical composition profile including the self-diffusion at the interface.

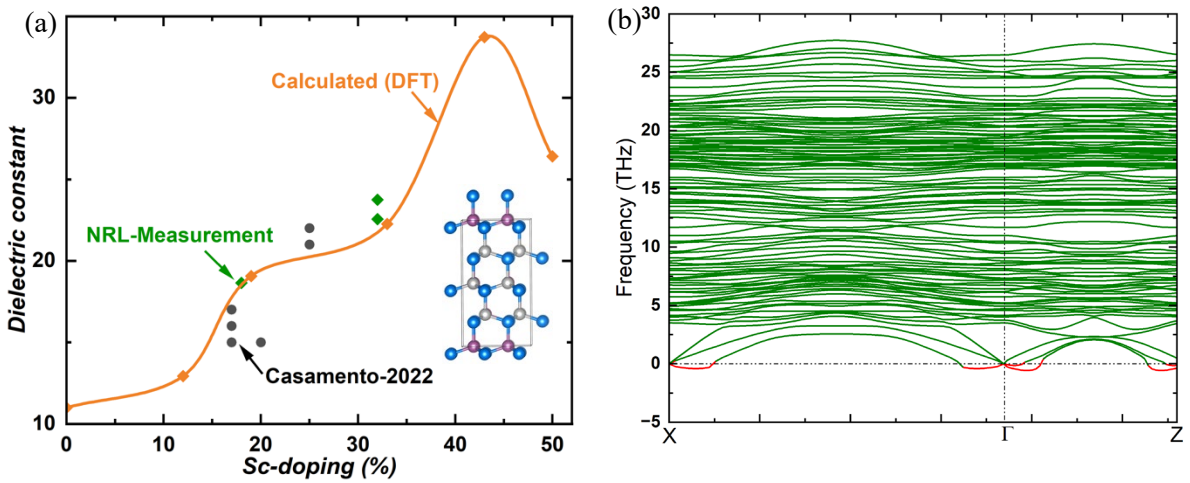

Figure 2. (a) Calculated dielectric constant of ScAlN as a function of Sc doping concentration from density functional theory (orange diamonds; the orange line is to guide the eyes) along with the data from experiments at NRL (green diamonds) and from literature (black circles). The schematic model of the unit cell is also given in the inset. (b) Phonon dispersion of ScAlN at a 50% Sc doping concentration. The red sections of the dispersion show imaginary modes, indicating instability of the structure at this doping concentration.

Title: Numerical Studies of Semiconductor Nanostructures
Author(s): T.L. Reinecke[1] and I. Welland[2]
Affiliation(s): [1]U.S. Naval Research Laboratory, Washington, DC; [2]National Research Council Research Associate at the U.S. Naval Research Laboratory, Washington, DC
CTA: CCM

Computer Resources: HPE SGI 8600, HPE Cray EX [AFRL, OH]

Research Objectives: To make first-principles calculations of the optical and acoustic properties of a range of monolayer and multilayer transition-metal dichalcogenide materials as a basis for determining their deformation potentials and optically induced stresses and to use these results as a basis for demonstrating novel approaches for high-frequency acoustic devices based on these materials.

Methodology: First-principles density functional methods using Quantum Espresso were used to calculate the electronic properties of a number of natural monolayer and multilayer transition-metal dichalcogenide materials, including WSe_2, MoS_2, and ReS_2, as functions of applied in-plane and out-of-plane strains. These results were used to obtain the deformation potentials of these materials and were compared to results of photoacoustic experiments at NRL.

Results: The present work involves calculations of a broad range of optical properties of natural monolayer and multilayer materials composed of WSe_2, MoS_2, and ReS_2 that are of interest in theoretical and experimental research involving potential ultrafast acoustic properties that are controlled optically. These materials are layered semiconductors with weak binding between layers and relatively complex electronic properties. Calculations of their electronic properties gave a number of conduction band minima and valence band maxima for their direct and indirect bandgaps. They have shown that material properties depend sensitively on the number of layers in the materials and that different semiconductor band minima and maxima have different deformation potentials for stresses along different crystal directions. These results can provide a basis for the development of ultrafast tunable acoustic systems composed of weakly bonded layered materials using optical control.

DoD Impact/Significance: It has been demonstrated that accurate theoretical results can be obtained for a wide variety of novel monolayer and multilayer materials using density functional approaches and that the results can be used to guide experimental research at NRL. Theoretical insights into the experimental observations will inform the development of terahertz photoacoustic devices using the novel properties of these materials.

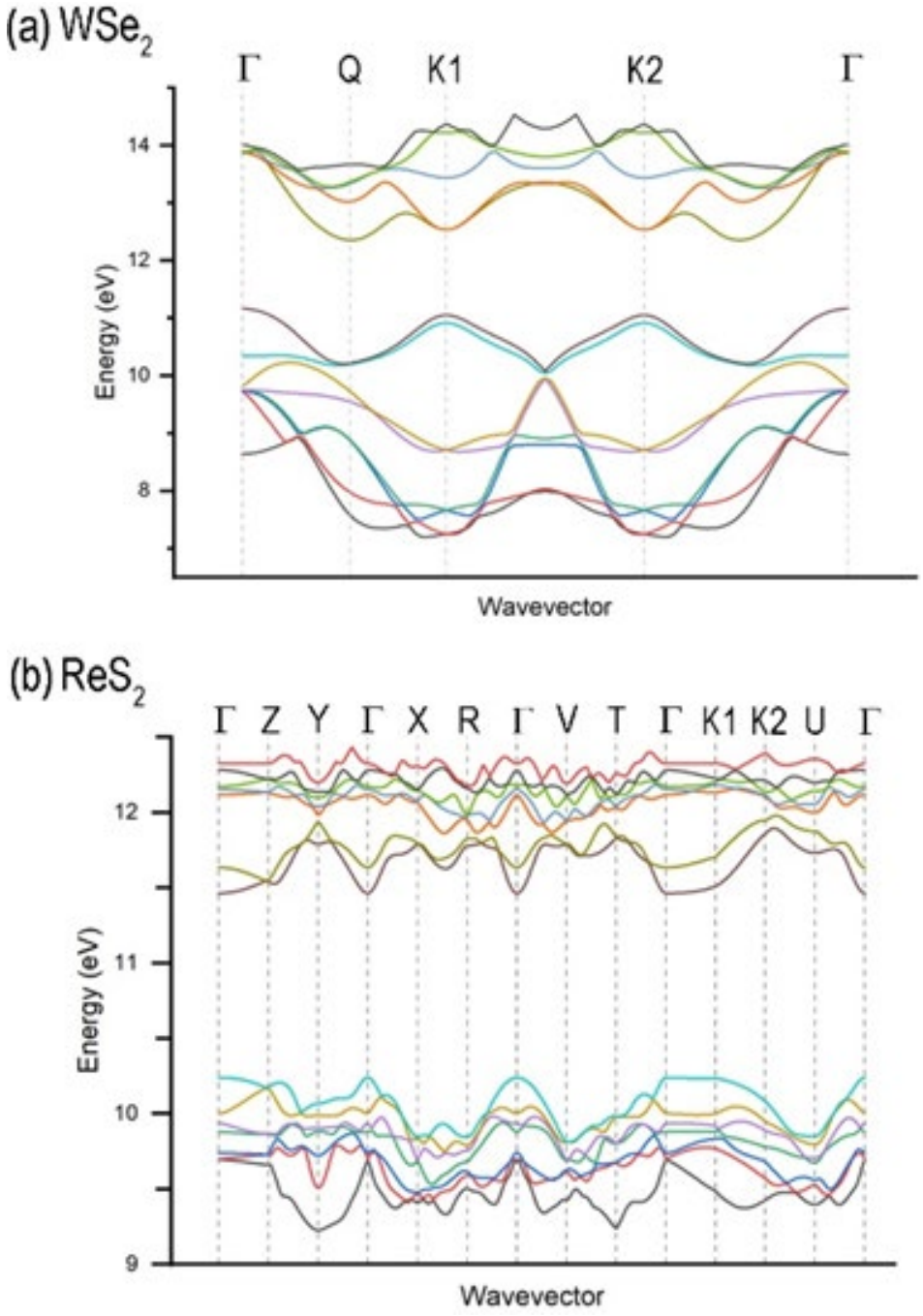

Figure 1. Density functional theory-calculated electronic band structures for (a) WSe_2 and (b) ReS_2. High symmetry points are labeled.

Title: Machine Learning Interatomic Potentials for Materials Science
Author(s): M.W. Swift
Affiliation(s): U.S. Naval Research Laboratory, Washington, DC
CTA: CCM

Computer Resources: HPE Cray EX 4000 [ERDC, MS]; Penguin Open Compute Platform (OCP) [AFRL, OH]; Liqid [ARL, MD]

Research Objectives: To train machine learning interatomic potentials to predict energies, forces, and stresses for a variety of Navy-relevant materials. To employ the trained potentials to predict structure-property-performance relationships.

Methodology: Machine learning interatomic potentials (MLIPs) are a cutting-edge approach in computational materials science, leveraging advanced machine learning algorithms to model the complex interactions between atoms in a material, enabling accurate, efficient predictions of material properties and behaviors at much lower computational cost than quantum methods such as density functional theory (DFT). The MACE potential, which relies on high-order equivariant message-passing neural networks for its operation, recently has been trained on the enormous "Materials Project Trajectory" database. The resulting model, MACE MP, achieved impressive accuracy — competitive with the best existing universal interatomic force fields. The true potential of this model can be unlocked using neural-network transfer learning: a small amount of fine tuning for a specific material system allows the model to achieve a very high level of accuracy that is competitive with DFT. For each target system, we fine-tuned MACE MP based on energies, forces, and stresses calculated using DFT. We then used the force field for molecular dynamics (MD) to predict relevant properties.

Results: In FY23, we studied three-dimensional (3D) solid-state batteries and lithium-sulfur batteries. MLIP training for both systems was successful, achieving energy errors in the few-MeV-per-atom range, competitive with the best fine-tuned interatomic potentials available.

For 3D solid-state battery systems, cross-linking behavior of the polymer electrolyte was simulated. Hydroxide conduction mechanisms were simulated using molecular dynamics simulations with the trained MACE MLIP. Analysis of these simulations is ongoing.

For lithium-sulfur batteries, bonding of the lithium polysulfide to a polymer coating was simulated in a realistic battery solvent. This polymer coating is used in experiments and has been shown to reduce the parasitic "polysulfide shuttle" process that occurs when the polysulfides cross the membrane to the anode side rather than being fully reduced on the cathode side. The simulations support the conclusion that the lithium polysulfide binds weakly to the polymer, weakly enough that the active material is not lost, but strong enough to prevent polysulfide crossover.

DoD Impact/Significance: 3D solid-state batteries have the potential to dramatically increase energy density, power density, and safety compared to traditional lithium-ion batteries, enabling smaller and cheaper electrified UAVs, UUVs, and UGVs, as well as improving safety and longevity of mobile electronics for the dismounted warfighter. Lithium-sulfur batteries are a cheaper alternative to lithium-ion batteries because sulfur is abundant and has a robust supply chain compared to cobalt and rare earths in traditional lithium-ion battery cathodes. This will contribute to operational resiliency, e.g., for grid-scale storage and backup systems.

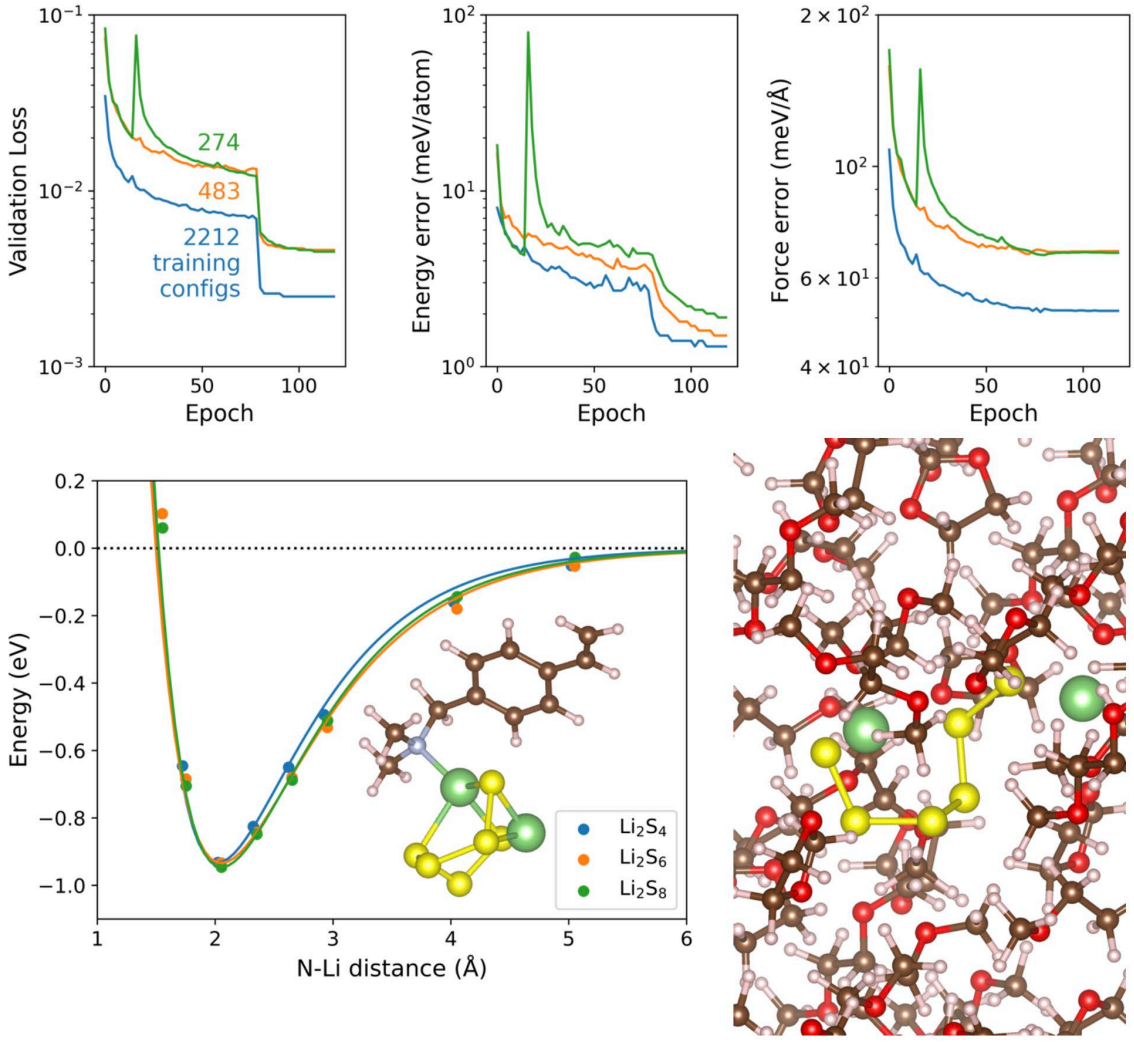

Figure 1. (top) learning plots for fine-tuning of MACE force field for polysulfide system, showing validation loss, energy error, and force error as a function of training epoch. The blue curve, which uses all the training data, shows that a large training set is required for good accuracy. (bottom left) Energy as a function of N-Li distance for a lithium polysulfides bonded to a DMAMS monomer, which makes up the polymer coating. An atomistic visualization of the bonding config of Li_2S_6 is inset, with hydrogen in gray, carbon in brown, nitrogen in blue, lithium in green, and sulfur in yellow. (bottom right) Atomistic visualization of lithium polysulfide in a realistic battery electrolyte. Colors are the same as before, plus oxygen in red.

Title: Materials Properties of Surfaces and Two-dimensional Systems
Author(s): M. Phillips
Affiliation(s): U.S. Naval Research Laboratory, Washington, DC
CTA: CCM

Computer Resources: HPE SGI 8600 [AFRL, OH]; Cray XC40/50 [ERDC, MS]

Research Objectives: Characterize and explain the origin of the localization of electrons in twisted two-dimensional transition metal dichalcogenide (TMD) bilayers.

Methodology: We use density functional theory (DFT) code implemented on the HPC machines to study these twisted TMD systems. DFT requires the identification of a periodic repeat unit cell. For our systems, this periodic cell can contain thousands of atoms. We undertake these huge DFT calculations to compute the relaxation of atoms in twisted TMD systems, which allows us to define a displacement field describing the relaxation of each atom. We also compute the electronic wavefunctions using DFT to see where electrons are localized. To understand this localization, we compute local electronic polarization in our systems using an expression that depends on both the displacement field and the Born effective charge tensors. We use smaller support DFT calculations to compute the Born effective charge tensors. Then we compute the charge density by taking the negative divergence of the polarization.

Results: We focus specifically on the $MoSe_2/WSe_2$ twisted-bilayer system, and we find that during relaxation, the atoms in the metal layers effectively rotate about two out of the three high symmetry points in the material (ABBA and BB sites). However, the wavefunctions are localized at the third high symmetry point, AA. In support of this finding, we find that the computed polarization points at the AA region, and the computed electronic charge density is localized in the AA regions in both Mo and W layers. In doing these calculations, we also have shown that the Born effective charge tensors for untwisted systems are accurate enough to use in the polarization calculations of twisted systems, which saves computational time.

DoD Impact/Significance: The localization of electronic states in twisted TMD bilayers is thought to lead to correlated electron behavior, which, in turn, leads to the realization of exotic electronic phases such as superconducting states and Mott insulating states. In TMD bilayers, these states are "highly switchable," i.e., one can tune into and out of these exotic states by applying a back-gate voltage. This is in contrast to many other materials, which require more involved techniques to induce exotic electronic phases such as chemical doping. The accessibility of "highly switchable" exotic electronic states makes twisted TMD bilayers attractive platforms for technologies based on switching (e.g., transistors). In the future, switchable twisted-TMDs may be utilized in lightweight and low-power devices for communication, information technology, and next-generation computing, which are relevant in many DoD scenarios.

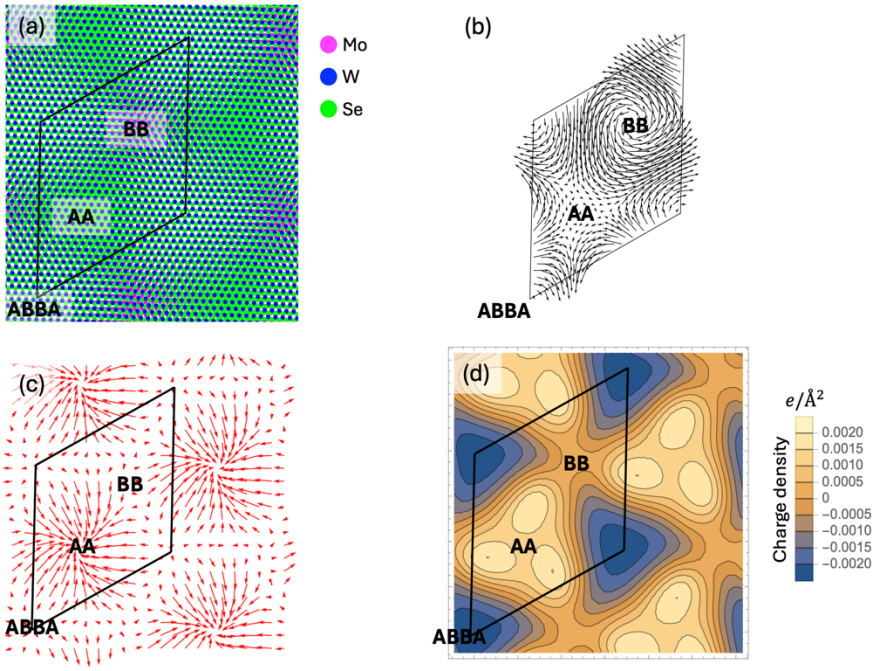

Figure 1. Origin of localized charge density in $MoSe_2/WSe_2$ bilayer. (a) Relaxed atomic positions of 62.45° twisted $MoSe_2/WSe_2$ bilayer. The three clear stacking regions are BB, with chalcogens aligned in the two layers, AA, with metals aligned in the two layers, and ABBA, with metals aligned with chalcogens in the two layers. (b) The displacement field of the Mo atoms in a 62.45° twisted bilayer. Upon relaxation, the Mo atoms rotate counterclockwise around the BB-aligned point in the unrelaxed lattice, rotate clockwise around the ABBA point, and are basically fixed around the AA point. (c) Computed polarization ($\overrightarrow{P''}$) for the Mo atoms in a 62.45° twisted bilayer. Though the atoms are fixed around the AA region in figure (b), the polarization is directed toward AA. (d) Electronic charge density, $\rho = -\nabla \cdot \overrightarrow{P''}$, in the 62.45° twisted bilayer is greatest around the AA regions.

Title: Multiple Length and Time Scale Simulations of Material Properties
Author(s): N. Bernstein
Affiliation(s): U.S. Naval Research Laboratory, Washington, DC
CTA: CCM

Computer Resources: HPE SGI 8600, Penguin Open Compute Platform (OCP) [AFRL, OH]; Liqid [ARL, MD]

Research Objectives: To understand and predict mechanical, structural, and energetic material properties.

Methodology: Atomic energy, force and stress calculation using density functional theory (DFT) to generate reference fitting data for machine learning interatomic potentials. The software implementing these methods includes VASP for DFT simulations, MACE for machine learning potential development, ASE for interfacing between various programs, and the wfl Python package for job workflow management. The MACE neural network used GPGPUs via the PyTorch library.

Results: We used VASP DFT calculations to evaluate reference data for machine learning interatomic potentials in two different contexts. The first is the creation of a ***universal*** foundation model that spans nearly the entire periodic table. The initial work on MACE-MP0 (https://arxiv.org/abs/2401.00096) showed that it was possible to fit a fairly stable potential for such a wide range of compositions, and we extended it by calculating about 15,000 additional configurations at smaller volumes to ensure that it is stable as atoms come closer together. In addition, we developed a workflow for fine-tuning this base model into more accurate system-specific potentials. Using the wfl Python library, we used HPC resources to compute reference data for $Ni(OH)_2 + H_2O$. These calculations used a DFT hybrid functional, which is much more computationally demanding than conventional functionals, and the fine-tuning approach was vital for making the amount of needed data small enough to be practical.

DoD Impact/Significance: Machine learning interatomic potentials have revolutionized atomic resolution simulations of materials properties during the past few years by matching the accuracy of first principles methods such as DFT, to which they are fit, with orders-of-magnitude-lower computational cost. Materials with technological usefulness to the DoD, whether for structural applications such as armor or hypersonics, or for functional applications such as sensing or energy storage, usually involve several elements. The existence of a universal machine learning interatomic potential makes it possible to tackle new materials with arbitrary compositions without having to develop a new potential laboriously from scratch for each such application. The stability of the potential during dynamics simulation is essential, and our calculations dramatically improved the stability of the next-generation universal model building on MACE-MP0 currently under development. Nickel hydroxide is a proton conductor with energy-storage applications, but its structure degrades under environmental conditions. The interatomic potential we have developed is the first to capture the Ni-O bonding, which previously could be done only with computationally expensive hybrid functional DFT simulations. It enables dramatically increased simulation speeds, making it possible to predict how the material evolves with time under different hydration conditions and what factors control its degradation and how to prevent it.

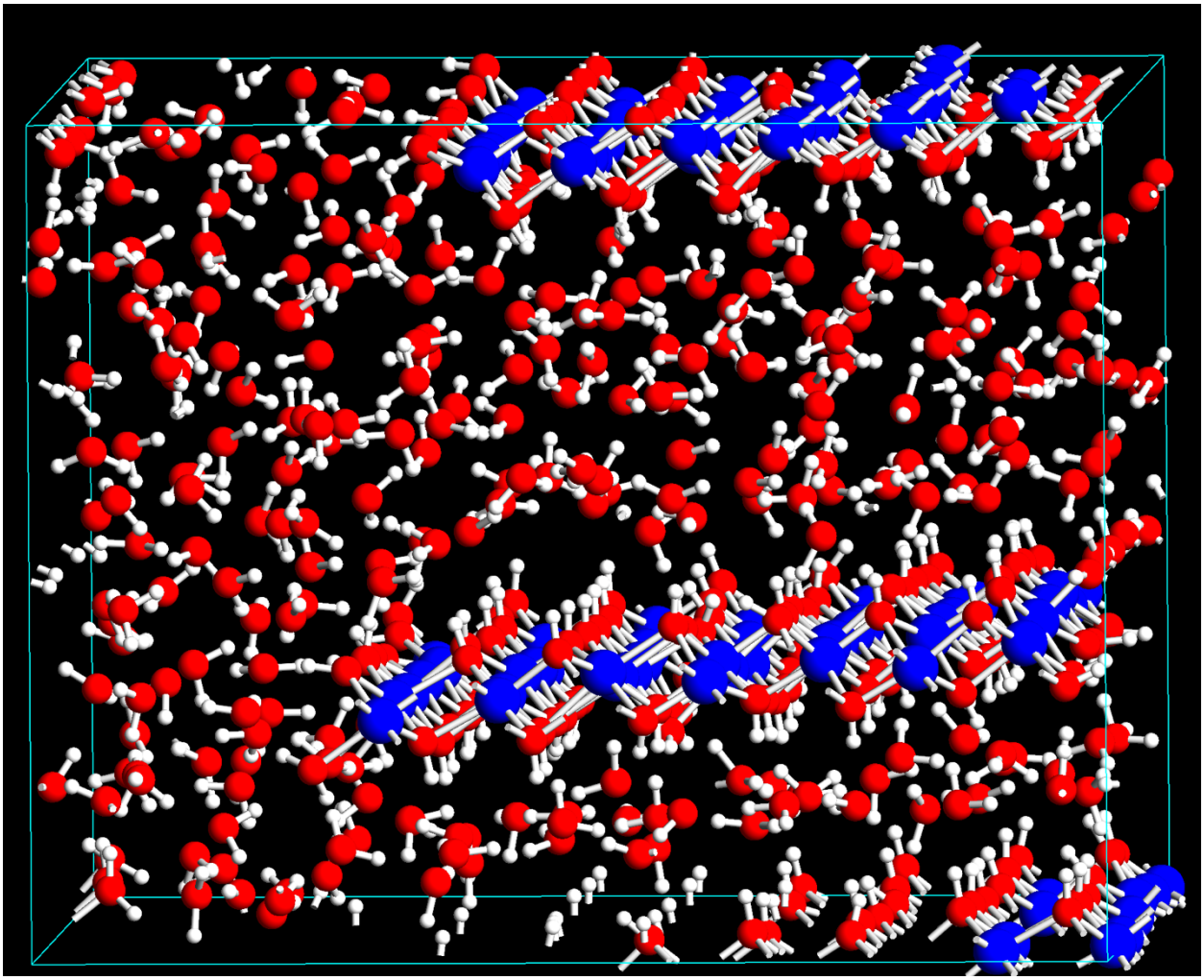

Figure 1. Snapshot from a 1197-atom simulation of $Ni(OH)_2 + H_2O$ using a MACE machine learning interatomic potential fit to HSE hybrid functional DFT calculations. Two layers of nickel hydroxide are shown, with a monolayer of intercalated water between two and a thicker water layer between the other two. Blue, red, and white spheres indicate Ni, O, and H atoms, respectively.

Title: Optimization Algorithms for Quantum Computers
Author(s): C.S. Hellberg
Affiliation(s): U.S. Naval Research Laboratory, Washington, DC
CTA: CCM

Computer Resources: HPE SGI 8600, Penguin Open Compute Platform (OCP) [AFRL, OH]; Liqid [ARL, MD]; HPE Cray EX 4000, Cray XC40/50 [ERDC, MS]; HPE Cray EX [NAVY, MS]

Research Objectives: Derive cost functions for optimization problems that are amenable to solutions using current noisy quantum computers.

Methodology: We derived cost functions for satellite schedules using two different encoding schemes. Each encodes the problem in quantum bits or qubits, but the meaning of qubits differs. The two encodings are:

1. **Time encoding**: Time is coarsely grained, and a grid of qubits is defined with each corresponding image to a certain target at a certain time. If a target cannot be imaged at a given time because the satellite is too close to the horizon, no qubit is defined for that time, which reduces the resources required for this encoding.

2. **Route encoding**: Each qubit corresponds to a pair of targets or an edge in the solution graph. If qubit (i,j) is "on," target j follows target i in the solution. If target j cannot follow target i, no qubit (i,j) is defined, reducing the resource requirements.

To simulate each encoding using the classical HPC computers, we generate a complete Hilbert space of all possible 2^N states for the N qubits and solve for the lowest cost.

Results: We can simulate up to $N = 42$ qubits on a single node. The code scales very efficiently, and we could push this higher, if needed, by running on more nodes. We validated that the cost functions derived for both encodings are accurate and give the solutions we expect. Additionally, we find that for dense problems in which the targets rise and set nearly simultaneously, as shown in the figure, route encoding can yield solutions that cannot be completed in time. We are exploring simultaneous time and route encodings that should be able to fix this problem.

DoD Impact/Significance: Optimization problems have broad DoD impact. Here, we developed algorithms for solving satellite scheduling on a quantum computer. Once the currently noisy quantum computers improve, these algorithms may become more efficient than their classical counterparts for scheduling problems.

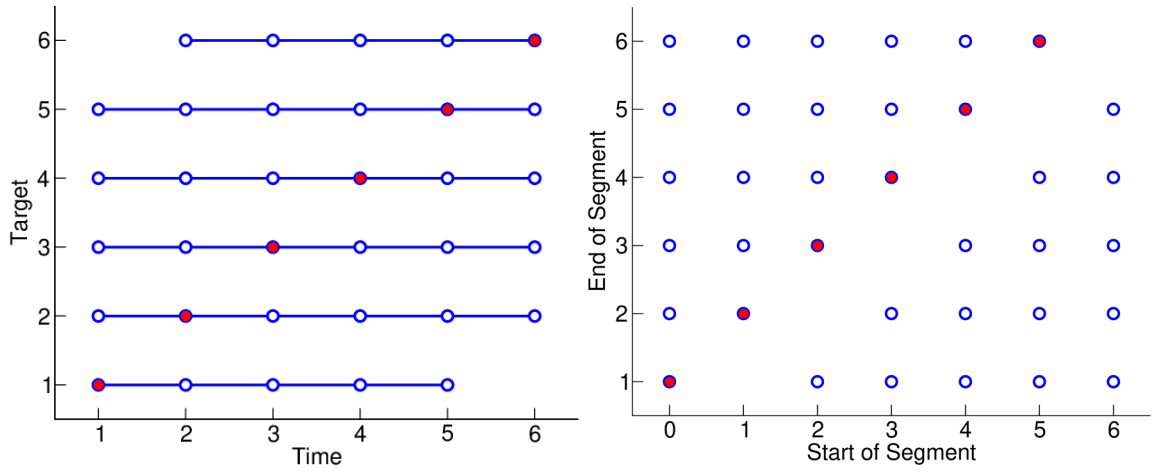

Figure 1. Two encodings and solutions for satellite scheduling. The circles indicate qubits in both figures. Filled red circles show the "on" qubits in the solution. The left panel shows time encoding: The *x*-axis is coarse-grained time, while the *y*-axis indicates the target. The optimal solution images target 1 at time 1, etc. The right panel shows route encoding. Each qubit represents an edge of the graph between starting and ending targets. The route starts with fictitious target 0. There are no edges between identical targets, so the qubits along $x = y$ are missing.

Title: Evaluating the Active Site of Metal-Zeolite Combinations for Selective Catalytic Reactions
Author(s): C.F. Holder,[1] A.R. Shabaev,[1] and J.R. Morse[2]
Affiliations: [1]U.S. Naval Research Laboratory, Washington, DC; [2]Applied Research Laboratory at Penn State University, State College, PA
CTA: CCM

Computer Resources: HPE SGI 8600, HPE Cray EX [AFRL, OH]; HPE Cray EX 4000, Cray XC40/50 [ERDC, MS]; HPE Cray EX [NAVY, MS]

Research Objectives: To provide insights into the adsorption of Pt clusters within zeolites of varying pore sizes. This study is part of the foundational work to investigate Pt clusters imbedded in zeolites for selective organic transformations.

Methodology: We used density functional theory and the projector augmented-wave method as implemented in the Vienna Ab Initio Simulation Package (VASP) to investigate differences in the chemical and physical properties after imbedding eight-atom clusters of Pt into the LTL zeolite archetype. Additionally, VASP simulations also were undertaken to explore the incorporation of Al into the SiO_2 framework to better simulate the typical zeolitic framework.

Results: This study looked at developing models of the LTL zeolite, and initial demonstrations started with a pure SiO_2 framework. The LTL zeolitic framework consists of a one-dimensional array of channels with pore sizes of 7.1 Å. Variations of this silicate model then were undertaken by substituting an Al atom for a Si atom at specific sites. In order to account for the differences in charge between the original Si^{4+} and the incoming Al^{3+}, protons also were included. Four sites were selected, and the resulting energies were compared to each other. The prerelaxed and relaxed models of the Al-substituted zeolite framework are shown in Fig. 1.

Following these initial experiments at developing the base LTL material, a cluster of eight Pt atoms was placed into the pores of the LTL zeolite. These studies were aimed at investigating the charge density differences between the zeolite framework with the substituted Al/H atoms and the Pt cluster. Figure 2 shows the preliminary results of this study, which suggested that the zeolite was transferring electronic charge to the Pt cluster at the cluster/zeolite interface. The next steps of this project will examine the differences in charge transfer to or from the Pt cluster when various zeolite frameworks and alkali metal promoters are present.

DoD Impact/Significance: Pt clusters imbedded into zeolites have attracted significant attention recently for their use as highly active thermocatalysts. The high surface area, the high reactivity of Pt, and the selectivity that can be obtained through appropriate zeolite selection make these materials highly tunable across a wide range of reactions. To enhance carbon utilization further during the process of making sustainable aviation fuel, our group at NRL is interested in utilizing the light end carbons (C4–C8) to produce the necessary aromatics and cyclic compounds needed for fuels such as JP-5.

The work accomplished in the past year using the HPC resources has enabled a better understanding of the Pt/zeolite catalysts that we are synthesizing and testing at the lab scale for the aromatization and cyclization of small-chain hydrocarbons. The foundational work established in the past year will enable a larger sweep of zeolite phase space in FY 25 to help determine the optimal zeolite pore size, Si:Al ratio, and Pt cluster size, and the effects of alkali metal promoters. These results then will help guide synthetic experiments in the lab to narrow in on particular Pt/zeolite combinations that may have promising catalytic activity for cyclization reactions.

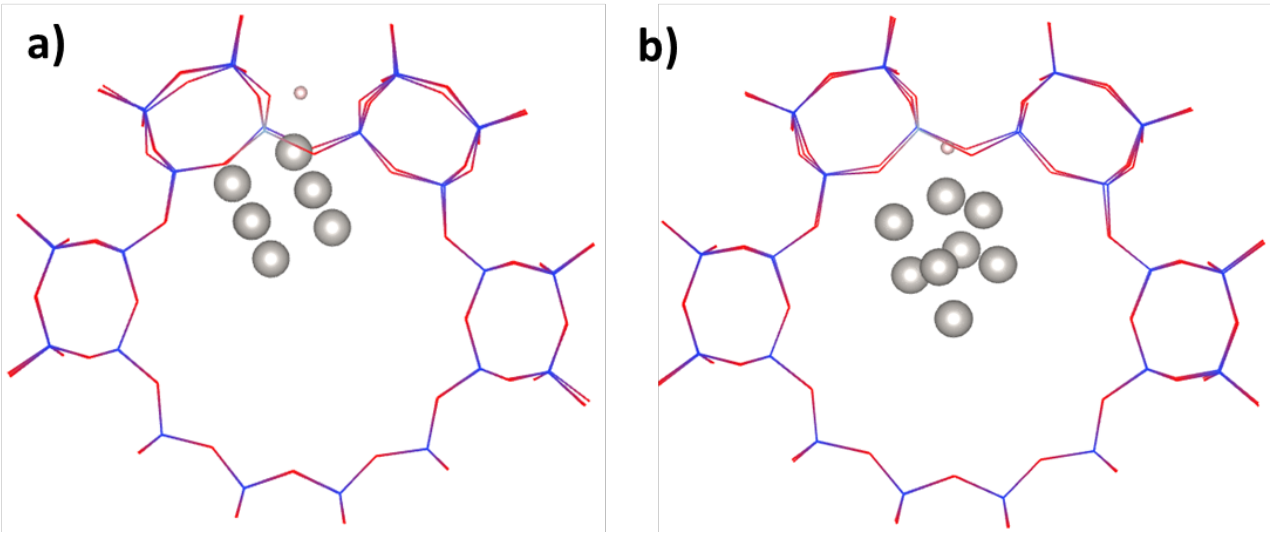

Figure 1. (a) Preconverged and (b) converged Pt clusters placed into the pores of an LTL zeolite, respectively. An Si atom has been replaced with an Al atom and the charge has been compensated for by the addition of an H atom.

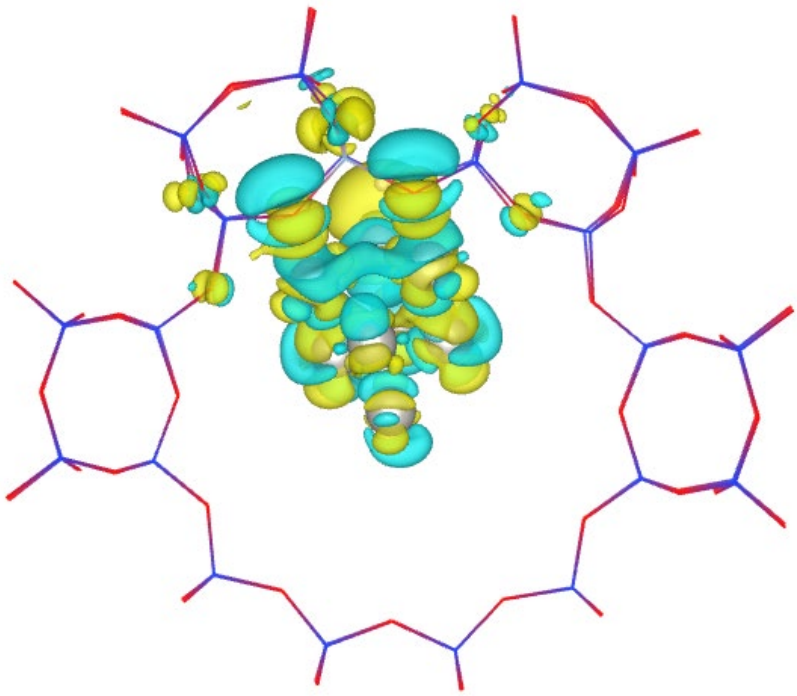

Figure 2. A charge density difference map is shown of the converged Pt/LTL structure, with yellow isosurfaces representing an increase in electron density and blue representing a decrease in electron density.

Title: Target Material Detection by Comparison of Measured and DFT-calculated Absorbance Spectra
Author(s): A.R. Shabaev, C.F. Holder, and S. Lambrakos
Affiliation(s): U.S. Naval Research Laboratory, Washington, DC
CTA: CCM

Computer Resources: HPE SGI 8600, HPE Cray EX [AFRL, OH]; HPE Cray EX 4000, Cray XC40/50 [ERDC, MS]; HPE Cray EX [NAVY, MS]

Research Objectives: The objective of this research is to aid target-material detection by spectroscopy using density functional theory (DFT). Detection methodologies such as infrared (IR) spectroscopy are based on identification of unknown materials by comparison of measured spectra with reference spectra associated with known materials. DFT-calculated IR absorption spectra corresponding to vibrational excitation states of molecular structures provide quantitative estimates of IR spectra that can be correlated with additional information obtained from laboratory measurements or spectra associated with detection in the field.

Methodology: The general methodology adopted for this task element involves DFT calculation of absorption spectra of various prototypical target materials of interest. These materials include, but are not limited to, microporous structures such as zeolites and adsorbate/support structures. Initial prototype materials included simple support structures and metal cluster deposition on zeolites for hydrogenation reactions. Correlation of DFT-calculated absorption with measured IR spectra will provide an interpretation of various spectral features for detection and help to understand and control catalytic reactions.

Results: The DFT calculation of absorption spectra for prototypical target materials of interest coupled with experimentally measured spectra provide an understanding of signature features of various adsorbate/support models. For example, Fig. 1a and 1b depict two different adsorption sites of CO_2 on the surface of Mo_2C, a known catalyst for CO_2 hydrogenation reactions. These relaxed models show various molecules adsorbed onto the surface, including CO_2, CO, and O. The difference in molecular species resulted in unique IR signatures, which are shown in Fig. 1c and d, respectively. These results then will be used to develop next-generation catalysts that leverage these findings to achieve improved catalytic activity and provide interpretation of signature features associated with experimentally measured spectra that are significant for realistic detection problems associated with detection of target materials.

DoD Impact/Significance: The proposed task, which provides a foundation for real-world deliverability of results, is that absorption spectra of major target molecules of interest are to be constructed using existing off-the-shelf software technology, including DFT software such as VASP and GAUSSIAN, as well as existing postprocessing software. Accordingly, it follows that a secondary deliverable of the proposed task element will be more optimal procedures for calculation of response spectra using atomic orbitals basis functions and potential energy functions, which represent the basic information for modeling vibrational spectra using DFT.

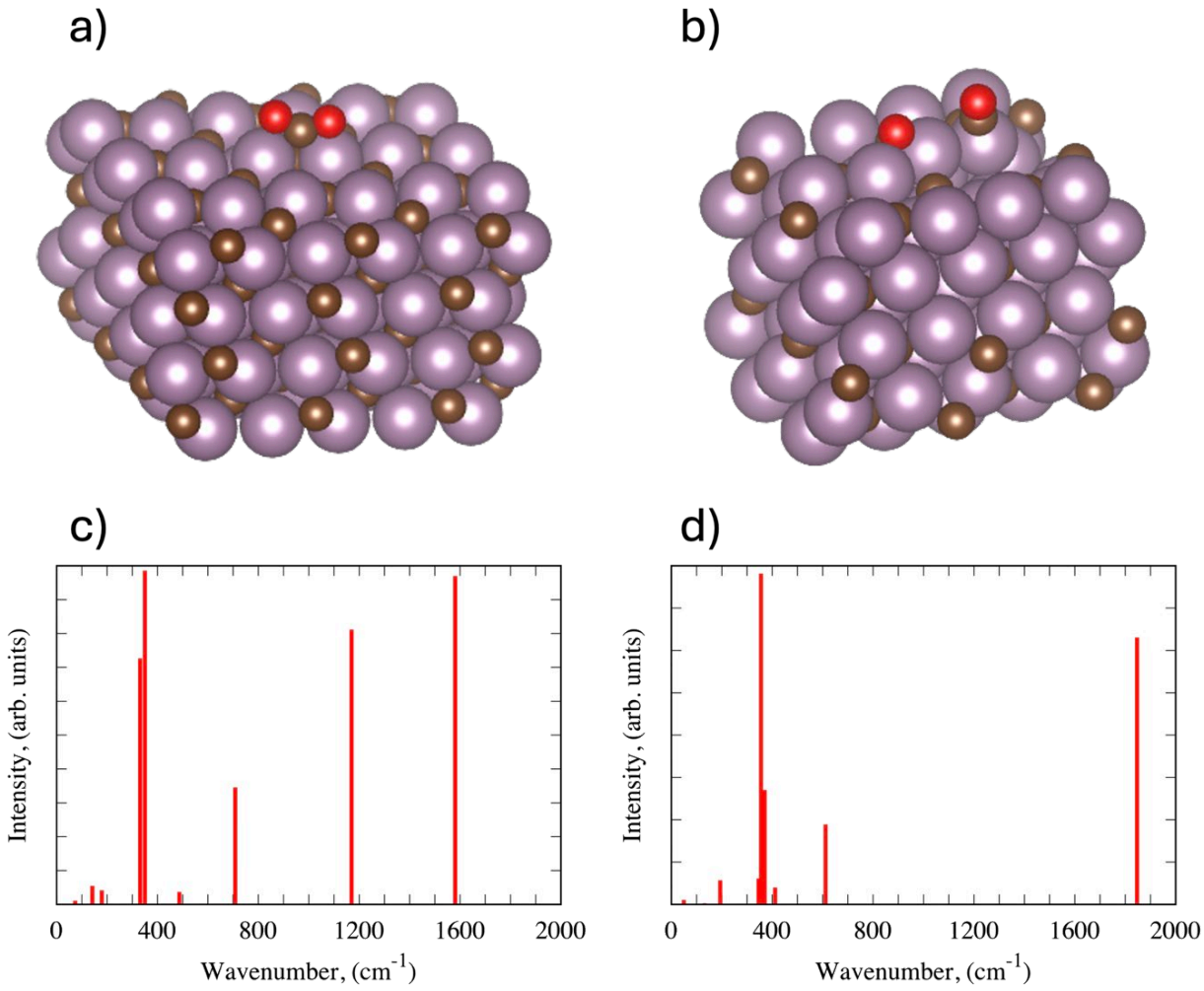

Figure 1. CO_2 molecule on Mo_2C surface at two varying adsorption sites: (a) in a hollow where the CO_2 molecule is adsorbed and bent, (b) atop Mo atoms where an oxygen is detached, forming a separate CO pair. The simulated IR spectra (c and d) of the relaxed geometries then can be used to verify and detect the presence of certain molecular species to determine the pathway of CO_2 adsorption on Mo_2C.

Title: Surfaces and Interfaces in Oxides and Semiconductors
Author(s): C.S. Hellberg
Affiliation(s): U.S. Naval Research Laboratory, Washington, DC
CTA: CCM

Computer Resources: HPE SGI 8600 [NAVY, MS]

Research Objectives: To determine the atomic reconstruction in twisted moiré van der Waals heterostructures and effects of the reconstruction on the electronic structure.

Methodology: First-principles density function calculations of bilayers of two-dimensional (2D) semiconducting transition metal dichalcogenides that are twisted relative to each other were performed. The constituent materials include $MoSe_2$, WSe_2, MoS_2, and WS_2. At certain angles, twisted bilayers form periodic structures that can be modeled with density functional codes; at all other angles, the twisted bilayer is incommensurate. The size of the periodic structures increases with decreasing twist angles; we have performed calculations without spin-orbit coupling of supercells containing up to 3,786 atoms, which corresponds to a twist angle of 2.28 degrees. The layers are bound to each other via the weak van der Waals interaction. We used the VASP density functional theory (DFT) code at the AFRL, NAVY, ERDC, and ARL HPC centers. It is important to converge the atomic positions fully, as the structural relaxation provides the confining potential within the layers due to the intrinsic piezoelectricity of the materials.

Results: The bilayers exhibit localized electronic states below critical twist angles. In this part of the project, we focused on homobilayers, particularly on WSe_2/WSe_2 and WS_2/WS_2, which are more readily constructed experimentally. In general, we found homobilayers develop localized states at smaller twist angles than heterobilayers. For these specific combinations, we find localized electron and hole states in WS_2/WS_2 at twist angles of 3.2 degrees and below. For WSe_2/WSe_2, we find localized hole states at 2.9 degrees and below. The electron states in WSe_2/WSe_2 are not localized at 2.9 degrees, but it appears in the band structure that the states are nearly localized. These calculations are particularly challenging because the spin-orbit coupling doubles the size of the Hamiltonian matrices. In future work, we hope to examine the WSe_2/WSe_2 electron states at the next commensurate twist angle of 2.6 degrees. Interestingly, the states in homobilayers have higher degeneracies than heterobilayers, which may allow them to form superconducting phases more readily. At large twist angles, all relative shifts between the layers are including in the supercell. At small twist angles, this is not the case. To test the effects of relative shifts, we performed calculations at 38.2 degrees, shown in the figure. The changes in the band structures are minimal.

DoD Impact/Significance: Moiré dichalcogenide bilayers are candidates for hosting strongly correlated electrons because the dispersion of the electrons can be tuned by adjusting the angle of the twist. Our results quantify the twist angles at which the electron and hole bands separate from the bulk bands, a signature of strong correlation. In this regime, the ground state of the materials may be Mott-insulating, ferro- or ferrimagnetic, or superconducting. In future work, we will derive the effective interacting Hamiltonians of these systems to examine these instabilities using many-body approaches.

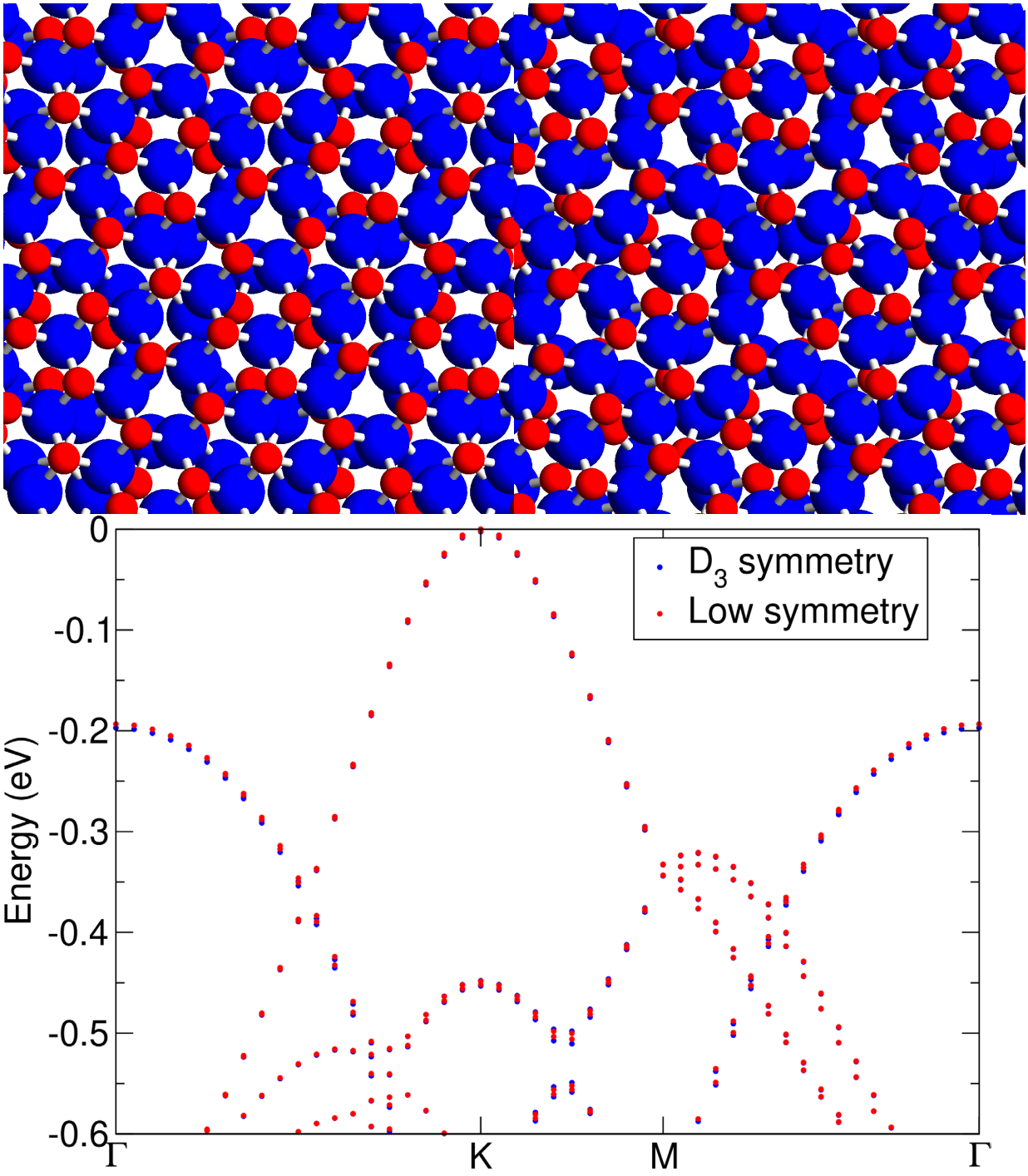

Figure 1. Relaxed atomic positions and band structure of WSe_2/WSe_2 bilayers twisted at 38.21 degrees. The atomic structures are shown in the top. W atoms are red, and Se atoms are yellow. The left structure has D_3 symmetry: notice each moiré cell has one W directly over another W and one pair of Se directly over the Se in the bottom layer. The right structure is twisted at the same angle but has no symmetries. Both computed valence band structures are plotted. The differences are very small. The differences in the conduction bands (not shown) are even smaller.

Title: First-principles Simulations of Condensed-phase Decomposition of Energetic Materials
Author(s): I.V. Schweigert
Affiliation(s): U.S. Naval Research Laboratory, Washington, DC
CTA: CCM

Computer Resources: HPE SGI 8600 [AFRL, OH]

Research Objectives: To predict thermal, chemical, and mechanical properties of molecular crystals, polymers, and molecular compounds of interest to the DoD.

Methodology: We use various methods of quantum chemistry to predict molecular and crystal properties of target materials. Structure optimizations based on density functional theory (DFT) and gas-phase or periodic models are used to determine atomic coordinates and crystal lattice parameters. DFT-derived electronic energies and vibrational frequencies are used to compute thermochemical properties such as formation and reaction enthalpies. Ab initio electron-correlation methods are used to compute accurate electronic energies and to correct the DFT values. Quantum molecular dynamics (QMD) simulations are used to quantify effects of elevated temperatures and pressures on crystal structures as well as to identify possible reaction mechanisms. Infrared absorption (IR) spectra, nuclear magnetic resonance (NMR) shifts, and X-ray photoelectron spectra (XPS) are simulated to enable comparisons with experiments. To facilitate these simulations, we develop automated workflows for preparation of input files, job submission, detection and remediation of errors, and processing and analysis of the simulation results.

Results: This year, we focused on predicting gas-phase bond dissociation enthalpies (BDEs) in molecular nitramines. To eliminate the need to specify target bonds manually for a large number of compounds, we implemented a numerical algorithm that identifies all single bonds in input molecular structures and generates atomic coordinates for the radical fragments that result from breaking these bonds. The generated fragment coordinates are labeled by the parent molecule, the bond type, and the reaction site, and are saved to a database. The in-house workflows then are used to optimize structures for the parent molecules and their radical fragments, to compute vibration frequencies and thermodynamic partition functions, to estimate the formation enthalpies, and to compute the corresponding BDEs. For the initial tests reported here, we extracted all nitramines with eight or fewer non-H atoms from the Pubchem open chemistry database. We further selected compounds that were neutral, were covalently bound, and were found to be stable in preliminary simulations. The BDEs for the resulting 205 molecular nitramines were computed with the G4(MP2) composite ab initio method, which is known to yield reaction enthalpies for various classes of reactions to within 2 kcal/mol of the experimental values. Interestingly, our simulations predict a large range of BDE values in nitramines, from 14 to 54 kcal/mol (Fig. 1a). We analyzed possible correlations between the predicted BDEs and the formation enthalpies (Fig. 1b), N-N bond distances (Fig. 1c), and the atomic environments of the N-N bonds (Fig. 1d), but found no obvious trends. The origins of such large variations in N-N BDEs in nitramines currently are being investigated. We also tested the feasibility of using the M06-2X hybrid DFT method in place of G4(MP2), because the latter has a much lower computational cost (Fig. 1e). We found that M06-2X consistently overestimated the G4(MP2) values (Fig. 1d), with a mean absolute difference of 6 kcal/mol and several values differing by as much as 15 kcal/mol. However, preliminary simulations (not shown here) suggest that using isodesmic reactions to evaluate BDEs with M06-2X can improve the agreement between the two methods significantly.

DoD Impact/Significance: Research completed this year focused on quantum chemical predictions of gas-phase bond dissociation enthalpies in a series of molecular nitramines. The generated values will be used to improve existing machine learning models for predicting reactive properties of nitramine-based explosives. We are also extending the workflow to enable predictions of bond dissociation enthalpies in polymers and high-energy-density molecular crystals of interest to the DoD.

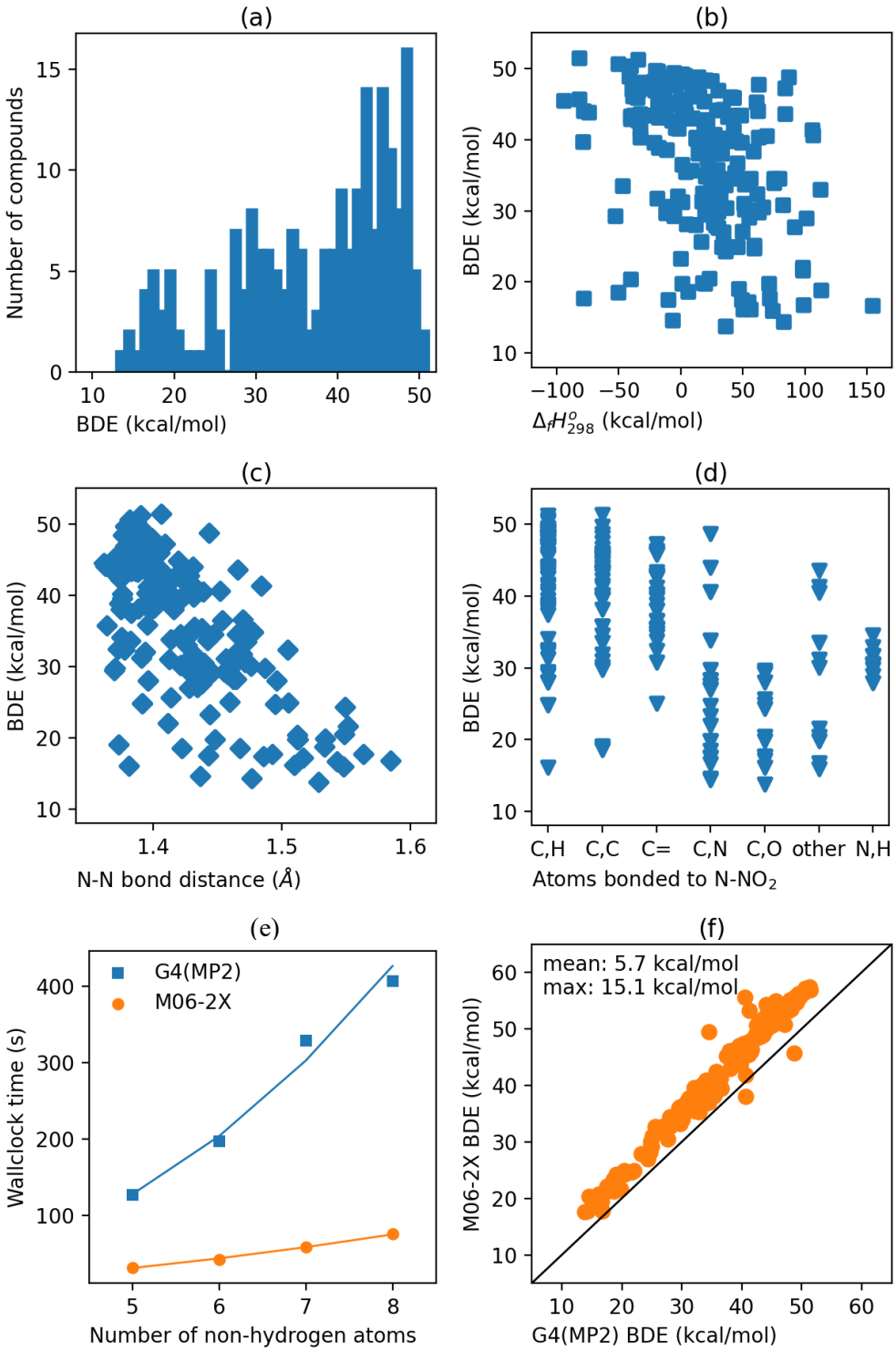

Figure 1. Predicted N-N bond dissociation enthalpies (BDEs) for 205 molecular nitramines: (a) distribution of the BDEs computed with the G4(MP2) composite ab initio method, (b) relation between the BDEs and formation enthalpies ($\Delta_f H^o_{298}$) computed at the same level of theory, (c) relation between the BDEs and N-N bond distances, (d) relation between the BDEs and the atomic environments of the N-N bonds, (e) wall-clock times for the BDE calculations with G4(MP2) and the M06-2X hybrid DFT method, (f) relation between the BDEs computed with G4(MP2) and M06-2X.

Title: Marine Biofilm Metaproteomics
Author(s): W.J. Hervey, M.R. Kardish, and G.J. Vora
Affiliation(s): U.S. Naval Research Laboratory, Washington, DC
CTA: CCM

Computer Resources: HPE SGI 8600, Penguin Open Compute Platform (OCP) [AFRL, OH]; HPE Cray EX 4000 [ERDC, MS]; Penguin TrueHPC [NAVY, MS]

Research Objectives: To maintain and update data analysis workflows for large-scale multiomics analytics, namely metagenomics and metaproteomics. Previous investments in distributed bioinformatics software development via the HPC Application Software Initiative (HASI) have enabled large-scale characterization of biological samples from complex environmental matrices, such as marine biofilms and other substrates of interest. In FY24, we updated resources and tools available for both metagenomic and metaproteomic analyses of complex environmental matrices.

Methodology: In FY24, updates were made to the available software tool sets applied to metagenomic and metaproteomic workflows. Metagenomic resources leveraged reproducible workflows to assemble raw sequence data, to annotate resulting assemblies, and to bin representative members of microbiomes. New tools deployed in FY24 were used to infer the composition of microbiomes distributed on marine substrates of interest. Existing software tools used for metaproteome analyses were benchmarked across a multilaboratory proteomics study targeting ocean metaproteomic filter samples.

Results: Metagenomic profiling results across marine substrates of interest are shown in Fig. 1. Across two disparate substrates, no significant differences were observed in terms of composition (via 16S profiling, Fig. 1a) or richness (Fig. 1b). Across both substrates, 119 metagenome assembled genomes (MAG) were profiled using the ATLAS pipeline [1]. For this sample, the profile was dominated by α- and γ-proteobacteria. Results of the multilaboratory ocean metaproteomic intercomparison study assessed results across eight disparate software workflows that used field-standard applications for peptide-spectrum matching. A consensus of more than 2,300 core peptides was identified across four labs participating in the study [2]. Deeper trends were not straightforwardly apparent due to the range of different applications used across labs.

DoD Impact/Significance: This HPC subproject has broad significance across both the Naval Research Enterprise (NRE) and larger DoD enterprise. Our subproject's general workflow for metagenomics and metaproteomics is applicable to the Navy focus area of "Sensing and Sense-Making" from large data. Biotechnology is listed as a seed area of emerging opportunity by OUSD(R&E) and is a Reliance 21 Community of Interest.

References

[1] Kieser, S., Brown, J., Zdobnov, E., Trajkovski, M., and McCue, L. A., ATLAS: a snakemake workflow for assembly, annotation, and genomic binning of metagenome sequence data. In: BMC Bioinformatics, 2020, vol. 21, n° 1, p. 257. doi: 10.1186/s12859-020-03585-4
[2] Saito, M. A., Saunders, J. K., McIlvin, M. R., Bertrand, E. M., Breier, J. A., Brisbin, M. M., Colston, S. M., Compton, J. R., Griffin, T. J., Hervey, W. J., Hettich, R. L., Jagtap, P. D., Janech, M., Johnson, R., Keil, R., Kleikamp, H., Leary, D., Martens, L., McCain, J. S. P., Moore, E., Mehta, S., Moran, D. M., Neibauer, J., Neely, B. A., Jakuba, M. V., Johnson, J., Duffy, M., Herndl, G. J., Giannone, R., Mueller, R., Nunn, B. L., Pabst, M., Peters, S., Rajczewski, A., Rowland, E., Searle, B., Van Den Bossche, T., Vora, G. J., Waldbauer, J. R., Zheng, H., and Zhao, Z.: Results from a Multi-Laboratory Ocean Metaproteomic Intercomparison: Effects of LC-MS Acquisition and Data Analysis Procedures, EGUsphere [preprint], https://doi.org/10.5194/egusphere-2023-3148, 2024

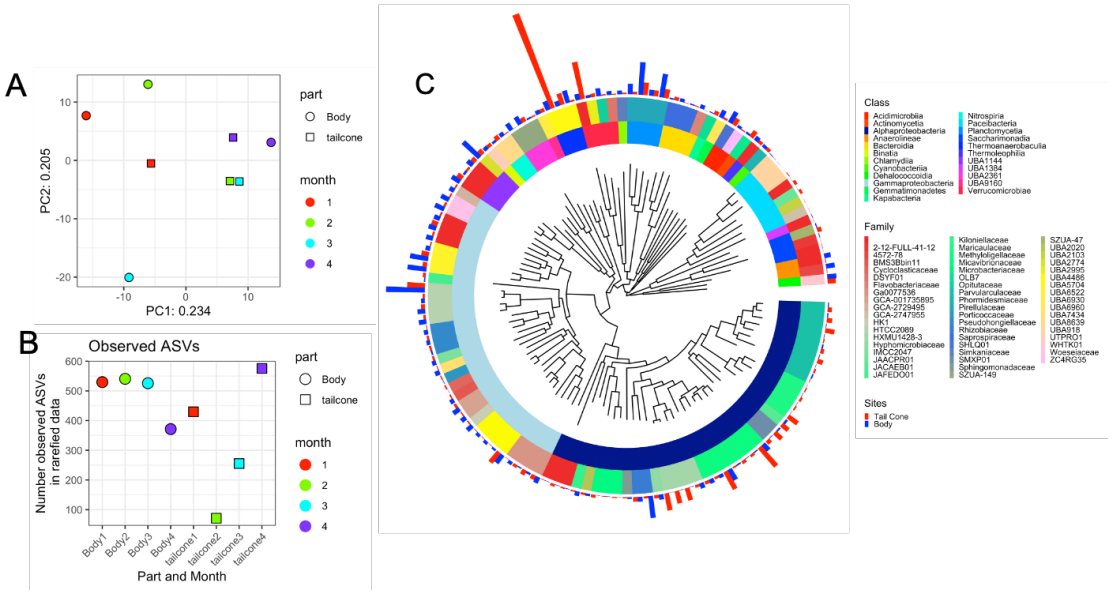

Figure 1. Metagenomic profiling of marine substrates by ATLAS. (A) Principal component analysis between 16S profiles from the two marine substrates. (B) Observed richness between the two marine substrates. (C) Metagenome assembled genomes (MAGs) of one microbiome time point. Metagenome sequencing reads from 199 MAGs were represented largely by α-proteobacteria species (dark blue, outer circle) and γ-proteobacteria species (light blue, inner circle) in the metagenome profile.

Title: Synthetic Biology for Military Environments
Author(s): W.J. Hervey and G.J. Vora
Affiliation(s): U.S. Naval Research Laboratory, Washington, DC
CTA: CCM

Computer Resources: HPE SGI 8600, Penguin Open Compute Platform (OCP) [AFRL, OH]; HPE Cray EX 4000 [ERDC, MS]; Penguin TrueHPC [NAVY, MS]

Research Objectives: To engineer and deploy synthetic biology tools for biomaterials production. Routinely, biotechnology and synthetic biology research leverage knowledge of model genomic species, such as the bacterium *E. coli*, the yeast *S. cerevisiae*, and the fly *D. melanogaster*. Though tremendous amounts of knowledge have been accrued for each of these model genomic species, previous background may not be extensible to emerging synthetic biology chassis or targeted organisms. Here, we have applied the synthetic biology "design, build, test, learn" (DBTL) paradigm to measurements of species of interest for novel biological insight.

Methodology: In FY24, DBTL paradigm foci (Fig. 1) included proteome profiling in the "test" phase and resulting signal intensities in the "learn" phase. In the "test" phase, proteome profiling, or other -omics-level measurement (e.g., genomics, transcriptomics, and/or metabolomics) can be performed on entire biological systems of interest. A high-level overview of the large-scale measurement's features, such as signal intensity, yields input that can drive the "learn" phase and iterative feedback into subsequent DBTL cycles.

Results: In FY24, large-scale genomic and proteomic measurements were performed on emerging species of interest in synthetic biology and biotechnology. FY24 allocations were leveraged to assist with genome sequencing of *Serratia sp.* from PFAS-impacted soil [1] and proteome profiling of *A. amphitrite* organic matrices [2].

DoD Impact/Significance: This HPC subproject has broad significance across both the Naval Research Enterprise (NRE) and the larger DoD enterprise. Insights from actionable biological data are applicable to the Navy focus area of "Sensing and Sense-Making" from large data. Biotechnology is listed as a seed area of emerging opportunity by OUSD (R&E) and is a Reliance 21 Community of Interest.

References

[1] Baker, I. R., Matzen, S. L., Schuler, C. J., Toner, B. M., and Girguis, P. R. (2023). Aerobic iron-oxidizing bacteria secrete metabolites that markedly impede abiotic iron oxidation. *PNAS nexus*, *2*(12), pgad421
[2] Schultzhaus, J., Hervey, J., Fears, K., and Spillmann, C. (2024). Proteomic comparison of the organic matrices from parietal and base plates of the acorn barnacle Amphibalanus amphitrite. *Open Biology*, *14*(5), 230246

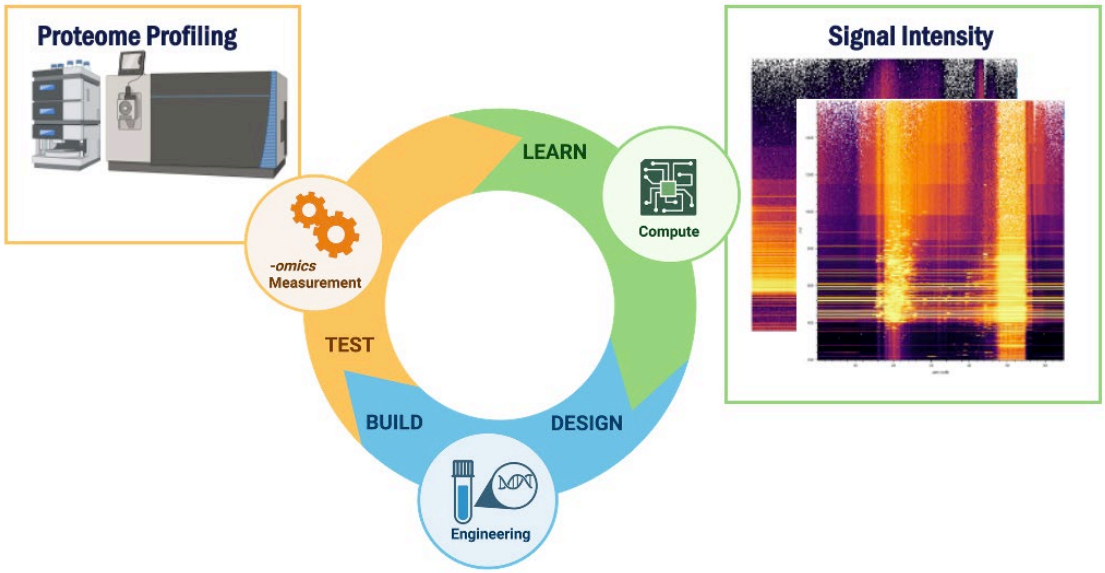

Figure 1. Synthetic biology “design, build, test, learn” (DBTL) paradigm. The test phase of the DBTL paradigm can be assessed by a number of -omics level measurements. Here, proteome profiling is shown as the representative measurement to evaluate output of the design and build phases. In the learn phase, representative data features from the -omics measurement, in this case signal intensity, provide primary feedback that may guide subsequent cycles or iterations of the DBTL paradigm.

Title: Atomistic Simulations of Navy-relevant Materials
Author(s): D. Fragiadakis
Affiliation(s): U.S. Naval Research Laboratory, Washington, DC
CTA: CCM

Computer Resources: HPE Cray EX, Penguin TrueHPC [NAVY, MS]; Penguin Open Compute Platform (OCP) [AFRL, OH]

Research Objectives: The objective of the work conducted was to determine the most favorable reaction pathways for the crosslinking of a series of novel phthalonitrile-based high-temperature resin systems.

Methodology: Structures of the relevant chemical species and transition states were optimized using density functional theory calculations at the M06-2XD3/def2-TZVPP level of theory. Reactants and products connected by each transition state were verified using intrinsic reaction coordinate computations. The Gaussian 16 software package was used to conduct the calculations on HPCMP resources, with in-house software for data analysis.

Results: The reactions of phthalonitrile (PN) with each of three model molecules at a temperature of T = 533K were investigated. Variants of these structures are being synthesized and studied experimentally at NRL and are expected to follow similar reaction pathways. The key results are summarized below.

N,N'-4,4'-diphenylmethane-bismaleimide (BMI): The most favorable pathway begins with a reaction between two the maleimide moieties on two BMI molecules to form a biradical, similar to what has been observed in the self-initiated polymerization of maleimide. Each radical site is able to attach to either the carbon or the nitrogen of a phthalonitrile -CN group, which then can promote attachment of additional phthalonitrile molecules (with or without closure of an isoindoline ring) to form either a triazine structure, a linear polymer, or a cyclic tetramer. Alternatively, a hydrogen atom transfers from the central methyl of the bismaleimide onto the biradical; the resulting diphenylmethyl radical also can promote phthalonitrile polymerization, though less readily.

N,N'-4,4'-diphenylmethane-bis(2-methyl)maleimide (MBMI): This differs from the above only in having a methyl group attached to the maleimide moiety. Here, there are two pathways with similar activation free energies. The first begins with two MBMI molecules that combine to form a dimer with a 2-methylene-succinimide moiety. A nitrile then can add to the C=C bond in the latter, yielding a primary imine. PN polymerization reactions then can proceed in an analogous manner to those in amine-catalyzed phthalonitriles. The second pathway begins with an ene reaction between a nitrile group and the 2-carbon atom on the 2-methyl-maleimide group, forming the primary imine directly and proceeding from there in a way similar to the first pathway.

N-Cinnamylideneaniline (NCA): The curing reaction between NCA and PN is particularly complex, with several pathways of relatively similar activation free energies. However, the reaction step that initiates PN polymerization appears to begin with a Diels-Alder reaction between two NCA molecules to form a dimer consisting of a central tetrahydropyrimidine ring with one phenylethenyl and three phenyl substituents. PN polymerization then can initiate via an ene reaction of a CN group with the double bond in the phenylethenyl and then proceed as described above.

DoD Impact/Significance: The results of this study contribute to the understanding of the fundamental mechanisms of curing chemistry in complex phthalonitrile-based systems, which will enable rational design of novel resins and reaction conditions to tailor structure and properties to DoD applications.

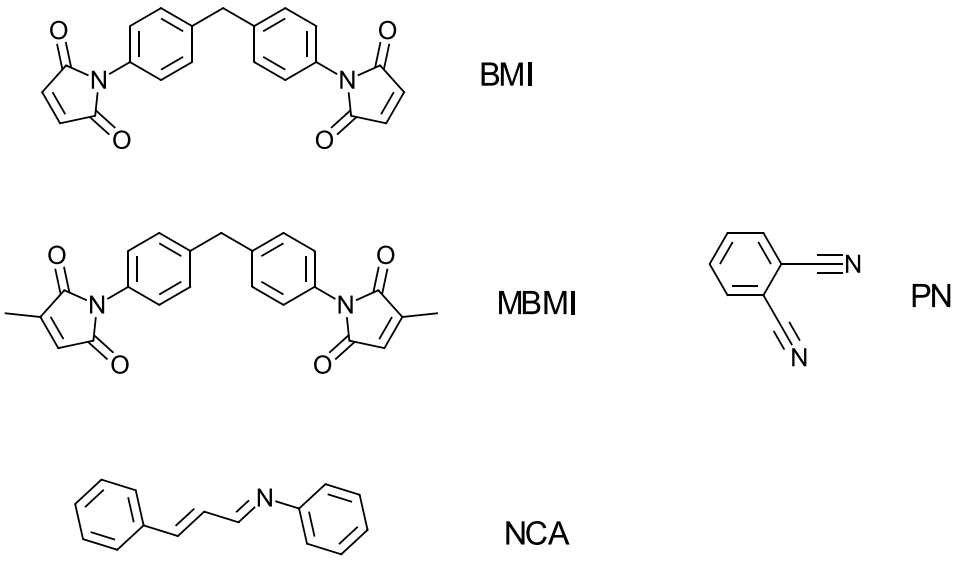

Figure 1. Chemical structures of the monomers studied.

THIS PAGE INTENTIONALLY LEFT BLANK

CEA

Computational Electromagnetics and Acoustics

CEA covers two primary computational disciplines. Computational electromagnetics covers the high-resolution multidimensional solutions of Maxwell's equations. DoD applications include calculating radio frequency (RF) sensor performance, radar scattering of tactical ground, air, and sea vehicles, the electromagnetic signature of buried munitions, high-power microwave performance, and the interdisciplinary applications in magnetohydrodynamics and laser systems. The computational acoustics area covers the high-resolution multidimensional solutions of the acoustic wave equations in solids and fluids. DoD applications include the modeling of acoustic fields for surveillance and communication, seismic fields for mine detection, and the acoustic shock waves of explosions for antipersonnel weapons.

Title: Low Grazing Angle Radar Backscatter
Author(s): J.V. Toporkov, M.A. Sletten, and J.D. Ouellette
Affiliation(s): U.S. Naval Research Laboratory, Washington, DC
CTA: CEA

Computer Resources: Penguin Open Compute Platform (OCP), HPE Cray EX [AFRL, OH]; HPE Cray EX 4000, Cray XC40/50 [ERDC, MS]; HPE Cray EX, Penguin TrueHPC [NAVY, MS]

Research Objectives: Reflections from the sea surface are observed in many radar systems operating in the ocean environment, often under low-grazing-angle (LGA) setting. They may be perceived as clutter that masks a target return, but they also can carry information about local ocean conditions. Understanding the properties of sea scatter, their dependence on environmental parameters, and how they differ from those of man-made target echoes is key to improving or even enabling performance of such radar systems and applications. This project studies detailed characteristics of radar returns from the ocean surface under both monostatic and bistatic observation geometries. The task is accomplished through simulations that involve both direct numerical solution of the scattering problem and, where suitable, numerical implementations of approximate scattering models.

Methodology: The approach combines a physics-based model for an evolving ocean surface with computationally efficient evaluation of the scattered electromagnetic field. The most rigorous implementation is limited to the two-dimensional (2D) space but is relevant for commonly occurring three-dimensional (3D) geometries (e.g., oncoming or receding long-crested waves). A wind-driven surface is represented by realizations of a Gaussian random process defined by a certain wave spectrum. Hydrodynamic nonlinearities and associated wave-wave interactions are modeled via Creamer transformation. This affects shape and motion of smaller ripples that have great impact on scattering of decimeter- and centimeter-scale electromagnetic waves. The field scattered by a "time-frozen" scene at a particular frequency is found by iteratively solving a boundary integral equation (BIE) for the induced surface current. This first-principles formulation automatically accounts for many phenomena (multiple scattering, shadowing) that could be problematic for analytical treatment. The 3D code implementation thus far relies on the small-slope-approximation (SSA) scattering model in lieu of the exact BIE-based solver. The calculations can be run at many frequencies covering a certain band to simulate pulse scattering. The procedure is repeated for every surface profile in the sequence representing temporal evolution. OpenMP parallelism is used.

Results: We have focused on developing and testing the 3D scattering model based on the state-of-the art ocean wave spectrum by P. Hwang and the second-order small slope approximation. At present, the accepted way to relate the normalized radar cross section (NRCS) to the near-surface wind speed has been through the empirically derived geophysical model functions (GMFs). Those are based on the data of a particular sensor and are limited to that sensor's frequency and viewing geometry. The developed model should overcome those limitations. Figure 1 shows the NRCS predictions from the model at L band (24 cm). Comparisons with the "measured data" from two GMFs are also shown and generally demonstrate superior agreement. The source of minor discrepancies (more noticeable in Fig. 1 for the crosswind radar look) were investigated further. Those seem to reflect continuing uncertainty in the directional spreading functions adopted in the ocean spectrum model. There are a number of proposed versions, as shown in Fig. 2 (our initial model used the Donelan-Plant angular spread). A detailed look at the azimuth dependencies of the NRCS (Fig. 3a) shows that while the differences are minor, they can be conceptually significant (e.g., the downwind NRCS not exceeding the crosswind NRCS). Figure 3b gives a broader picture by examining crosswind-to-downwind NRCS ratios for different models. Apparently, the Du spreading function results in the best match.

DoD Impact/Significance: The efforts under this project contribute to improving the Navy's ability to assess and predict fleet sensor performance through the development and integration of advanced model physics.

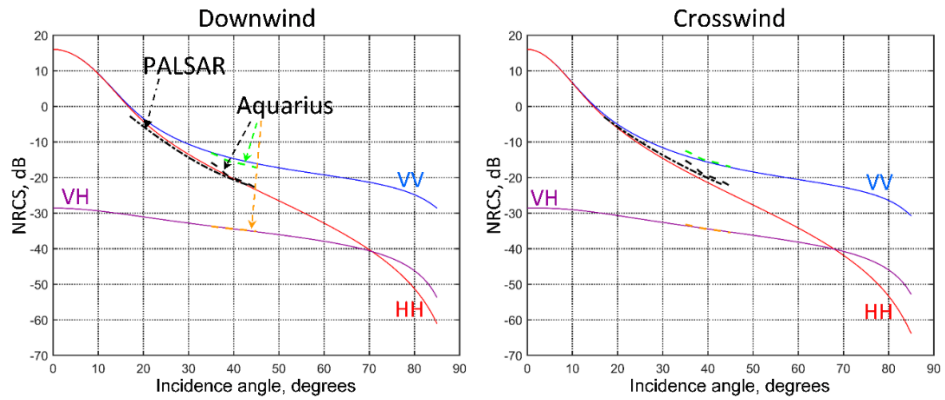

Figure 1. Backscattered normalized radar cross sections calculated at L band for 7 m/s wind. The measurements in form of geophysical model functions for PALSAR and Aquarius sensors show good agreement. Hwang sea spectrum with Donelan-Plant spreading function were used in the calculations.

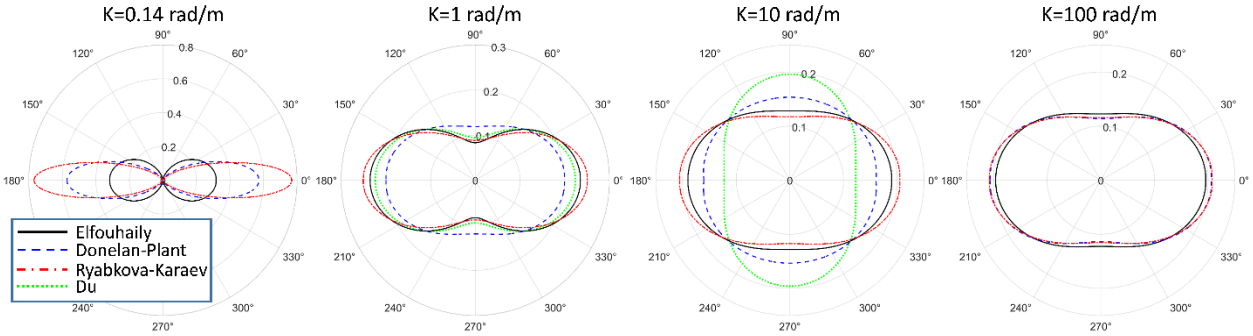

Figure 2. Sample contours of the spreading functions considered in this study evaluated for the wind speed of 7 m/s (the left panel corresponds to the spectral peak wavenumber).

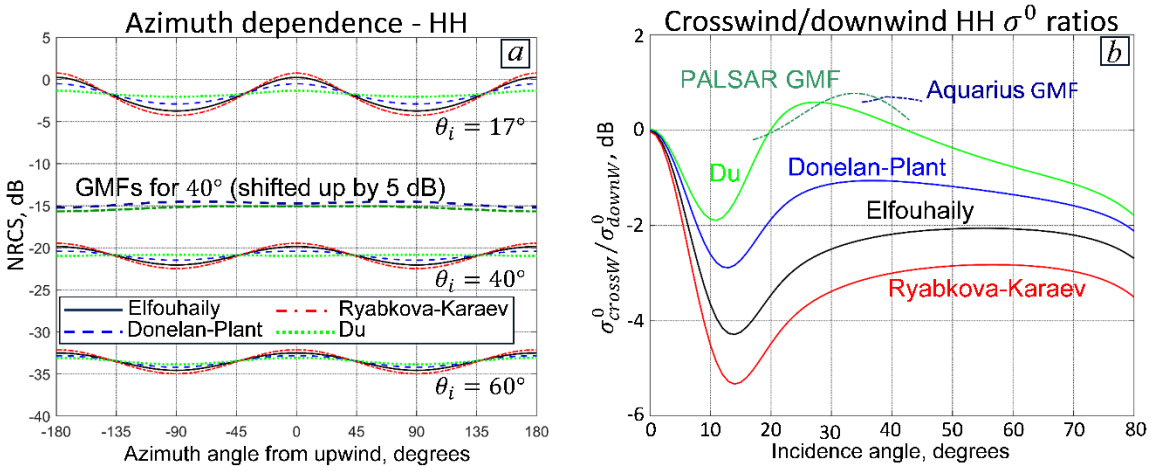

Figure 3. a) Azimuth dependence of the simulated normalized radar cross section for 7 m/s seas for different spectral spreading functions. b) Impact of the choice of the spreading function on the crosswind/downwind ratio of the calculated NRCS for wide range of incidence angles.

Title: Acoustic Parameter Variability over an Ocean Reanalysis (AVORA)
Author(s): B.A. Melzer
Affiliation(s): U.S. Naval Research Laboratory, Stennis Space Center, MS
CTA: CEA

Computer Resources: HPE SGI 8600, HPE Cray EX, Penguin TrueHPC [NAVY, MS]

Research Objectives: Translating ocean fields to acoustically significant parameters is important in the development of products to support Navy operations. Likewise, the advancement of geophysical products to characterize the environment along the seafloor requires extensive data processing and testing. The objectives of this effort are to analyze these environments and to develop tools and prototypes to increase the capabilities of acoustic modeling in the ocean and seabed environments.

Methodology: Develop techniques to identify acoustically sensitive environments from ocean reanalyses and global seabed models that can inform a user of the optimal acoustic simulations to compute for real-world applications and scenarios. Analyze decades of ocean reanalysis to develop products that quantify the variability of acoustic properties on different time scales across multiple regions and areas of interest within each region. Investigate differences in acoustic simulations initialized with various model configurations and observational datasets.

Results: We moved subsets of the global Hybrid Coordinate Ocean Model (HYCOM) reanalysis output to local machines through the transfer queue for use in several projects, including model evaluation, data assimilation, and acoustic parameter characterization. Using these HYCOM subsets, we analyzed the spatial/temporal scales on which HYCOM sound speed profiles change over multiple geographic study areas. We ran acoustic simulations with both forecast and reanalysis data to assess further the impacts of forecast uncertainty on propagation pathways. Steps were taken in conjunction with the HPCMP PET program to transition existing code from the decommissioned systems, Gaffney and Koehr, to the architecture of Narwhal and Nautilus.

DoD Impact/Significance: “In Joint Vision 2020, the Department of Defense’s strategic plan to ensure battlespace dominance in the 21st century, a key element is information superiority enabled by emerging technologies ...” “An important aspect of information superiority is situational awareness. This implies knowing where you are, where allied and coalition forces are and where enemy forces are. It means understanding the environment, from the sea floor to the top of the atmosphere.” [Heart of ForceNet: Sensor Grid, Advanced Command and Control By RADM Steven J. Tomaszeski]. Our efforts directly inform environmental variability as it applies to acoustics.

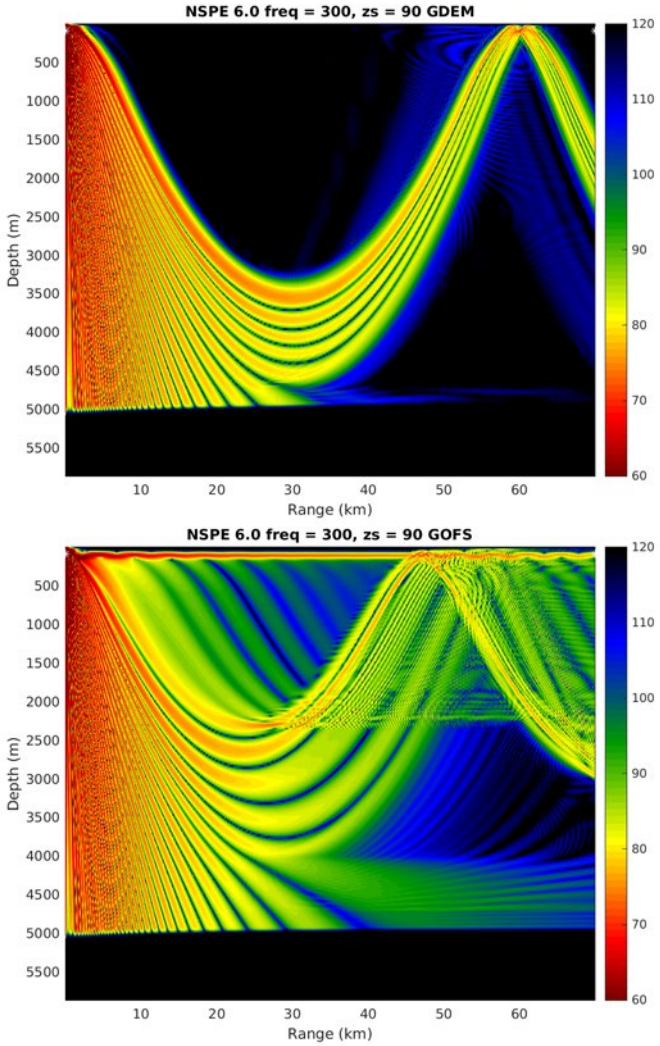

Figure 1. Simulated acoustic transmission loss (dB) along a 70 km radial from a 300 Hz source at 90 m depth from (top) GDEM (climatology) sound speed fields, and (bottom) Global Ocean Forecast System (GOFS) sound speed fields. Warm colors indicate stronger sound signals.

Title: Computer-Aided Design of Vacuum Electronic Devices
Author(s): G. Stantchev,[1] S. Cooke,[1] J. Petillo,[2] A. Jensen,[2] and S. Ovtchinnikov[2]
Affiliation(s): [1]U.S. Naval Research Laboratory, Washington, DC, [2]Leidos, Tewksbury, MA
CTA: CEA

Computer Resources: HPE Cray EX 4000 [ERDC, MS]; HPE SGI 8600 [NAVY, MS]

Research Objectives: 1) Continue to improve the Leidos MICHELLE charged-particle-beam optics code, the NRL TESLA, NEPTUNE and CHRISTINE large-signal codes, and the new Leidos COMPASS design environment that works with the AFRL Galaxy Simulation Builder (GSB) to take advantage of DoD HPC hardware and software enabling significantly larger high-fidelity simulations, optimizations, and sensitivity studies. 2) Further reduce simulation runtimes and boost user productivity in the design and development of vacuum electronic components and systems of interest to DoD. 3) Employ the new capability in the design of next-generation vacuum electronic components with optimized performance.

Methodology: The MICHELLE/xVoyager code has been extended to a flexible, heterogeneous computing framework that can be deployed on distributed memory HPC clusters and includes support for accelerators such as multicore CPUs and graphics processing units (GPUs). Also developed are several high-level interfaces to existing DoD HPC mesh generation, visualization, and simulation environments and productivity tools included in the pipeline of HPC-based optimizations. The new Leidos COMPASS user design environment has been extended to transition the user from the initial design phase of building parametric CAD models and single simulations for early scoping to the optimization phase, allowing optimized parameter sets to be built, providing the backbone for the HPC GSB/DAKOTA optimization.

I. **Exploitation of heterogeneous computing architectures:** Leveraging existing and emerging DoD HPC architectures with distributed memory HPC clusters and multicore CPUs and GPUs.
II. **Integration into the existing DoD HPC ecosystem:** This includes the DoD CAPSTONE CAD/Mesh generator (CREATE-FT), and DoD HPC tools including AFRLs GSB, and Kitware's ParaView visualization software, available and supported through the DAAC.

In pursuit of the above objectives, we develop the software capabilities enabling the Leidos/NRL team to bridge the software gap faced in design and commissioning of advanced vacuum electronics components.

Results: The focus of the project during FY24 has been on continuing the integration of the HPC version of MICHELLE and the other NRL physics codes as well as the integration with HPC productivity tools. Figure 1 shows an advanced COMPASS optimization of an electron gun. The beam diameter and current are optimized, and most importantly, the beam scalloping is minimized. The optimization is being used to develop optimization techniques for running COMPASS on the HPC. Figure 2 shows an application of an object traveling through the ionosphere in low Earth orbit (LEO). The application uses the MICHELLE code to model the ions impacting and flowing around the object, where the electrons are included using a Boltzmann relation for the charge density. This is an excellent model when the object is large compared to the electron Debye length and is fully self-consistent, and with streaming ions impacting the object, a plasma sheath forms around it. The figures show on the upper left the object in green and the self-consistent electron charge density that results. The ion trajectories are shown in the upper-right-hand figure. The particles witness an almost vertical magnetic field of Earth, locking the motion of electron trajectories to spiral around the field lines. The lower-left figure shows electrons entering the bottom and either going past the object (green) or impacting the plasma sheath around the object and returning to the bottom (red/blue). The close-up figures bottom right show the electrons impacting the object.

DoD Impact/Significance: This development has impacted several DARPA, ONR, IARPA, AFRL and NRL programs in vacuum electronics by providing the ability to perform rapid analysis and optimization of mission-critical vacuum electron devices, previously deemed intractable via state-of-the-art methods.

Acknowledgment: This research is based upon work supported in part by the Office of the Director of National Intelligence (ODNI), Intelligence Advanced Research Projects Activity (IARPA), via 2023-23060200005. The views and conclusions contained herein are those of the authors and should not be interpreted as necessarily representing the official policies, either expressed or implied, of ODNI, IARPA, or the U.S. Government. The U.S. Government is authorized to reproduce and distribute reprints for governmental purposes notwithstanding any copyright annotation therein.

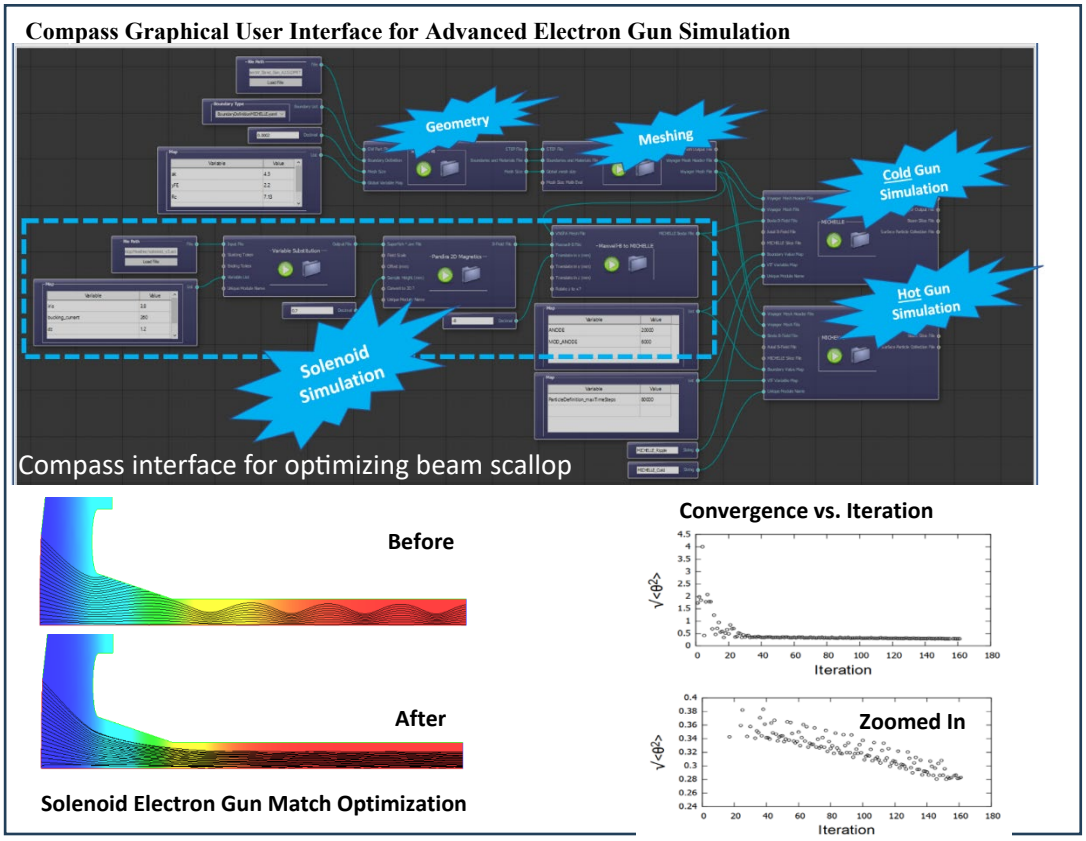

Figure 1. DoD high-performance computing (HPC) for vacuum electronics and space plasmas

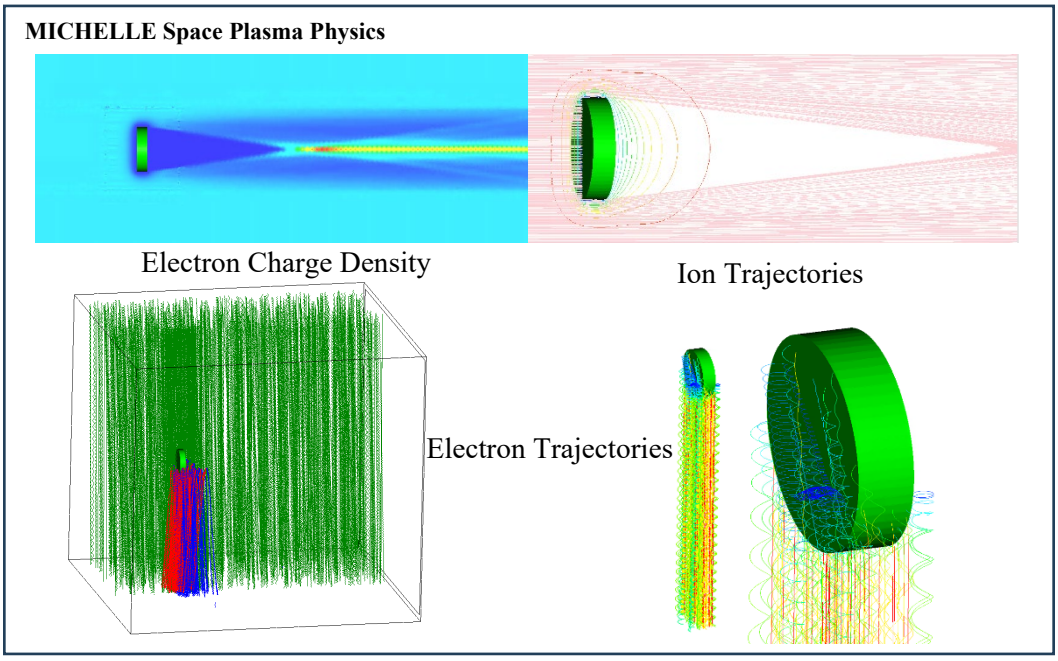

Figure 2. An application of an object traveling through the ionosphere in low Earth orbit

Title: Particle-In-Cell Simulations of Two Cylindrical Reflex Triodes in Parallel
Author(s): I.M. Rittersdorf, B.V. Weber, S.B. Swanekamp, and D.D. Hinshelwood
Affiliation(s): U.S. Naval Research Laboratory, Washington, DC
CTA: CEA

Computer Resources: HPE SGI 8600, HPE Cray EX, Penguin TrueHPC [NAVY, MS]

Research Objectives: The CRT is a bremsstrahlung diode that is notable for its ability to create low-endpoint X-ray spectra useful for radiation-matter interaction studies. The primary objective of this research is to perform particle-in-cell (PIC) simulations that can predict the X-ray output of multiple cylindrical reflex triodes (CRTs) either in series or in parallel.

Methodology: PIC simulations of two CRTs in parallel were performed in a two-dimensional (2D) cylindrical geometry using the code Chicago. The simulation was driven by a voltage waveform as measured on an experiment performed on NRL's Gamble II pulsed-power generator. During the pulse, currents are sufficiently large that the electrons are magnetically insulated from the anode. Electrons travel to the anode tip and scatter through the foil multiple times, creating bremsstrahlung radiation as they do so. PIC simulation lists of scattering electrons are output to be used as inputs for the 2D radiation transport code Cyltran to predict X-ray outputs.

Results: Figure 1 shows electron densities from each CRT near the peak power of the pulse. The current is magnetically insulated from the anode and, instead of flowing directly across the anode-cathode gap, the flow of current is swept down toward the tip of the anode foil (downstream). As the electrons connect with the anode foil, they scatter through because the foil is so thin and create X-rays via bremsstrahlung. The electrons scatter in the foil multiple times, a process known as reflexing, and as they do so, they travel in the negative-z direction (upstream). Figure 1 shows coupling of the CRTs with electrons emitted from the outer (inner) CRT ending up in the inner (outer) CRT. Figure 2 shows two electron test orbits during the peak power of the pulse. These test orbits verify that coupling is occurring in the simulations. The blue electron orbit travels to the end of the anode foil and then it reflexes back up the foil. The red electron orbit travels to the inner anode foil. Scattered electrons in the foil are logged and used as inputs to Cyltran, a 2D radiation transport code. Figure 3 shows the resultant X-ray dose as a function of radius at a test plane downstream of the source. The blue curve is the Cyltran calculation and the red points are measurements from the experiment. Figure 3 shows that the simulation and the experiment are in good agreement. There is a 10% underprediction by the code on axis (r = 0 cm). The source of this underprediction is not yet understood and is an area of future computational study. Figure 3 also shows the X-ray output from a simulation in which the two CRTs were isolated and shows a reduction in the dose in the absence of coupling.

DoD Impact/Significance: The simulations described here show that 2D simulations of two CRTs connected in parallel offer good X-ray output predictive capabilities. This technique then can be used to inform future simulations and experimental studies to increase the X-ray performance of such devices.

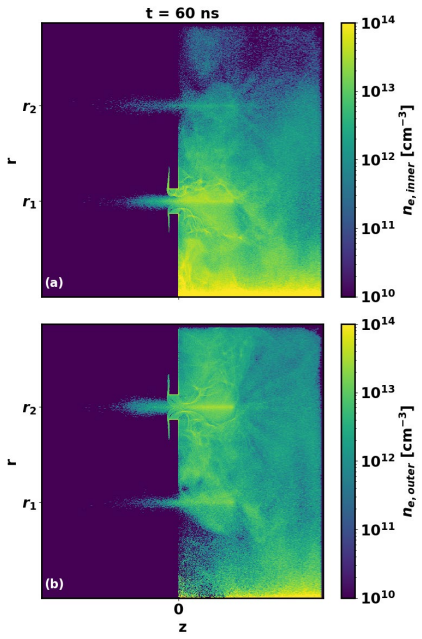

Figure 1. Densities for electrons emitted from the inner and outer cathodes at time t = 60 ns, a time that is near the peak power of the pulse. In each image, electrons emitted from one triode can be found in the other triode, offering evidence of coupling.

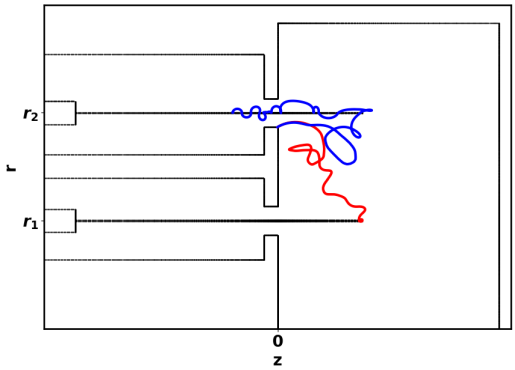

Figure 2. Two test particle orbits released from the same outer cathode location at different times near the peak of the pulse. The test particle orbits show that coupling between the triodes is happening. The blue electron orbit travels to the end of the anode foil and then it reflects back up the foil. The red electron orbit travels to the inner anode foil.

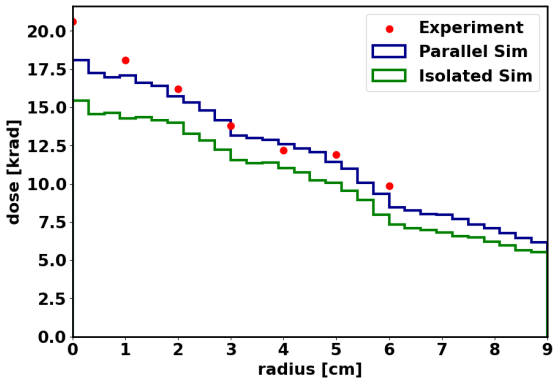

Figure 3. X-ray dose outputs as a function of radius at a test plane downstream of the vacuum chamber. The parallel simulation (blue) shows good agreement with the experiment (red) except for directly on axis, where the simulation underpredicts the experiment by 10%. An isolated simulation (green), where the two CRTs were electrically isolated, shows a reduction in the overall dose.

Title: Three-Dimensional Empire Particle-in-cell Simulations of a Magnetically-insulated Transmission Line Terminated by a Large-area Diode
Author(s): S.B. Swanekamp,[1] J.C. Zier,[1] N.D. Isner,[1] I.M. Rittersdorf,[1] A.R. Vazsonyi,[1] and M.D. Johnston[2]
Affiliation(s): [1]U.S. Naval Research Laboratory, Washington, DC; [2]Sandia National Laboratories, Albuquerque, NM
CTA: CEA

Computer Resources: HPE Cray EX, Penguin TrueHPC [NAVY, MS]

Research Objectives: A magnetically insulated transmission line (MITL) is a key element in modern pulsed-power architectures. The primary objective of this research is understanding the electron beam distribution on the anode of a large-area diode driven by an MITL. The three-dimensional (3D) simulations are performed with Sandia's unstructured PIC code EMPIRE.

Methodology: PIC simulations of a magnetically insulated transmission line (MITL) terminated by a large-area diode (LAD) were performed with the 3D Empire particle-in-cell code. Cubit was used to generate the unstructured tetrahedral grid used by Empire. Power is delivered to the LAD using an MITL and is simulated by the particle-in-cell method. The output of the simulations is visualized using the ViSit software.

Results: A large-area diode (LAD) is a common element in pulsed-power systems. The LAD is used to spread the energy density of the electron beam over a large area on the anode. This is useful for keeping the energy deposition on the anode below the threshold for ion emission. Suppressing ion emission can prevent the electron beam from pinching to the axis. This report presents cutting-edge 3D particle-in-cell simulations of the coupling between an MITL and an LAD. The peak voltage, current, and pulse duration for the simulations are 8 MV, 200 kA, and 50 ns, respectively. The 3D MITL/LAD simulations show that the current density of the electron beam breaks up into filaments in the azimuthal direction as the beam lifts off the MITL and approaches the anode. This creates regions of about 80 local hot spots on the anode. The pseudocolor image of the electron beam current density at t = 50 ns for several positions in the MITL is shown in Figs. 1a–d.

DoD Impact/Significance: Electron beam diodes like the LAD are used to generate intense bremsstrahlung X-rays for materials related research. The 3D simulations of the coupling between an MITL and a high-power diode show an instability that causes the electron beam to break up into filaments. These results may have implications on the physics of other high-power bremsstrahlung radiation sources.

Acknowledgment: This work was supported by Sandia National Laboratories. Sandia National Laboratories is a multimission laboratory managed and operated by National Technology and Engineering Solutions of Sandia, LLC., a wholly owned subsidiary of Honeywell International, Inc., for the U.S. Department of Energy's National Nuclear Security Administration under contract DE-NA0003525.

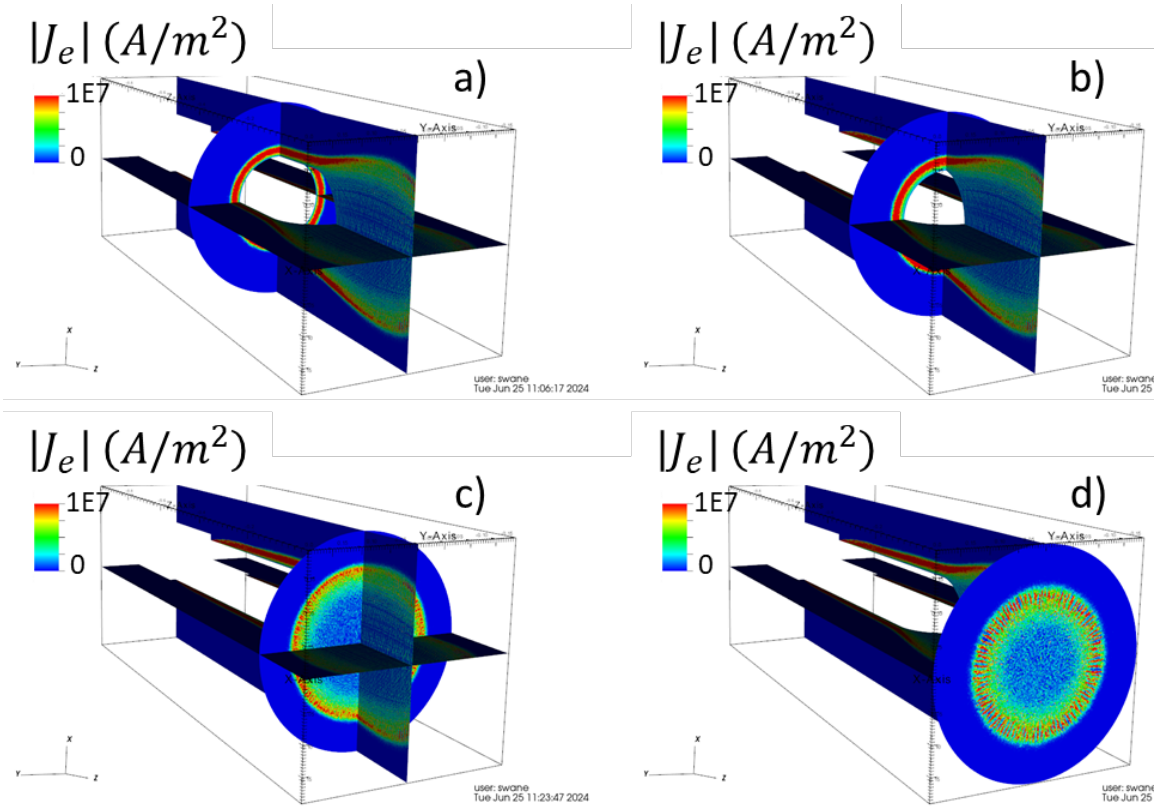

Figure 1. A pseudocolor image of the magnitude of the electron current density at t = 50 ns for several z-slices: a) z = −45 cm, b) z = −30 cm, c) z = −15 cm, d) z = 0 cm.

Title: Infrared Scattering by Micro-particles
Author(s): R. Furstenberg and A.R. Shabaev
Affiliation(s): U.S. Naval Research Laboratory, Washington, DC
CTA: CEA

Computer Resources: HPE SGI 8600 [AFRL, OH]; HPE Cray EX 4000, Cray XC40/50 [ERDC, MS]; HPE SGI 8600, HPE Cray EX [NAVY, MS]

Research Objectives: An accurate description of infrared scattering spectra is of importance for the development of detection instrumentation and in other fields such as atmospheric research. The main goal of this research is to develop a predictive tool for spectral signatures of liquid and solid aerosols as a function of size and shape. We investigate spectral features of microparticles, especially those with irregular shapes (i.e., nonspherical), commonly found in solid aerosols and surface contaminants. For these particles, the spectral features differ from their bulk values. These differences are most pronounced in the Mie regime, where the wavelength of light is comparable to the size of the particles. For perfect spheres, Mie theory provides exact (analytical) solutions, but those equations cannot be applied widely to irregularly shaped particles, most often found in solid aerosols and other trace contamination on surfaces.

Methodology: We have developed a method and a code implementation to generate random particles. Each particle is characterized by the three-dimensional (3D) shape parameters (aspect ratios, convexity, sphericity, etc.) and a complex refractive index, n+ik, of a given bulk material. For these particles, we calculate the angle-dependent scattering cross-sections for a range of frequencies in which optical constants (n and k) vary. These calculations are performed using established electromagnetics codes that are suitable for solving the scattered electromagnetic field. The datasets are analyzed statistically to identify which shape parameters influence the scattering cross-sections the most. This analysis provides the basis for predictive models. The datasets are also used to build a multidimensional lookup table or a trained neural network, essential tools for the rapid prediction of scattering response.

Results: In FY24, we continued to model the scattering response that provides foundation for the analysis of a small number of shape parameters that are responsible for the majority of the observed scattering cross-section. This characterization is needed to limit the required dimensionality of the lookup table and, therefore, to allow for the formulation of a reasonably accurate predictive model that can be used both by detection instruments (in the field) or for research purposes (in the lab) in various scientific fields, such as atmospheric and environmental science, and for detection of hazardous materials. Figure 1 shows results of calculations for a particle of rectangular shape made of sodium chloride. In the range of wavelengths near 6 μm, sodium chloride is a dielectric material with zero conductivity and nearly constant index of refraction. The figure shows how the differential cross-section varies with the orientation at the wavelength of 6 μm. The angular distribution of scattered intensity is shown by the stereographic projections of scattered intensity. In FY24, we prepared the necessary codes to go beyond regular shapes (spheres, cubes etc.) and to generate particles or irregular shapes. This will be the main focus of our future FY25 work.

DoD Impact/Significance: Better understanding of spectral signatures from microparticles is of great interest to the DoD in general and to the Navy in particular. Protecting the warfighter in contested and hazardous environments as well as the homeland from attacks by monitoring the environment is greatly enhanced from higher sensitivity and lower false-alarm rates possible when the exact spectral signatures of the hazardous materials are known. As an immediate use of the expertise developed under this HPC project, we continued to support the IARPA PICARD program in FY24 as part of their T&E team. Our predictive models are used for detection algorithm development and to provide synthetic datasets to augment experimental data.

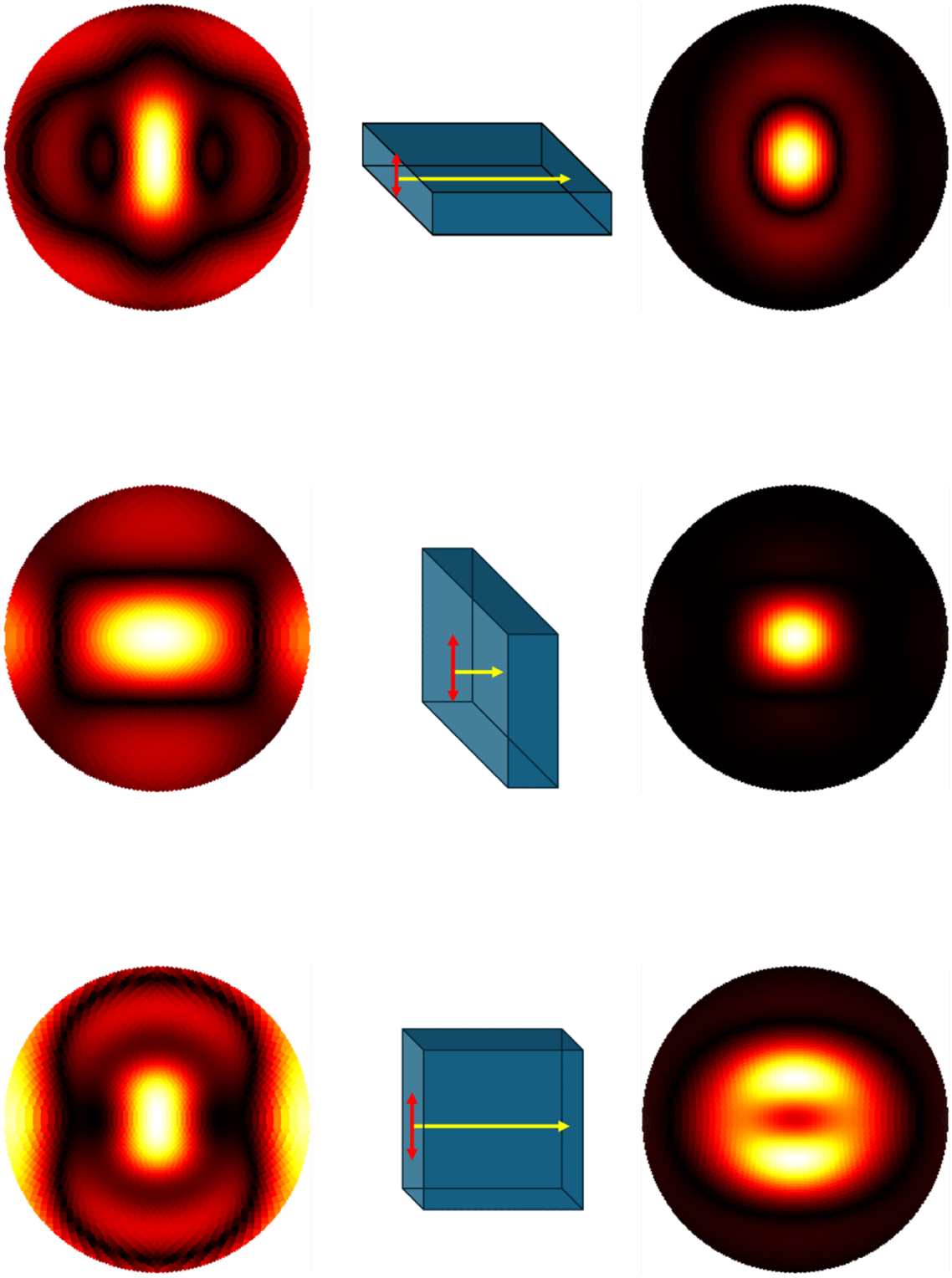

Figure 1. Light scattering by a small crystal of sodium chloride. The crystal is in the shape of an oblate rectangular prism that is 5 μm × 5 μm × 2.5 μm. The wavelength of light is 6 μm. The pattern of scattering intensity in the backward (left) and forward (right) directions vary with the direction of incident light and crystal orientation. Arrows show directions of polarization (red) and propagation (yellow).

Title: Three-Dimensional Acousto-Elastic Modeling
Author(s): S. Dey
Affiliation(s): U.S. Naval Research Laboratory, Washington, DC
CTA: CEA

Computer Resources: HPE SGI 8600 [AFRL, OH]; Penguin TrueHPC [NAVY, MS]

Research Objectives: Generate a high-fidelity near-field structural acoustic response ensemble from canonical targets to verify and improve accuracy of fast-running approximate surrogate models for scattering.

Methodology: We utilized a high-order hp-finite and infinite element-based solver (STARS3D) developed at NRL for solving the coupled elastoacoustics problem. This enables highly accurate solution of the scattering response up to the midfrequency regime. The use of high-order hierarchic basis combined with infinite elements that automatically satisfy the far-field radiation condition ensures an accurate first-principles-based solution of the acoustic field both near the target and far away from it.

The high-fidelity solutions are used for verification of the solution using fast-running surrogates that use simple point-reacting scattering models. Eventually, a careful set of high-fidelity solutions will be used to improve the accuracy of the fast-running surrogates.

Results: Figure 1 depicts the canonical domain used in the study. Figure 2(a) depicts the last two cases of hp-mesh convergence plots for the bistatic response for $\theta = 0$. One can note the expected symmetry of the response for a numerically converged solution. The monostatic acoustic-color plot showing the form function in dB as a function of θ and frequency is shown Fig. 2(b).

DoD Impact/Significance: Fast-running and sufficiently accurate digital surrogates for structural acoustics provide timely data for use in the design, operation, and maintenance of complex undersea systems.

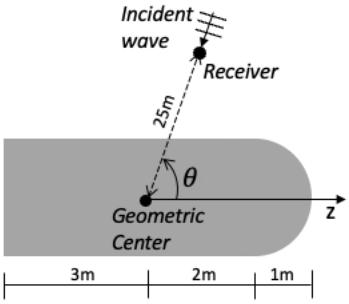

Figure 1. Canonical model setup for monostatic near-field scattering response.

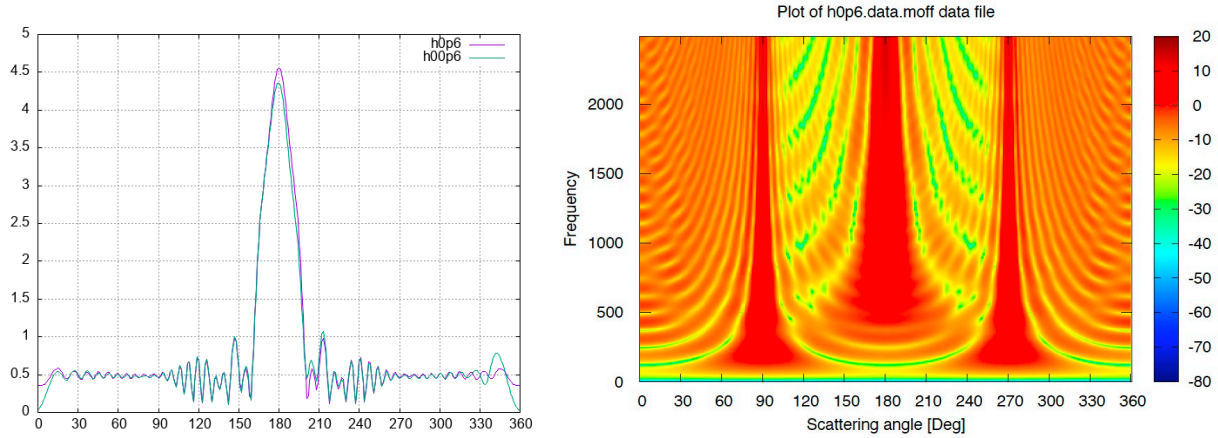

(a) (b)

Figure 2. (a) Mesh convergence showing expected symmetry in the bistatic response at a 0 degree angle on incidence. (b) Monostatic target strength in dB at the receiver in near-field location. Horizontal axis is the aspect and vertical axis is the frequency.

Title: Underwater Electrical Impedance Tomography
Author(s): G.R. Gatling and E.M. Tejero
Affiliation(s): U.S. Naval Research Laboratory, Washington, DC
CTA: CEA

Computer Resources: HPE Cray EX [NAVY, MS]

Research Objectives: Use computational resources of the HPCMP to generate Jacobians and sensitivity matrices for electrical impedance tomography, both in plasma and underwater, to facilitate two-dimensional (2D) measurements of plasma density and 2D imaging of underwater impedance structures. Investigate image reconstruction methods for resolution and stability and discover novel algorithms to improve inclusion detection and signal-to-noise ratio and to decrease computing costs.

Methodology: Impedance tomography is an inverse problem with a goal of using measurements of voltage and current at the boundary of a region of interest to construct an image of the interior. In the case of water and plasma tomography, the boundary of this region may be ill-defined, as contrasted with medical impedance tomography, where the boundary is often well-defined by the patient's skin. Solving this inverse problem requires two steps, the first being the solution to the forward problem, in which the electrode voltages and currents are predicted using an assumed impedance distribution. For this research, the forward solver is implemented using Python and several open-source tools, including Gmsh for generating arbitrary meshes, scikit-fem, a finite-element assembler, numpy, a library of fast numeric algorithms for Python based on LAPACK, and scipy, which includes a library of sparse matrix routines used to solve the system of equations generated by the FEM. These tools have been built into an NRL-developed electrical resistance tomography code and have been used to explore the performance of arrays of electrodes placed onto the edges of polygons. The second step is to generate an image, given an actual measurement of the voltages and currents on the electrodes, by searching the space of all possible impedance distributions for one that predicts the observed voltages and currents. In FY2024, this search was performed using the Jacobian, or sensitivity matrix, in a single update against an assumed background. A primary goal of the research in 2025 is to reduce the cost of computing this Jacobian to enable iterative search methods.

Results: One of the key results of FY2024 was the discovery of surface waves on the electrodes in the solution of the forward problem when using the complete electrode model for plasma impedance probes (pCEM). These surface waves are shown in Fig. 1. These waves form at interfaces between plasmas and other surfaces and are vital to the operation of plasma antennas, which are currently being studied at NRL due to their tunable resonant transmission properties. The pCEM represents a more straightforward and simpler method to arrive at the underlying physics of plasma surface waves than what is currently present in the literature and presents an opportunity to make quick advances in our understanding of the phenomenon.

DoD Impact/Significance: This work is significant to the DoD because noninvasive, remote sensing with electrical impedance tomography is an emerging technology with a wide range of DoD applications, including biomedical imaging, characterizing fusion plasma, underwater imaging, under-seafloor mine detection, resource prospecting, and a variety of fluid process-monitoring applications. However, impedance tomography methods continue to present critical challenges in low signal-to-noise ratio, inherently limited resolution, intense computational costs, and slow reconstructions. Overcoming these challenges will keep the DoD on the frontier of imaging capability.

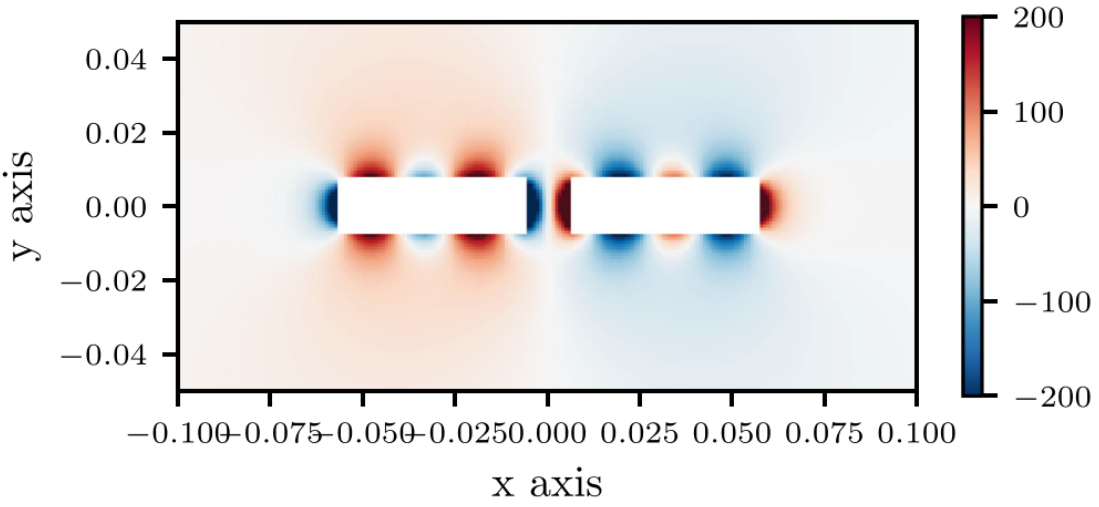

Figure 1. A simulation of the spatial potential around a dipole immersed in a plasma shows tangential electric fields at the surface of the electrode. This simulation is based on the complete electrode model for plasma impedance probes and differs from Balmain's analytic model by supporting nonzero tangential electric fields through the use of the contact impedance. The underlying physics of plasma surface waves is critical to improving our understanding of the operation of plasma antennas, currently being studied at NRL for their tunable resonant transmission.

THIS PAGE INTENTIONALLY LEFT BLANK

CWO

Climate Weather Ocean Modeling

CWO focuses on the accurate numerical simulation of the Earth's atmosphere and oceans on those space and time scales important for both scientific understanding and DoD operational use. This CTA includes the simulation and forecasting of atmospheric variability (e.g., temperature, winds, pressure, relative humidity, cloud cover, precipitation, storms, aerosols and trace chemicals, surface fluxes, etc.) and oceanic variability (e.g., temperature, salinity, currents, tides, waves, ice motion and concentration, sediment transport, optical clarity, etc.). Numerical simulations and real-time forecasts are performed from the very top of the atmosphere to the very bottom of the ocean. CWO also includes the development of numerical algorithms and techniques for the assimilation of in situ and remotely sensed observations into numerical prediction systems. CWO has DoD applications on a daily basis for specific warfare areas, mission planning, and execution (air, ground, sea, and space), as well as for flight and sea safety, search and rescue, optimal aircraft and ship routing, and weapon system design. This CTA provides the DoD with: 1) real-time, high-resolution weather and oceanographic forecasts leading to incisive decision making and enhanced operational capability in adverse weather and ocean conditions, and 2) realistic simulations of the dynamic oceanic and atmospheric environment to permit effective mission planning, rehearsal and training, and materiel acquisition.

Title: COAMPS-TC® Tropical Cyclone Rapid Intensification Prediction
Author(s): J.D. Doyle
Affiliation(s): U.S. Naval Research Laboratory, Monterey, CA
CTA: CWO

Computer Resources: HPE SGI 8600, HPE Cray EX, Penguin TrueHPC [NAVY, MS]

Research Objectives: The predictions of tropical cyclone (TC) paths or tracks have improved significantly during the past few decades, in contrast to intensity predictions that have lagged behind them, particularly for TCs that undergo rapid intensification (30 kt increase in maximum winds over a 24 h period). This disparity can be attributed to our limited capability to model accurately the physical processes governing TCs and the inherent sensitivity of TC forecasts to initial conditions. The primary aim of this project is to advance and evaluate COAMPS-TC®, a numerical weather-prediction system for TCs. This system supports Navy, DoD, and civilian operations. The COAMPS-TC® system is currently in operation at the Fleet Numerical Meteorology and Oceanography Center (FNMOC) and has undergone advancements for both the deterministic and ensemble prediction systems. The objective is to improve COAMPS-TC's® predictions of TC track, intensity, and wind field.

Methodology: In the past year, advanced versions of the COAMPS-TC® deterministic and ensemble systems have been tested. The first type of experiments involves rapid development and prototyping of COAMPS-TC®. Rigorous testing is essential for assessing the system's performance in a statistically significant manner and requires hundreds of individual cases for evaluation. This approach is indispensable for analyzing the impact of every advancement to the software, such as increased resolution or improved parameterizations. This rapid prototyping is important for the evaluation and transition of the operational version of COAMPS-TC® at FNMOC. A second type of application of COAMPS-TC® relates to the near-real-time execution of an experimental version of COAMPS-TC® that contains advanced capabilities relative to the operational version. This protyping of the experimental COAMPS-TC® system is conducted for numerous TCs across the globe.

Results: In the past year, a suite of COAMPS-TC® configurations was tested over a large number of TCs worldwide, particularly in the Atlantic Ocean and Pacific Ocean basins. Advanced versions of the deterministic and ensemble COAMPS-TC® systems were transitioned to FNMOC operations in the past two years. As an illustration of the 21-member COAMPS-TC® demonstration ensemble system, Fig. 1 shows an ensemble forecast for Hurricane Helene from 0000 UTC 26 September 2024. The ensemble captured the forecast position/timing more than 24 h in advance (Fig. 1a) and the landfall intensity of 122 kt (category 4) was consistent with the 75% probability of a Category 4 storm (113 to 136 kt) (Fig. 1b). COAMPS-TC is one of the top TC prediction models worldwide for track, intensity, and storm structure (storm size). This new, advanced version of COAMPS-TC®, developed on the DSRCs HPE SGI 8600, the HPE Cray EX, and the Penguin TrueHPC, indicates even greater accuracy for improved research and operational tropical cyclone applications.

DoD Impact/Significance: Tropical cyclones continue to pose a substantial hazard to Navy missions. Improving the accuracy of tropical cyclone forecasts should yield substantial cost benefits for the Navy. The latest version of COAMPS-TC® deterministic and ensemble systems will enable new decision-making capabilities for fleet sorties and will reduce exposure to hazardous weather conditions. The real-time testing and development of the system using the HPC DSRC platforms have resulted in major enhancements in the predictive capabilities of COAMPS-TC®. Additionally, these advancements facilitate quicker integration into Navy operations at FNMOC. These improvements will play a crucial role in shaping the future of tropical cyclone model development in support of the Navy, the DoD, and the civilian sector. This is particularly pertinent as computational capabilities increase, enabling higher-resolution forecasts and more accurate representation of physical processes, as demonstrated in this project.

(a)

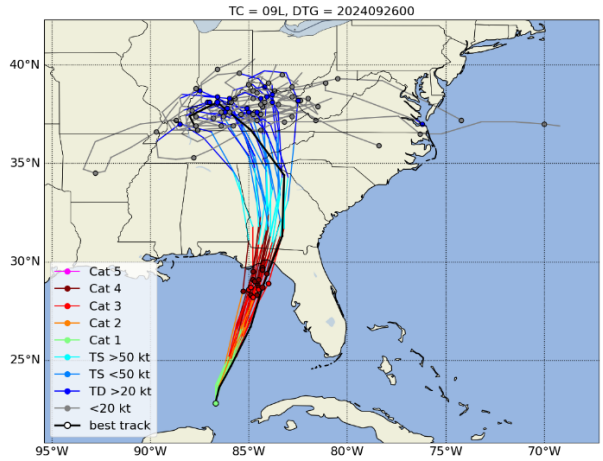

(b)

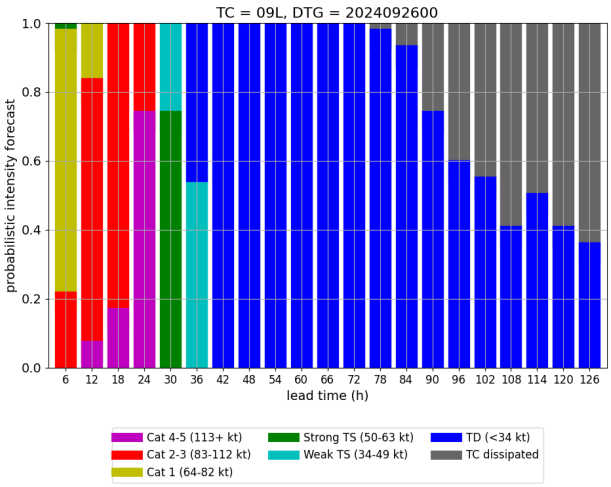

Figure 1. (a) Track and (b) intensity probability forecasts from NRL's experimental 21-member CTCX ensemble for Hurricane Helene from 0000 UTC 26 September 2024. In the track forecast depicted in (a), the best (observed) track (black line) and ensemble members (colored by the intensity category according to the legend) are shown with circles indicating the storm's position in 24 h increments. In the intensity probability forecast shown in (b), the probabilities of the intensity categories during successive 6 h periods are indicated, ranging from Category 4–5 (≥ 113 kt, magenta) to dissipation stage (gray).

Title: Improved Mixed Layer Depth and Upper Ocean Structures via Turbulent Mixing Advancements
Author(s): Y. Fan
Affiliation(s): U.S. Naval Research Laboratory, Stennis Space Center, MS
CTA: CWO

Computer Resources: HPE SGI 8600 [NAVY, MS]

Research Objectives: Improve upper ocean predictions in the Navy's operational ocean models by developing a new mixing parameterization that builds on three new theories of turbulent processes associated with Langmuir circulation in the oceanic mixed layer and improves on the shortcomings of each.

Methodology: This project utilized extensive numerical studies using the Naval Coastal Ocean Model (NCOM) and the NCAR large-eddy simulation (LES) model. The new K-Profile Parameterization proposed by Solano and Fan [1] with enhanced Langmuir turbulence (KPP-LT) was implemented in NCOM and reevaluated two other parameterizations, Mellor and Yamada [2] and Kantha and Clayson [3], previously implemented in NCOM, observations, and LES simulations.

Carefully designed numerical experiments were conducted at Ocean Station Papa, a deep-water station (with a water depth of more than 4 km) located at (144.9°W, 50.1°N), ~850 miles off the British Columbia coast. The station is within the subpolar northeastern Pacific gyre, and thus experiences strong, frequent winter storms. Hourly meteorological (10 m wind, net surface heat flux) and oceanographic (temperature, salinity) data for the NCOM runs are obtained for year 2011 from the moorings at OSP operated by the Ocean Climate Stations (OCS) group at Pacific Marine Environmental Laboratory of the National Oceanic and Atmospheric Administration (NOAA/PMEL) [4]. Time-varying wind stress was calculated from these data using the vectorized COARE 3.5 algorithm modified from Fairall et al. [5] by Woods Hole Oceanographic Institution (WHOI).

Results: The new KPP parameterization, KPP-LT, first was evaluated in monthly runs (Table 1). Its performance is generally better than the other two parameterizations in sea surface temperature (SST) simulations with slightly larger mean and root-mean-square errors in March and May. The performance of KPP-LT on mixed-layer-depth (MLD) simulations is a bit mixed. We see improvements in the fall and winter months but degradations in the spring and the summer.

However, consistent improvements using the KPP-LT scheme were observed from the full-year simulation for both SST and MLD (Fig. 1). While we see improvements throughout the simulation period, significant improvements start in July and persist for the rest of the year, being consistent with the monthly evaluations. Further investigation suggests that all mixing parameterizations assessed in this study are more robust for shear-driven mixing scenarios that are more common in the fall and winter but have deficiencies when the ocean is under mild wind, with surface warming such that the double-diffusive mixing plays a dominant role in mixed-layer turbulence. The reason that we see better model performance using the KPP-LT scheme with the yearlong run than the monthly runs is because the monthly runs were reinitialized each month at the start of the simulation, so errors from the previous month were not accumulated in the model as in the yearlong run.

DoD Impact/Significance: This study will improve the battlespace environment forecasting accuracy for ocean models with more accurate vertical thermal profiles and better predication of acoustic and optic properties in the upper ocean to support the Navy's search, sanitize, and avoid operations.

Monthly Comparison

SST

	Jan		Feb		Mar		Apr		May		Jun		Jul		Aug		Sep		Oct		Nov		Dec	
	ME	RMS	ME	RMS	ME	RMS	ME	RMS	ME	RMS	ME	RMS	ME	RMS	ME	RMS	ME	RMS	ME	RMS	ME	RMS	ME	RMS
MY2.5	0.070	0.084	0.075	0.086	0.07	0.091	0.39	0.54	0.84	0.98	1.16	1.36	1.42	1.58	1.40	1.52	0.66	0.76	0.49	0.57	0.33	0.36	0.02	0.12
KC04	0.071	0.083	0.076	0.088	0.068	0.087	0.37	0.52	0.8	0.94	1.13	1.32	1.36	1.52	1.37	1.48	0.63	0.73	0.48	0.55	0.31	0.34	0.02	0.12
KPP-LT	0.055	0.067	0.066	0.077	0.077	0.098	0.2	0.29	0.83	0.97	1.0	1.15	1.16	1.29	0.73	0.90	0.08	0.22	0.10	0.14	0.10	0.12	0.003	0.1

MLD ($\Delta\sigma_\theta$<0.1kg/m^3)

	Jan		Feb		Mar		Apr		May		Jun		Jul		Aug		Sep		Oct		Nov		Dec	
	ME	RMS	ME	RMS	ME	RMS	ME	RMS	ME	RMS	ME	RMS	ME	RMS	ME	RMS	ME	RMS	ME	RMS	ME	RMS	ME	RMS
MY2.5	1.35	2.09	1.32	2.46	1.21	3.17	30.4	43.3	29.6	32.4	17.8	19.8	12.6	15.1	11.21	12.6	6.15	8.07	-1.15	3.90	12.6	13.9	-6.21	6.79
KC04	1.13	1.92	1.13	2.28	1.04	3.05	29.1	42.4	28.5	31.4	17.3	19.4	12.2	14.8	10.9	12.3	5.72	7.75	-1.44	3.98	11.9	13.2	-6.31	6.88
KPP-LT	0.82	1.99	0.58	1.67	1.95	3.47	19.5	31.7	30.3	32.9	17.9	20.1	13.2	15.6	9.4	11.9	3.35	8.00	-4.81	6.13	1.09	2.92	-5.91	6.61

Table 1. Mean error (ME) and root-mean-square error (RMS) comparisons among NCOM monthly simulations using the Mellor and Yamada [2] (noted as MY2.5), Kantha and Clayson [3] (noted as KC04), and KPP-LT scheme. Red boxes highlighted the months when KPP-LT showed degradations.

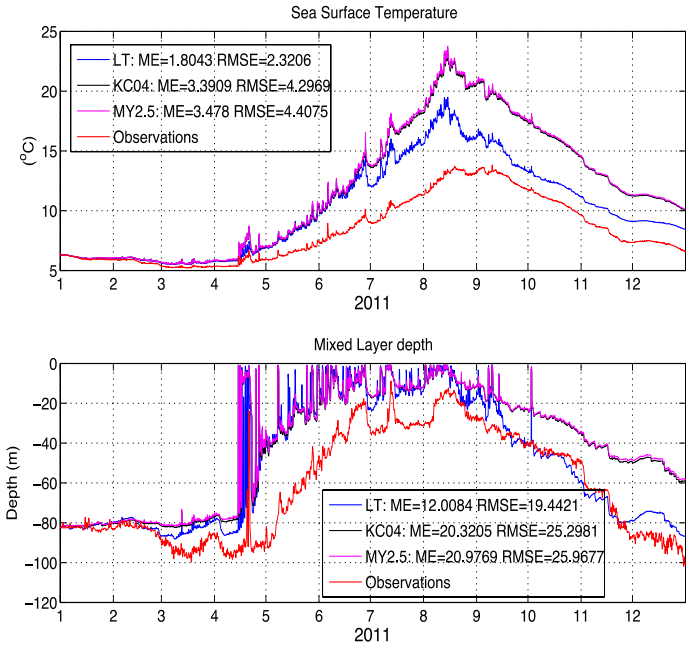

Figure 1. Sea surface temperature (SST) and mixed layer depth (MLD) comparisons between observations (red) and NCOM simulations using the MY2.5 (purple), KC04 (black), and KPP-LT (blue) schemes. The ME and RMSE for each run were given in the legend.

References

[1] Solano, M., and Fan, Y. (2022). A new K-profile parameterization for the ocean surface boundary layer under realistic forcing conditions. *Ocean Modelling*, *171*, 101958

[2] Mellor, G. L., and Yamada, T. (1982). Development of a turbulence closure model for geophysical fluid problems. *Reviews of Geophysics*, *20*(4), 851-875

[3] Kantha, L. H., and Clayson, C. A. (2004). On the effect of surface gravity waves on mixing in the oceanic mixed layer. *Ocean Modelling*, *6*(2), 101-124

[4] Send, U., Davis, R., Fischer, J., Imawaki, S., Kessler, W., Meinen, C., Owens, B., Roemmich, D., Rossby, T., Rutnick, D., Toole, J., Wijffels, S., and Beal, L. (2010). A global boundary current circulation observing network. *Proceedings of OceanObs*, *9*, 21-25

[5] Fairall, C. W., Bradley, E. F., Hare, J. E., Grachev, A. A., and Edson, J. B. (2003). Bulk parameterization of air–sea fluxes: Updates and verification for the COARE algorithm. *Journal of climate*, *16*(4), 571-591

Title: Dynamics of Coupled Models
Author(s): I. Shulman, S. Cayula, E. Jarosz, and E.J. Metzger
Affiliation(s): U.S. Naval Research Laboratory, Stennis Space Center, MS
CTA: CWO

Computer Resources: HPE SGI 8600, HPE Cray EX [NAVY, MS]

Research Objectives: Improve our understanding of coupled bio-optical and physical processes in the coastal zone and the variability and predictability of the coastal ocean's optical properties on time scales of 1–5 days. Investigate the coupled dynamics of ocean bio-optical, physical, and atmospheric models.

Methodology: The approach is based on using nested, coupled physical-bio-optical models of the coastal region together with bio-optical and physical in situ and remotely sensed observations. Data-assimilation techniques for both physical and bio-optical fields are being used to examine project research issues and objectives. Approach is also based on joint studies of the bioluminescence (BL) potential and inherent optical properties (IOPs) over relevant time and space scales. Dynamical, biochemical, physical, and BL potential models are combined into a methodology for estimating BL potential and nighttime water-leaving radiance (BLw).

Results: We published refereed paper "Dynamics of the Polar Front in the southwestern area of Svalbard, Norway," in which we have investigated the dynamics of the polar front (PF) in the southwestern area of Svalbard. In order to investigate the hydrographic history of the modeled water masses circulating to the area of the southwest of Svalbard, we conducted numerical experiments with the adjoint to the tracer model. The adjoint tracer distribution provides information on the model tracer history and identifies the origin and pathways of the model tracer-tagged water masses in the past, which circulated into the area of interest (red box on Fig. 1). In other words, the adjoint quantifies where water masses were, for example, three days before circulating into a specific geographical area of interest. Therefore, adjoint distributions show the hydrographic history of water masses advected and mixed into the area of interest at the evaluation time T. Figure 1 presents the hydrographic history of water masses for different depths. Those adjoint maps show areas where the model tracer-tagged water masses were four days before circulating into the area of interest (the red box) on October 11 at 12Z. For all seeding depths (with the same horizontal area of interest but different depths of adjoint seeding), our results demonstrated that the water masses were circulating into the area of interest from the eastern and southeastern parts of the Svalbard and were flowing along the southern tip of Svalbard. These water masses were mixed with the water masses coming from the southeast to the area of interest.

DoD Impact/Significance: Emerging Navy electro-optical (EO) systems under development and special operations missions require an improved understanding of the ocean optical environment. This is critical for operations and weapon deployment, especially in the coastal and littoral zones. Improved basin-scale-to-mesoscale forecast skill is critical to both military and civilian use of the oceans, particularly on the continental margins.

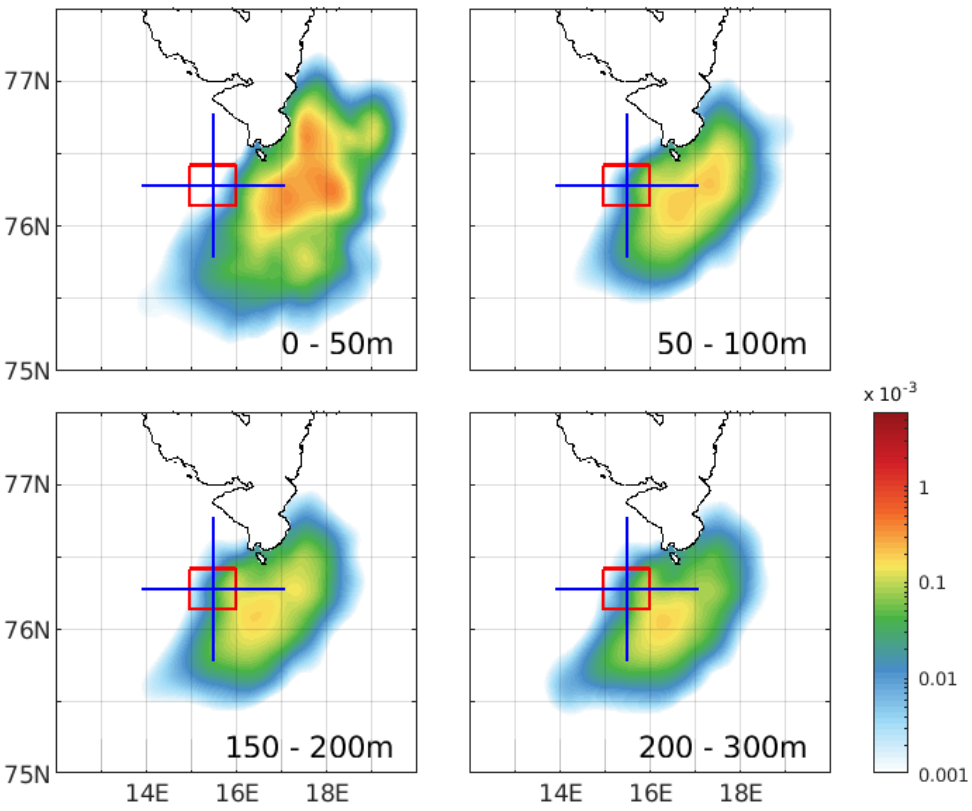

Figure 1. Adjoint distribution maps in the southwestern area of Svalbard, Norway. (top left) the adjoint was seeded in the top 50 m of the red box on October 11 12Z. The map shows distribution of the adjoint after four days of backward integration of the adjoint equation (therefore, on October 7 12Z). The vertically integrated adjoint for each model grid is shown (also normalized by the volume of the red box); (top right) as in top left, but the adjoint was seeded between 50 m and 100 m depths on October 11 12Z; (bottom left) as in top left, but the adjoint was seeded between 150 m and 200 m on October 11 12Z; (bottom right) as in top left, but the adjoint was seeded between 200 m and 300 m.

Title: Coastal Mesoscale Modeling
Author(s): P.M. Finocchio
Affiliation(s): U.S. Naval Research Laboratory, Washington, DC
CTA: CWO

Computer Resources: HPE SGI 8600, HPE Cray EX, Penguin TrueHPC [NAVY, MS]; Penguin Open Compute Platform (OCP) [AFRL, OH]; Cray XC40/50 [ERDC, MS]

Research Objectives: The coastal zone is characterized by mesoscale weather phenomena that adversely affect Navy operations. Sharp gradients of wind, temperature, moisture, aerosols, refractivity, and visibility exist in the lowest kilometer of the atmosphere in the coastal zone. Such mesoscale variability also exists in the ocean. Accurate prediction of coastal mesoscale meteorological phenomena requires coupled land-ocean-atmosphere numerical forecast systems that represent dynamics from the synoptic scales to the scales of the largest eddies. The objective of this project is to develop and validate a coastal/littoral modeling system that can be used to provide high-resolution (< 5 km) analysis/nowcast/short-term (0–120 h) coupled forecast guidance for tactical-sized areas of the world. This system also can be used for basic and applied research leading to improvement in our understanding of atmospheric and oceanic processes.

Methodology: The primary tool being developed, tested, and utilized for research in this project is the Coupled Ocean/Atmosphere Mesoscale Prediction System (COAMPS®). The atmospheric component of COAMPS® is made up of a data-assimilation system, an initialization procedure, and a multinested, nonhydrostatic numerical model. The numerical model includes parameterizations for cloud, precipitation, and radiation processes, as well as for surface and boundary-layer effects. The NRL Coastal Ocean Model (NCOM) is currently used for the simulation of the mesoscale ocean circulation response to the atmospheric forcing in one-way and two-way interactive modes. The Noah Land Surface model currently is used to simulate land-surface processes and exchanges with the atmosphere. COAMPS® also has been modified to predict electro-optical quantities of interest for directed-energy applications.

Results: In FY24, HPC resources were used to develop new techniques for assimilating novel observations of boundary-layer height into COAMPS®. Assimilation of boundary-layer height corrects temperature and moisture profiles in analyses for Navy numerical weather-prediction models and increases the utility of lidar measurements in analyses. New applications of this technique to other observing platforms are being explored. HPC hours also were crucial in continued research using very-high-resolution (<10 m) simulations to understand the physical processes that affect the evolution of the atmospheric boundary layer over the ocean. Several additional research projects that relied on HPC resources resulted in publications in FY24. These include projects focused on developing a new tangent linear model for applications in cloud microphysics parameterizations, improving forecasts of marine fog in COAMPS®, quantifying the predictability of high-impact weather such as polar lows and tropical cyclones, understanding contributions of the coastal land surface to Navy forecasts in the littoral zone, and training machine learning models for improved cloud forecasts. The development of the Navy's next-generation global numerical weather prediction system, NEPTUNE, also continued in FY24.

DoD Impact/Significance: COAMPS® continues to play a significant role in providing atmospheric forecasts in support of Navy missions involving the deployment of weapon systems, strike warfare, radar propagation, and search and rescue. Research and development performed at HPC DSRCs have led to significant improvements in the predictive skill of COAMPS® that will benefit the operational performance of COAMPS® greatly. The HPC DSRCs will be the primary computing resources in FY25 and beyond for the development of the fully coupled COAMPS® system, including the emerging electromagnetic and electro-optical (EM/EO) and ensemble capabilities for COAMPS®.

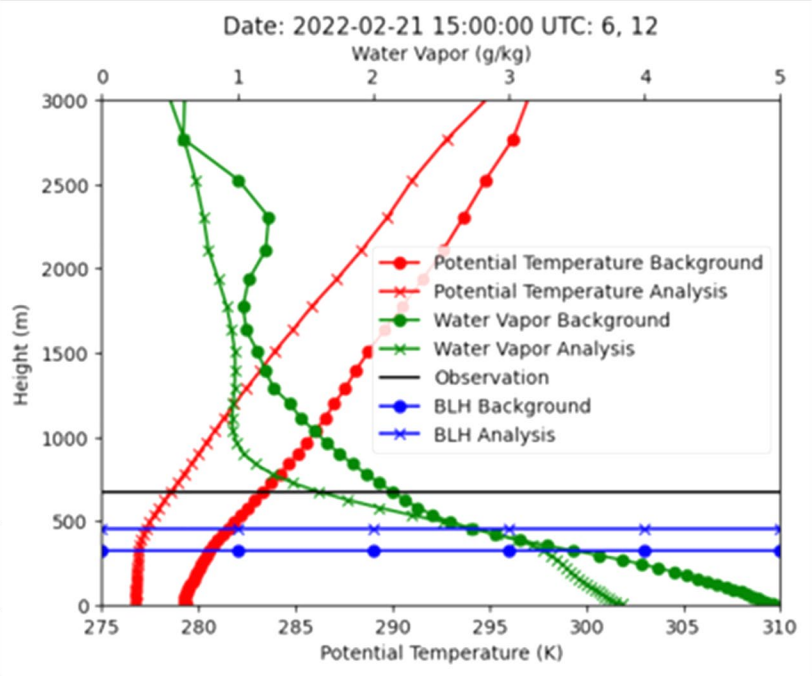

Figure 1. Demonstration of assimilating an observation of boundary layer height (black line) into the Coupled Ocean/Atmosphere Mesoscale Prediction System (COAMPS®). The initial (filled circle) and updated (crosses) boundary layer height (blue), and profiles of potential temperature (red, bottom x-axis) and water vapor mixing ratio (green, top x-axis) demonstrate how assimilating boundary layer height observations (black line) affect the structure of the lower troposphere in COAMPS®. (Courtesy: Dr. Clark Amerault, NRL Code 7533)

Title: Eddy-Resolving Global/Basin-Scale Ocean Modeling – Winter Convection and Water Mass Formation in the Northern Arabian Sea
Author(s): P.G. Thoppil
Affiliation(s): U.S. Naval Research Laboratory, Stennis Space Center, MS
CTA: CWO

Computer Resources: HPE SGI 8600 [NAVY, MS]

Research Objectives: The primary aim of this project is to identify and isolate the key physical processes that govern the convective formation of water masses and quantify the associated mechanisms. The long-term goal is to understand the influence of mesoscale-to-submesoscale eddies on air-sea interaction to determine how these interactions impact upper-ocean convection and water mass formation through surface heat fluxes. This research will shed light on how submesoscale dynamics and their interactions with the atmosphere can modify the structure and variability of upper-ocean processes in ways that affect ocean stratification, mixing, and water mass properties.

Methodology: The project utilizes both perturbation and realistic simulations using high-resolution ocean models, the HYbrid Coordinate Ocean Model (HYCOM), complemented by data analysis.

Results: In the northern Arabian Sea, high salinity levels are sustained primarily by year-round evaporation, driving the convective formation of Arabian Sea high-salinity water (ASHSW) during the winter monsoon (November–February). Although precipitation largely has been discounted as a critical controlling mechanism for winter convection, recent years have seen a notable increase in extreme cyclones over the Arabian Sea, particularly in postmonsoon cyclones (September–December) since 2014. However, the extent to which these cyclone-induced freshwater inputs disrupt the region's freshwater balance (evaporation–precipitation) and impact ASHSW formation remains unclear. Here, we present observational evidence supported by a suite of model simulation experiments, revealing a significant weakening in ASHSW formation triggered and sustained by extreme tropical cyclones. The addition of fresh water reduces the density of high-salinity water, augmenting stratification and disrupting the convective sinking process, ultimately limiting the depth of convective mixing. This strengthened stratification stabilizes the water column, exacerbating warming trends and destabilizing the freshwater balance between the Arabian Sea and the Bay of Bengal. These findings underscore the profound implications of extreme cyclone-induced freshwater inputs.

DoD Impact/Significance: Ocean convection occurs in regions of surface buoyancy loss in winter and plays an important role in the stratification of water columns. Convective mixing is highly inhomogeneous in regions of mesoscale eddy activity, where propagation of sound speed becomes complex and less predictable. Improved knowledge of the interaction between mesoscale eddies and convective mixing will lead to a better representation of acoustic parameters in ocean models.

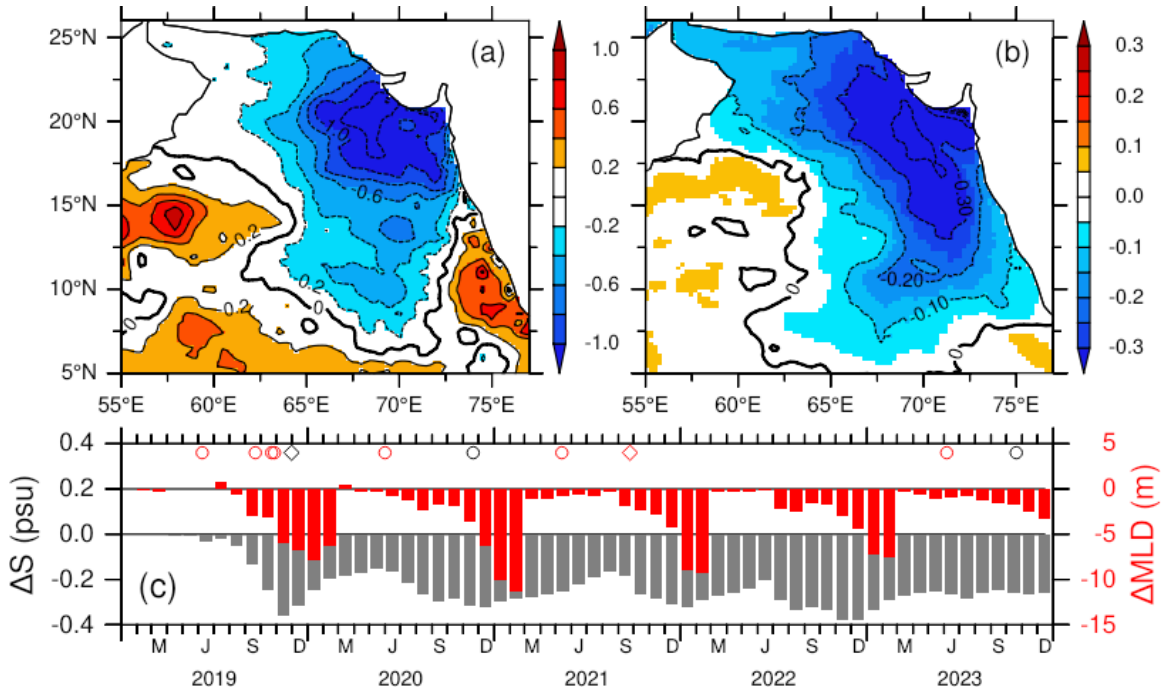

Figure 1. Differences between the control (CNTL) and the perturbation experiment $PPE_{2019\text{-}2023}$ (CNTL – $PPE_{2019\text{-}2023}$) during the five-year period spanning 2019–2023 in (a) surface salt flux (10^6 psu m s^{-1}) and (b) salinity in the upper 50 m. Temporal evolution of differences in (c) mixed layer depth (MLD, m) and salinity in the upper 50 m averaged over the northern Arabian Sea 60°–75°E, 20°–25°N. MLD is calculated from the density increase equivalent to a 0.5°C temperature decrease from the surface. Negative values indicate (a) decrease in salinity due to excess precipitation over evaporation, (b) lower salinity, (c) shallower MLD, and lower salinity in the CNTL compared to $PPE_{2019\text{-}2023}$ experiment. The perturbation experiment isolates the effect of cyclone-induced precipitation on salinity freshening during 2019–2023 by persisting the 2018 precipitation forcing while maintaining all other forcings intact. By contrasting $PPE_{2019–2023}$ with the control simulation, we isolate the precipitation events responsible for the observed freshening during the period 2019–2023. Cyclone occurrences are marked in (c) with circles and diamonds.

Title: Eddy-Resolving Global/Basin-Scale Ocean Modeling
Author(s): E.J. Metzger
Affiliation(s): U.S. Naval Research Laboratory, Stennis Space Center, MS
CTA: CWO

Computer Resources: HPE Cray EX [NAVY, MS]

Research Objectives: Run a sequence of 45-day forecasts at the ensemble resolution of the Earth System Prediction Capability version 2 (ESPC-E v2) for 12 members. The output is used to perform the verification and validation (V&V) of the atmosphere, ocean, sea ice, and wave model components to compare against the existing operational ESPC-E v1 system.

Methodology: The cylc metascheduler is used for job management of ESPC forecasts. As the forecast model integrates forward in time, cylc uses the built-in dependencies to initiate tasks to postprocess the output from each model component. Some tasking creates model/observation matchups, i.e., sampling both at the same spatial and temporal location to compute error metrics, and thus to determine model skill. All error metrics are combined into a validation test report that details the strengths and shortfalls of the new system compared to the old.

Results: Many error metrics are computed for each model component. Typically, these involve bias, root-mean-square error (RMSE), scalar and vector correlation coefficients, anomaly correlation, and others. An example for the atmosphere is shown in Fig. 1 that examines RMSE over three regions (Northern Hemisphere, Tropics, and Southern Hemisphere) and for five variables. Green indicates superior performance of ESPC-E v2 over the operational ESPC-E v1 system. For some variables (Tropical 500 hPa geopotential height and Southern Hemisphere Extratropics 2m air temperature), the new system exhibits large gains throughout the entirety of the 45-day forecasts. Much of the improved skill is due to overall lower bias. It is also noted that operational ESPC-E v1 is underdispersive relative to ESPC-E v2, where new modeling capabilities have led to better atmospheric ensemble skill. Surface wave forecast skill from ESPC-E v2 is measured against the Advanced Climate Analysis and Long Range Forecasting System (ACAF). Examining both the RMSE and the correlation coefficient shows that ESPC-E v2 ensemble mean provides a superior forecast over ACAF out through approximately a 15-day lead time, whereafter the two have essentially the same error out to 45 days. The coupling between the atmosphere and wave models contributes to the skill of longer forecasts.

DoD Impact/Significance: The atmosphere, the ocean, sea ice, and waves all affect Navy operations. The Navy's Earth System Prediction Capability will meet U.S. Navy needs for global Earth system prediction from the top of the atmosphere to the bottom of the sea on time scales from days to months, supporting tactical to strategic decision making and long-range planning. Examples of ESPC ensemble products in use by the fleet are: a) maps of weekly averaged atmospheric conditions provide the Joint Typhoon Warning Center (JTWC-Guam) with long-range forecasts of enhanced/diminished tropical cyclone development in the western Pacific Ocean, b) forecasts of the oceanic mesoscale eddy field provide mission planners an understanding of the ocean environment before deploying assets, and c) the U.S. National Ice Center uses extended forecasts for environmental mission support in the Arctic (biannual Ice Experiment (ICEX) scientific mission) and the Antarctic (Operation Deep Freeze - McMurdo resupply mission). ESPC deterministic products provide tactical scale ocean forecasts out to 16 days and are shown to be superior to climatology, thereby extending the lead time beyond the traditional one-week forecast window.

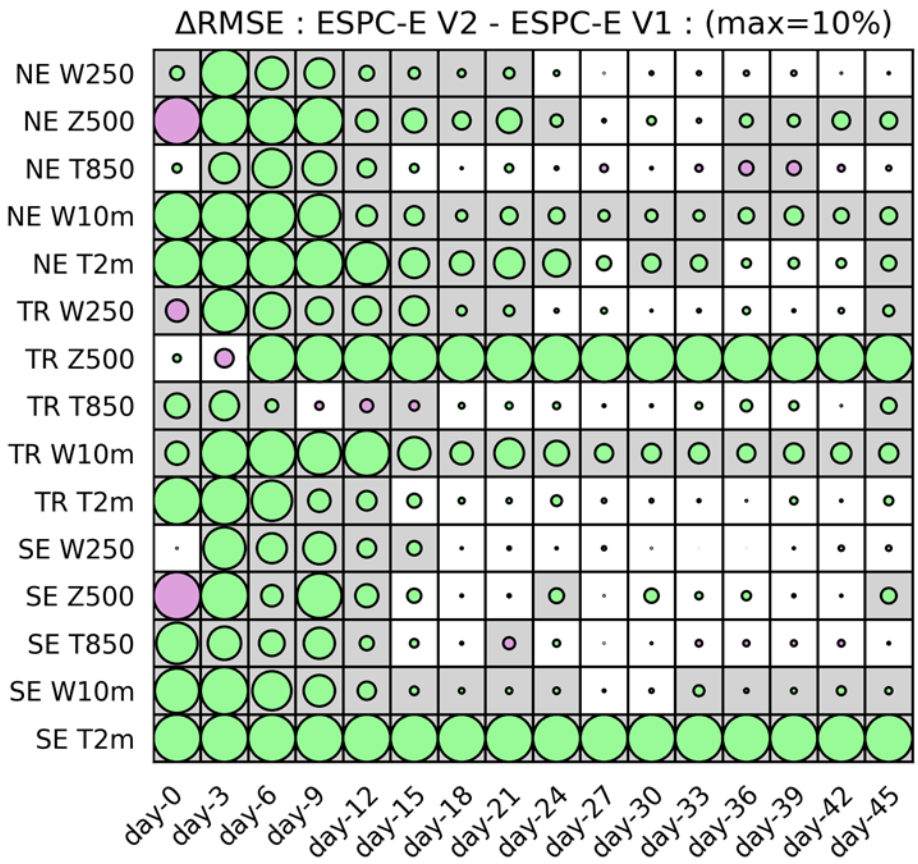

Figure 1. Ensemble-mean root-mean-square error (RSME) scorecard for ESPC-E v2 vs ESPC-E v1 for the Northern Hemisphere Extratropics (NE – top five rows), the tropics between 20°S and 20°N (TR – rows 6–10), and the Southern Hemisphere Extratropics (SE – bottom five rows) for variables: 250 hPa wind speed (W250), 500 hPa geopotential height (Z500), 850 hPa air temperature (T850), 10 m wind speed (W10m), and 2 m air temperature (T2m). The x-axis is forecast lead time. Green indicates ESPC-E v2 outperforms ESPC-E v1. Purple indicates that ESPC-E v1 outperforms ESPC-E v2. The size of the circle is proportional to the percent RMSE difference, with the maximum circle size indicating a 10%-or-greater difference. When the panels are colored gray, the difference is statistically significant at the 95% level.

Title: Eddy-Resolving Global/Basin-Scale Ocean Modeling – Phase-accurate Internal Tides in a Global Ocean Forecast Model: Potential Applications for Nadir and Wide-swath Altimetry
Author(s): J.F. Shriver and E.J. Metzger
Affiliation(s): U.S. Naval Research Laboratory, Stennis Space Center, MS
CTA: CWO

Computer Resources: HPE SGI 8600, HPE Cray EX, Penguin TrueHPC [NAVY, MS]

Research Objectives: To assess how well HYCOM represents internal tides in comparison to observations. To examine this research question, we used the 0.04˚ global HYbrid Coordinate Ocean Model (HYCOM) with tides and data assimilation and the satellite altimeter-based High Resolution Empirical Tide Model (HRET 8.1) to address this important question.

Methodology: We investigate the degree to which an operational tide-resolving ocean forecast system based on HYCOM can be used to provide quantitatively accurate predictions of internal tides as measured by baroclinic tidal SSH. Previous evaluations focused on qualitative comparisons because these earlier runs were not constrained by data assimilation, a critical ingredient in simulating internal tides. Data assimilation improves the stratification and the accuracy of oceanic features such as fronts and eddies. The observations we compare HYCOM internal tides to are those derived from the Jason-2 satellite altimetry mission using HRET 8.1. Satellite altimeter measurements of sea surface height are the only global data set that can be used for an assessment such as this.

Results: The analysis period we are considering spans 2017–2019. A global map of M_2 internal tide SSH amplitudes in HYCOM is presented in Fig. 1a. The map is constructed after regridding the data from altimeter track points to a uniform 0.5° latitude-longitude grid. A visual comparison of individual M_2 internal tide SSH peaks and troughs (Fig. 1b) in HRET8.1 and the 3-year HYCOM analysis in the HAWAII region demonstrates that HYCOM can replicate the spatial variability of internal tide amplitudes and phases with reasonable accuracy.

A technique (termed “variance reduction”) used to assess the skill of internal tide predictions is to subtract them from observations and note the change in variance. If the variance is reduced, then your prediction has skill. HYCOM can reproduce the geographical pattern of phase-locked internal tide SSH variance reduction seen in HRET8.1 at both semidiurnal and diurnal frequencies (Fig. 2a–d). The HYCOM variance reduction for the total tide, the sum of the phase-locked and modulated components, exceeds that of HRET8.1 in some regions, especially those with strong internal tides.

Our research shows that a data-assimilative forecast system based on HYCOM can provide accurate predictions of the internal tide, capturing both the phase-locked (long-term) and non-phase-locked (modulated) internal tides. The predictions of the phase-locked internal tide with HYCOM are somewhat less accurate than those of an empirical model, HRET8.1. In contrast, we demonstrated the capacity for making skillful predictions of the modulated tides, something that is not possible with HRET8.1 or any other empirical model of the phase-locked internal tide.

DoD Impact/Significance: Data-assimilative eddy-resolving models are important components of global ocean and sea ice-prediction systems. Tactical decision aids (TDAs) and mission planning tools (MPTs) based on these systems provide vital enabling capabilities for the Navy at spatial scales ranging from operational areas to entire theaters and over time horizons ranging from a few hours to many months. An estimate of the accuracy of the simulated internal tides in global HYCOM would be valuable guidance for those who would use these models as decision-making aids or boundary conditions for regional models.

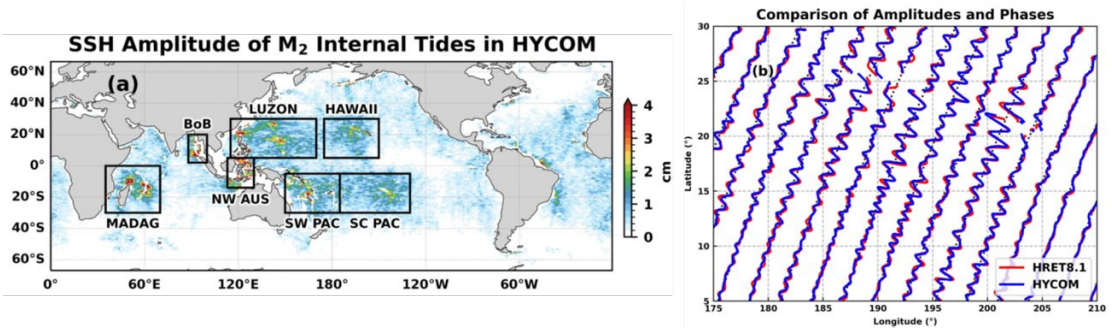

Figure 1. (a) Amplitude (in cm) of M_2 internal tide SSH fields extracted from 3-year harmonic analysis of HYCOM. Boxes represent regions with strong internal tide activity: region near Luzon Strait (LUZON), region near Hawaii Islands (HAWAII), region near Madagascar Island (MADAG), the southwestern Pacific (SW PAC), the south-central Pacific (SC PAC), the Bay of Bengal (BoB), and the region above northwestern Australia (NW AUS). Regions shallower than 1,500 m are masked out. (b) Comparison of M_2 phase-locked internal tides in terms of quadrature waveform (imaginary part of harmonic constants) — in other words, (amplitude * sin(phase)) — between HRET8.1 and the 3-year analysis of HYCOM for ascending tracks in the HAWAII region.

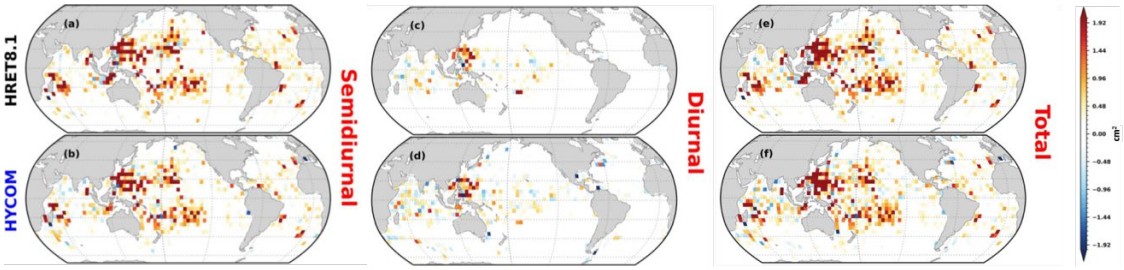

Figure 2. Global maps of internal tide SSH variance reduction (in cm^2) in nadir altimetry by HRET8.1 (a, c, e) and HYCOM (b, d, f) at semidiurnal frequency (a, b), diurnal frequency (c, d) and their total (sum of semdiurnal and diurnal) (e, f). The HYCOM results are from the harmonic analysis applied over 3 years. The results are averaged over 4° bins for visualization.

Title: Eddy-Resolving Global/Basin-Scale Ocean Modeling – Optimization of Ice Rheology for Advancing Sea Ice Forecast
Author(s): G. Panteleev, D. Hebert, M. Yaremchuk, and R. Allard
Affiliation(s): U.S. Naval Research Laboratory, Stennis Space Center, MS
CTA: CWO

Computer Resources: HPE SGI 8600 [NAVY, MS]

Research Objectives: The project aims to find the way to advance sea ice forecasting on a tactical scale. Polynyas and ridges present a typical phenomenon in the Arctic Ocean characterized by regular, elongated structures 50–1000 km long and 5–20 km wide. These structures are a subset of linear kinematic features (LKFs), and their positions and shapes are defined by the combined impact of sea ice divergence and shear on the ice cover. Currently, all sea ice models have a problem accurately forecasting LKFs. We analyzed the simple option to develop an advanced system to forecast LKFs on tactical scales.

Methodology: The project utilizes a standalone CICE6 sea ice model forced by the output from GOFS-3 reanalysis and complemented by data analysis.

Results: Proper forecasting of LKFs (i.e. $(\text{divergence}^2 + \text{shear}^2)^{0.5}$ is important for naval operations in the Arctic Ocean because they are regions of safe (polynyas) and dangerous (ridging) navigation. Panteleev et al. [1] demonstrated feasibility of optimizing spatially varying model parameters (e.g., P*(x)) of the EVP model. This resulted in a significant improvement of the sea ice forecast. The application of this approach to the in situ observations in the Beaufort Sea revealed that P* varies in space and has a clear seasonal cycle [1]. Thus, the underlying hypothesis of the constant P* is incorrect and should be reconsidered. In particular, this suggests LKFs can be predicted better through the optimization of the temporally and spatially varying P* fields within the CICE6 model. Similarly, Korosov et al. [2] demonstrated that LKFs can be predicted through the analysis of high-resolution sea ice velocity maps by adjusting spatial variation of the elasticity parameter E_o based on Brittle-Bingham-Maxwell (BBM) rheology. Currently, we have a large volume of daily sea ice concentration (SIC), velocity (SIV) and thickness (SIT) observations.

CICE6 model results are controlled strongly by the initial conditions, atmospheric forcing, and rheological parameters. The influence of the initial sea ice velocity (SIV) is very limited due to high viscosity in pack ice. Because of this, the only option to use a significant volume of high-resolution SIV observations is to derive a method to convert SIV information into the spatially varying rheological parameters (e.g., P*(x)) of the CICE6 model. This can be done through the simplified empirical algorithm based either on the analysis of the SIV high-resolution data or on a more advanced data-assimilation procedure, for example, as in [1]. At this stage, we completed the following tasks: a) generalized the CICE6 code by introducing spatially varying rheology parameters such as P*(x), b) extracted SIV and sea ice divergence and shear observations from the Copernicus Marine Environment Monitoring Service (CMEMS) database [3], c) constructed regional models collocated with the available CMEMS observations, and d) proposed a simple empirical relationship between P*(x) and sea ice deformation data based on empirical parameters. Results are shown in Fig. 1.

DoD Impact/Significance: This approach directly addresses the Navy's need to predict ice conditions (thickness, concentration, sea ice polynyas, ridging areas and landfast ice position) accurately to support safety of navigation in ice-covered waters. The ability to predict LKFs ensures the Navy will maintain tactical advantage by knowing where it is safe for both U.S. and adversary forces to operate in sea ice.

References
[1] Panteleev, G., Yaremchuk, M., Stroh, J. N., Francis, O. P., and Allard, R. (2020). Parameter optimization in sea ice models with elastic–viscoplastic rheology. *The Cryosphere*, *14*(12), 4427-4451
[2] Korosov, A., Rampal, P., Ying, Y., Ólason, E., and Williams, T. (2023). Towards improving short-term sea ice predictability using deformation observations. *The Cryosphere*, *17*(10), 4223-4240
[3] Saldo, R. (2020) Global Ocean – High Resolution SAR Sea Ice Drift, Copernicus Marine Service [data set], https://doi.org/10.48670/moi-00135

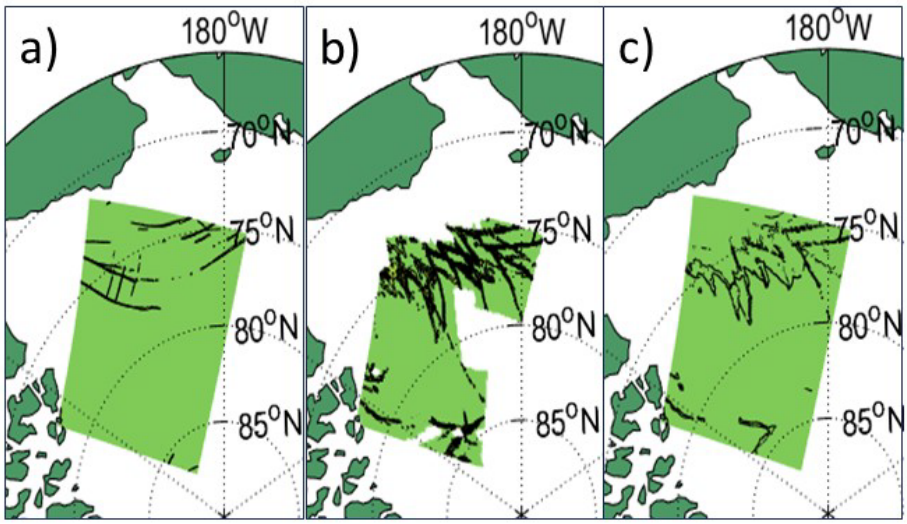

Figure 1. Linear kinematic features from: a) the conventional CICE6 model run, b) the high-resolution (10 km) velocity observations from sequential SAR images, c) the CICE6 model run with modified dependence of the maximum ice strength parameter on spatial coordinates.

Title: Eddy-Resolving Global/Basin-Scale Ocean Modeling – Ocean Forecast Compression for Resource-limited Environments
Author(s): C.B. Trott
Affiliation(s): U.S. Naval Research Laboratory, Stennis Space Center, MS
CTA: CWO

Computer Resources: HPE Cray EX, Penguin TrueHPC [NAVY, MS]

Research Objectives: The goal of this project is to enable reliable communication of ocean forecast products to forward operating forces over low-bit-rate data links using an approach called SABRE (Selected Analogous Battlespace Reanalysis Environment). Each profile in an operational forecast is paired with an analogous, SABRE-identified profile sourced from 30 years of Global Ocean Forecast System (GOFS) 3.1 reanalysis and is sent to forward units in communications-limited scenarios to permit onboard reconstruction of the battlespace environment.

Methodology: The technical approach for SABRE compresses individual profiles in the forecast field using a clustering algorithm to identify matching profiles in the 30-year GOFS 3.1 reanalysis. In this way, each profile is reduced to a single index value, yielding 250:1 compression, depending on the complexity of the indexing scheme. The GOFS reanalysis profiles are clustered by water mass and acoustic properties to reduce the number of brute-force searches. Each profile's analogue falls within the same cluster as its original profile based on cluster means. Then, the cluster is sorted into profiles with the same sonic layer depth. This subsetted cluster then is searched for the profile with the most similar vertical gradient of sound speed. The resultant profile after this multilevel search is considered the analogous environment and its integer identifier is transmitted to the platform that also would have a copy of the GOFS 3.1 reanalysis on board for reconstruction.

Results: For SABRE, cluster analysis of 30 years of GOFS 3.1 reanalysis data has been completed for January and has begun for July. As of the beginning of July clustering, there has been high throughput on both Navy DSRC machines (Nautilus and Narwhal) and no script stoppages due to bugs. The project is on track to provide a quarterly analysis (January, April, July, October) for the Northern Hemisphere. Next, the Northern Hemisphere will be clustered for the remaining months.

With each reconstruction of an operational forecast field, full-column root-mean-square error (RMSE) of the vertical gradient of sound speed is computed that evaluates the accuracy of the vertical gradient of sound speed between the operational forecast and its analogous environment. Outputs are saved as netCDF files. Figure 1 presents a sample RMSE for the East China Sea region for an operational GOFS 3.1 forecast on January 1, 2023. Highest errors are along the shelf break, whereas lowest errors are on the continental shelf.

DoD Impact/Significance: METOC forecast files are large, even for small areas, and increase in size with each advance in forecast model resolution. Advanced data-compression techniques are required so that communications-disadvantaged operators can derive maximum benefit from these Navy METOC Enterprise capabilities. Compression of METOC forecast data will enable communications-disadvantaged operators to maintain environmental situational awareness, reducing risk and enhancing decision making.

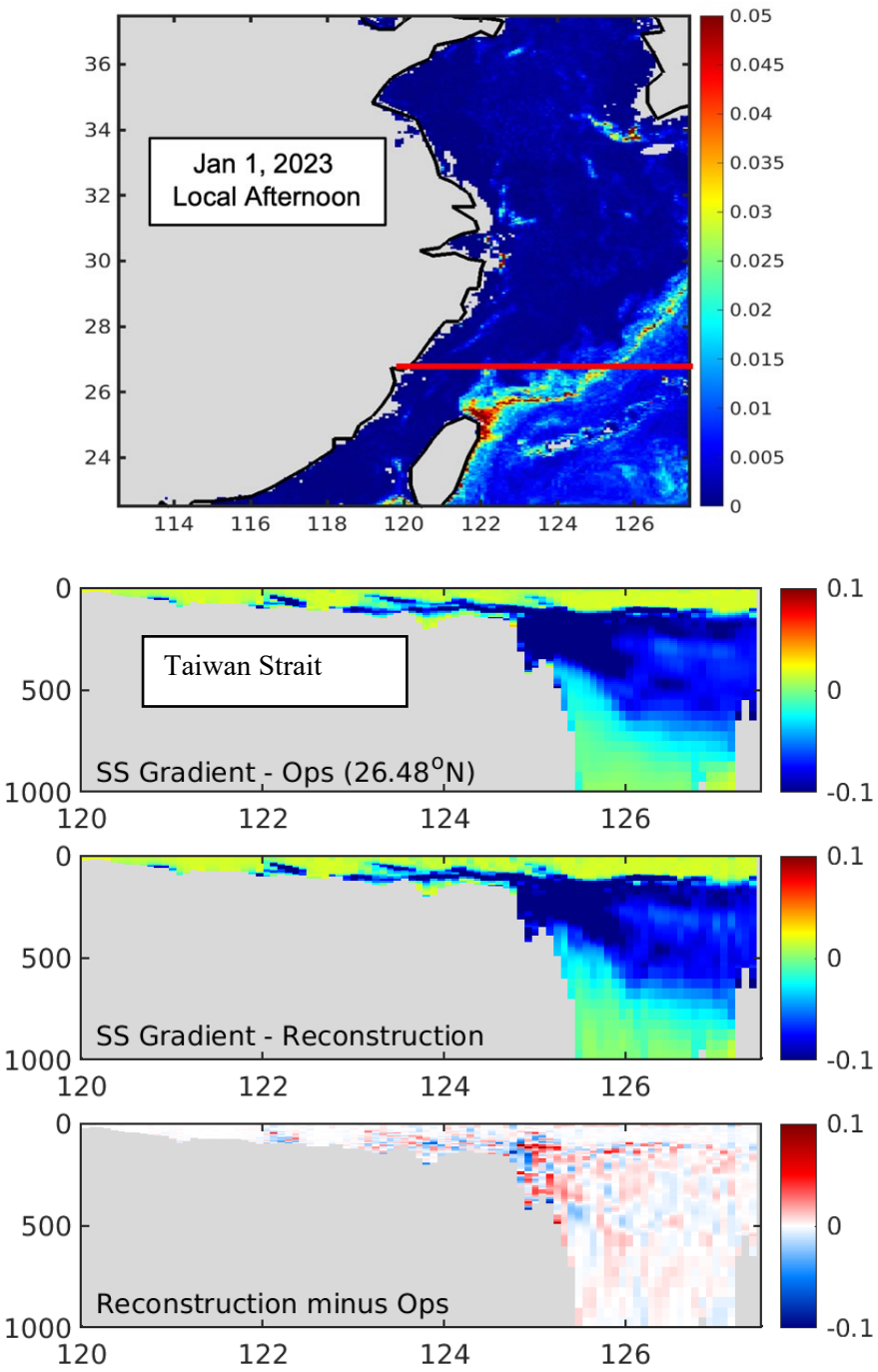

Figure 1. Root-mean-square error of vertical gradient of sound speed (s^{-1}) in the East China Sea (top panel). The operational GOFS 3.1 forecast is from January 1, 2023 (local afternoon). Sections of vertical gradient of sound speed (s^{-1}) from the same reconstruction as that shown along the red line for (second panel) an operational GOFS 3.1 forecast field, (third panel) an analogous environment reconstructed from 30 years of GOFS 3.1 reanalysis data, and (bottom panel) the difference between the top two panels.

Title: Eddy-Resolving Global/Basin-Scale Ocean Modeling – Dynamical Controls of the East China Sea/Yellow Sea
Author(s): J.F. Shriver and L.T. Gulliver
Affiliation(s): U.S. Naval Research Laboratory, Stennis Space Center MS
CTA: CWO

Computer Resources: HPE Cray EX [NAVY, MS]

Research Objectives: The East China Sea and the Yellow Sea (ECSYS) constitute a dynamic environment heavily influenced by complex topography and an energetic Kuroshio, contributing to an intricate system of permanent and temporary flows. Fleet users have documented the requirement for increased prediction accuracy for upwelling regions in the ECSYS, but the scarcity of in situ observations dictates the necessity of enlisting high-resolution models to discern the unique ocean processes. This project aims to isolate the dynamics related to upwelling in Navy ocean-forecast systems by using a regional numerical model to identify areas of interest (AOI) where vertical motion is significant. Simulations are conducted with and without remote tidal forcing at the boundaries to assess its impact on upwelling circulation, the dynamical insights from which will lead to better representation of water mass structure and prediction of the acoustic environment.

Methodology: A regional HYbrid Coordinate Ocean Model (HYCOM) of the Western Pacific was created using output from a global HYCOM reanalysis at the open boundaries from 2018 to 2022. Six simulations were conducted, half with bottom-boundary-layer parameterization (BBL). Four included barotropic tides, which were enabled in the regional model interior concurrent with the application of Oregon State University's TOPEX/Poseidon Global Inverse Solution tidal model (TPXO) as time-varying conditions at the open boundaries. TPXO was used at the open boundaries in order to permit the impact of remotely generated barotropic tides from outside the study area.

Results: A method was developed for identifying AOIs that quantified the percentage of time there was significant (> 1 m/day) upwelling or downwelling in a given area. Many of the AOIs aligned nicely with areas identified in previous observational studies. The first AOI chosen for further examination was a permanent downwelling zone (PDZ) ~350 km east-northeast of Taiwan along the 200 m isobath where the Kuroshio runs parallel along the continental slope as shown in Fig. 1. Analysis of daily mean vertical velocity from 50 m to 100 m shows a 9,000 km^2 zone of strong-and-persistent downwelling, where negative vertical velocity of 3 m per day is observed nearly 93% of the time over the 5-year analysis period. Seasonally, the flow reduces in intensity during the winter (Fig. 2a) in conjunction with a Kuroshio core that moves from the surface above the shallow shelf in the summer to the deeper waters of the Okinawa Trough in winter (Fig. 2b–e). Figure 2 also shows that from summer to winter, both the average Kuroshio and the downwelling velocity decrease by about a third. An upslope counterflow also appears to exist along the seafloor beneath the PDZ. This year, other AOIs will be explored with the intent of understanding the effects of remote tides on upwelling throughout the region.

DoD Impact/Significance: The results of this research will produce a better representation of the water mass structure that in turn will lead to improved prediction of the acoustical environment, such as more accurate surface and subsurface duct depths, which are sensitive to temperature variations that occur in areas of upwelling/downwelling. Being able to predict the complex ECSYS environment accurately without increasing computational resources will allow operators, such as those at NOAC, to provide warfighters with superior environmental intelligence, giving us a tactical advantage over our adversaries.

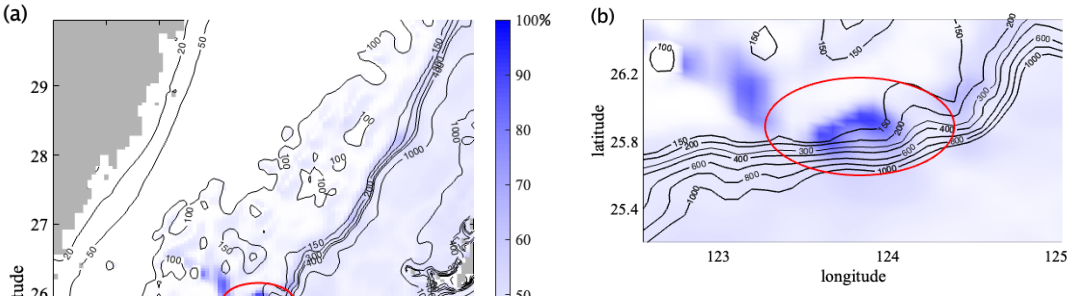

Figure 1. A region in the East China Sea is analyzed for vertical motion. The blue represents percentage in a 5-year experiment where the hourly snapshot of vertical motion at 100 m depth is above a significant downward velocity threshold, in this case,
> 5m/day. The prominence of the PDZ (circled in red) is displayed in comparison to the region in (a), while (b) is a zoomed-in view of the same area, with isobaths added to show its location with regard to topography.

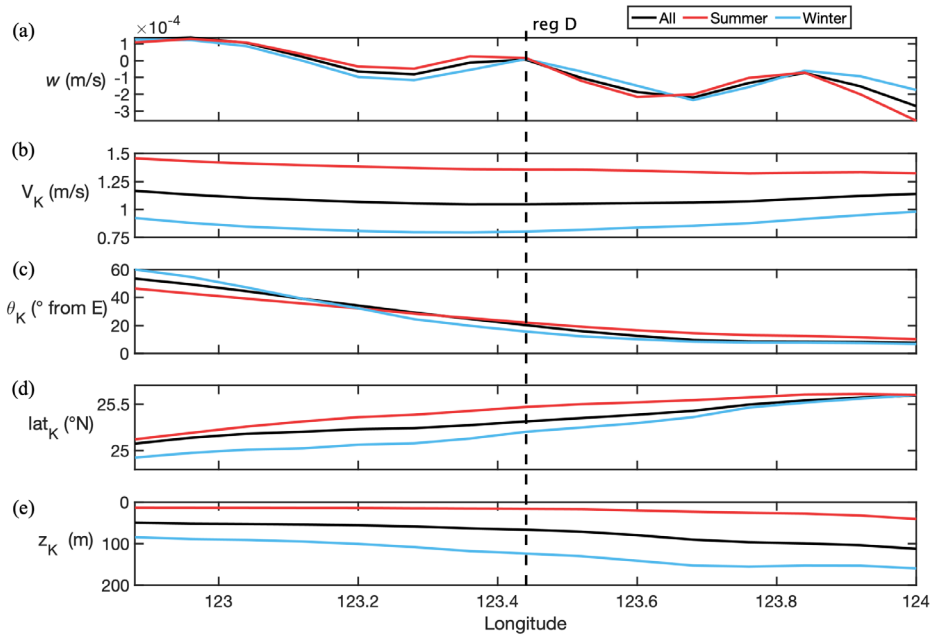

Figure 2. Comparison of mean (a) vertical motion, *w*, integrated in depth along the 25.8˚N parallel against the Kuroshio maximum horizontal velocity (b) magnitude, (c) direction in degrees from east, (d) latitude and (e) depth from 2018 to 2022. Black lines are total average for all years, red is an average of all summer months (June, July, August) and blue of all winter months (December, January, February). The dashed line represents the boundary between the area west of the PDZ and the PDZ itself on the right. Average *w* is +2.8 m/day west of the dashed line versus −12 m/day in the PDZ, highlighting the intensity of the downwelling region. From west to the PDZ, the Kuroshio core changes direction from NNE to nearly due east and is 35 m deeper on average. Seasonal variations in the Kuroshio also coincide with downwelling intensity.

Title: Eddy-Resolving Global/Basin-Scale Ocean Modeling – Accelerating Ocean Forecasts Through Mixed Precision Data Representation
Author(s): C. Rowley
Affiliation(s): U.S. Naval Research Laboratory, Stennis Space Center, MS
CTA: CWO

Computer Resources: Penguin TrueHPC [NAVY, MS]

Research Objectives: Our objective is to reduce the memory-access bandwidth in Navy ocean forecast models through the targeted use of mixed-precision data representation in the software. The overall goal is to advance speed and skill in current- and next-generation ocean forecast systems, with model errors evaluated in the context of a probabilistic forecast system, in which an ensemble of forecast models is used to represent and account for errors in initial conditions and in the model physics and numerics.

Methodology: We are working primarily with the HYbrid Coordinate Ocean Model (HYCOM). HYCOM is the global ocean forecast model used in the operational Earth System Prediction Capability (ESPC) systems, and the resource requirement for HYCOM is a limiting factor in the ensemble size and forecast range of the ESPC ensemble forecast system. In FY24, our work included testing of a HYCOM modification to allow for some computationally expensive processing to be performed less frequently than every time step, reducing the cost of a model simulation.

Results: We modified the HYCOM code to enable user-configurable time-step intervals for the computations of the vertical mixing and the tracer advection. After initial code development and testing, we implemented the changes in the ESPC system to evaluate the impact on timing in the coupled air-ocean-ice-wave model. We only completed a short set of 48 h simulation tests, but the results are promising. A short run configured to call both the vertical mixing and tracer advection routines every six time steps (versus every time step) showed a reduction in the HYCOM run core routine timer from 947 s to 796 s, a 15% reduction. This reduction will not reflect directly in the fully coupled model wall-clock time, but after extending the testing to larger intervals and subsequent load-balancing among the component models, we expect to be able to reduce the overall wall-clock cost of the coupled forecast. We will evaluate the performance of the ensemble forecast, not the individual member forecasts, so some increase in model error is acceptable.

DoD Impact/Significance: Reducing the overall cost of the ocean models used in regional and global ocean-only and coupled air-sea ensemble forecast systems will allow us to reallocate computational resources toward larger ensemble sizes, higher horizontal or vertical resolution, or more expensive physics calculations without increasing wall-clock time.

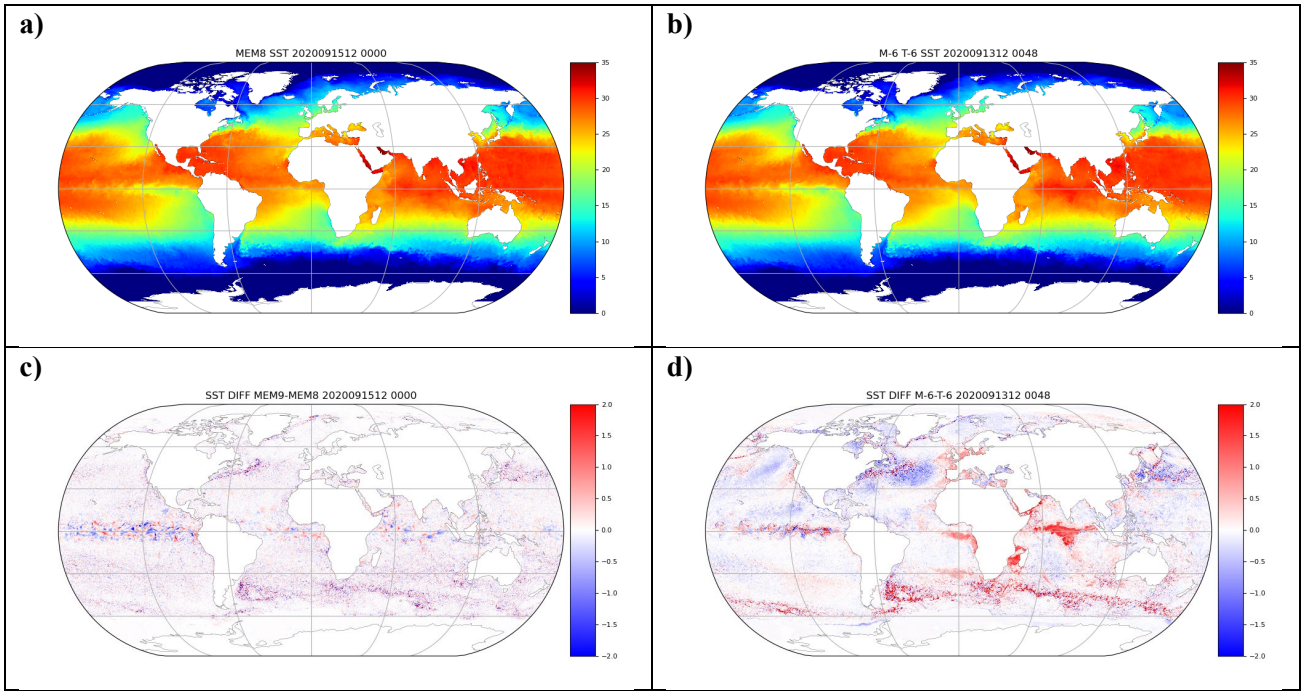

Figure 2. a) Sea surface temperature (SST, °C) from the global coupled ESPC ensemble v2 validation run member 8 at the analysis time, b) the member 0 48 h forecast SST calculated with mixing and tracer advection performed every six time steps, c) the SST difference between validation members 9 and 8 at the analysis time, d) the 48 h forecast SST difference between two experiments (mixing and tracer advection calculated every time step vs. every six time steps). All forecasts are valid 1200 UTC 15 September 2020.

Title: Eddy-Resolving Global/Basin-Scale Ocean Modeling – Ocean Submesoscale Eddy Evolution
Author(s): J. May, T. Smith, J.M. D'Addezio, D. Hebert, and B. Krause
Affiliation(s): U.S. Naval Research Laboratory, Stennis Space Center, MS
CTA: CWO

Computer Resources: HPE Cray EX, Penguin TrueHPC [NAVY, MS]

Research Objectives: This project aims to gain a fundamental understanding of ocean submesoscale eddy life cycle progression. It will study the dynamics, physics, and surrounding ocean environment impacts of ocean submesoscale eddies throughout their generation, evolution, and dissipation. Long-term goals of this project are to demonstrate the key mechanism for submesoscale eddy penetration past the mixed layer and to determine the impact each stage of the eddy evolution has on ocean stratification, heat exchange, and vertical transport both within and below the mixed layer.

Methodology: The project utilizes idealized simulations using the Coupled Ocean/Atmosphere Mesoscale Prediction System (COAMPS®) and the Navy Coastal Ocean Model (NCOM), complemented by data analysis.

Results: To investigate and understand the impacts of submesoscale eddies both within the eddies themselves as well as on the surrounding ocean environment, high-resolution ocean model simulations must be used. We have run a 6-month 1.125 km horizontal ocean model simulation with 128 vertical levels over the western Pacific of high resolution. For comparison, we also have started a 375 m horizontal ocean model simulation, also with 128 vertical levels. From these high-resolution (in both the horizontal and vertical) simulations, we are able to identify and isolate individual submesoscale eddies. The submesoscale eddy-selection process is performed on the small-scale relative vorticity field. The small-scale field is obtained by applying a 50 km Gaussian filter to the full vorticity field. Closed contours are identified on the small-scale relative vorticity field using an Okubo-Weiss threshold check. The closed contours then are tested further for circularity by comparing the major and minor axes. This submesoscale eddy-selection process is performed at all depth levels within the model. This allows for both the vertical and horizontal structure, the extent, the characteristics, and the impacts to the surrounding ocean environment to be evaluated.

DoD Impact/Significance: Ocean submesoscale eddies are strong features, often with larger magnitudes compared to the mesoscale. These features exist throughout the global ocean and often extend past the mixed layer. Submesoscale eddies are areas of strong convergence zones and will impact search-and-rescue domain size and location. Additionally, submesoscale eddies change the ocean stratification, which then impacts sound speed channels, sound speed gradients, and surface ducts. Improved knowledge of the interaction between submesoscale eddies and the surrounding ocean environment will lead to better representation of the effects within ocean forecasts.

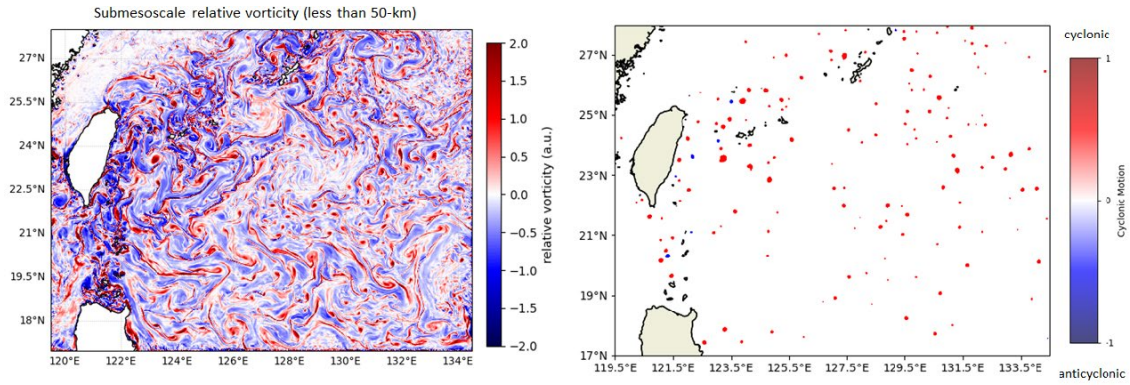

Figure 1. Small-scale relative vorticity is shown on the left for the western Pacific region for 1 February 2022 at 00Z. After applying the eddy-selection process, the identified cyclonic (red) and anticyclonic (blue) submesoscale eddies are shown on the right.

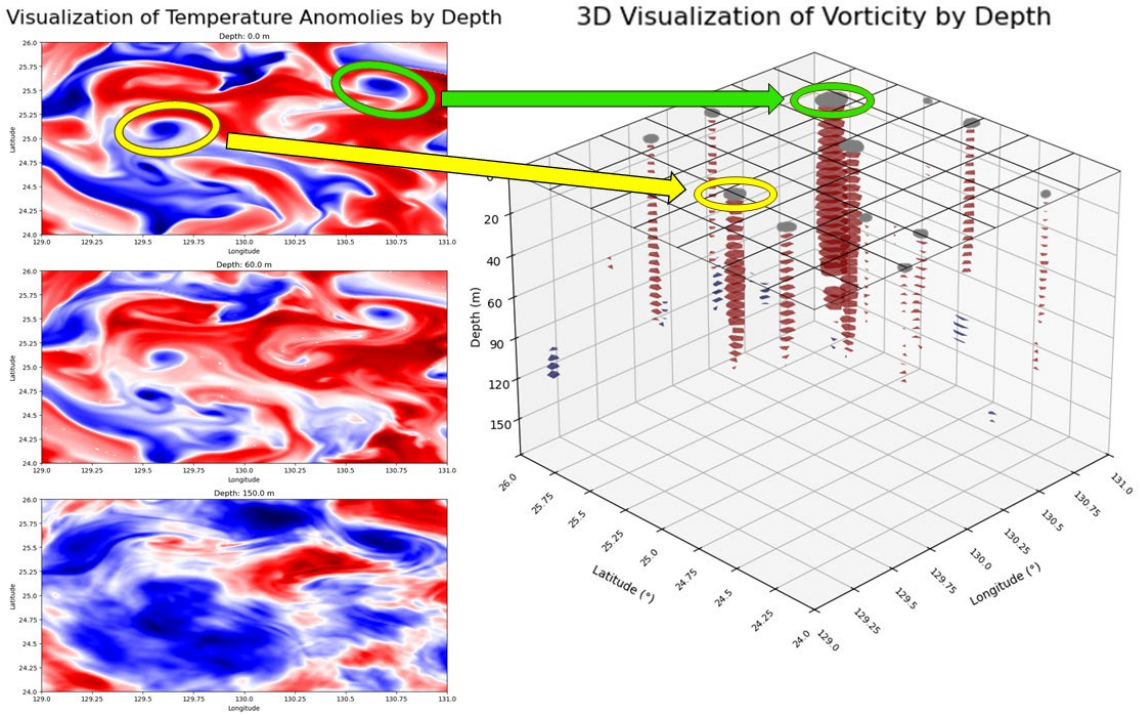

Figure 2. Three-dimensional (3D) visualization of submesoscale eddies. For a given area within the western Pacific (24°–26°N and 129°–131°W), the submesoscale eddies can be defined for each depth within the model simulation. The identified submesoscale eddies are shown on the right with vorticity. The corresponding temperature anomalies (left) for the given area at depths of 0 m (top), 60 m (middle), and 150 m (bottom) also are shown.

Title: Eddy-Resolving Global/Basin-Scale Ocean Modeling - Resolving Northern High Latitude Water-mass Formation Mechanisms
Author(s): S.R. Smith,[1] R.W. Helber,[1] and H. Kaur[2]
Affiliation(s): [1]U.S. Naval Research Laboratory, Stennis Space Center, MS; [2]University of Southern Mississippi, Hattiesburg, MS
CTA: CWO

Computer Resources: HPE SGI 8600, HPE Cray EX, Penguin TrueHPC [NAVY, MS]

Research Objectives: The goal of this project is to determine the physical mechanisms causing deep-water formation off the coasts of southeastern Greenland and Iceland as a source of deep, dense water found exiting the Irminger and Iceland Basins. These mechanisms also are believed to be responsible for water-mass intrusions that create acoustic channels. The unique advantage of this research will be greater understanding and modeling capabilities to predict the evolutionary processes of high-latitude, dense water that have a significant impact on the water mass properties in the region. This also will help us understand and quantify the kinematics and dynamics governing the evolution of high-northern-latitude-originated water and the circulation feeding the lower limb of the Atlantic Meridional Overturning Circulation.

Methodology: In recent decades, the source of deep-water formation in the North Atlantic and Arctic Oceans supporting the large-scale ocean thermohaline circulation has moved southward. It has been observed that the North Atlantic's deep, dense water is now formed south of the Greenland-Scotland Ridge in the Irminger and Iceland Basins (Fig. 1, Panel D), suggesting that deep water is still being formed, but no longer in the Greenland Sea. In addition, recent observations suggest that while deep convection does occur in the Labrador Sea, it does not appear to contribute to the deep water flowing into the deep layers of the Atlantic Ocean. These findings indicate that the Irminger and Iceland Basins are the new high-northern-latitude locations where deep water is formed. The physical mechanisms responsible for the deep-water formation in the Irminger and Iceland basins, and their exact locations, remain uncertain. The goal of the project is to resolve the relevant processes causing the formation of water found exiting these basins at depth. One of the approaches is to perform high-resolution modeling off the eastern coast of Greenland (Fig. 1, Panel C) using the Navy Coastal Ocean Model (NCOM) to investigate the impact that freshwater runoff from ice melt off Greenland and Iceland has on the circulation in the region.

Results: High-resolution (1 km) ocean modeling experiments were performed off the eastern Greenland coast using HPC resources. We added additional freshwater sources to NCOM to account for the ice melt that occurs during the summer months. NCOM originally did not include these types of sources. To examine the impact of this additional freshwater source, twin model experiments were performed. One included freshwater runoff from ice melt and the other did not. Panels (A) and (B) of Fig. 1 show profiles of root-mean-square (RMS) difference for temperature and salinity, respectively, relative to profile observations collected in the Irminger Basin (black dots in panel C). These results reveal that including freshwater runoff in the model improves the accuracy of the predictions. Panel (D) shows a new, high-resolution model domain that encompasses a large section of the North Atlantic and Arctic oceans. This new domain has 1600 × 1200 horizontal grid points and 200 levels and has just been started on the HPC.

DoD Impact/Significance: The Navy needs accurate ocean forecasts, and because of amplified high-latitude warming, circulation in the tactically relevant Greenland/Iceland/United Kingdom (GIUK) gap is changing. Decreasing sea ice coverage and subsurface hydrographic changes in the seas surrounding the Arctic Ocean are causing the origins of the Atlantic Ocean's deep water to change. This research accounts for this variability, leading to new forecasting capabilities for high-resolution ocean circulation and sea ice predictions useful for Navy operations in the GIUK region.

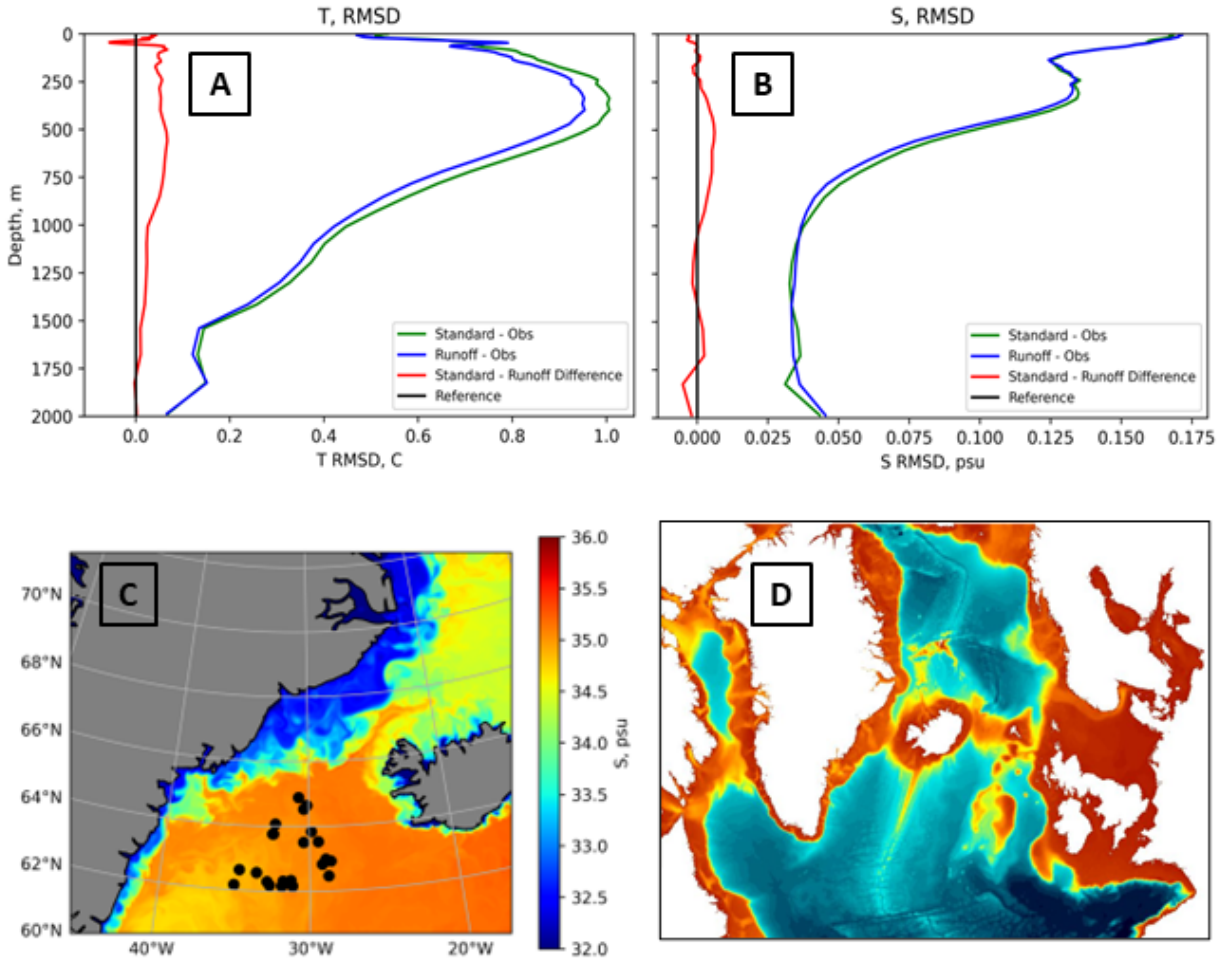

Figure 1. Comparison of root-mean-square (RMS) differences between two high-resolution model runs performed off the eastern coast of Greenland (panel C); one included freshwater runoff from ice melt and the other did not. Panels (A) and (B) show profiles of RMS difference for temperature and salinity, respectively, relative to profile observations collected in the Irminger Basin (black dots in panel C). Panel (D) shows a new, high-resolution model domain that encompasses a large section of the North Atlantic and Arctic oceans. This new domain has 1600 × 1200 horizontal grid points and 200 levels and has just been started on the HPC.

Title: Data Assimilation Studies Project
Author(s): J. Tsu and W.F. Campbell
Affiliation(s): U.S. Naval Research Laboratory, Monterey, CA
CTA: CWO

Computer Resources: HPE SGI 8600, HPE Cray EX, Penguin TrueHPC [NAVY, MS]

Research Objectives: Our objective is to improve the quality of numerical weather predictions (NWP) by leveraging vast quantities of observations. Data assimilation (DA) corrects model analyses of the atmosphere, the ocean, or the surface using a nonhomogenous collection of observations. This project develops, tests, and improves: 1) the development version of the U.S. Navy operational atmospheric global Hybrid 4D-Var assimilation system, which is coupled to our global model NAVGEM (Navy Global Environmental Model), 2) fully ensemble-based DA, 3) coupled ocean-atmosphere global DA, 4) 4D-Var DA for our regional model COAMPS® (Coupled Ocean/Atmosphere Mesoscale Prediction System), 5) the next-generation global model, the Navy Environmental Prediction System Utilizing a Nonhydrostatic Engine (NEPTUNE) DA system, and 6) preparation and testing of new assimilation methods and new observational data types. Our goal is to assimilate traditional data (generally in situ, e.g., weather balloon, ship, or buoy reports) as well as data from a variety of new sources (often spaceborne) efficiently and effectively to provide the best environmental analysis and ultimately to improve numerical weather forecast performance.

Methodology: A variety of experimental setups are designed to develop and test the global and regional models and the associated DA systems. These require, at a minimum, porting and compiling the code to the various HPC platforms, as well as maintenance of large Earth observation repositories covering several years, to be accessed by the various researchers, including in situ and satellite-based observations as well as initial conditions of the modeling systems.

Results: Because DA has a multitude of applications, numerous types of research take place under this project using the Navy's latest global (Hybrid Ensemble NAVGEM, NEPTUNE) and mesoscale (COAMPS®) models, along with our global (NAVDAS-AR, hybrid NAVDAS-AR, and coupled hybrid NAVDAS-AR, JEDI) and mesoscale (COAMPS-AR) DA systems. Results from research performed in FY24 include: 1) assimilating EUMETSAT hyperspectral three-dimensional (3D) wind retrievals in NAVGEM over a two-month (February and April 2023) experiment; the 3D winds contributed modest beneficial impact in terms of adjoint-based forecast sensitivity to observations (FSOI), which is comparable to other satellite wind products; however, an evaluation of statistics from an observing system experiment produced mixed results, 2) potential application of wind retrievals from bistatic high-frequency radar (HFR) for NWP by assimilating hourly HFR wind retrievals from the New York bight in COAMPS®, identified areas where HFR wind vector differences relative to the Un-Restricted Mesoscale Analysis (URMA) were largest and recommended updates for the retrieval algorithm; ultimately, we found that assimilating these HFR winds currently had negligible impact on COAMPS® forecasts in terms of adjoint-based forecast sensitivity to observations and comparison to a control experiment, 3) fixed and improved features, such as NOAA's cloud-liquid-water flag, of AMSR2 assimilation in NAVGEM, 4) transitioned verification software using MET to assess NAVGEM ensemble performance, 5) tested NAVGEM and COAMPS® assimilation of new NOAA-21 AMVs, 6) release testing NAVDAS for COAMPS® 2.8.13, 7) testing a candidate for the next version of NIMO, which likely will be a hybrid of ANCHOR and NRLSAMI, and running additional experiments with the NRLSAMI-EnKF, 8) exploring performance of Desrozier's statistics governing observation uncertainty of assimilated observations in NAVGEM, 9) development and testing of the Ensemble Navy Aerosol Analysis Prediction System (ENAAPSv1.1) and the ENAAPS aerosol data assimilation.

DoD Impact/Significance: The advancements of NEPTUNE, JEDI, NAVDAS-AR, NAVGEM, and COAMPS-AR systems would not have been possible without the HPCMP systems. The core and future of Navy DA capabilities are being developed using the resources provided by HPCMP. In summary, the ability to access the HPCMP resources is critical to prepare technology for successful transfer to operations.

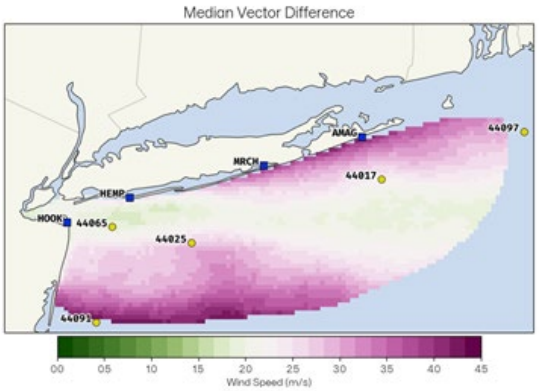

(Left) Median 10 m wind vector difference of HFR hourly winds relative to URMA for the winds considered for assimilation (prior to data thinning) for March 1–23, 2022.

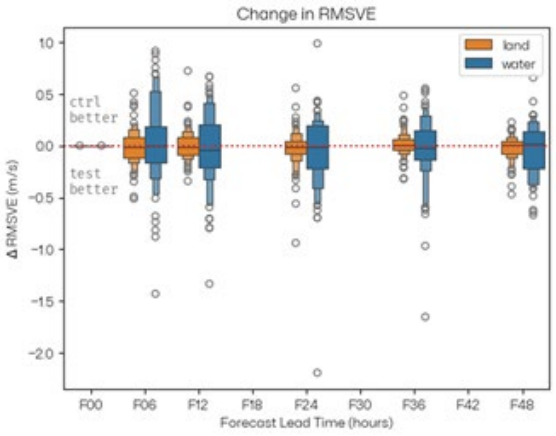

(Right) Change in COAMPS® 10 m wind forecast root-mean-square vector error relative to URMA for 0–48-hour forecasts between a test and control COAMPS® experiment. There was no significant change in the wind forecast accuracy when HFR winds are assimilated.

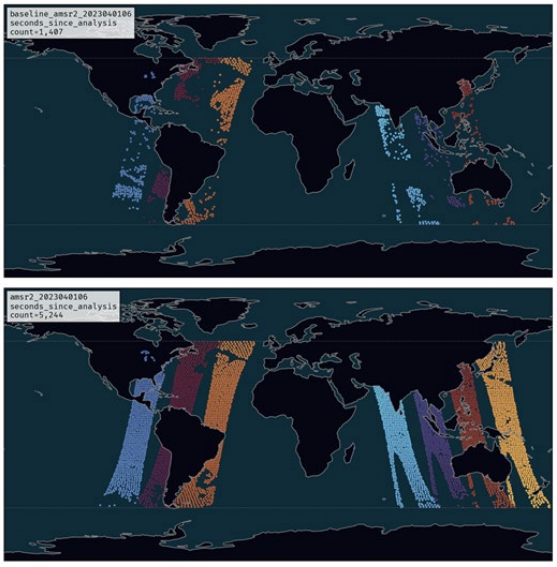

(Left) Unique AMSR2 profiles, colored by observation time, assimilated before (top) and after (bottom) the updates to the AMSR2 preprocessing code for the 06 UTC cycle on April 1, 2013.

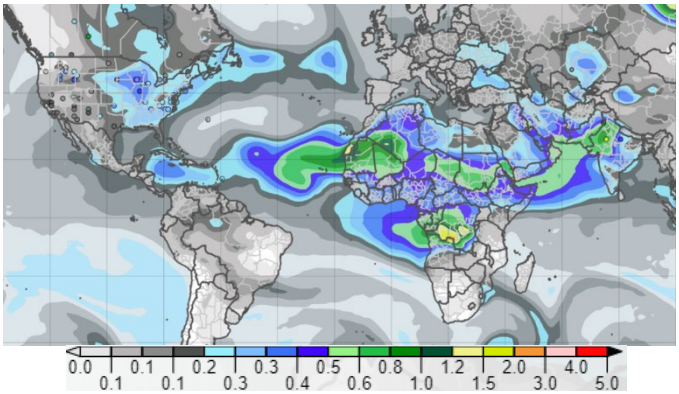

(Right) ENAAPS v1.1 24-hour mean AOD forecast with AERONET obs (circles) valid July 16, 2024 00Z

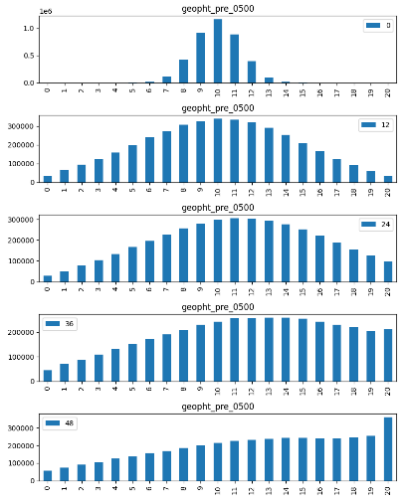

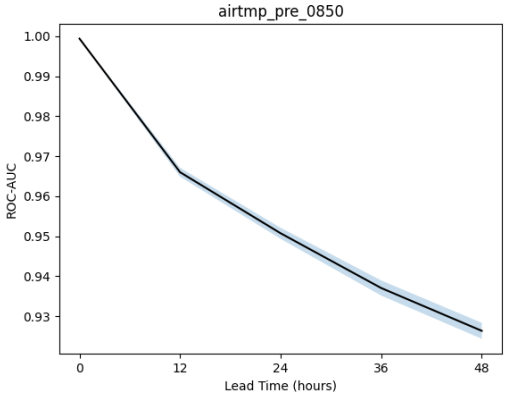

(Left) Ranked histogram (RHIST) and (right) relative operating characteristics-area under the curve (ROC-AUC) results from comparison of a NAVGEM ensemble to ECMWF analysis using Model Evaluation Tools (MET) version 11.0.1 at 12-hour intervals from analysis time to lead time 48.

Title: Performance Study and Potential Optimization Exploration of an Ocean Modeling Code
Author(s): Y. Khine
Affiliation(s): U.S. Naval Research Laboratory, Washington, DC
CTA: CWO

Computer Resources: HPE Cray EX, Penguin TrueHPC [NAVY, MS]

Research Objectives: The goal of this project is to study the performance of HYbrid Coordinate Ocean Model (HYCOM) on various DoD HPC systems using available compilers and profilers. HYCOM is used widely by the U.S. Navy as the ocean component of a global coupled ocean-atmospheric-ice-wave prediction system.

Methodology: In FY24, we continued investigating the performance of HYCOM code on various DoD HPC systems. It is an open-source code and consists of approximately 50 routines and 10 header files written in Fortran 90. The code is implemented with MPI and OpenMP. HYCOM is also one of the benchmarks of HPCMP. We studied the available benchmark test cases as well as a realistic setup of Gulf of Mexico simulation in which the simulation began after 44 days of initial run. The test cases were simulated using different compilers on various HPC platforms. Various profilers including HPCToolkit, VTune, CrayPat, and Tuning and Analysis Utilities (TAU) were used to profile HYCOM on different platforms. The performance of MPI and OpenMP of the code was studied and the possible ways to improve the code were explored.

Results: Figure 1 presents a sample Gulf of Mexico temperature variations after a two-day simulation. The grid size is 541 × 385 with 36 Z-layers. Approximately 150,000 cells represent water. The yellow and orange regions near the land show higher temperatures, while the blue region represents cooler temperatures in the Gulf. The gray area represents the land.

Figure 2 presents a one-day simulation of HYCOM on the Penguin TrueHPC system at the Navy DSRC (Nautilus) using one node. The comparison is between four MPI ranks in red and four OpenMP threads in yellow for the same test case. The efficiency of the top eight most time-consuming routines was presented here, and the last set of columns presents the total efficiency of the simulation. For most of the routines, MPI performs much better than OpenMP, especially for the most time-consuming “momtum” routine. The overall efficiency of the MPI run is much higher than that of the OpenMP run. Because the performance of OpenMP lags behind MPI, poor performance is observed for hybrid (MPI+OpenMP) simulations. In addition, load imbalance is observed when running with a large number of processors. We have identified the ways to improve the performance of OpenMP as well as the overall performance of the code, and the recommendations are presented to the HYCOM group, who utilizes the code for large-scale simulations for forecasting weather.

DoD Impact/Significance: Since ocean modeling requires a large computational domain on the scale of kilometers and a long physical time that is “many days” forecast, it is important to achieve results in a desired time frame. The performance studies of the HYCOM code indicate potential bottlenecks in the code that prevent the code from performing efficiently on state-of-the-art DoD HPC systems. The recommendations were made to improve the performance of the code in order to utilize the HPC resources efficiently. Accurate ocean forecasting is very important to DoD to achieve successful missions and it is also vital in preventing potential natural disasters.

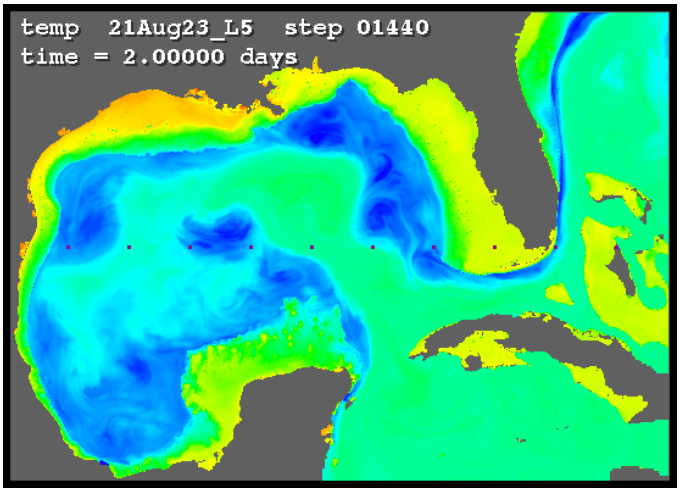

Figure 1. Sample Gulf of Mexico simulation.

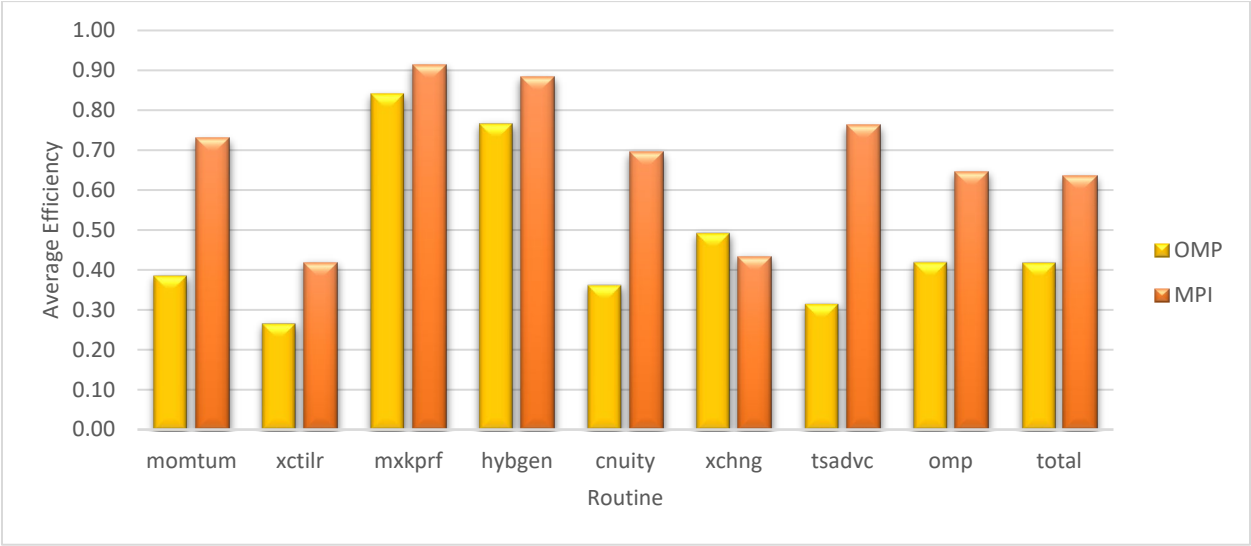

Figure 2. Details of MPI and OpenMP profiling results of Gulf of Mexico one-day simulation.

Title: Ocean Data Assimilation – Multiscale, Multiphysics Ocean Data Assimilation
Author(s): J.M. D'Addezio,[1] A.J. Iversen,[2] G. Jacobs,[1] and S.R. Smith[1]
Affiliation(s): [1]Naval Research Laboratory, Stennis Space Center, MS; [2]Peraton, Stennis Space Center, MS
CTA: CWO

Computer Resources: HPE SGI 8600 [NAVY, MS]

Research Objectives: NRL's multiscale ocean data-assimilation technology has been demonstrated by Souopgui et al. [1] and currently is moving toward operation. While the technology is novel, much of the core algorithm is based on older technology embedded within the Navy Coupled Ocean Data Assimilation (NCODA) system. One such system is the Improved Synthetic Ocean Profile (ISOP), which transforms a sea surface height anomaly (SSHA) observation into a temperature/salinity profile that then is assimilated into the ocean model. ISOP uses a set of climatologically based covariances to make the synthetic profiles, and the multiscale assimilation system uses those same covariances in each of the two analysis steps that are performed. This is problematic because the second analysis step, which is meant to correct smaller scales, has ocean features that deviate significantly from climatology. Our work this fiscal year has addressed this current shortcoming so that the small-scale step of the multiscale ocean assimilation system makes synthetic ocean profiles that are more consistent with the true ocean physics at smaller scales.

Methodology: Four years of model data were analyzed to produce both large- and small-scale temperature/salinity covariances as a function of depth. Those depth-depth covariances were used to replace the current climatology-based covariances within ISOP. Then, using an observing system simulation experiment (OSSE), we ran experiments in which we were able to compare the prior multiscale ocean data-assimilation algorithm directly to our new version using scale-dependent depth-depth temperature/salinity covariances. The ocean model we used was run at 1 km horizontal resolution with 100 vertical layers over a very large geographic area off the U.S. West Coast (Fig. 1). Given these considerations, our experiments could be run only on HPC, which proved invaluable for deriving the results we detail below.

Results: Using our OSSE setup, we harvested simulated observations from our "truth" simulation and assimilated them into three simulations that started at a different initial condition from the "truth," each using a different ocean assimilation method: single-scale assimilation, multiscale assimilation, and multiscale, multiphysics assimilation. Figure 1 shows an example of the types of ocean model corrections made by the two multiscale assimilation methods. Figure 2 compares the two multiscale methods directly while also comparing with the single-scale assimilation. The multiscale, multiphysics assimilation, our novel methodology, often outperforms both the single-scale and multiscale assimilation methods or does at least as well. This short period of testing shows that our methodology is promising, and we will continue the experiments throughout FY25.

DoD Impact/Significance: Navy ocean models are used frequently to provide to warfighters valuable information related to the battlespace environment. A critical element to the ocean-modeling system is the process of data assimilation. Model errors grow exponentially over time, making having an accurate initial model condition vital to the modeling process. The data-assimilation process takes recent observations and corrects the ocean model. Recent observation types now observe both large- and small-scale ocean features. Older Navy data-assimilation systems could not correct smaller-scale ocean features. The Navy's multiscale ocean data-assimilation system can, but the system required some modification to account for both the spatial scales and the physics of both large- and small-scale processes. We anticipate that this modification will increase the accuracy of the Navy's modeling system further, thereby providing more accurate information to warfighters.

References

[1] Souopgui, I., D'Addezio, J. M., Rowley, C. D., Smith, S. R., Jacobs, G. A., Helber, R. W., Yaremchuk, M., and Osborne, J. J. (2020). Multi-scale assimilation of simulated SWOT observations. *Ocean Modelling*, *154*, 101683

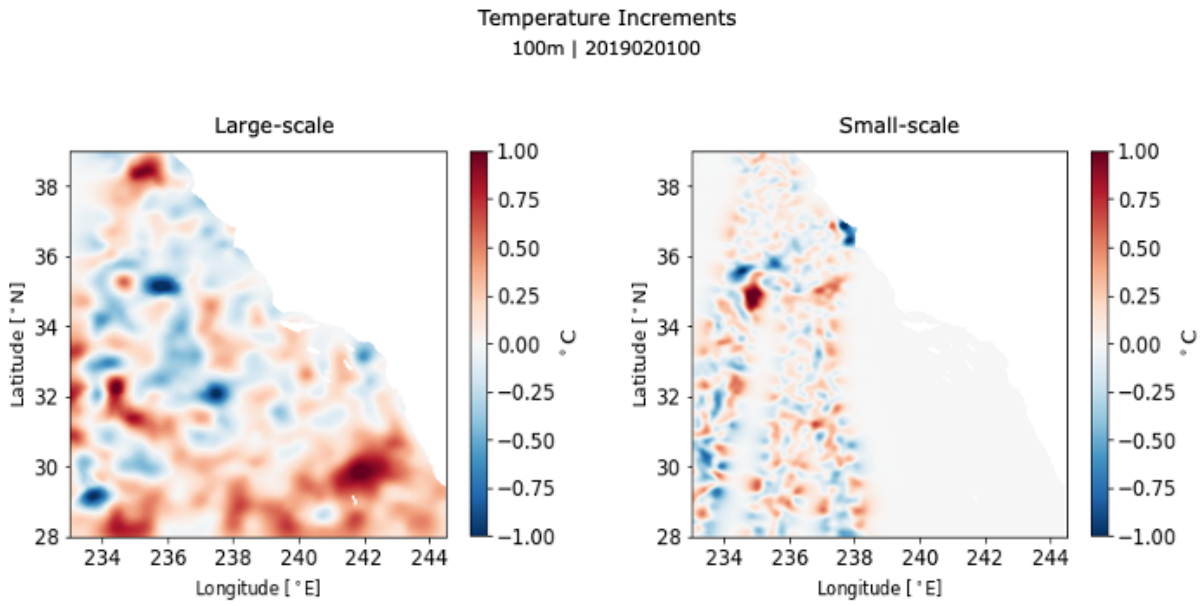

Figure 1. Example of ocean model corrections produced by the Navy's multiscale ocean data-assimilation system. (left) large-scale update from the first assimilation step and (right) small-scale update from second assimilation step.

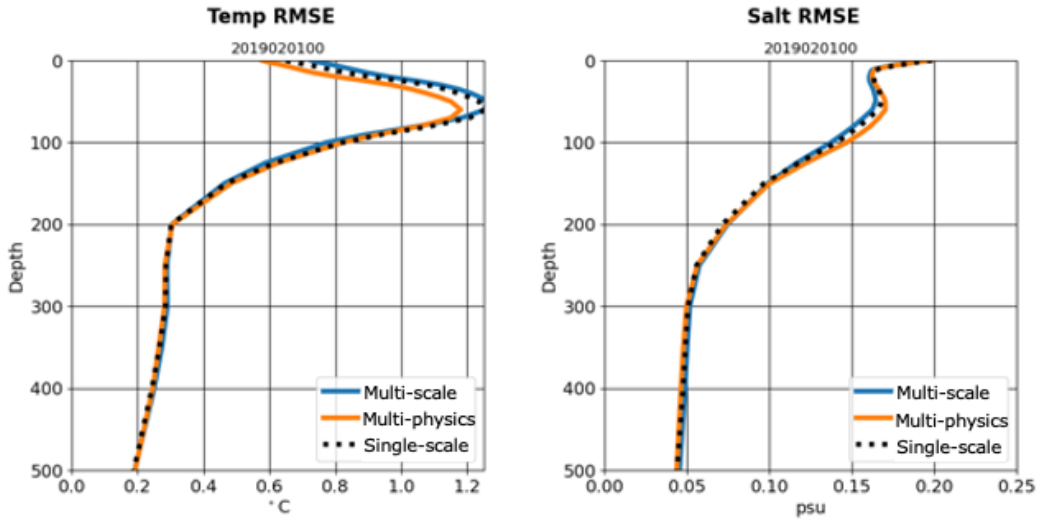

Figure 2. Example root-mean-square (RMS) (left) temperature error and (right) salinity error with depth comparing a single-scale assimilation (dashed, black line), a multiscale assimilation (blue line), and a multiscale, multiphysics assimilation (orange line).

Title: Velocity Data Assimilation
Author(s): S.R. Smith, R.W. Helber, and G. Jacobs
Affiliation(s): U.S. Naval Research Laboratory, Stennis Space Center, MS
CTA: CWO

Computer Resources: HPE SGI 8600, HPE Cray EX, Penguin TrueHPC [NAVY, MS]

Research Objectives: The scope of this project is to continue the validation of the velocity data-assimilation capability so it can be transitioned and used in the operational prediction systems in the upcoming fiscal year. In FY24, the primary focus was getting the velocity data-assimilation capability to work within the Navy Coupled Ocean Data Assimilation (NCODA) system version 4.4, which is embedded in the Coupled Ocean/Atmosphere Mesoscale Prediction System (COAMPS®) version 2023. We also began embedding the velocity data-assimilation capability in NCODA ver. 5.1, which will be the official version that will go into the next transitions of COAMPS® and ESPC.

Methodology: The velocity data-assimilation capability has been developed and was tested in the Gulf of Mexico. Two papers and a validation test report were published detailing this effort. This test, however, used an older version of NCODA and COAMPS®. To transition this capability into operations, it had to be embedded into the system versions that are going to be transitioned. Therefore, in FY24, we performed experiments using NCODA ver. 4.4 and COAMPS® ver. 2023 in both the Gulf of Mexico and the western Atlantic (Fig. 1, panels A and B, respectively). These locations were selected because a large deployment of drifters was conducted, signified by the black dots and lines in panels A and B of Fig. 1. Because NCODA is designed to resolve geostrophic dynamics, the velocity observations that are assimilated need to be processed to include just the geostrophic component. This is accomplished by computing Eulerian velocities using a long time period between successive drifter locations. We use a period of 24 hours here, which is roughly the inertial oscillation period for this region, to filter out much of the small-scale or high-frequency features not resolved by our assimilation system and to focus on the components of velocity more likely to be in geostrophic balance.

Results: The first validation in the Gulf of Mexico was a repeat of the initial test that was used to write the validation report and two papers. The only difference was that the latest versions of NCODA and COAMPS® were used. This was a short test just to verify that the results are like those found in the initial test. Panel C of Fig. 1 shows analyses of this experiment on four consecutive days in the northeastern portion of the domain. The color contour in these plots is temperature at 100 m, the black vectors are surface velocity, and the green vectors are the drifters that were assimilated. These results are very similar to the initial experiment, and the flow of the analyses generally matches the flow of the drifters. The next validation effort that was performed in FY24 was a twin experiment performed on a 1 km horizontal grid with 100 levels within the northwest Atlantic (WATL) domain (Panel B of Fig. 1). The first experiment is a control run that had velocity assimilation turned off. This control run was initiated using the Global Ocean Forecasting system on February 1, 2022, and assimilating the normal operational data stream of observations. The other experiment was initiated using the CNTRL run on March 1, 2022, and includes the assimilation of velocity observations in addition to the standard stream of observations used in the control run. Velocity observations come from the LANT drifter data set (black dots in Panel B of Fig, 1), which lasted from March 2022 through February 2023. Both experiments were performed through the end of December 2022.

DoD Impact/Significance: The assimilation experiments tested under this project went toward improving the Navy's capability of forecasting the ocean environment and directly address Navy priorities as outlined in the following documents: OPNAVN2N6E FY 2021 RDT&E Priorities Letter 3062, Ser N2N6E/20U119707 (March 26, 2020), and the NRL ocean modeling roadmap developed in consultation with the Navy operational modeling centers the Naval Oceanographic Office (NAVOCEANO) and the Fleet Numerical Meteorology and Oceanography Center (FNMOC).

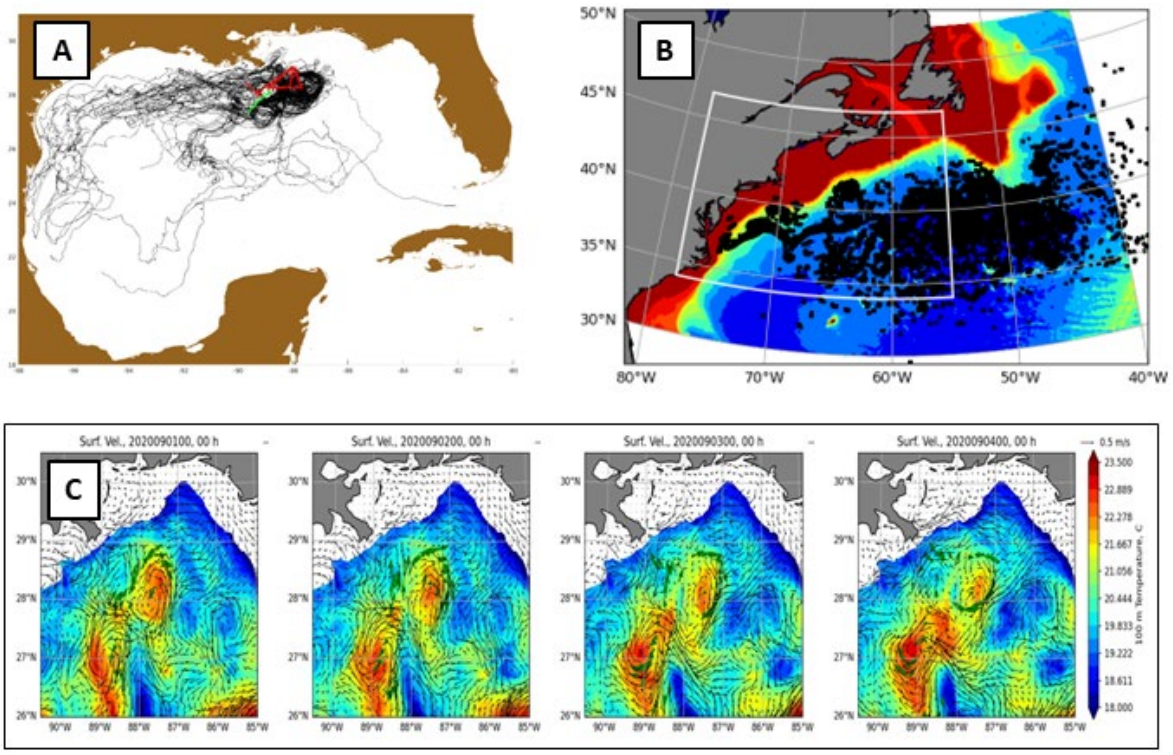

Figure 1. The velocity data-assimilation capability has tested and is being tested in the Gulf of Mexico (Panel A) and a western Atlantic domain (white box in Panel B). Velocity derived from drifters (black dots and lines in Panels A and B), deployed by the Ocean of Things field study, are being assimilated. Panel C is snapshots of the velocity data-assimilation analyses on four consecutive days in the northeastern portion of the Gulf of Mexico domain. The color contour is temperature at 100 m, the black vectors are surface velocity, and the green vectors are the drifters that were assimilated.

Title: Impact of SWOT Observations on the Ocean Subsurface
Author(s): B. Rester[1] and M.J. Carrier[2]
Affiliation(s): [1]American Society for Engineering Education Postdoctoral Fellow at the U.S. Naval Research Laboratory, Stennis Space Center, MS; [2]U.S. Naval Research Laboratory, Stennis Space Center, MS
CTA: CWO

Computer Resources: HPE SGI 8600 [NAVY, MS]

Research Objectives: To examine the impact of wide-swath altimeter observations, as collected by NASA's Surface Water and Ocean Topography (SWOT) mission, on the ocean model subsurface features of mixed layer depth (MLD), thermocline depth (TD), and downstream acoustic simulations.

Methodology: The model domain for the experiments presented here covers the Southern California region (SoCal) from 118° W to 130° W and from 30° to 42° N. The model uses a spherical projection with a horizontal resolution of 3 km for the assimilative model and 1 km for the nature run. For this work, we ran three assimilation experiments to determine the impact of SWOT observations on the ocean subsurface: 1) using standard 3DVAR assimilation with standard nadir altimeters, 2) using standard 3DVAR assimilation with SWOT observations, and 3) using multiscale 3DVAR (MS3DVAR) assimilation with SWOT observations. The multiscale 3DVAR method uses multiple outer loops of the assimilation and gradually reduces background error correlation scales to progressively correct the ocean model state from large to small scales. Each experiment assimilated SSH from −120 hours to +12 hours relative to the analysis time. The assimilation runs differ from the nature run regarding horizontal resolution, 1 km for the nature run and 3 km for the assimilation runs, as well as in the vertical resolution, 100 levels for the nature run and 50 levels for the assimilation runs. The assimilation runs also had a different initial condition from the nature run, offset in time by 15 days. These differences result in an assimilation model that is, initially, very different from the nature run model solution.

Results: The OSSE for this work is configured for the Southern California domain and the experiment was run from 1 October 2022 through 31 December 2022. The accomplishments of this work in FY24 involve configuring the OSSE environment, running the high-resolution nature run model, simulating the observations from the nature run, and running the assimilation experiments. In this case, the experiments run include: 1) standard 3DVAR using standard altimeters, 2) standard 3DVAR using SWOT, and 3) multiscale 3DVAR using SWOT. The results indicate that the multiscale 3DVAR with SWOT outperformed the other two runs, as expected. We are now examining the impact on the ocean subsurface characteristics as well as the impact to acoustic simulations, which rely on the ocean model output to characterize the environment.

DoD Impact/Significance: The impact of wide-swath altimeters on the ocean subsurface can have a substantial positive impact on downstream acoustic modeling. Determining the best methods for incorporating these observations into the Navy's ocean models will improve the acoustic modeling and tactical decision aids that the warfighter relies on.

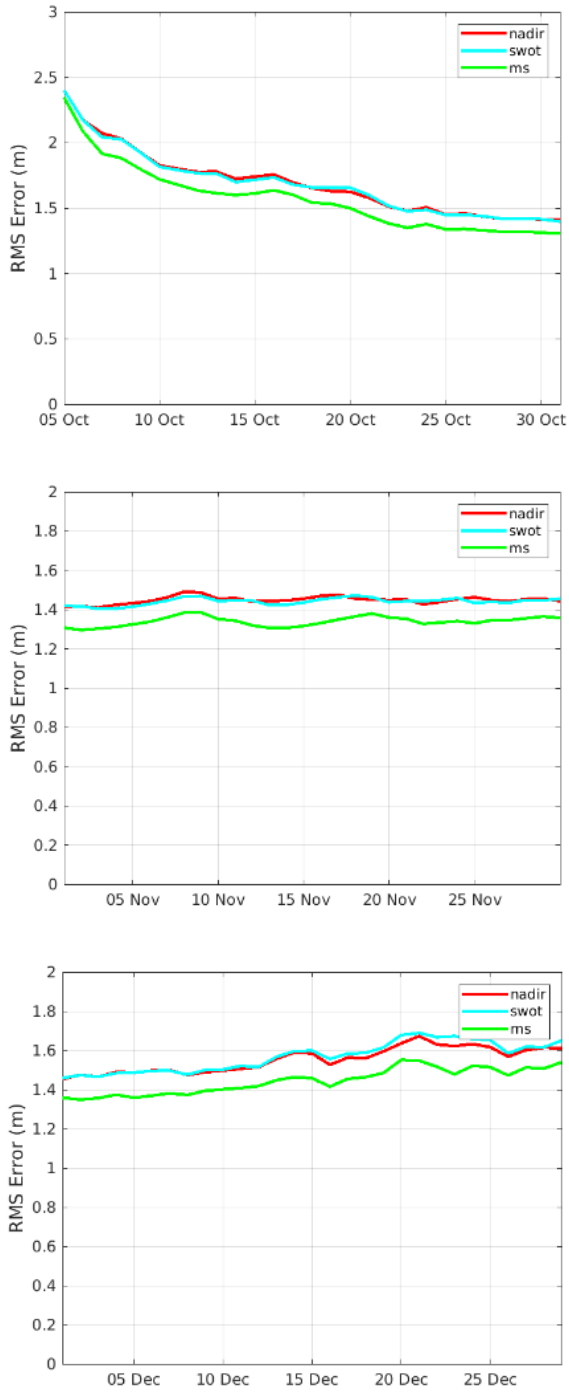

Figure 1. Error in the ocean model 24-hr forecast thermocline depth, averaged over the entire model domain daily for the 3DVAR using nadir altimeters (red line), 3DVAR using SWOT altimeters (blue line), and multiscale 3DVAR using SWOT altimeters (green line).

Title: Ocean Modeling for Acoustic Impacts
Author(s): J.J. Osborne,[1] C.M. Amos,[2,3] G. Jacobs,[1] J.W. Book,[1] C.N. Barron,[1] and A. Lawrence[4]
Affiliation(s): [1]U.S. Naval Research Laboratory, Stennis Space Center, MS; [2]American Society for Engineering Education Postdoctoral Fellow at the U.S. Naval Research Laboratory, Stennis Space Center, MS; [3]Applied Physics Laboratory, Johns Hopkins University; [4]Peraton, Inc., Stennis Space Center, MS
CTA: CWO

Computer Resources: HPE SGI 8600 [NAVY, MS]

Research Objectives: This work investigates vertical structure of the ocean and how temperature and salinity features impact underwater sound speed, with particular emphasis on features located below the surface mixed layer/surface duct and above the deep sound channel. Ocean-acoustic features in both the Pacific Ocean along the U.S. West Coast and the North Atlantic Ocean have been analyzed.

Methodology: Both observations and data-assimilating ocean model results are analyzed to understand ocean vertical structure. Observations utilized include both sources of opportunity (ARGO floats, commercial ship data) as well as dedicated field experiments (gliders, research vessels) collected by the Office of Naval Research's Task Force Ocean research programs in the Pacific and the North Atlantic. Model results are from a series of models covering the study areas with configuration appropriate to local dynamics. Data assimilated includes "routine" data from national and international observation networks (sea surface temperature, sea surface height, ARGO float profiles) and dedicated project observations (gliders, ship CTDs, ship XBTs, and other ship-based underway sensors). Cyber infrastructure was developed to share, process, and ultimately, to assimilate project observations in real time. Real-time model results enabled so-called "adaptive sampling" to conduct acoustic transmission experiments (principal investigator: YT Lin, Scripps Institute of Oceanography) in ocean-acoustic features of interest. Without real-time model results, the ability to conduct acoustic transmission experiments in features of interest is reduced greatly (depending on the feature). Real-time model results also were used to generate glider guidance (PIs: Donglai Gong, Virginia Institute of Marine Science, and Karim Sabra, Georgia Institute of Technology) for sampling ocean-acoustic features.

Results: A major set of results from this work includes an analysis of ocean vertical structure on the U.S. West Coast, specifically, vertical gradients of temperature and salinity and understanding how those properties change from assimilation of 1) remotely sensed data, 2) remotely sensed data in combination with in situ data, or 3) assimilation of no data at all (*Impacts of Assimilating Satellite and In Situ Observations of Modeling Thermocline and Halocline Properties off Oregon, USA;* Amos, Osborne, and Jacobs, 2024, in submission to *Journal of Ocean Modelling*). Assimilating data results in vertical gradients with up to a 60% reduction in error versus assimilating no data at all. For the North Atlantic study area, results are recently available, and analysis is ongoing. A significant finding is the skillful prediction of a parcel of cold water that was transported > 200 km over ~14 days (Fig. 1). The presence of this parcel was modeled in real time and was used to place acoustic transmission experiments through adaptive sampling.

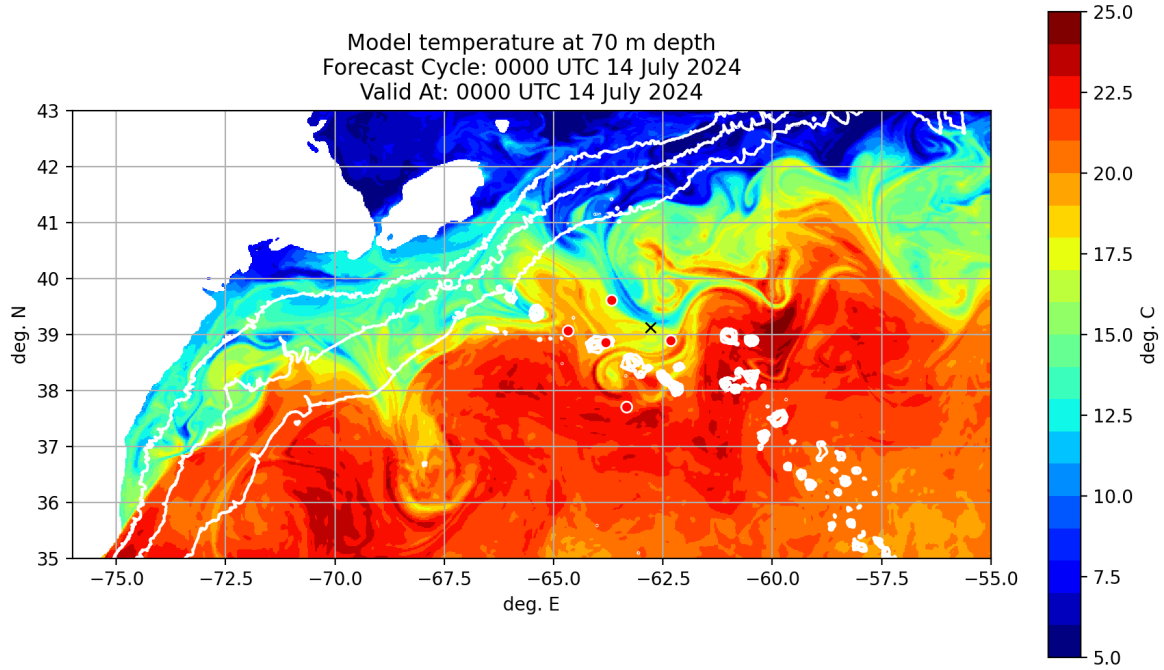

Figure 1. Ocean model temperature at 70 m depth in North Atlantic Ocean along the U.S. East Coast. Five red circles clustered near −63.0°E, 39.0°N mark the position of oceanographic moorings. The black X near −63.0°E, 39.0°N marks the location of an observed water parcel with temperature 5°C. The model places the water parcel within a few kilometers after transporting the parcel from the Scotian shelf and then along the edge of an eddy, originating more than 200 km to the northeast of the observed location.

Title: Atmospheric Process Studies
Author(s): J.A. Ridout, T.R. Whitcomb, M.A. Janiga, and J.M. McLay
Affiliation(s): U.S. Naval Research Laboratory, Monterey, CA
CTA: CWO

Computer Resources: HPE SGI 8600, HPE Cray EX, Penguin TrueHPC [NAVY, MS]; HPE Cray EX [AFRL, OH]; Cray XC40/50 [ERDC, MS]

Research Objectives: The objectives of this project are to improve the Navy's global weather-prediction capability and, from a basic research perspective, to improve our understanding of the dynamical and physical mechanisms that operate in the atmosphere, including its interactions with land and ocean. Basic research helps to inform forecast system development, so this component complements our more direct efforts to enhance Navy battlespace awareness.

Methodology: The project this year focused largely on features and applications of our operational global atmospheric forecast system NAVGEM (Navy Global Environmental Model). Efforts were directed at development of model physics, as well as improved ensemble forecasting techniques, including development of postprocessing methods involving both bias and variance correction. The work addressed both the "stand-alone" (uncoupled) NAVGEM as well as NAVGEM as a component of the Navy Earth System Prediction Capability (ESPC) coupled system.

Results: We made significant progress on updates to the Navy ESPC configuration of the NAVGEM model physics. Development was supported by a combination of NAVGEM uncoupled data-assimilative cycling runs, as well as hindcast tests in Navy ESPC. Progress on a Navy ESPC v2.1 system prototype through this project included updates to the treatment of turbulence mixing, as well as the representation of land-surface roughness.

NAVGEM ensemble system development included experimental runs for each of two prospective upgrades to the system: an increase in ensemble size from 20 to 30 members, and an increase in horizontal resolution from 37 km to 31 km. In addition, European Center for Medium-Range Weather Forecasting (ECMWF) ERA5 global analyses were used to extend benchmark postprocessing of NAVGEM ensemble cloud cover forecasts to the global scale. We demonstrated that the system is very effective in reducing forecast bias in operationally relevant regions in the Pacific (Fig. 1). We also generated an extended 24-year NAVGEM reforecast ensemble dataset that will facilitate advanced neural network postprocessing of global ensemble cloud cover.

Postprocessing tests also were carried out with operational forecasts from the Navy ESPC-E v1 ensemble. A range of fields that are used in operational products were bias corrected, resulting in some very significant reductions in forecast biases. In addition, a variance-correction procedure was applied, bringing the variance/squared-error ratio to near unity in all regions for the fields that were tested, indicating a well-calibrated ensemble (Fig. 2). This is a substantial improvement from the original forecasts, which suffered from underdispersion.

DoD Impact/Significance: Advances in forecast skill and in our understanding of atmospheric processes and forecast uncertainty targeted through this project enable delivery to decision makers of more accurate weather information for environmentally sensitive risk assessment. HPCMP resources are critical in this work, the downstream impacts of which are mediated through other closely connected Navy efforts supported by HPCMP. An example is the deployment to Navy operations this year of the first deterministic high-altitude version (ESPC-D v2.0) of the Navy ESPC system, the culmination of a multiyear development cycle.

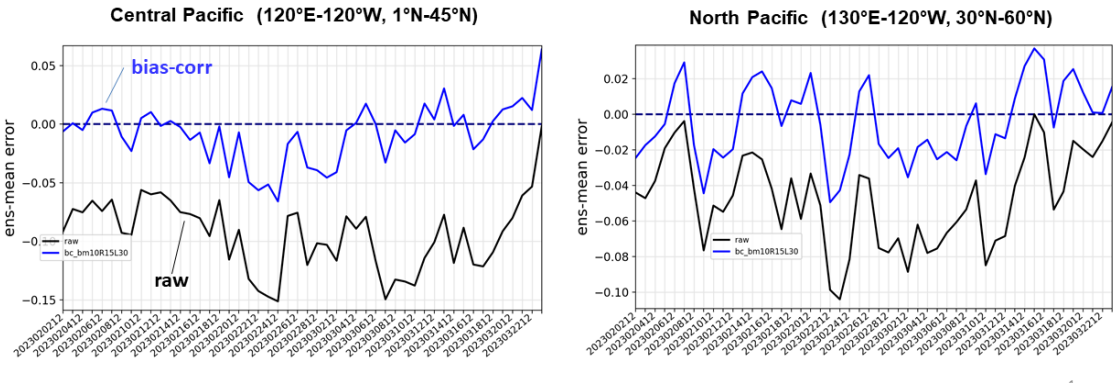

Figure 1. Bias-correction of NAVGEM ensemble-mean fractional cloud-cover forecasts. Error at 48 h from daily forecasts from February 2 to March 23, 2023 (black curve – raw data, blue curve – bias corrected). Significant improvements are shown for regional averages for a portion of the central Pacific (left) and a partially overlapping region centered farther north (right).

Title: Coupled Ocean-Wave-Air-Ice Prediction System
Author(s): R. Allard,[1] T. Campbell,[1] E. Douglass,[1] D. Hebert,[1] T. Jensen,[1] G. Panteleev,[1] M. Phelps,[2] and T. Smith[1]
Affiliation(s): [1]U.S. Naval Research Laboratory, Washington, DC; [2]Peraton, Inc., Stennis Space Center, MS
CTA: CWO

Computer Resources: HPE SGI 8600, HPE Cray EX [NAVY, MS]

Research Objectives: Perform research studies with the Coupled Ocean/Atmosphere Mesoscale Prediction System (COAMPS®), which is six-way coupled with the Navy Coastal Ocean Model (NCOM), WAVEWATCH-III® (WW3) and SWAN wave models and the COAMPS® atmospheric model. Perform modeling studies with the Community Ice Code (CICE v6), which includes a landfast ice parameterization.

Methodology: For accurate simulation and prediction on regional scales in the tropics, we have used various configurations of NRL's state-of-the-art fully coupled atmosphere-ocean-wave model system COAMPS® with very high spatial and temporal resolution. One component under development for COAMPS® is the generation of spatially varying coefficients for grounding and tensile strength for landfast ice in Arctic regions. These spatially varying parameters will be used in regional COAMPS-CICE and Navy Earth System Prediction Capability (ESPC) V2 ensemble and deterministic forecast systems.

Results: We performed landfast ice (LFI) studies using CICE6 for the Arctic. We added two Kara Sea regions for landfast ice studies. We used a conjugate gradient technique to produce optimized spatially varying grounding parameters (k_1) for landfast ice studies. GOFS 3.1 reanalysis fields were used for CICE initial/boundary conditions. NAVGEM atmospheric forcing was used to drive the yearlong simulations. Validation studies for the COAMPS-CICE system will be performed in FY25. We have identified three test areas: 1) the Beaufort Sea for the 2015 ONR Sea State Experiment, 2) MOSAiC for 2019–2020 in the region between Greenland and Norway where we are investigating Arctic cyclones, and 3) the Baltic Sea. In all three domains, we will perform studies with the fully coupled COAMPS-CICE system and will compare against operational systems such as GOFS 3.1 and observed data. We performed multiyear testing of Antarctic landfast ice with CICE6 on a 1/12° regional SH domain. We found that increasing the CICE6 subcycles to 720 and using tensile strength value of $k_t = 0.2$ gave best results. Testing subsequently was performed with ESPC-D (1/25°), showing good results for the Ross Sea. Figure 1 depicts the National Ice Center analysis for January 12, 2024, showing the presence of landfast ice. The figures on the right show how well the landfast ice is captured in ESPC-D for the same date. We made recommendations for ESPC V2.1 for model settings. We began testing with the new C-grid discretization in CICE v6.5.0, which allows transport in channels that are one grid cell wide — a capability that is not possible with the B-grid. CICE v6.5.0 was modified to read HYCOM ocean forcing on both the B and C grids, allowing for uncoupled tests. We are presently performing initial testing with this new code. We identified and added missing fluxes within the COAMPS® framework, including sea ice melt rate, sea ice velocity, freshwater flux, and shortwave flux through sea ice. This captures more physical processes in the coupled ice/ocean/atmosphere system.

DoD Impact/Significance: The development of a coupled air-ocean-wave prediction system can have a pronounced effect on Navy forecasting by improving ASW performance, tropical cyclone prediction, and search-and-rescue and mission planning. The relocatable COAMPS-CICE system will provide high-resolution Arctic forecasting of ice thickness, ice drift, and concentration to support navigation. Inclusion of landfast ice in the Navy's global ice prediction systems will yield a more realistic representation of pan-Arctic sea ice.

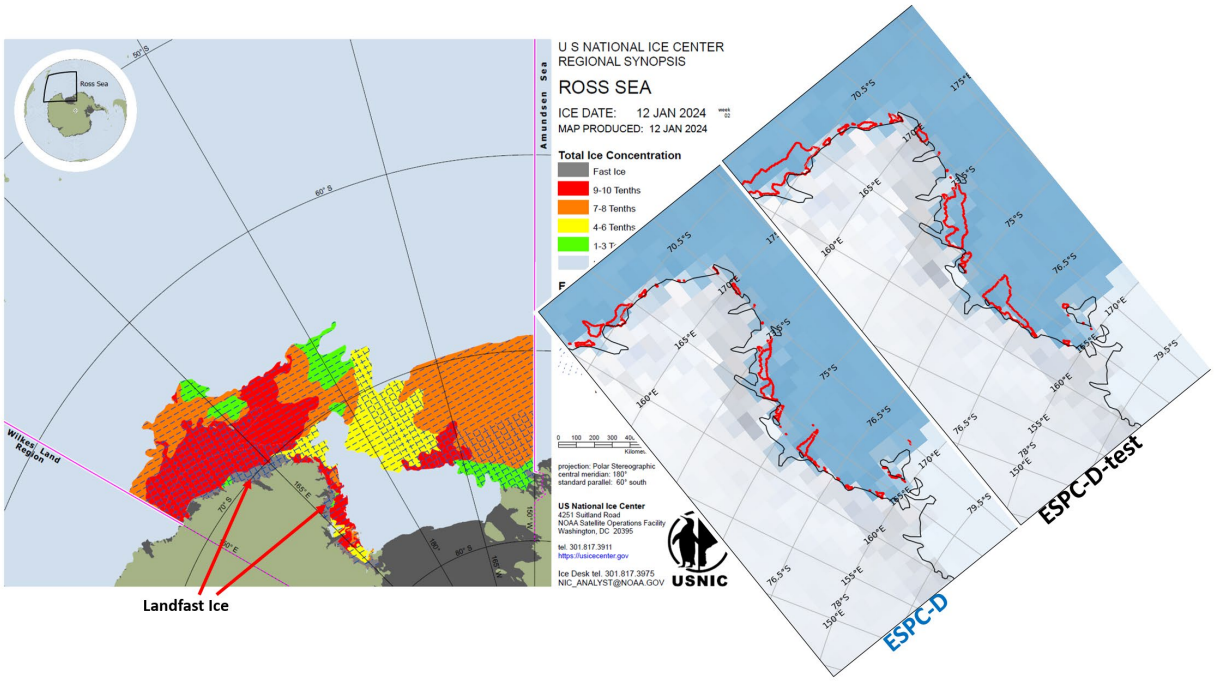

Figure 1. Left) NIC analysis of landfast ice (gray shade) in the Ross Sea on January 12, 2024. Middle) ESPC V2 landfast ice extent (red lines) on January 12, 2024. Right) Improved landfast ice extent on the same date using optimized landfast ice parameters.

Title: Multiscale Characterization and Prediction of the Global Atmosphere from Ground to the Edge of Space using Next-Generation Navy Modeling Systems
Author(s): C.A. Barton, S.D. Eckermann, J.F. Kelly, M.A. Herrera, K.W. Hoppel, D.D. Kuhl, D.R. Allen, J. Ma, and T. Rhodes
Affiliation(s): U.S. Naval Research Laboratory, Washington, DC
CTA: CWO

Computer Resources: Cray XC40/50 [ERDC, MS]; HPE SGI 8600, HPE Cray EX, Penguin TrueHPC [NAVY, MS]

Research Objectives: To develop and test new, seamless atmospheric specification and prediction capabilities from 0 to 500 km altitude for future Navy Earth System Prediction Capability (ESPC) and ground-to-space numerical weather-prediction systems, linking prediction of the ocean, atmosphere, and space over time scales from hours to decades.

Methodology: This project develops and tests key components of state-of-the-art systems required for improved modeling, prediction, and analysis of the extended operational environment for Navy applications, focusing on the atmosphere, the near space, and the geospace. Several model prototypes and operational systems are under development, including: a) two high-altitude versions of the Navy Global Environmental Model (NAVGEM), based on upward extensions of the Navy's operational global numerical weather prediction (NWP) system into 1) the middle atmosphere for seasonal prediction (NAVGEM-MA) and 2) the upper atmosphere for thermospheric prediction and data assimilation (NAVGEM-HA), and b) two high-altitude extensions of the next-generation Navy NWP model NEPTUNE (Navy Environmental Prediction system Utilizing a Nonhydrostatic Engine) comprising 1) a "middle atmosphere" extension (NEPTUNE-MA) for seasonal prediction and 2) a ground-to-space prototype extended into the thermosphere (NEPTUNE-HA).

Results: Major results directly facilitated by HPC resources during FY24 include: a) production of deep-atmosphere data-assimilation runs from NAVGEM-HA for backgrounds of gravity-wave models and initialization of NEPTUNE forecasts, b) completion of a suite of seasonal NAVGEM-MA forecasts with bias correction obtained from long-term meteorological analysis products covering 11 contiguous years, c) study of dynamics and predictability of sudden stratospheric warmings and planetary wave propagation in the NAVGEM-MA coupled forecast/data-assimilation system (Fig. 1), d) continued validation of new wind measurements from meteor radar and satellite observations to improve the NAVGEM-HA reanalysis of the mesosphere and the lower thermosphere, e) development of ground-to-space NAVGEM and NEPTUNE modeling capabilities using advanced numerical algorithms that enable the dynamical cores to operate at high altitudes, including a complete refactor of upper-atmosphere physics schemes to comply with the Common Community Physics Package framework used by NEPTUNE and a complete merger of the high-altitude NEPTUNE capability into the release version of NEPTUNE as a latent capability (Fig. 2), and f) development and demonstration of a "file-drop" coupler driving SAMI3 ionospheric forecasts with thermospheric specification from NAVGEM-HA data-assimilation runs and NEPTUNE-HA forecasts.

DoD Impact/Significance: This research addresses Navy/DoD requirements to develop and test new high-altitude atmospheric specification and prediction capabilities leading to 1) a planned Navy Earth System Prediction Capability (ESPC) and 2) a Navy space weather-prediction capability. This project performs the R&D needed to install high-altitude (both middle- and upper-atmosphere) specification and forecast capability in next-generation Navy NWP systems, ultimately providing improved near-space specification and prediction to the warfighter over both tactical and strategic time frames. HPC resources for this project provide critical support for the development of novel ground-to-thermosphere NWP models fully coupled to ionospheric models and data assimilation to address key space-environment prediction goals of the Defense Advanced Research Projects Agency's Space Environment Exploitation (DARPA SEE) program.

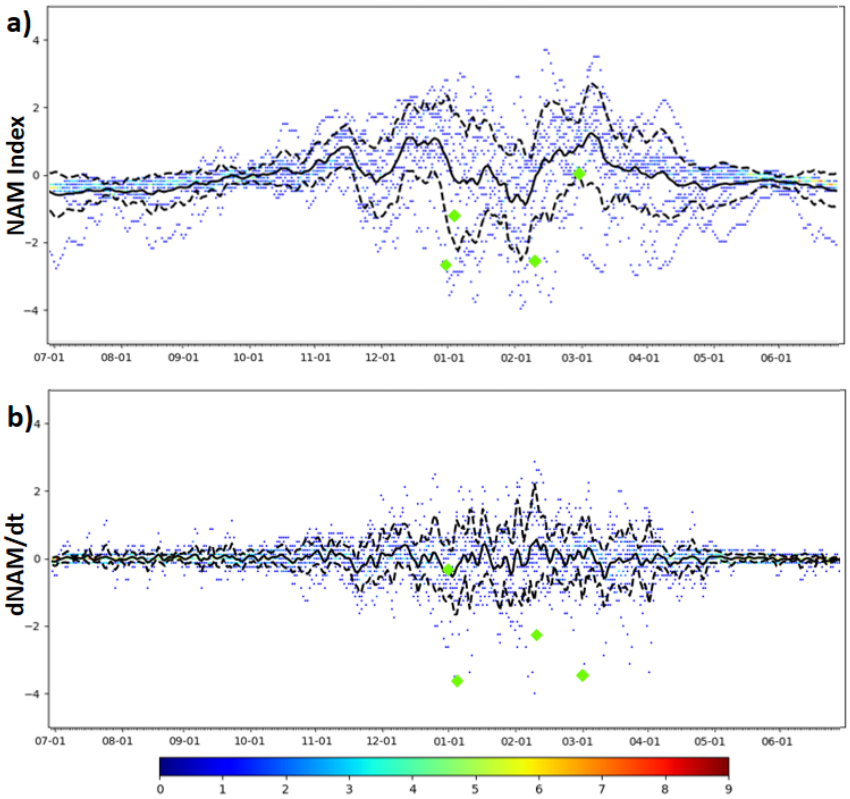

Figure 1. Binned count of number of days of the year between 2010 and 2021 with a value of NAM (top) or dNAM/dt (bottom), with sudden stratospheric warming onset days indicated by the green diamonds, analyzed from NAVGEM-MA 6-hour reanalysis run using HPC resources.

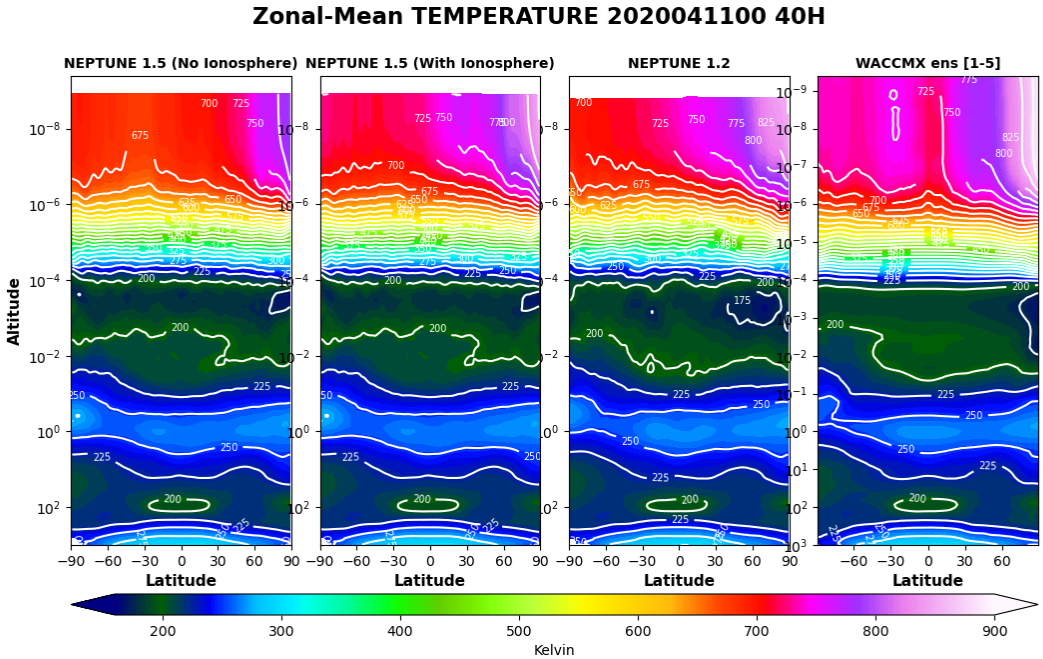

Figure 2. Comparison of NEPTUNE-HA full-physics forecasts against WACCM-X data (right) to validate the new "version 1.5" NEPTUNE-HA with dynamics and physics merged into the release build.

THIS PAGE INTENTIONALLY LEFT BLANK

ENS

Electronics, Networking, and Systems/C4I

ENS focuses on the use of computational science in support of analysis, design, modeling, and simulation of electronics from the most basic fundamental, first-principles physical level to its use for communications, sensing, and information systems engineering. Accordingly, ENS activity ranges from the analysis and design of nanodevices to command, control, communications, computers, intelligence, surveillance, and reconnaissance (C4ISR) systems of systems. This focus ties together nanoelectronics, acoustoelectronics, microelectromechanics, optoelectronics, photonics, circuits, and networks through the exploration of passive/active devices, detectors, emitters, and their physical integration and system deployment in a network-centric warfare environment. ENS has developed computational methods for investigating phenomena at the nanoscale and smaller. These include studies of electronic structure, charge transport, optical and photonic interactions, and the behavior of analog/digital circuits. ENS also addresses system-level challenges in communications, sensing, and networked information systems, focusing on areas like data links, signal propagation, and performance analysis for information warfare and large tactical networks.

Title: Simulation of Passively Mode-locked and Frequency Modulated Interband Cascade Laser Frequency Combs
Author(s): M. Povolotskyi,[1] I. Vurgaftman,[2] and J.R. Meyer[2]
Affiliation(s): [1]Jacobs, Hanover, MD; [2]U.S. Naval Research Laboratory, Washington, DC
CTA: ENS

Computer Resources: HPE SGI 8600, Penguin Open Compute Platform (OCP), HPE Cray EX [AFRL, OH]; HPE SGI 8600 [NAVY, MS]

Research Objectives: 1) Use the HPC cluster to extend the numerical modeling software for interband cascade laser (ICL) frequency combs. 2) Perform a numerical study of key factors affecting amplitude modulated (AM) combs in ICL.

Methodology: The light propagation inside the cavity is modeled in the slowly varying envelope approximation with a single-transverse-mode cavity being considered. The group velocity dispersion (GVD) of the mode without the active-layer effect is obtained from an external simulator. A stable algorithm based on the fast Fourier transform for the pulse-propagation simulation allows us to treat the GVD effects up to an arbitrary order. The active-layer effect is included in the light-propagation equation via a dipole polarization term. The polarization is computed by solving the semiconductor Bloch equations for the coupled electric-field/electron/hole system. The major difference between interband and intraband systems is that in the interband system, the transition energy depends on the electron wavevector. Therefore, the laser's performance depends on the distribution of electrons and holes over the Brillouin zone. Modeling of a nonequilibrium electron gas distribution over energy is a challenging task. In this research, it is assumed that the electron and hole relaxation times are constant, so the electrons and holes gradually thermalize to the local Fermi distributions. Previously, we used a model in which electrons and holes were delivered to the active well by a constant injection current. A new model has been developed in which each stage of the ICL contains an electron injector, a multiple quantum well structure that can accumulate and release electrons before they are injected into the active well (Fig. 1c). The transfer of electrons between the injector and the active well is modeled assuming elastic scattering with an energy-independent scattering time. The injector is doped by donors to improve the ICL performance. The process of dopant ionization and recombination is modeled using the mass action law.

Results: Two types of structures have been simulated: a homogeneous-cavity structure (Fig. 1a) and a structure in which the cavity has a saturable absorber (SA) (Fig. 1b). The homogeneous structure has a CW output with periodic modulation (a frequency-modulated (FM) comb). Experiment has shown a nonmonotonic dependence of the threshold current on the injector doping density [1]. The simulation is able to reproduce this dependence quite well (Fig. 1d). The minimal threshold current corresponds to the doping value that leads to equal densities of electrons and holes in the active well (Fig. 1e). For AM comb operation, the injector doping affects the comb formation (Fig. 2). A low doping density leads to broad output pulses, hence narrow spectra. At very high doping, the AM combs cannot be generated. A moderate optimal doping density is predicted to deliver a narrow pulse, provided that electrons and holes are removed from the SA efficiently. The SA optimization is part of ongoing research. Use of the HPC facility is critical for this work because the ICL needs to be simulated for 200 ns of operation time until the AM comb stabilizes. A single simulation requires 2 hours of wall time on 96 CPU cores.

DoD Impact/Significance: AM combs in type-II ICLs have not yet been realized experimentally. The simulations suggest that the holes in the existing designs are not removed from the SA active well during the round-trip time, which prevents AM comb phase locking. The modified designs with optimized doping of the injector will enable more rapid removal of the holes.

References
[1] Vurgaftman, I., Bewley, W. W., Canedy, C. L., Kim, C. S., Kim, M., Merritt, C. D., Abell, J., Lindle, J. R., and Meyer, J. R., Rebalancing of internally generated carriers for mid-infrared interband cascade lasers with very low power consumption, *Nature Communications*, 2(1):585, 2011, DOI: 10.1038/ncomms1595

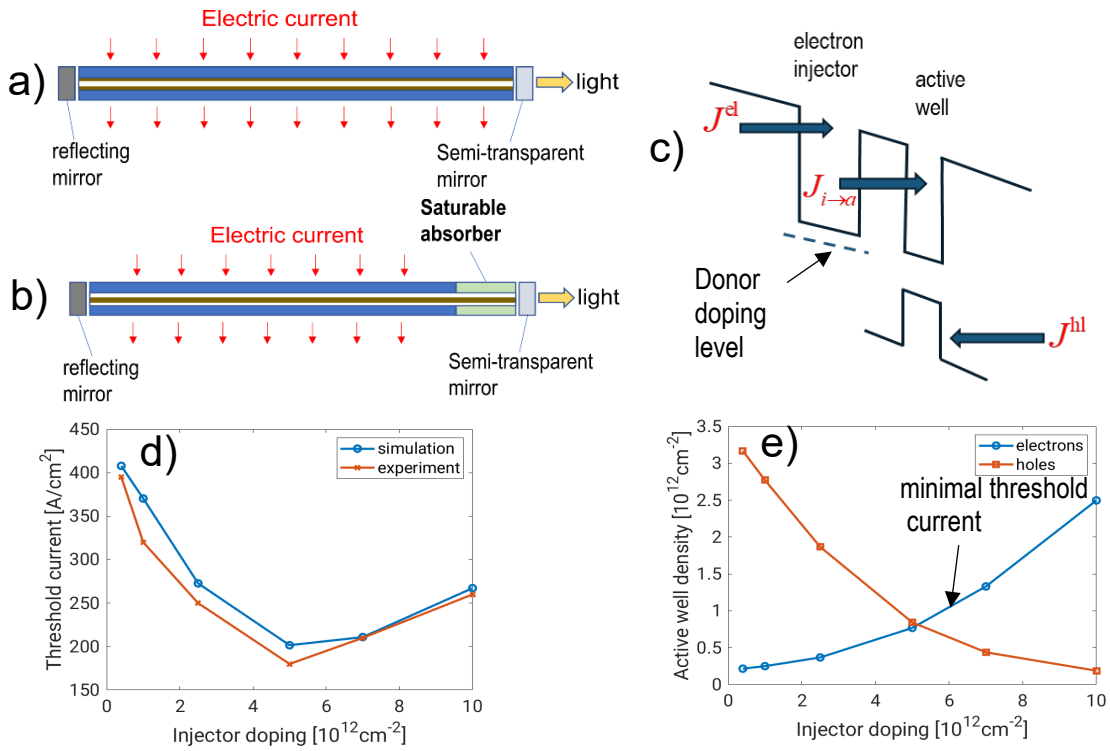

Figure 1. Simulation results for the AM comb. a, b) Schematic layout of the laser structures for FM and AM combs, respectively. c) Band diagram for the laser stage used in the model. d) Threshold current vs. injector doping density. e) Electron and hole density in the active well for the above-threshold regime vs. injector doping density.

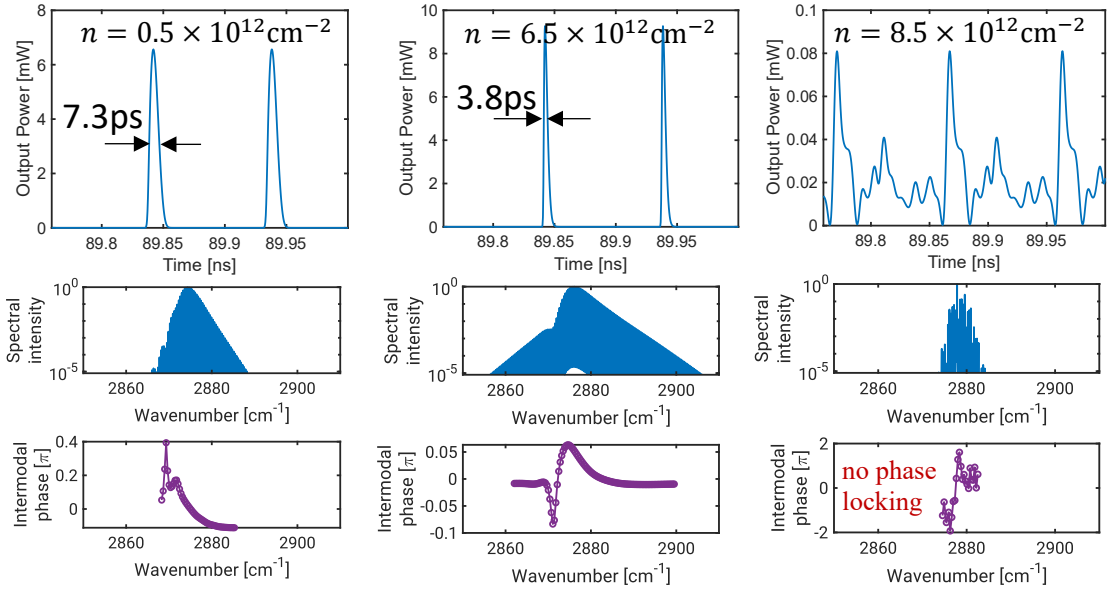

Figure 2. ICL output computed for different doping densities. Top: output power for different injector doping densities: 0.5×10^{12} cm^{-2}, 6.5×10^{12} cm^{-2}, and 8.5×10^{12} cm^{-2}. Bottom: Output spectral intensity and intermodal phases for different injector doping densities.

THIS PAGE INTENTIONALLY LEFT BLANK

SIP

Signal Image Processing

SIP covers the extraction of useful information from sensor outputs in real time. DoD applications include surveillance, reconnaissance, intelligence, communications, avionics, smart munitions, and electronic warfare. Sensor types include sonar, radar, visible and infrared images, and signal intelligence (SIGINT) and navigation assets. Typical signal-processing functions include detecting, tracking, classifying, and recognizing targets in the midst of noise and jamming. Image-processing functions include the generation of high-resolution, low-noise imagery, and the compression of imagery for communications and storage. The CTA emphasizes research, evaluation, and testing of the latest signal-processing concepts directed toward these embedded systems. Usually, such processors are aboard deployable military systems and hence require hefty packaging and minimum size, weight, and power. System affordability is expected to improve by an order of magnitude through the development of scalable codes running on flexible HPC systems. This will enable the traditional expensive military-unique “black boxes” required to implement high-speed signal/image processing to be replaced by COTS HPC-based equipment.

Title: Retrieving Surface Soil Moisture from CyGNSS Reflectivity Measurements
Author(s): J.D. Ouellette, E.M. Twarog, L. Li, and S.M. Grossman
Affiliation(s): U.S. Naval Research Laboratory, Washington, DC
CTA: SIP

Computer Resources: HPE Cray EX [NAVY, MS]

Research Objectives: Measuring surface soil moisture (SSM) at global scale is an important component in forecast models of the Earth's water and carbon cycles. SSM serves to regulate the separation of incident solar radiation into sensible and latent heat flux and thus helps to determine the flow of water between the Earth's surface and the atmospheric boundary layer. The Cyclone Global Navigation Satellite System (CyGNSS) is a NASA-funded constellation, presently comprising seven operational microsatellites, each of which receives Global Positioning System (GPS) signals reflected from the Earth's surface. The primary science goal of CyGNSS is to characterize ocean surface winds during tropical cyclone conditions but, given the properties of land surface reflections measured by CyGNSS, several investigations have been launched into producing SSM and inundation products using CYGNSS data. This project investigates the derivation of soil dielectric properties and volumetric SSM from CyGNSS by applying a change-detection algorithm to a time series of conditioned CyGNSS reflectivity observations. This serves as a less computationally intensive alternative to existing machine learning algorithms.

Methodology: The approach employs a matrix-based change-detection algorithm to derive SSM estimates from CyGNSS reflectivity data. An NRL Karles Fellowship supported development of the original version of this SSM retrieval algorithm, referred to as the time series ratio (TSR) method. The algorithm relies on ratios between consecutive radar backscatter or reflectivity values within a time series of observations. These ratios, which populate the off-diagonal terms of the sparse TSR matrix equation, theoretically change only with changes in SSM, given that changes in surface roughness and/or vegetation are negligibly small between each repeat pass. The TSR method originally was conceived for use with L-band radar and radiometer data from NASA's Soil Moisture Active/Passive (SMAP) mission. TSR method error performance with SMAP data has been assessed since using in situ data; the TSR method outperformed the official SMAP algorithm, and furthermore, it required no training data and minimal ancillary information. The same algorithm has been applied since to CyGNSS under this project, with significant modifications being necessary for application to this sensor suite, including reflectivity preconditioning. This preconditioning includes screening for coherence-dominant or low-signal-to-noise-ratio reflectivity values and also includes a novel denoising procedure known as diagonal loading.

Results: Error analyses for the CyGNSS/TSR algorithm were performed over a roughly three-year period from late 2018 through late 2021. Figure 1 shows the increased coverage, both as a global map and as a function of land cover type, which results from the relaxation of quality-control thresholds made possible by the diagonal loading denoising and preconditioning technique employed here. Figure 2 shows the algorithm root-mean-square error (RMSE) using the Soil Moisture Active/Passive level-2 product as a standard. Note that RMSE values are reported with the relaxed quality-control thresholds applied. It has been found that the relaxation of these thresholds does not impact the accuracy of the SSM estimates in a significant way.

DoD Impact/Significance: Navy forecasting tools use models of soil moisture, derived from precipitation measurements, in order to constrain storm forecasts. This project addresses the following science and technology areas identified by the Navy: Assure Access to Maritime Battlespace, Information Dominance, and Platform Design and Survivability.

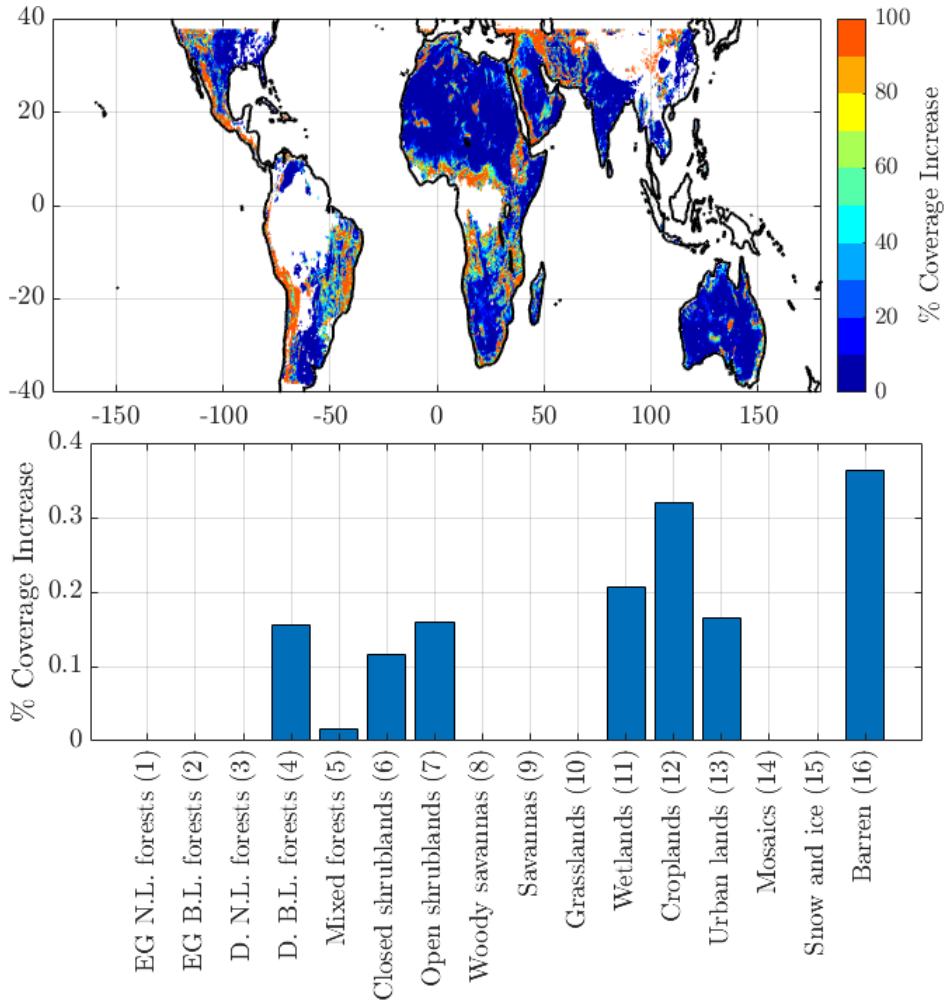

Figure 1. Increased coverage resulting from relaxation of quality-control thresholds on signal coherence and signal-to-noise ratio, made possible by the introduction of a diagonal loading denoising technique. Percentages are reported as an increase compared to the legacy quality-control thresholds.

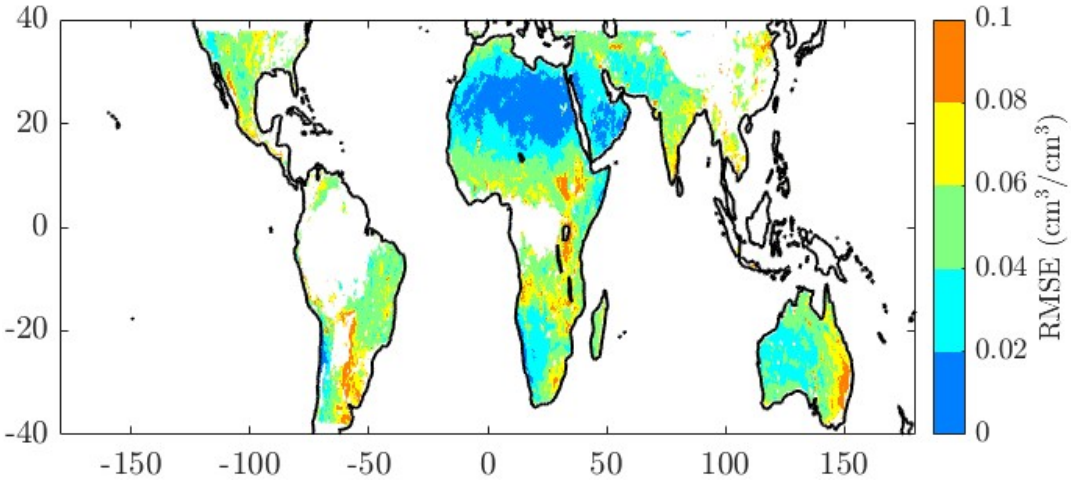

Figure 2. Global root-mean-squared error of the CyGNSS/TSR algorithm over a 3-year assessment period, using the official SMAP level-2 SSM product as a baseline for comparison.

Title: Application of Physics-based Machine Learning to Navy Problems
Author(s): L.N. Smith
Affiliation(s): U.S. Naval Research Laboratory, Washington, DC
CTA: SIP

Computer Resources: Penguin Open Compute Platform (OCP), HPE Cray EX, [AFRL, OH]; Liqid [ARL, MD]; Penguin TrueHPC [NAVY, MS]

Research Objectives: The overarching goal of our Improving Generalization of Neural Networks for Physics Domains project in FY24 was to investigate and develop various generalization methods across three critical physics domains: acoustics, meteorology, and materials science. Our primary focus aimed to bridge existing gaps in research to enable neural networks to excel at physics tasks across various physical environments and boundary conditions.

Methodology: Our technical approach made significant strides in this regard. Deep learning techniques have demonstrated exceptional success in computer vision and language tasks. However, there remain significant gaps in the field's research that hinder their successful application to physics problems. Our research endeavored to fill these gaps and to provide valuable insights into the fundamental workings of neural networks in this context.

In FY24, we developed a neural network-based emulator for modified refractivity in the marine atmospheric surface layer (MASL), a dynamic environment with varying vertical profiles of thermodynamic variables, including temperature, humidity, pressure, and wind. This emulator complemented our existing work in the acoustics domain, where the input "image" represents undersea physical properties that impact sound travel in the ocean, known as the sound speed profile (SSP). The output "image" is the transmission loss predicted by the acoustics simulator.

Results: We conducted extensive experiments with a range of well-known generalization methods to test our hypothesis that they would improve generalization in the physics domains. However, our experiments demonstrated that these methods were ineffective in this context. Consequently, we shifted our focus to experimenting with novel approaches to generalization, such as a Contrastive Language Image Pre-training (CLIP) method for creating a "foundation model" for a specific physics domain. This technique involves using unsupervised learning to train encoder parts of two generative systems on vast amounts of data with a loss function that rewards correct matching of input/output pairs and punishes incorrect matches. The encoders are then frozen, and training of only the decoders is performed on specific areas of the world. Our hypothesis is that this pretraining enables greater generalization abilities.

In addition to our research efforts, we also refactored our codebase and performed software engineering to improve performance. Emulation of physics simulators in both acoustics and meteorology problems obtained speedups of more than two orders of magnitude.

DoD Impact/Significance: Our work demonstrates that applying machine learning to a variety of physics problems is sound. We are now applying machine learning methods to solve other challenges in various physics domains in order to enable substantially improved environmental and situational understanding by our fleet. In addition, the understanding gained by the experiments on the HPC GPU servers builds on all the previous understanding gained from previous experiments, and this understanding is crucial for our future progress in the field.

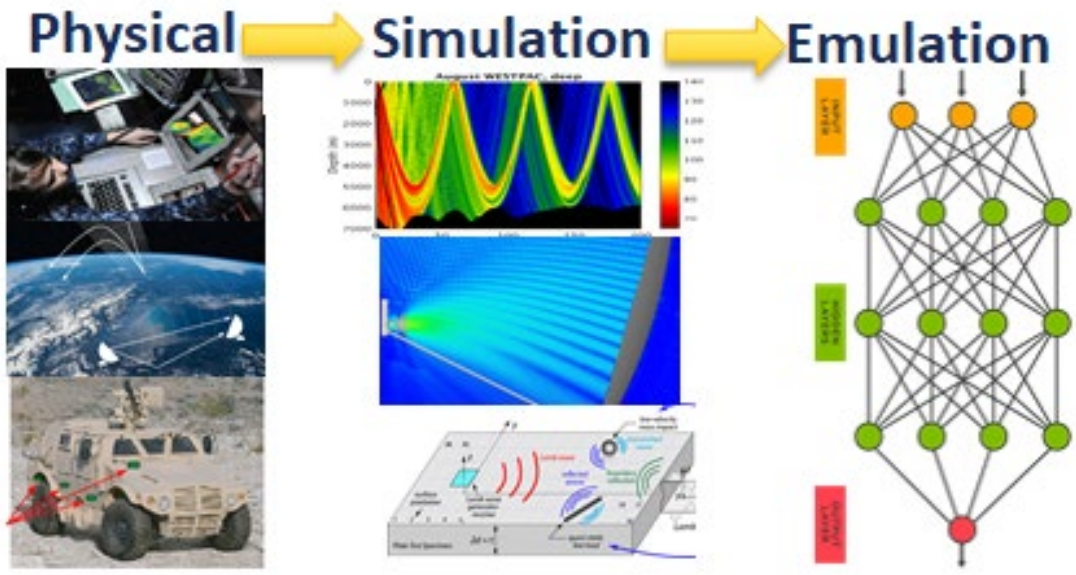

Figure 1. This figure represents the concept of using generative neural network models to emulate the results of a computationally expensive physics simulator. Our emulations run orders of magnitude faster than physics simulations, providing a substantial advantage for warfighters in computationally constrained environments.

Title: Task Force Lima
Author(s): L.N. Smith
Affiliation(s): U.S. Naval Research Laboratory, Washington, DC
CTA: SIP

Computer Resources: Liqid [ARL, MD]

Research Objectives: The overarching goal is to develop, evaluate, recommend, and monitor generative AI capabilities, including large-language models, to support operational and enterprise requirements. The objective of this project was to develop and test a proof-of-concept prototype for utilizing generative AI (Gen AI) as "mission engineering." Our primary goals for this project are twofold: significantly reduce mission planning time and enhance the quality of mission plans. By harnessing Gen AI, we aim to transform the mission-planning process, making it more efficient and effective while ensuring high-quality outcomes.

Methodology: Our first tasks included establishing the core infrastructure for prototype development, which requires a significant investment in initiating this project. Our GAME plan involved acquiring high-quality data, open-source large language models (LLMs), and computing resources, alongside an in-depth analysis of the project's requirements and crafting a strategic implementation plan. We worked on HPC systems because of the high resource requirements of LLMs. We created proxy unclassified data to facilitate our investigations. The current best open-source LLMs that we used included Llama-3, Mixtral-8-32B, and Google's Gemma.

Secondly, we investigated the essential elements of a "mission record" such that the record concisely and completely contains the salient information leading to the decision steps of the mission plan (i.e., mission orders, supporting information, plans, lessons learned, and outcomes).

Results: Our efforts centered around three key initiatives: refining TravelPlanner, developing a fuel planner, and creating an action wargame simulation. TravelPlanner saw remarkable improvements in accuracy when we delved into prompt engineering techniques. However, the most significant strides were made when we adopted a hybrid approach, combining LLMs with deterministic helper functions. This fusion of methodologies yielded the most substantial leaps in precision.

The fuel planner project posed a unique challenge: creating a scheduling algorithm for aerial refueling that addressed the complexities of tanker and receiver coordination. Through our work, we were able to develop a solution that effectively tackled these issues.

NEXUS, our wargame simulation, was designed to simulate intricate scenarios using LLM-driven personas built on sophisticated, prompt engineering techniques. This approach allowed us to provide realistic and strategic challenges, further highlighting the potential of LLMs in real-world military applications.

DoD Impact/Significance: In summary, our work on the GAME project has demonstrated the vast potential of LLMs to improve mission-planning processes significantly. The solutions we have developed are not only robust but also scalable, offering promising applications in real-world military contexts.

Our agentic approach, combining LLMs with verification and algorithm components, showed great promise in achieving unparalleled speed and precision in next-generation tactical planning. Furthermore, the integration of LLM personas into wargame simulations enhanced the strategic depth and realism of the Red Team decisions, offering varied and dynamic gameplay experiences. The ExpeL framework was explored to communicate the LLM's thought process linguistically to both the user and the LLM itself, enabling self-reflection and insight extraction.

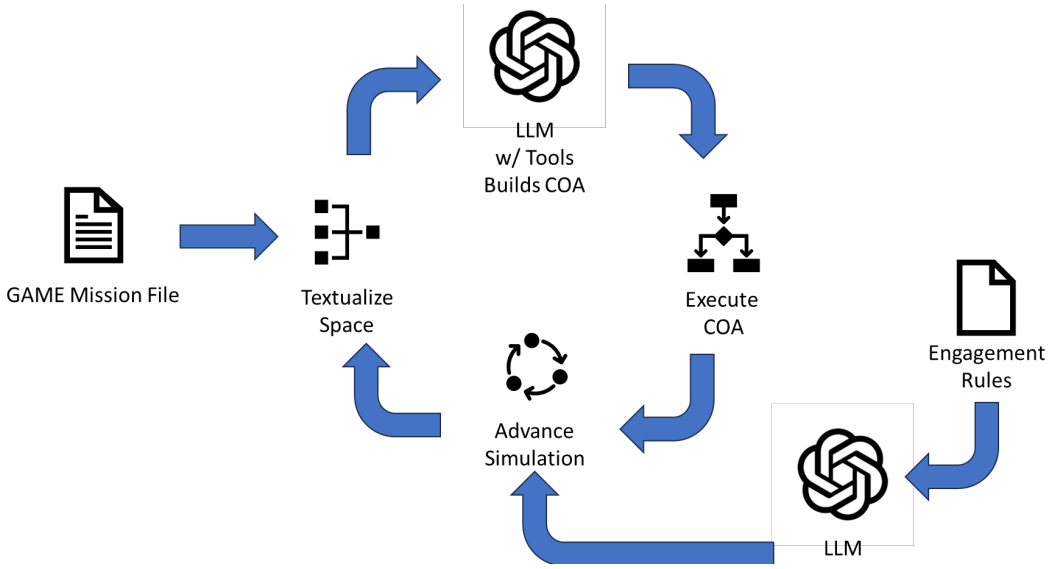

Figure 1. This figure represents the concept of using language-based generative neural network models (a.k.a. large language models) as an agent for mission planning.

THIS PAGE INTENTIONALLY LEFT BLANK

SAS

Space and Astrophysical Science

Space and astrophysical science (SAS) research and development advance understanding, specification and prediction of the Earth's atmospheric and space domains to exploit the extended operational environment for military advantage and to minimize environmental impacts on military operations. The SAS Computational Technology Area (CTA) embodies the use of mathematics, computational science, and engineering in the analysis, design, identification, modeling, and simulation of the space and near-space environment, and of all objects therein, whether artificial or natural. The SAS CTA encompasses foundational discovery research to study the atmospheres of the Sun and the Earth, including solar activity and its effects on the Earth's atmosphere and ionosphere and near-Earth space, and the unique physics and properties of celestial sources. SAS employs an extensive array of physical and empirical models and analysis tools to integrate observations and theoretical understanding for ever-improving DoD enterprises within, and exploitation of, the extended operational environment. The CTA melds the strengths of a broad range of physical sciences — atomic and molecular physics, materials science, plasma physics, applied optics, radiation survivability, electronic warfare, directed-energy technology, astronautics and space propulsion, orbital mechanics, space situational awareness, and remote sensing — into a structure that helps the DoD multiply force combat effectiveness.

Title: Searches for Millisecond Pulsars and Pulsar Emission Modeling
Author(s): P.S. Ray[1] and J. Deneva[2]
Affiliation(s): [1]U.S. Naval Research Laboratory, Washington, DC; [2]George Mason University, resident at U.S. Naval Research Laboratory, Washington, DC
CTA: SAS

Computer Resources: Cray XC40/50 [ERDC, MS]; Penguin TrueHPC [NAVY, MS]

Research Objectives: The first goal of this project is to search for millisecond pulsars in ground-based data from the Robert C. Byrd Green Bank Telescope (GBT) in West Virginia as well as a backlog of survey data from the decommissioned Arecibo Telescope in Puerto Rico. These searches require high-performance computing resources because of the massive parameter spaces that must be searched. The second goal of the project is to model the X-ray emission of pulsars based on data from the NICER X-ray telescope that is currently on the International Space Station.

Methodology: We use custom codes to search for pulsations in our radio data sets. These correct for frequency-dependent delays caused by interstellar dispersion and variable Doppler shifts caused by orbital acceleration in a binary system, then search over a broad range of candidate frequencies using very large Fourier transforms and harmonic summing. We split up the trials over a set of nodes on the cluster. We use another custom code to model pulsar emission. This is an iterative, computationally intensive process involving multithreaded calculations of the Bayesian likelihood of a number of model parameters.

Results: We used Raider to fit several emission models of PSR J1231-1411. Each model includes known pulsar parameters such as the rotation period and pulse shape, unknown parameters such as the pulsar's mass and radius, and the locations and shapes of the hot spots on the pulsar's surface that produce the X-ray emissions. In addition to using NICER data in conjunction with data from XMM (the X-ray Multi-Mirror telescope, a spacecraft operated by the European Space Agency) we improved on our previous modeling work by incorporating the SCORPEON background model. Each letter in the model's name stands for a component responsible for a subset of events triggering the NICER detectors that do not originate from pulsars and are not necessarily X-rays. These background components include the South Atlantic Anomaly, cosmic rays, polar and precipitating electrons, non-X-ray particle interactions, and noise events within the NICER detectors.

On Nautilus, we processed GBT data on 20 pulsar candidates. Some of the candidates were selected by their locations within the error ellipses of Fermi-unidentified sources with pulsar-like gamma-ray spectra, and others were selected based on their steep, pulsar-like radio spectra in data from the VLA Low-band Ionosphere and Transient Experiment 1 (VLITE). While so far, we did not detect any pulsed radio emission from the candidates, the GBT observing program is ongoing and will continue into FY25. We also processed data from the Arecibo 327 MHz drift survey for pulsars and transients (AO327). This made possible the compilation of the first AO327 online catalog and data release of various data products describing pulsars detected by the survey. The catalog is hosted by West Virginia University at http://ao327.nanograv.org

DoD Impact/Significance: The main goal is to identify millisecond pulsars that are very stable rotators and therefore are useful for detecting gravitational waves with a pulsar timing array (PTA). Among the ~3,300 known pulsars, only 35 fit this criterion, and any addition to this set is a significant contribution to the nanohertz gravitational wave detection effort, as it improves the sensitivity of the PTA. The PTA approach to gravitational wave detection effort is complementary to LIGO and is sensitive to a different range of gravitational wave frequencies. The first PTA detection of the nanohertz gravitational wave background was published in 2023. The objective of modeling pulsar emissions is to obtain fits for as many pulsar mass-radius pairs as possible, in order to constrain the equation of state of neutron star matter, an extreme state of matter that cannot be reproduced in a laboratory.

Figure 1. The maximum-likelihood model to the emission of the MSP J1231-1411 includes two hot spots on the pulsar's surface where the X-ray emission originates. The panels show posterior distributions for the pulsar's radius and mass and their ratio for three modeling runs of the pulsar emission using NICER and XMM-Newton data. Red curves show the results of a hydrogen atmosphere model. Blue curves show the results of a helium atmosphere model. Yellow curves show the results of a hydrogen atmosphere model with a radius assumed or known to be greater than 8 km (figure from Salmi et al. 2024).

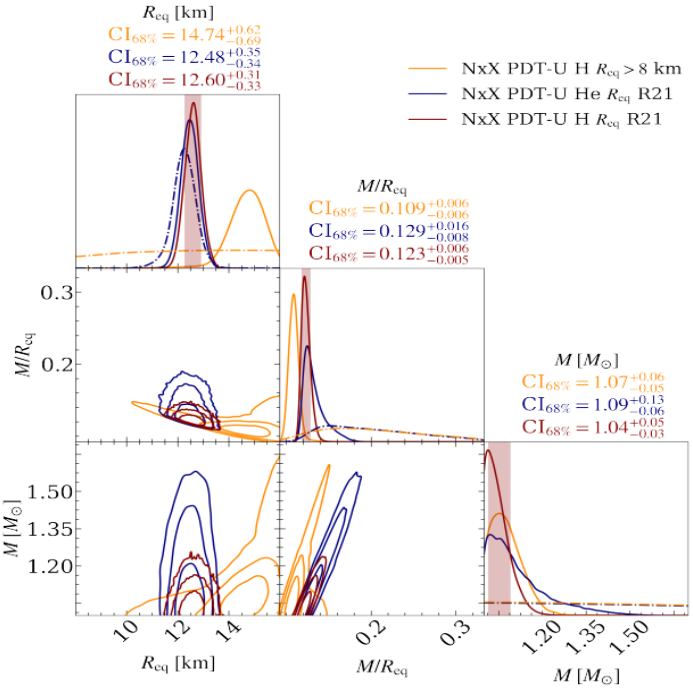

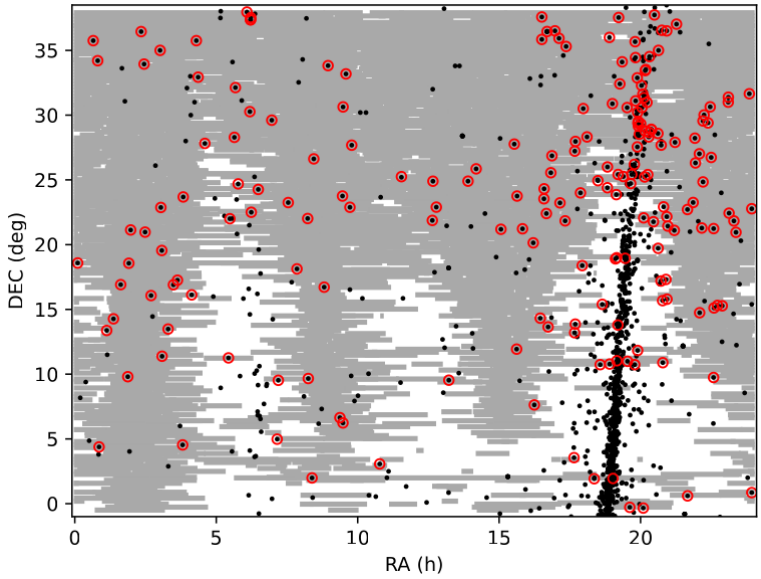

Figure 2. Sky coverage of the AO327 survey for radio pulsars and transients is shown in gray. The sky coverage is incomplete due to the collapse of the Arecibo telescope in 2020. Black points denote all known pulsars within the sky area accessible to the Arecibo telescope. They were discovered at a range of radio frequencies since the 1960s. The concentration of pulsars near right ascension of 18–20 h corresponds to the inner galactic plane. Pulsars included in the AO327 catalog are indicated with red circles. They include previously known objects as well as pulsars discovered by AO327. Whether a pulsar could be detected at the survey's observing frequency of 327 MHz depends on instrument properties such as observing bandwidth and system temperature, intrinsic pulsar properties such as rotation period and radio spectrum, and the scattering and dispersion properties of the ionized gas along the line of sight between Earth and the pulsar.

Title: Modeling Propagation of Ionospheric Disturbances Initiated by Magnetospheric Substorms
Author(s): J. Haiducek and J. Helmboldt
Affiliation(s): U.S. Naval Research Laboratory, Washington, DC
CTA: SAS

Computer Resources: HPE Cray EX [NAVY, MS]; HPE SGI 8600 [AFRL, OH]

Research Objectives: This program aims to develop data-assimilation capabilities for space weather applications, particularly focusing on SAMI3 (SAMI3 is Another Model of the Ionosphere), an ionospheric simulation code. Our long-term goal is to assimilate total electron content (TEC) observations from radio interferometers. In the short term, we are utilizing GNSS TEC observations to test the assimilation process. We aim to use the resulting data-assimilation system to better understand transient ionospheric phenomena such as ionospheric irregularities and traveling ionospheric disturbances (TIDs).

Methodology: To support the assimilation of data into SAMI3, we have developed a new parallel data-assimilation tool called LightDA. LightDA is modular software library written in Fortran that provides data-assimilation capabilities in a generic way applicable to any model whose state can be represented as a one-dimensional (1D) array of real numbers. LightDA updates an ensemble of model states to better fit a set of observations. The assimilation is performed using an ensemble Kalman filter. Interfaces to LightDA have been created for SAMI3, and a generic model consisting of a random state vector was created to test LightDA's parallelism.

Results: During FY24, we added instrumentation to LightDA to enable profiling the software in ways that are not possible with existing profiling tools. This enables us to examine questions relating to the relative performance of different parallelization strategies. One of these relates to the optimal distribution of the model state among the MPI processes. It was hypothesized previously that randomly distributing segments of the model state would enable optimal load balancing; however, this appears not to be the case. The new instrumentation enables us to identify bottlenecks such as situations in which many processes sit idle while waiting for other processes to complete. We also improved the interpolator code used as part of LightDA observation operators. Previously, the interpolator was designed to output a line integral over a vertical column within the model domain; now, it provides a vertical profile above a specified latitude and longitude. The line integral is computed from this vertical profile, and the profile can also be used to compute values for other observation types, such as electron density profiles derived from ionosondes.

DoD Impact/Significance: SAMI3 can simulate a variety of ionospheric phenomena that can impact DoD operations by altering radio signals used for radar and communications. The data-assimilation capabilities developed in this program will provide insights into how these ionospheric features develop and will influence the future development of ionospheric forecasting capabilities.

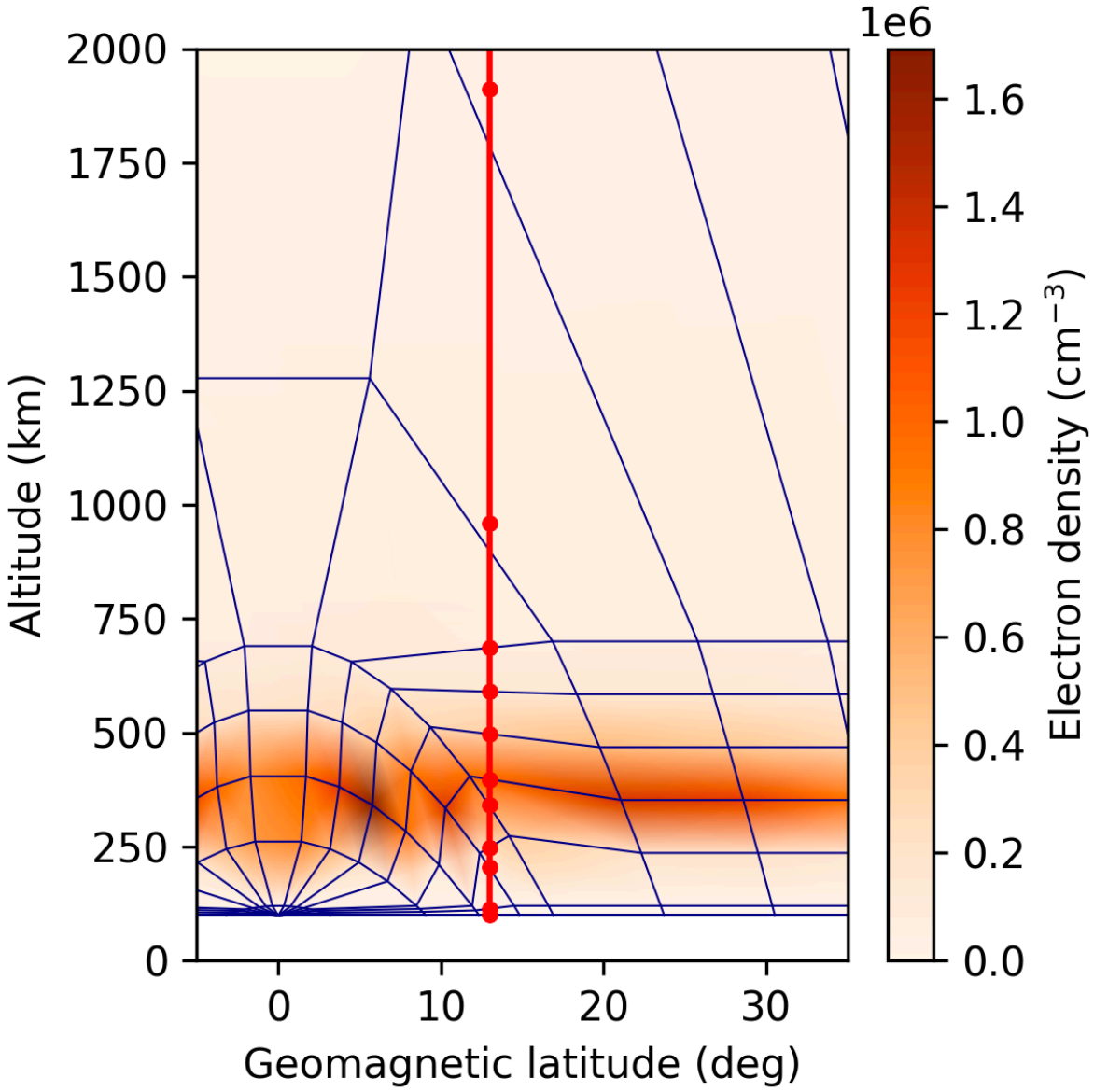

Figure 1. Illustration of the interpolation process, showing gridded electron density from PyIRI (an empirical ionosphere model used for testing algorithms intended for use with SAMI3). A vertical path drawn through the grid is marked with the locations of points output by the interpolator where a vertical line intersects with the grid. Some of the points are slightly offset from the grid edges shown because the interpolator accounts for subgrid curvature along magnetic field lines, while the routine used to plot the grid simply draws straight lines between grid points.

Title: Particle-in-Cell Simulations of Plasma Waves and Turbulence
Author(s): A.R. Soto-Chavez and J.D. Huba
Affiliation(s): U.S. Naval Research Laboratory, Washington, DC
CTA: SAS

Computer Resources: HPE SGI 8600, HPE Cray EX [AFRL, OH]; Cray XC40/50 [ERDC, MS]; HPE Cray EX [NAVY, MS]

Research Objectives: 1) Support NRL and DARPA's SMART sounding rocket experiment program by developing the capability to simulate near-Earth space plasmas on both a kinetic scale and a macroscopic scale in order to predict and assess possible scenarios. 2) Gain deeper understanding of the nonlinear induced scattering process in a turbulent plasma and the Barium evolution in the ionosphere. 3) Also, support NRL's space chamber experiments by performing nonlinear simulations of plasma-beam instabilities and apply the understanding of turbulence gained from the SMART experiment to the turbulence in the solar wind.

Methodology: We used the Tristan-MP code, which is a massively parallel (MP) PIC code that has been tested in HPC systems for the kinetic physics, and the three-dimensional (3D) SAMI3 code for the global ionosphere physics.

Results: Last year, we published one important paper on physics of plasmas (accepted September 13, 2023, but it was published in October 2023 so it would be part of this FY24 report). Therein, we presented our two-dimensional (2D)-PIC simulations of ion-ring instability leading to the successful excitation and creation of whistler waves with the Tristan-MP PIC code. The whistler waves are the result of the nonlinear scattering of lower-hybrid (LH) waves via plasma particles. This nonlinear scattering is at the heart of the SMART experiment and is something that we needed to test. The major results we found were:

1) The confirmation of the generation of whistler waves by the nonlinear scattering mechanism, shown in Fig.1. There, we see that in the right panel, the LH wave (E_ky) is saturated by the whistler waves (B_ky), confirming the scattering mechanism.

2) We varied the ion-to-electron mass ratio, with the objective of testing theory, experiment, and other PIC simulation results. In all cases, we find the excitation of the whistler waves.

We also performed 3D global ionospheric simulations using SAMI 3D code. The background plasma parameters in the code were chosen as close to the ionospheric and magnetospheric conditions that the SMART experiment encountered. In order to simulate the global ionosphere, we use SAMI3. Figure 2a shows a 2D interpolation at 500 km of altitude of the global electron density (Ne). The red dot represents the island where the SMART experiment will be launched. Figure 2b shows the ion (nH^+, nO^+) and electron densities at the launch site as a function of altitude. We are currently testing the addition of a third ion species in the code. This third element will provide the seed for the LH to be generated.

We continued the work of plasma-beam interactions to support the NRL Space Chamber. This year, we conducted two new simulations, each with a different beam radius, to study this interaction, (see Fig. 3). We submitted a paper to *Phys. Plasmas* in which some of these results are reported; the article is currently in review.

DoD Impact/Significance: The SMART experiment and associated simulations ultimately will demonstrate the formation of turbulence and its coupling between the ionosphere and the magnetosphere. The production of whistler waves and their impact on the magnetospheric particles is an active area of research in the space physics community. It is the Earth's magnetosphere where most of the DoD's and the U.S. Navy's reliance on spaceborne assets are. Furthermore, plasma-beam interactions are very important in understanding the escaping radiation from the sun's upper atmosphere. Therefore, understanding both processes in the space environment gives the Department of the Navy new capabilities to predict, to prepare for, to respond to, and to recover from space weather events.

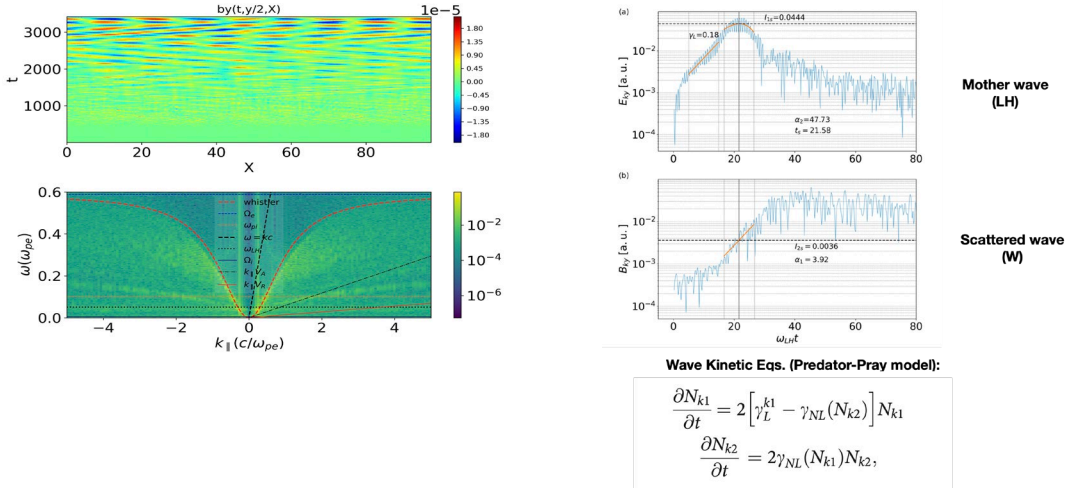

Figure 1. The whistler wave generation snapshot from our 2D PIC simulation. Top left: the B_{ky} magnetic field magnitude (wave fronts) in x-t format. Bottom left: The whistler wave dispersion relation (indicated with the red, dashed line in the bottom). Right: The LH wave E_{ky} (top), and the whistler wave B_{ky} (bottom) in k-space. This confirms the generation of whistler waves.

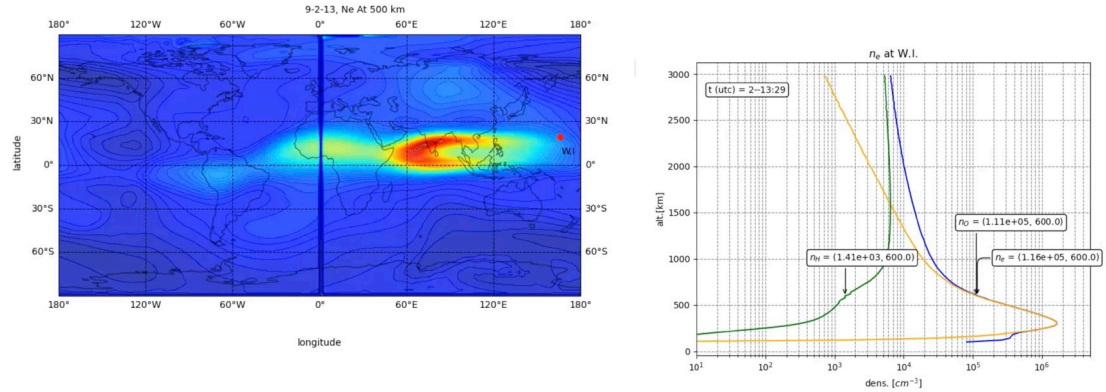

Figure 2. Left: 2D plot of the global electron density at 500 km of altitude. Right: the ion and electron densities at the launch location as a function of altitude.

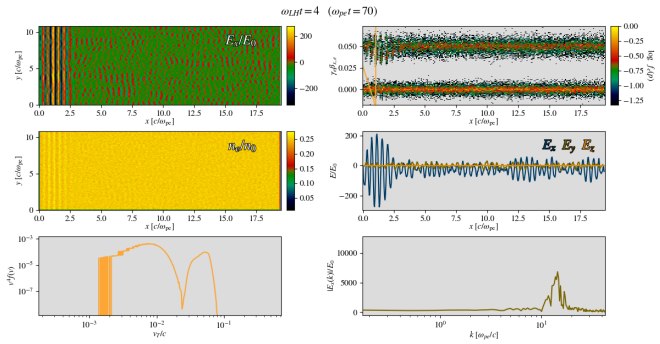

Figure 3. Electrostatic nonlinear subpackets created by the interaction of an electron beam (top left) and plasma in a 2D geometry. Middle panel: 2D density and 1D electric fields. Bottom left: beam distribution and power spectrum in k-space.

Title: Thermosphere & Ionosphere Numerical Models and Ensemble Methods
Author(s): D.P. Drob, M. Jones, and J. Emmert
Affiliation(s): U.S. Naval Research Laboratory, Washington, DC
CTA: SAS

Computer Resources: HPE SGI 8600, HPE Cray EX [AFRL, OH], [NAVY, MS], Penguin TrueHPC [NAVY, MS]

Research Objectives: This effort seeks to specify and predict the hourly, seasonal, and episodic behavior of the Earth's ionosphere and thermosphere at altitudes between 90 and 2000 km for various DoD applications. First-principles numerical forecast model biases, time-correlated model errors, and specification of solar and magnetospheric system drivers are the primary sources of poor space weather model forecast skill. This differs from meteorological numerical weather prediction, where forecast model skill almost exclusively depends on accurate specification of the forecast model's initial conditions. This year's objective was to identify and rank the key physics-based numerical forecast model parameters systematically within the SAMI4/HWM/MSIS ionosphere/thermosphere forecast model ecosystem that 1) result in largest systematic forecast model biases of ionospheric state parameters relevant to high-frequency (HF) radio wave propagation and 2) subsequently can be adjusted dynamically using available observations during the previous 24 hours to improve forecast model skill.

Methodology: The relative significance of a change in forecast model output characteristics to a corresponding adjustment of an uncertain (but locally constant) global forecast model parameter can be quantified by computing the cross-correlation between a distribution of different model output states and the ensemble distribution values of a specific model parameter used to produce those states. Furthermore, this relation taken over multiple time steps at every grid point generally forms a cross-correlation or Kalman gain matrix utilized in an ensemble Kalman filter methodology to update SAMI4/HWM/MSIS model parameters dynamically at every forecast cycle. Following from the central limit theorem and the weak nonlinearity of the physics-based SAMI4/MSIS/HWM forecast models at synoptic scales, utilizing only a 32-member SAMI4 ionospheric forecast model ensemble, up to 10 different uncertain model parameters could be examined per forecast to determine their potential contributions to model biases. As the systematic and/or stochastic uncertainties of the potentially biased, but tunable, model parameters within the SAMI4/MSIS/HWM forecast system are reasonably known, the linear-least-squares fit of forecasts over the model output domain versus parameter variations determines the total derivate relation between the output and model parameters. Maps these derivatives provide valuable insight into the ultimate contribution of specific model parameters to overall forecast model bias.

Results: Figure 1 shows an example of calculation of the key operational ionospheric parameter of MUF3000, which is the average isotropic maximum usable HF frequency to establish a HF Skywave communication link over a 3000 km path. Additional details are provided in the caption. Considered over multiple seasons and phases of the 11-year solar cycle, our sensitivity analysis in FY24 showed that the key underlying input parameters needed for actuate ionosphere specification and forecasting are 1) the amplitude and phase of the seasonal/latitudinal variation of atomic oxygen, 2) the correct scaling of a number of wavelength bands in the solar EUV input spectrum, 3) the global average exospheric temperature, and 4) the amplitude and phase of the in situ thermosphere (> 150 km) migrating tidal components in both neutral temperature and winds.

DoD Impact/Significance: The coupled physical-based ionosphere-thermosphere model validation studies performed here address the long-term DoD/Navy need for environmental prediction of space weather effects for tactical planning purposes, as well as the maximization of DoD space systems performance through adaption to the variable environment (ref: SECNAVINST 2400.2A).

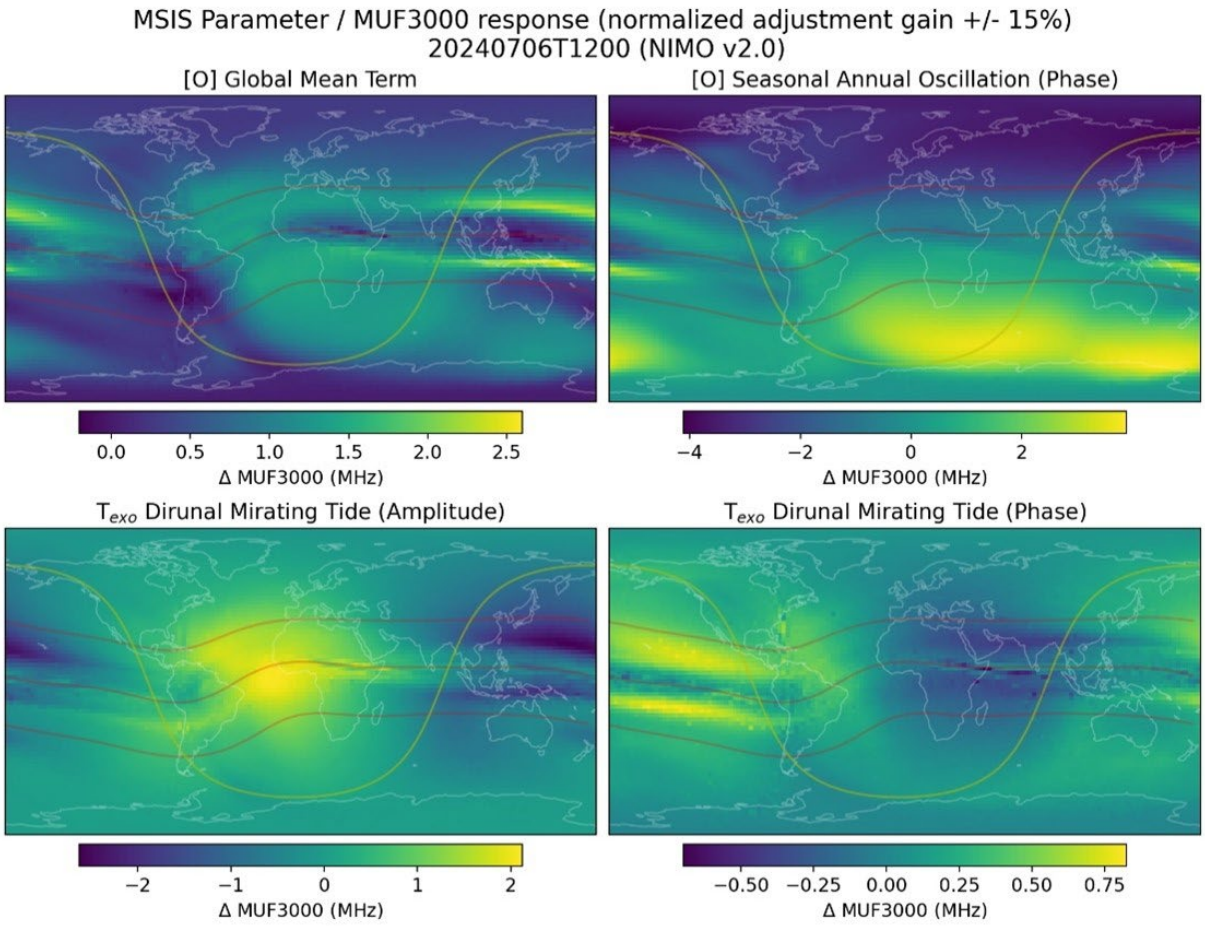

Figure 1. In the upper left panel, the MSIS atomic oxygen density was scaled uniformly, producing nonuniform responses of MUF3000 of up to 2.5 MHz. Note that this is 15% of the HF band and very likely has important operational consequences. The upper-right panel shows that the phase of the seasonal variation of atomic oxygen is also an influential parameter, and the bottom panels show that the diurnal migrating temperature tide has a similarly sized impact on the HF metric. Ionospheric sensitivity responds to horizontal wind variations in the amplitude and phase of the major tidal components DW1 and SW2 and altitude. Color scale indicates areas where ionosphere is enhanced (yellow) or reduced (blue) by variations in the tides.

Title: Navy Ionosphere Model for Operations
Author(s): M.R. Burleigh,[1] S.E. McDonald,[1] J.L. Tate,[2] E. Morgan,[1] C.A. Metzler,[1] D. Hodyss,[1] R. Schaefer,[3] and G. Romeo[3]
Affiliation(s): [1]U.S. Naval Research Laboratory, Washington, DC; [2]Computational Physics, Inc., Springfield, VA; [3]Johns Hopkins University Applied Physics Laboratory, Laurel, MD
CTA: SAS

Computer Resources: HPE Cray EX [AFRL, OH]; Cray XC40/50 [ERDC, MS]; HPE SGI 8600, HPE Cray EX, Penguin TrueHPC [NAVY, MS]

Research Objectives: The objective of this effort is to develop a physics-based ionosphere model coupled to an ionospheric data-assimilation system that provides global and regional electron density specifications and short-term forecasts (0–24 hour). This capability forms the basis of a Navy operational ionospheric forecasting system, running at multiple resolutions and fully coupled to operational atmospheric forecast models. In FY24, the main objectives were to continue development and testing of incremental releases of the Next-generation Ionosphere Model for Operations (NIMO) and to continue to improve our understanding of the lower atmospheric effects on the ionosphere using Another Model of the Ionosphere (SAMI3) coupled to whole-atmosphere models.

Methodology: NIMO consists of the physics-based ionosphere model, SAMI3, and a three-dimensional (3D) variational (3DVAR) data-assimilation system (IDA4D) that can ingest a wide variety of ionospheric datasets. NIMO utilizes the Earth System Modeling Framework (ESMF) for interpolating between the ionosphere and data-assimilation grids. For current testing and development, NIMO uses an empirical thermosphere comprising NRLMSIS 2.0 and HWM.

To investigate lower atmospheric effects on the ionosphere, SAMI3 is coupled to several whole-atmosphere models, including the Whole Atmosphere Community Climate Model Extended (WACCM-X), the Thermosphere Ionosphere Mesosphere Electrodynamics General Circulation Model (TIME-GCM), and the Navy Environmental Prediction System Utilizing the NUMA Engine (NEPTUNE).

Results: In FY24, HPC resources were used to perform multiple real-time and historical simulations with NIMO and supported the successful transition of NIMO v1.0 into operations. The use of these resources allowed us to provide critical ad hoc support for naval operations during operational outages and to simulate hotfixes for application support ahead of operational promotions to ensure smooth transitions into the operational environment. We produced and investigated near-real-time operational verification products to monitor ionospheric product quality, providing essential statistics for both operations and research and development. Additional simulations were performed to investigate the impacts of novel observations for model enhancements, further increasing the capability of NIMO to produce quality nowcasts of the ionosphere.

HPC resources also were used to run several simulations of SAMI3 coupled to a variety of whole-atmosphere models such as WACCM-X, TIME-GCM, NAVGEM-HA and NEPTUNE to investigate lower atmospheric effects on the ionosphere. This includes the yearlong simulation of SAMI3 coupled to TIME-GCM for all of 2020. Results from these simulations, as well as the NIMO work discussed above, identified areas of model improvement for SAMI3 that have been implemented.

DoD Impact/Significance: Development of an operational ionospheric forecast model will aid in the numerical forecasting of high-frequency (HF) radio wave propagation through the Earth's atmosphere and ionosphere across the range of conditions relevant to DoD/Navy operations.

Acknowledgement: This research is supported by the Office of Naval Research.

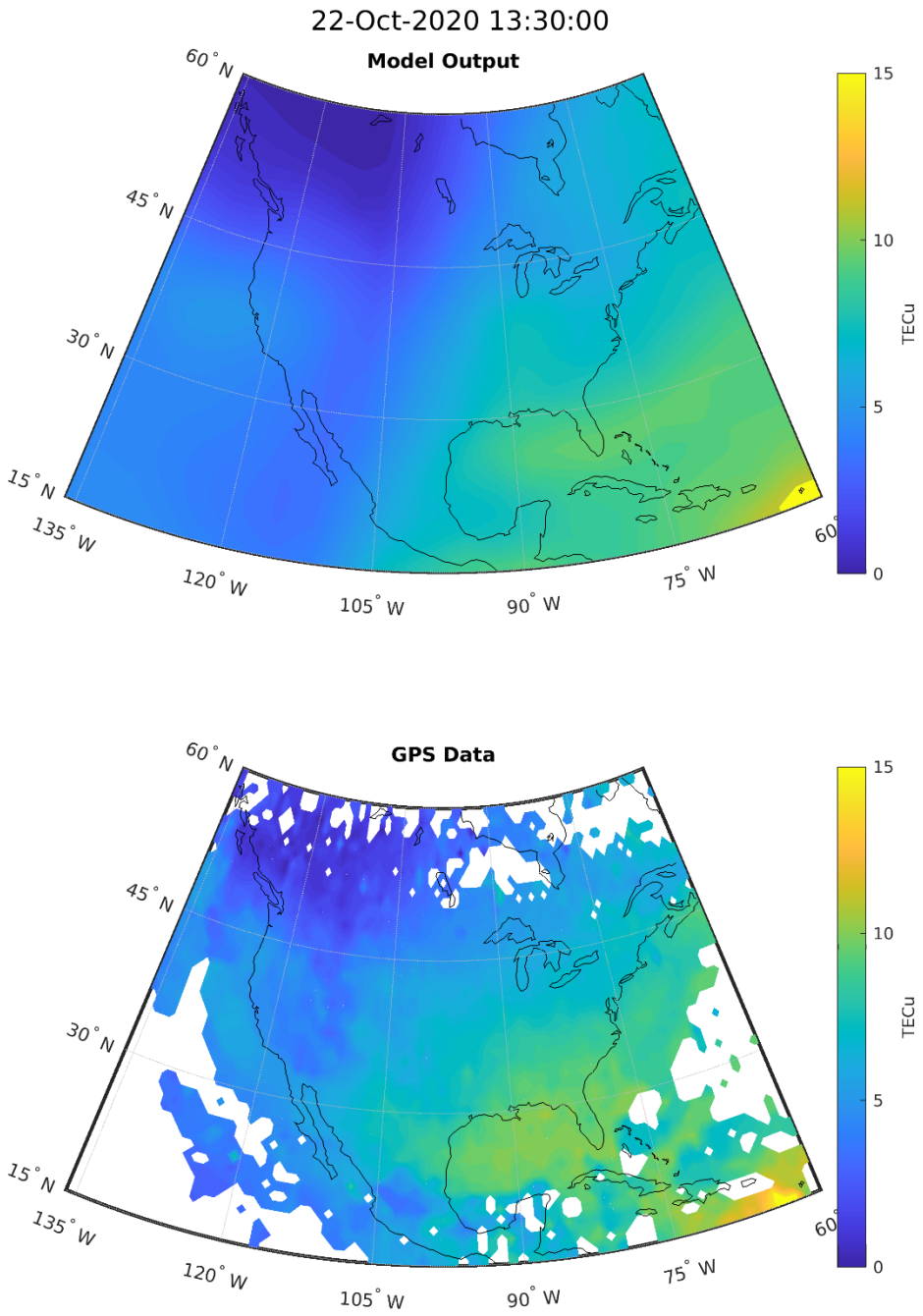

Figure 1. SAMI3/NEPTUNE model output and GPS data comparison of total electron content (TEC) for October 22, 2020.

THIS PAGE INTENTIONALLY LEFT BLANK

EQM

Environmental Quality Modeling and Simulation

The Environmental Quality Modeling and Simulation (EQM) CTA supports the investigation of DoD impacts on the environment and the impacts of this environment upon DoD activities. EQM technical activities involve the high-resolution modeling of hydrodynamics, geophysics, and multiconstituent fate/transport through the coupled atmospheric/land surface/subsurface environment and their interconnections with numerous biological species and anthropogenic activities. Within DoD, this technology is used for concerns ranging from stewardship and restoration of natural and cultural resources on military installations to evaluation of the impacts of environmental conditions on the DoD mobility operations in the battlespace.

Title: Data-Driven Prediction of Global Seabed Environmental Properties
Author(s): B.J. Phrampus and T.R. Lee
Affiliation(s): U.S. Naval Research Laboratory, Stennis Space Center, MS
CTA: EQM

Computer Resources: HPE Cray EX [NAVY, MS]

Research Objectives: NRL Code 7352 (Geology/Geophysics) aims to build, sustain, and update a data-driven, global, digital seabed model with estimates of Navy-relevant hydrological, biological, and geological properties. The prediction of high-resolution products and/or the utilization of large ("big data") datasets require the use of HPC systems to produce these models in acceptable time frames. The objective of this effort is to utilize DoD HPC capabilities to facilitate the production of necessary models, to build deliverables, and to maintain and test the scalability of future code development in support of the operational Navy. Such a capability allows the Navy to have a fast, repeatable method for providing critical environmental information for mission planning, in situ performance prediction, and deployment planning.

Methodology: NRL Code 7352 has developed a geospatial machine learning (GML) system to utilize seabed data to predict global properties. GML is used to link the production of geospatial statistics, machine learning (ML) and deep learning (DL) prediction of environmental parameters and the simulation of geophysical properties into one modular codebase. GML currently is used to produce regional and global databases and deliverables for use in the operational Navy. Here, we aim to leverage the HPC computational capabilities to improve upon the GML codebase and to produce models at higher global resolutions (i.e., global 15 arc seconds), to utilize larger datasets, and to use more advanced ML/DL algorithms. These efforts will accelerate the production of Navy-relevant properties with more accurate and realistic deliverables.

Results: The DSRC HPC is used with the GML framework to produce global and regional grids of geophysical and geoacoustic significance. This process is iterative and involves prediction-optimization and feature-selection methodologies, which can take significant computational power to complete. The HPC allows these methods to complete in reasonable and tactically useful time frames. We continue to work, in conjunction with the DoD High Performance Computing Modernization Program's Productivity and Enhancement Training (PET) program, to streamline and optimize our workflow to produce environmental parameters more rapidly and accurately. These results are used in products that are published publicly (e.g., Fig. 1), but most importantly, some products are used in support of both NAVO and NRL efforts to produce updated products for OPNAV. Finally, NAVOCEANO personnel utilize GML and the HCP in conjunction with NRL to update products, databases, and TDAs.

DoD Impact/Significance: The computational resources provided by the DoD HPC are in direct support of the Navy's seafloor prediction capabilities. Further, this project is aligned with FY25 OPNAV N2N6E Naval Oceanography RDT&E priorities for sensing, data processing, and dissemination technologies: "Techniques to enable absolute seafloor characterization …" and "Techniques to enable global bathymetric model generation …" Results from this proposal have produced and will continue to produce updated and high-resolution environmental properties in support of the operational Navy. Development on the HPC enables not only NRL, but also NAVOCEANO, to advance and maintain state-of-the-art capabilities in support of battlespace awareness across several warfare areas.

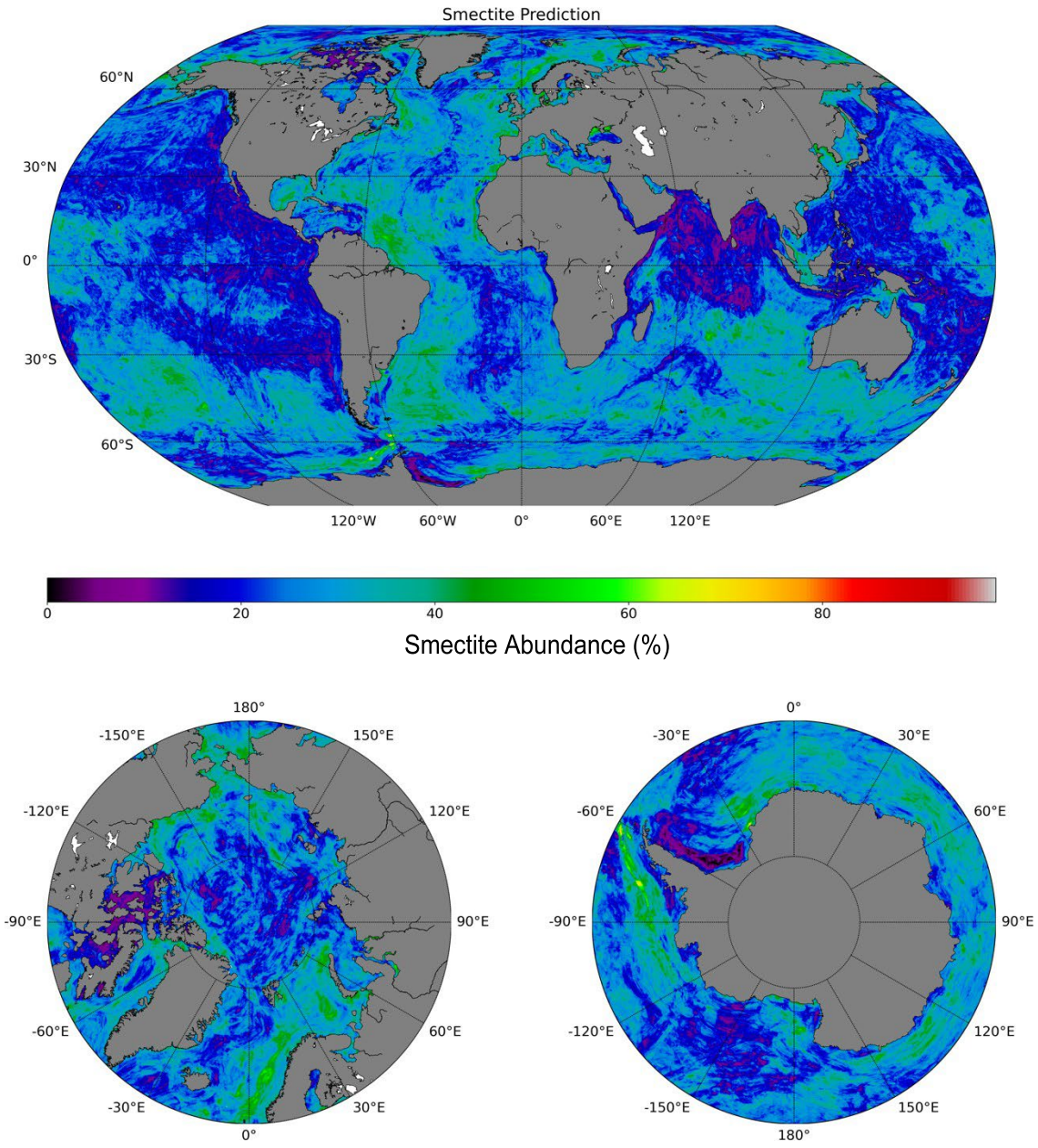

Figure 1. Global prediction of the smectite abundance (0–100%) in the upper 1 m of the seafloor. Smectite is a clay mineral and is important because it controls the compressibility, compatibility, and strength of seabed sediments. From Lee, T. R., Vander, T., Hill, T., Obelcz, J., Phrampus, B. J., Graw, J. H. (submitted). The Updated Distribution of Clay Minerals in the World Ocean. *Geophysical Research Letters*.

THIS PAGE INTENTIONALLY LEFT BLANK

DDA

Data and Decision Analytics

The Data and Decision Analytics (DDA) computational technical area (CTA) focuses on how the latest advancements in supercomputing can advance large-scale data analytics and machine learning. Recent advances in machine learning algorithms have opened the possibility to analyze and act upon the growing and increasingly accessible data collections of the DoD and the public. Current example applications, among many, include financial optimization from DoD record entries, analysis and prediction of helicopter maintenance from DoD records, and the generation of novel peptides from public protein databases. The CTA gives particular emphasis to research that will enable the analysis of high-dimensional data that was previously impossible and the discovery of new algorithms for graph analytics and machine learning. Additionally, the CTA will cover the entire supporting workflow for this research, including the software, hardware, storage, and networking. The goal of the CTA is to streamline the process of aggregating the data, the creation of these novel capabilities from analytic and machine learning methods, and the integration of the results into decision making.

Title: The Impact of Foam and Aerosol Dynamics on Fire, Explosion Safety, and Suppression (Mechanisms of Water Mist Suppression of a Burning Solid Surface)
Author(s): J.A. Cramer and R. Ananth
Affiliation(s): U.S. Naval Research Laboratory, Washington, DC
CTA: DDA

Computer Resources: HPE SGI 8600, HPE Cray EX [AFRL, OH]

Research Objectives: To develop machine learning (ML) methods to predict the fire-suppression capabilities of novel nonfluorinated surfactant concepts prior to synthesis, thus both streamlining and otherwise enhancing the development of alternatives to fluorinated fire-suppression materials.

Methodology: In-house firefighting-foam-performance data collections were collated and reformatted into an expansive database upon which to train future ML models. As a specific application, two ensembles of 10 artificial neural networks (ANNs) were trained to correlate area-under-the-curve (AUC) values obtained from 19 cm heptane pool fire extinction curves to the quantitative molecular descriptors associated with the primary surfactants found in the formulations used to obtain those curves. One ensemble included fluorinated aqueous film-forming foam (AFFF) fire-suppression agents in its training data, and one was trained only with nonfluorinated materials, thus, at least theoretically, providing internal validations of performance predictions. Both ANN model ensembles were used to evaluate proposed surfactant structure concepts to predict their effectiveness in real-world scenarios prior to laboratory synthesis and experimental fire-suppression trials, including the collection of additional 19 cm heptane pool fire extinction data.

Results: When considered in aggregate, the two ANN model ensembles predicted that a novel poly-dispersed (i.e., multiple PEO chain lengths) chlorotrisiloxane-polyethyleneoxide (PEO) surfactant concept would perform at least as well as the median-performance PEO surfactant found in the training data and might perform better than the highest-performing PEO surfactant, and perhaps even better than AFFF materials themselves. However, while these predictions were superficially promising, the fact that prediction averages for the same PEO chain lengths diverged considerably across the two model ensembles, and the fact that the average values seen across differing PEO chain lengths even trended in different directions between the two model ensembles (see Fig. 1), should have been considered causes for reconsideration prior to synthesis. In fact, the novel poly-dispersed PEO material, once synthesized, did not meet the expectations set forth by the ANN modeling insofar as it performed more poorly than not only the median performance PEO surfactant, but almost every other comparable PEO material in the training data as well. In hindsight, the divergences noted both within and between the model ensembles might have been an indication that the performance predictions were not based upon solidly modeled chemical information. While a negative result, said result is still considered important in the context of how to assess properly the probable real-world utility of machine learning predictions.

DoD Impact/Significance: Per- and polyfluoroalkyl substances (PFAS) in AFFF firefighting materials pose environmental and health problems. PFAS must be replaced per the National Defense Authorization Act (NDAA, passed by U.S. Congress in 2020). However, while fluorine-free foams can be much more environmentally friendly, these materials do not normally meet the exacting fire-suppression requirements set forth in MIL-PRF-24385F. Research into producing a robust pool of suitable fluorine-free surfactants is ongoing, but trial-and-error empirical development approaches are both inefficient and dependent upon preexisting expert knowledge. An ML-based capability to screen fire-suppression material concepts accurately prior to synthesis will allow for accelerated development cycles that in turn will allow for a much faster investigation of promising concepts that are both well-informed by expert knowledge and completely novel in the context of fire suppression.

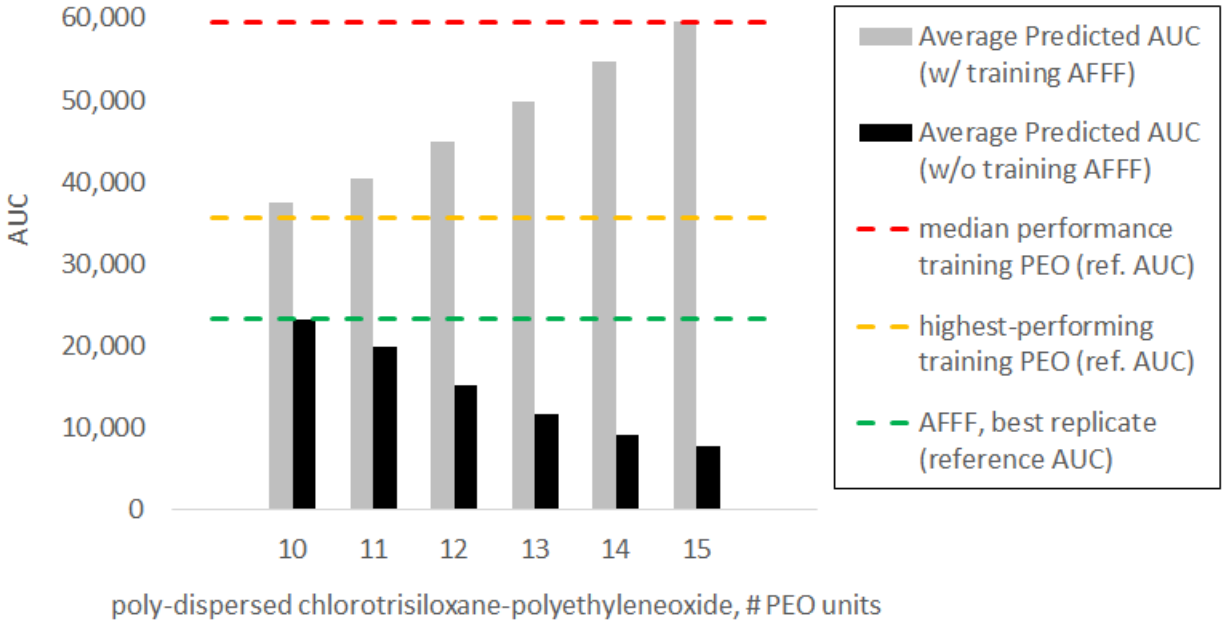

Figure 1. Average predicted 19 cm heptane pool fire extinction curve AUC results as obtained from the individual PEO chain lengths of a prospective poly-dispersed chlorotrisiloxane-polyethylene oxide firefighting surfactant, alongside reference AUC values that were obtained experimentally and incorporated into the training data used to train the ANN ensembles yielding these predictions.

THIS PAGE INTENTIONALLY LEFT BLANK

OTH

Other

Work that is not easily categorized as one of the other computational technology areas.

Title: Modeling Low-Temperature Plasmas for Atomic Precision Processing
Author(s): M. Meyer[1] and S.G. Walton[2]
Affiliation(s): [1]National Research Council Postdoctoral Research Associate at the U.S. Naval Research Laboratory, Washington, DC, [2]U.S. Naval Research Laboratory, Washington, DC
CTA: OTH

Computer Resources: Penguin TrueHPC [NAVY, MS]

Research Objectives: The objective of this program is to model low-temperature plasmas relevant for atomic precision processing efforts at NRL. Initially, this project will focus on benchmarking the results of the model against experimental measurements of the plasma sources. Once benchmarked, the model will be used to predict quantities in the plasma that are difficult to measure and to examine the dominant physical processes occurring in the plasma. The model will be used further to guide material-processing efforts by investigating a wide range of process conditions.

Methodology: The low-temperature plasma model used in this project is the Hybrid Plasma Equipment Model (HPEM). HPEM was developed by Mark Kushner at the University of Michigan (M. Kushner, *J. Phys. D: Appl. Phys.* 42, 194013 (2009)). HPEM is used widely throughout academia and industry to model plasma-processing tools. HPEM uses time-slicing algorithms to span the disparate time scales of processes occurring in the plasma. Each module in HPEM models a different physical process, and each module is updated on its relevant time scale and provides necessary output to other modules. Different methods are available in each module, allowing HPEM to be capable of simulating a wide range of plasma conditions and configurations.

Results: This project began in July of FY24, focusing on benchmarking the results of HPEM against experimental measurements. The plasma device modeled is a remote inductively coupled plasma (ICP), based on sources currently in use at NRL. A schematic of the remote ICP device is shown in Fig. 1. Initial simulations showed that using a kinetic method for electron energy transport better matched experimental measurements compared to a fluid method. In pure Ar, the electron density and plasma potential predicted by HPEM agreed reasonably well with experimental measurements in the ICP source and the afterglow. Initial results from HPEM showed a decrease in electron temperature in the afterglow, while measurements showed an increase in electron temperature. This discrepancy is potentially due to an underprediction of capacitive power coupling in the afterglow. Current work is focused on matching the trends in electron temperature in the afterglow as well as examining Ar/N_2 mixtures.

DoD Impact/Significance: Plasma-enhanced atomic layer processing systems are used for development of next-generation electronic, opto-electronic, and sensing devices of interest to the DoD. Applications include novel nonvolatile memory/transistors compatible with CMOS technology or ultralow-power computation, ultrawide-bandgap semiconductors for next generation RF and power devices, new meta-material structures, scalable nanoscale biosensing platforms, and enhanced electromagnetic radiation-specific detectors. A better understanding of these plasma sources and systems is integral to developing the process parameter to material property connection needed to advance device fabrication.

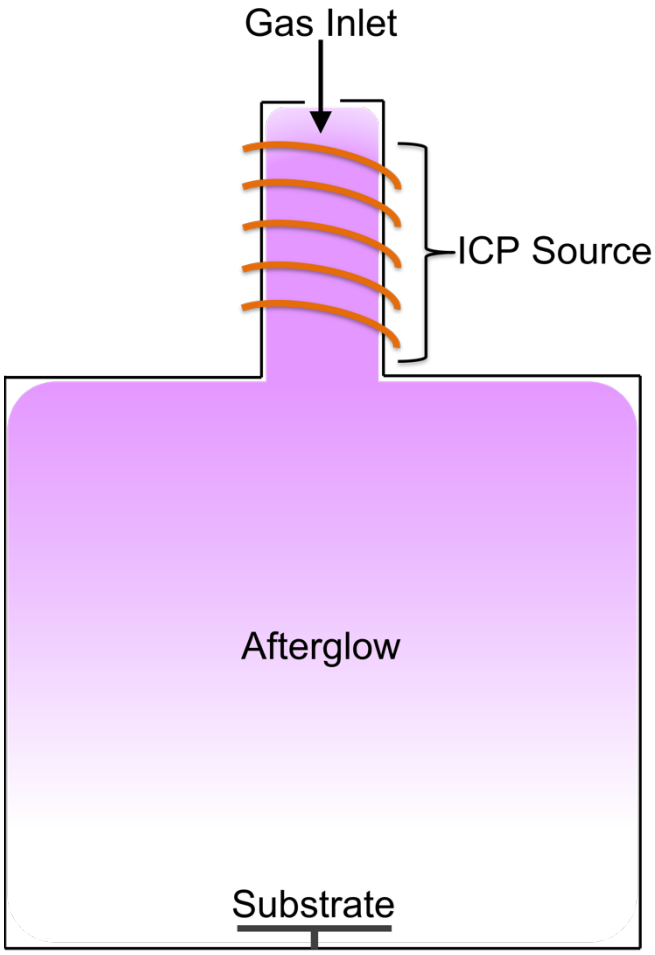

Figure 1. Schematic of a remote ICP system.

Title: Simulation of High Energy-Radiation Environments
Author(s): J. Finke and W. Duvall
Affiliation(s): U.S. Naval Research Laboratory, Washington, DC
CTA: OTH

Computer Resources: HPE Cray EX [NAVY, MS]

Research Objectives: 1) Use Monte Carlo radiation transport techniques to simulate radiation effects on electronics and humans in various venues including space, aviation, and terrestrial radiation environments. Also simulate radiation-detection system effectiveness in each venue, pulsed-power radiation sources and potential systems for the detection of special nuclear materials and radiological/nuclear materials. 2) Apply an improved model of the extragalactic background light (EBL), computed on HPC machines to new gamma-ray absorption data.

Methodology: 1) We used the SoftWare for Optimization of Radiation Detectors (SWORD) system for performing relevant radiation-transport simulations. SWORD is a vertically integrated, graphical user interface that allows users to simulate radiation quickly and easily in a number of environments, making use of industry-standard radiation-transport codes such as Geant4. 2) We applied the model of the EBL created by Co-PI Finke to new gamma-ray absorption data from blazars from the Fermi Large Area Telescope (LAT). The Fermi LAT data can be used with the model to get an independent measurement of the star-formation rate and overall EBL intensity.

Results: 1) SWORD on HPC has been used to simulate a variety of space, aviation, and terrestrial radiation-propagation problems. These include simulation of radiation effects on orbiting spacecraft to evaluate effects on electronics and on sensitivity of instruments. This is very compute intensive, hence the requirement for HPC resources. In support of aviation background studies, SWORD has been used to evaluate the effects of the in-flight radiation environment on passengers and cargo. Finally, SWORD has been used to evaluate shielding efficiency in high-radiation laboratory environments. 2) We are able to put updated constraints on the EBL (see Fig. 1). These constraints are based on preliminary gamma-ray observations. The EBL contains information about star formation, dust extinction, and the cosmological expansion of the universe.

DoD Impact/Significance: 1) The ability to use SWORD to simulate radiation effects in space, aviation, and terrestrial radiation environments allows studies that are becoming increasingly important for the DoD, particularly the Space Force and the Navy. By simulating radiation effects on electronics, detection systems, and personnel, large SWORD simulations in the various venues will predict the impact of radiation in these venues on the warfighter and warfighting systems. For example, radiation effects simulations allow for the development of spacecraft for sponsors such as NASA and the DoD Space Test Program. They also allow for the testing of operational radiation detection concepts in urban and maritime scenarios that are relevant to sponsors such as the Department of Homeland Security/Countering Weapons of Mass Destruction (DHS/CWMD) office and the Defense Threat Reduction Agency (DTRA). 2) Understanding the transparency of the universe is crucial to studying GRBs and other astrophysical objects that accelerate particles. Understanding particle acceleration in these sources can give insight into how particles accelerated elsewhere can impact DoD space assets.

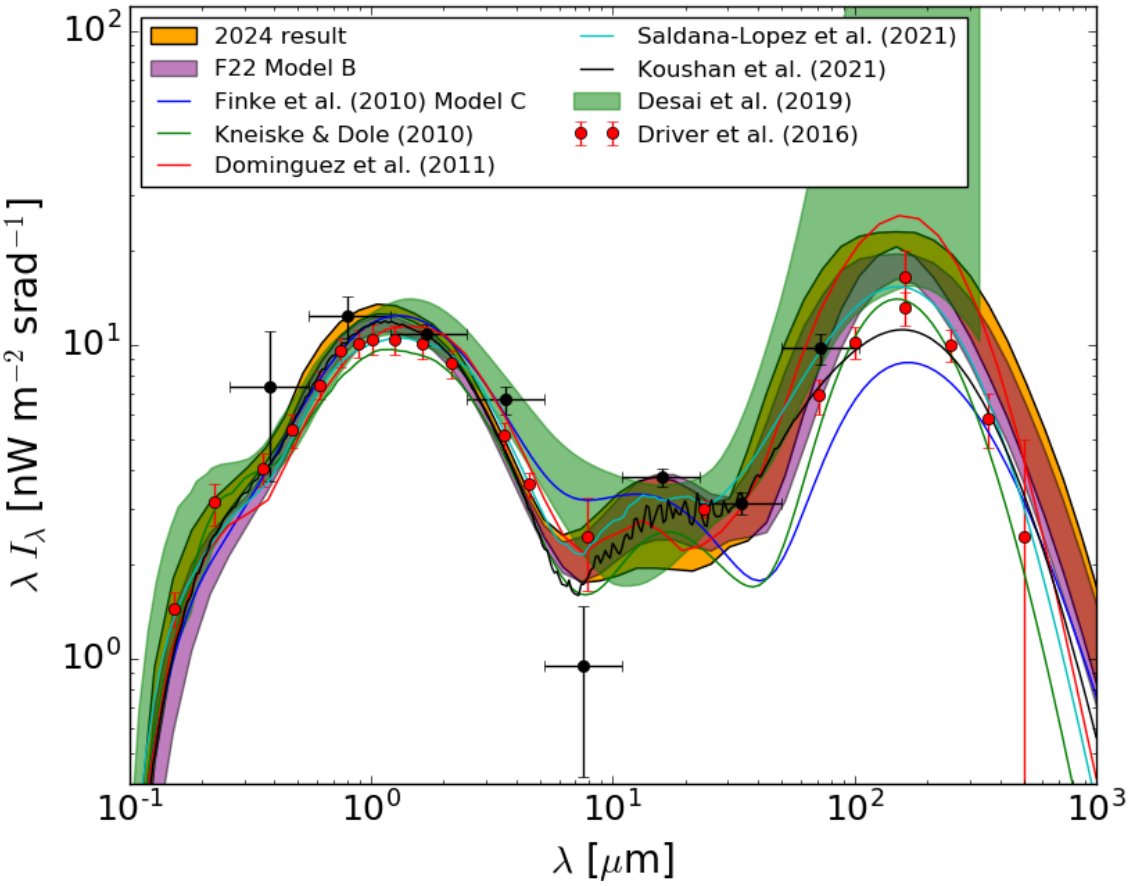

Figure 1. The EBL intensity from several measurements and models from the literature, as described in the legend. The most recent preliminary result is labeled “2024 result.”

THIS PAGE INTENTIONALLY LEFT BLANK

Author Index

Adams, I. ---------- 26
Allard, R. ---------- 100, 126
Allen, D.R. ---------- 128
Amos, C.M. ---------- 122
Ananth, R. ---------- 160
Antillon, E. ---------- 6
Arcari, A. ---------- 2

Barron, C.N. ---------- 122
Barton, C.A. ---------- 128
Bateman, S. ---------- 26
Bernstein, N. ---------- 48
Bojko, B. ---------- 22
Book, J.W. ---------- 122
Burleigh, M.R. ---------- 152

Campbell, T. ---------- 126
Campbell, W.F. ---------- 112
Carrier, M.J. ---------- 120
Cayula, S. ---------- 90
Chadwick, A. ---------- 4
Cooke, S. ---------- 72
Cramer, J.A. ---------- 160

D'Addezio, J.M. ---------- 108, 116
DeBoskey, R. ---------- 12
Deneva, J. ---------- 144
Dey, S. ---------- 80
Douglass, E. ---------- 126
Doyle, J.D. ---------- 86
Drob, D.P. ---------- 150
Duvall, W. ---------- 166

Eckermann, S.D. ---------- 128
Edwards, K. ---------- 26
Emmert, J. ---------- 150

Fan, Y. ---------- 88
Finke, J. ---------- 166
Finocchio, P.M. ---------- 92
Fragiadakis, D. ---------- 64
Furstenberg, R. ---------- 78

Gamezo, V.N. ---------- 18
Gatling, G.R. ---------- 82
Goodwin, G.B. ---------- 12
Grossman, S.M. ---------- 136
Gulliver, L.T. ---------- 104

Haiducek, J. ---------- 146
Hebert, D. ---------- 100, 108, 126
Helber, R.W. ---------- 110, 118
Hellberg, C.S. ---------- 50, 56
Helmboldt, J. ---------- 146
Herrera, M.A. ---------- 128
Hervey, W.J. ---------- 60, 62
Hess, A. ---------- 22
Hinshelwood, D.D. ---------- 74
Hodyss, D. ---------- 152
Holder, C.F. ---------- 52, 54
Hoppel, K.W. ---------- 128
Huba, J.D. ---------- 148

Isner, N.D. ---------- 76
Iversen, A.J. ---------- 116

Jacobs, G. ---------- 116, 118, 122
Janiga, M.A. ---------- 124
Jarosz, E. ---------- 90
Jensen, A. ---------- 72
Jensen, T. ---------- 126
Johannes, M. ---------- 38
Johnson, R.F. ---------- 22, 30
Johnston, M.D. ---------- 76
Jones, M. ---------- 150

Kardish, M.R. ---------- 60
Kaur, H. ---------- 110
Kelly, J.F. ---------- 128
Kessler, D. ---------- 22
Khine, Y. ---------- 14, 114
Krause, B. ---------- 108

Author Index

Kuhl, D.D. ---------- 128

Lambrakos, S. ---------- 54
Lawrence, A. ---------- 122
Lee, T.R. ---------- 156
Li, L. ---------- 136
Liu, J. ---------- 16
Lyons, J.L. ---------- 34

Ma, J. ---------- 128
May, J. ---------- 108
McDonald, S.E. ---------- 152
McLay, J.M. ---------- 124
Melzer, B.A. ---------- 70
Metzger, E.J. ---------- 90, 96, 98
Metzler, C.A. ---------- 152
Meyer, J.R. ---------- 132
Meyer, M. ---------- 164
Morgan, E. ---------- 152
Morse, J.R. ---------- 52
Moser, A.E. ---------- 8
Mott, D.R. ---------- 14
Mukhopadhyay, S. ---------- 40

Osborne, J.J. ---------- 122
Ouellette, J.D. ---------- 68, 136
Ovtchinnikov, S. ---------- 72

Panteleev, G. ---------- 100, 126
Patel, T.K. ---------- 22
Penko, A. ---------- 26
Petillo, J. ---------- 72
Phelps, M. ---------- 126
Phillip, R. ---------- 26
Phillips, M. ---------- 46
Phrampus, B.J. ---------- 156
Poludnenko, A.Y. ---------- 18
Povolotskyi, M. ---------- 132

Ramamurti, R. ---------- 24
Ray, P.S. ---------- 144
Reinecke, T.L. ---------- 42
Rester, B. ---------- 120
Rhodes, T. ---------- 128
Ridout, J.A. ---------- 124
Rittersdorf, I.M. ---------- 74, 76
Romeo, G. ---------- 152
Rowley, C. ---------- 106

Schaefer, R. ---------- 152
Schoenauer, S. ---------- 26
Schweigert, I.V. ---------- 58
Schwer, D.A. ---------- 28
Shabaev, A.R. ---------- 52, 54, 78
Shriver, J.F. ---------- 98, 104
Shulman, I. ---------- 90
Simeonov, J. ---------- 26
Sletten, M.A. ---------- 68
Smith, L.N. ---------- 138, 140
Smith, S.R. ---------- 110, 116, 118
Smith, T. ---------- 108, 126
Soto-Chavez, A.R. ---------- 148
Stantchev, G. ---------- 72
Swanekamp, S.B. ---------- 74, 76
Swift, M.W. ---------- 44

Tan, X.G. ---------- 8
Tate, J.L. ---------- 152
Teferra, K. ---------- 4
Tejero, E.M. ---------- 82
Thoppil, P.G. ---------- 94
Toporkov, J.V. ---------- 68
Trott, C.B. ---------- 102
Tsu, J. ---------- 112
Twarog, E.M. ---------- 136

Vazsonyi, A.R. ---------- 76
Veeramony, J. ---------- 26
Viswanath, K. ---------- 20
Vora, G.J. ---------- 60, 62
Vurgaftman, I. ---------- 132

Author Index

Wade, N. ---------- 2, 4
Walton, S.G. ---------- 164
Weber, B.V. ---------- 74
Welland, I. ---------- 42
Whitcomb, T.R. ---------- 124
Wickramaratne, D. ---------- 36
Wimmer, S.A. ---------- 2

Yaremchuk, M. ---------- 100

Zier, J.C. ---------- 76

Division/Branch Index

Systems Directorate (Code 5000)

Information Technology Division (Code 5500)

Navy Center for Applied Research in Artificial Intelligence (Code 5510) 138, 140

Optical Sciences Division (Code 5600)

Senior Scientist for Quantum Electronics (Code 5604) 132
Optical Physics (Code 5610) 132

Materials Science and Component Technology Directorate (Code 6000)

Laboratories for Computational Physics and Fluid Dynamics (Code 6040)……...12, 14, 16, 18, 20, 22, 24, 28, 30, 114

Chemistry Division (Code 6100)

Materials Chemistry and Dynamics (Code 6120)..... 64
Center for Corrosion Science and Engineering (Code 6130) 2
Navy Technology Center for Safety and Survivability (Code 6180) 58, 160

Materials Science and Technology Division (Code 6300)

Multifunctional Materials (Code 6350) 2, 4, 8
Materials and Sensors (Code 6360) 52, 54, 78
Center for Materials Physics and Technology (Code 6390)..... 6, 34, 36, 38, 44, 46, 48, 50, 56

Plasma Physics Division (Code 6700)

Charged Particle Physics (Code 6750) 82, 148, 164
Pulsed Power Physics (Code 6770) 74, 76, 148

Electronics Science and Technology Division (Code 6800)

Voluntary Emeritus Program Participant for Electronics, Science and Technology..... 42
Electromagnetic Technology (Code 6850) 40, 72
Electronic Materials (Code 6870)..... 42

Center for Biomolecular Science and Engineering (Code 6900)

Principal Scientist for Biotechnology (Code 6904)..... 60, 62
Laboratory for Bio/Nano Science and Technology (Code 6910) 60, 62

Ocean and Atmospheric Science and Technology Directorate (Code 7000)

Acoustics Division (Code 7100)

Physical Acoustics (7130)..... 80
Acoustics Simulation, Measurements, and Tactics (Code 7180) 70

Remote Sensing Division (Code 7200)

Radio/Infrared/Optical Sensors (Code 7210)..... 146
Remote Sensing Physics (Code 7220) 68, 128, 136, 152
Image Science and Applications (Code 7260)..... 68

Ocean Sciences Division (Code 7300)

Ocean Dynamics and Prediction (Code 7320) 26, 88, 90, 94, 96, 98, 100, 102, 104, 106, 108, 110, 116, 118, 120, 122, 126
Ocean Sensing and Processing (Code 7330) 90, 122
Seafloor Sciences (Code 7350)..... 26, 156

Marine Meteorology Division (Code 7500)

Senior Scientist for Mesoscale Meteorology (Code 7503)..... 86
Atmospheric Dynamics and Prediction (Code 7530) 92, 112, 124

Space Science Division (Code 7600)

Special Projects Office for High Altitude Numerical Weather Prediction (Code 7604) 128
Contracting Officer Representative Office for Space Science (Code 7608) 144
Geospace Science and Technology (Code 7630)..... 128, 150, 152
High-Energy Space Environment (Code 7650)..... 144, 166

Naval Center for Space Technology (Code 8000)

Space Systems Development Division (Code 8100)

Mission Development (Code 8110) 54

Spacecraft Engineering Division (Code 8200)

Design and Verification (Code 8220)..... 12

Site Index

DSRCs

AFRL	4, 6, 8, 16, 18, 22, 24, 30, 34, 36, 38, 40, 42, 44, 46, 48, 50, 52, 54, 58, 60, 62, 64, 68, 78, 80, 92, 124, 132, 138, 146, 148, 150, 152, 160
ARL	24, 44, 48, 50, 138, 140
ERDC	4, 6, 16, 18, 20, 24, 34, 36, 40, 44, 46, 50, 52, 54, 60, 62, 68, 72, 78, 92, 124, 128, 144, 148, 152
NAVY	2, 4, 8, 12, 14, 16, 18, 20, 22, 26, 28, 30, 40, 50, 52, 54, 56, 60, 62, 64, 68, 70, 72, 74, 76, 78, 80, 82, 86, 88, 90, 92, 94, 96, 98, 100, 102, 104, 106, 108, 110, 112, 114, 116, 118, 120, 122, 124, 126, 128, 132, 136, 138, 144, 146, 148, 150, 152, 156, 164, 166